Analysis of the structural basis for the gating and regulation of the human type 3 Inositol Trisphosphate Receptor

By

Emily Ann Schmitz

Dissertation
Submitted to the Faculty of the
Graduate School of Vanderbilt University
in partial fulfillment of the requirements
for the degree of

DOCTOR OF PHILOSOPHY

in

Chemical and Physical Biology

December 17, 2022

Nashville, Tennessee

Approved:

David Jacobson, Ph.D.

Ray Blind, Ph.D.

Teru Nakagawa, Ph.D.

Roger Colbran, Ph.D.

1 Acknowledgments

I would like to first acknowledge the funding sources that enabled me to complete this Ph.D. This list includes: the Molecular Biophysics Training Program Grant from the T32 GM008320 assigned to Walter Chazin, the start-up fund from Vanderbilt University to my advisor Dr. Erkan Karakas, the Vanderbilt Diabetes and Research Training Center Grant DK020593, and finally the NIH R01GM141251 grant.

I would like to next thank current and former members of the lab for their support. Cate Risener provided the initial training I received when joining the lab, and was the source of sunshine and fun in the lab. Mel Cutler provided critical molecular biology support with the endless number of IP_3R constructs planned for functional assays, biochemical assays, and future Cryo-EM projects in addition to being a friend for life. Hirohide Takahashi was an enjoyable person to work with and a calming influence on the lab for these years where it was just the two of us in the lab. He provided critical support with the Cryo-EM portions of this thesis, plunging and screening the grid conditions when I was unable to, and offering advice on liposome preparation. Erkan Karakas provided the opportunity to see how an academic lab is started and develops over time, which was a critical influence on my future career goals and decisions. He also single-handedly provided the vision for my project and determined the research strategy which successfully led to our publications. While not members of the lab, I would also like to thank Kevin Jagessar and Rich Stein for being great sources of life and career advice.

I would like to thank the Carrasco lab for the use of their plate reader and Silvia for helping with troubleshooting. For the Panoptic assays, Debbie Mi from the High-throughput screening core was incredibly helpful with training on the machines and with troubleshooting. Thanks to Drs. James Crowe Jr. and Lauren P. Jackson for the use of their ITC instruments. Thanks to the Vanderbilt Center for Structural Biology Instrumentation Core for the use of the Nanotemper Monolith NT.115 for the MST experiments. Special thanks to Caleigh Azumaya for collecting the data for the JBC paper on the FEI polara and FEI F20, and to Teru Nakagawa for helping with data processing. Thanks to Drs. Scott Collier, Elad Bishtein, and Melissa Chambers for training, data collection, and support along the way. For the open structure project, we thank Case Western University for the use of their Titan Krios in data collection. We acknowledge the

use of SBGrid supported software, the DORS storage system provided by National Institutes of Health Grant S10RR031634. Finally, the CPU and GPU resources of the Advanced Computing Center for Research and Education (ACCRE) greatly assisted with data processing and provided an excellent learning opportunity in high throughput computing.

I am grateful for the advice and help from all of my committee members, Drs. David Jacobson, Roger Colbran, Ray Blind, and Teru Nakagawa both in meetings and in conversations outside of them. And finally, I am most grateful for my husband, Sam, for reminding me that science can be fun and proofreading everything.

Table of Contents

List of Figures

List of Tables

4 Summary

The inositol 1,4,5-trisphosphate receptor (IP_3R or $InsP_3R$) is a key component in the cell's calcium signaling toolbox, synthesizing the combined effects of extracellular signals, propagated through G-protein coupled receptors (GPCRs) and receptor tyrosine kinases (RTKs), with modulatory binding proteins to produce a precisely spatiotemporally controlled Ca^{2+} signal. The released Ca^{2+} acts as a second messenger by binding to cytosolic Ca^{2+} buffers and binding proteins, which then transform the signal into tangible effects ranging from transcription to exocytosis. Of the three IP_3R isoforms, the type 3 IP_3R (IP_3R-3) is the predominant isoform localized at ER-mitochondrial contact sites. IP_3R-3 activation creates local Ca^{2+} hotspots, promoting Ca^{2+} transfer through the outer mitochondrial membrane (OMM) into the intermembrane space via the voltage-dependent anion channel (VDAC). The Ca^{2+} flow into the mitochondrial matrix is critical for cell bioenergetics and survival. Dysregulation of IP_3R activity leads to impaired Ca^{2+} signaling, which is part of the pathophysiology underlying neurological and metabolic diseases, as well as several cancers. The receptor is currently undruggable due to the lack of membrane permeable, isoform specific agonists, antagonists, or allosteric modulators to correct for aberrant IP_3R activity. A lack of structural information on different functional states of the receptor in the gating cycle, as well as how IP_3R binding proteins and compounds change the receptor's structure to impose their modulatory effects, has resulted in a dearth of pharmacological tools to precisely control the receptor in both laboratory and clinical settings. Determining the three IP_3R isoforms in multiple pre-active, active, and inhibited conformations is a critical step in understanding the differences between each isoform's activity, which may provide insight into future directions for developing isoform-specific modulator compounds.

The motivation of the three main projects in this dissertation is outlined in Chapter 5. The three main projects described are 1) the identification and description of a novel self-regulating peptide in a ligand-free human IP_3R-3 (hIP_3R-3) structure, 2) the determination of an ensemble of IP_3R-3 structures that includes the active conformation, and 3) current progress on the search for the optimal conditions to determine an inhibited IP_3R structure in complex with a chemical antagonist.

Chapter 6 describes the process of determining a Cryo-EM structure of the hIP$_3$R-3 in the apo, or ligand free, conformation, focusing the refinement strategy on a portion of the N-terminal domain that contains a self-binding peptide (SBP). Following the identification of the 27 residue SBP through Cryo-EM data processing, biochemical assays were used to show the effect of the SBP on IP$_3$ binding and conclude that the SBP competes against IP$_3$ for access to the binding pocket.

The following Chapter 7 discusses the search for and the identification of an active conformation of the IP$_3$R-3, also using Cryo-EM as the primary technique. The chapter discusses the three pre-active conformations (A-C), active conformation, and an inactive/desensitized structure that were determined from the same starting dataset. The propagation of domain and conformation changes throughout the large cytosolic N-terminal domain towards the transmembrane domain, which ultimately results in the pore opening is described in detail.

Chapter 8 describes recent progress on the efforts to determine a Cryo-EM structure of the IP$_3$R-3 in complex with a small molecule antagonist. A structure of IP$_3$R-3 obtained using samples incubated with saturating conditions of the non-specific inhibitor 2-Aminoethoxydiphenyl borate (2-APB) is reported, although no density could be attributed to the ligand. Further attempts to optimize the purification conditions of IP$_3$R-1 splice variants are described, with the goal of using some or all of these constructs for another future attempt at obtaining an IP$_3$R structure in complex with an inhibitor.

All three major projects comprising this dissertation are critically discussed in Chapter 9 with their potentials and limitations, and future strategies to improve upon and expand these results. The main takeaway is that the described ensemble of IP$_3$R-3 structures reveals the gating mechanism and activation of a flexible ligand-gated ion channel, and identify a novel regulatory mechanism whereby the receptor is capable of self-inhibition. The structural conformations that underlie the receptor's transition from an desensitized state back to an apo, licensed to respond, conformation remain unsolved. In addition, the underlying structural mechanism by which chemical antagonists modulate IP$_3$R activity and how this modulation differs based on receptor isoform remains to be determined.

5 Introduction

5.1 An overview of intracellular Ca^{2+}homeostasis and Ca^{2+} signalling

Multicellular eukaryotes utilize Ca^{2+} as a secondary messenger to stimulate different cellular processes, ranging from differentiation to exocytosis (Parys and H. De Smedt 2012; Berridge 2016). The exact nature of the response depends on the source of the calcium, as well as the spatial and temporal distribution of the signal (K. Samanta and Parekh 2017). Cells maintain a steep calcium gradient across the plasma membrane (PM), with 1-2.5 mM Ca^{2+} concentrations in the extracellular milieu (Guse, Gil Montoya, and B. P. Diercks 2021), and resting physiological cytosolic Ca^{2+} concentrations ranging from 50-100 nM (J. K. Foskett et al. 2007). Aside from the concentration gradient across the PM, cells also sequester high concentrations of calcium in the ER, which is the major source of intracellular calcium, the Golgi (Pinton, Pozzan, and Rizzuto 1998), lysosomes (H. Xu and Ren 2015), and nuclear envelope (Taufiq-Ur-Rahman et al. 2009). The ER lumen is estimated to contain around 1 mM Ca^{2+}. Much of this Ca^{2+} is bound to lumenal Ca^{2+}-binding proteins such as calsequestrin, calreticulin, GRP78, and GFP94 (Schwaller 2009). This limits the free Ca^{2+} concentration to a range between 100 and 700 μM (Alvarez and Montero 2002; Bassik et al. 2004; Bygrave and Benedetti 1996; Montero et al. 1995; Palmer et al. 2004; Pinton, Pozzan, and Rizzuto 1998; Verkhratsky 2005). The low cytosolic [Ca^{2+}] is maintained by a series of pumps, channels, and transporters in the plasma and ER membranes (Figure 1).

IP_3 is considered a global messenger. The calculated diffusion rate of IP_3 is approximately 280 $\frac{\mu M^2}{s}$ in cytoplasmic extracts and its estimated effective range is 25 μM (Allbritton, Meyer, and Stryer 1992). Although competing measurements using caged IP_3 suggest the messenger's effects are more localized, with an effective range of 5 μM due to a 30-fold slower diffusion rate (Dickinson et al. 2016). This lower diffusion rate is attributed to binding immobile IP_3Rs on the ER membrane, which diffuse at a rate of 0.1 $\frac{\mu M^2}{s}$ (I. F. Smith et al. 2014). IP_3Rs are one of two major Ca^{2+} release channels located on the ER membrane (J. K. Foskett et al. 2007), the other being the closely related ryanodine receptor family (RyR) (Hamilton 2005). Ca^{2+} release from acidic stores, such as the lysosome, is mediated by NAADP activation of two-pore channels (TPCs) (Morgan et al. 2011).

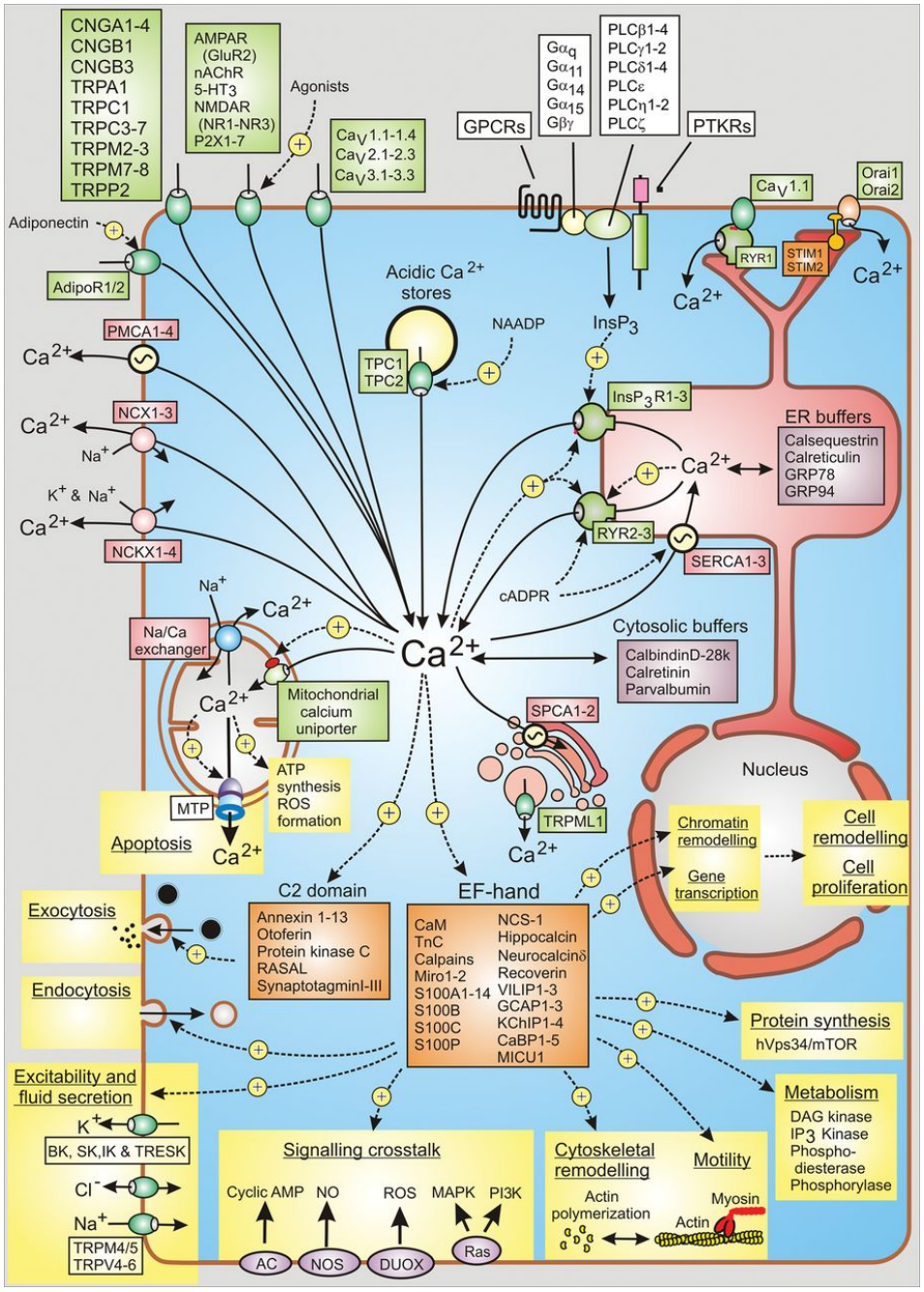

Figure 1: **A Sampling of Components in the Ca^{2+} signaling toolkit** Listed inside the green boxes are Ca^{2+} release channels, located either on the PM or ER, which when active promote Ca^{2+} entry into the cytosol. Listed inside the red boxes are the Ca^{2+} pumps and exchangers that either remove Ca^{2+} out of the cell or sequester the ion in the ER lumen. Listed in the purple boxes are the cytosolic and ER lumenal Ca^{2+} buffers. The orange and yellow boxes list the Ca^{2+} sensors, separated into either C2 or EF-hand domains, and effectors respectively. Image from (Berridge 2012).

There are voltage- and ligand-gated Ca^{2+} channels on the PM. They open upon changes in membrane potential or binding of ligands (such as neurotransmitters) allowing permeation of Ca^{2+} into the cytoplasm. Voltage-gated Ca^{2+} channels are involved in cardiac action potentials (Mesirca, Torrente, and Mangoni 2015), neurotransmitter release (Dolphin 2020), and muscle contraction (Catterall 2011). Ligand-gated Ca^{2+} channels are critical in synaptic transmission. For example, N-methyl-D-aspartate receptors (NMDARs) are a member of glutamate receptor family and their activation leads to Ca^{2+} uptake into neurons, leading to long term changes in the synaptic strength, a critical event in synaptic plasticity. Receptors from GPCR and RTK families couple extracellular signals, ranging from small molecules to peptides to proteins (Q. Zhou et al. 2019), to different phospholipase C (PLC) isoforms that generate inositol 1,4,5-trisphoshate (IP_3) by cleaving phosphatidylinositol 4,5-bisphosphate (PIP_2). On the PM, voltage-operated channels (VOPs), ligand-gated Ca^{2+} channels, Trp channels, and Orai mediate Ca^{2+} entry along its concentration gradient from the extracellular milieu. The exact mechanism of Ca^{2+} entry depends on cell type. The VOCs are divided into three families: CaV1 (L-type), CaV2 (N-, P/Q- and R-type) and CaV3 (T-type) (Berridge 2012), and are characteristically expressed in excitable cells where they are activated by membrane depolarization. The Trp channels are expressed on non-excitable cells and are divided into: TRPC, TRPV, TRPM, TRPN, and TRPA families (Venkatachalam and Montell 2007).

As the ER calcium store empties through the activity of P_3Rs and RyRs, store-operated calcium entry (SOCE) is triggered to replenish the loss. SOCE is believed to occur in most animal cells, and IP_3Rs were implicated in coupling ER calcium loss to capacitative Ca^{2+} entry from the extracellular milieu through Ca^{2+} channels on the PM (Irvine 1990). After decades of research, two proteins were identified as essential components of SOCE: stromal interaction molecule (STIM) and Orai (Murali Prakriya et al. 2006; Liou et al. 2005; Y. Zhou et al. 2010). STIM is the sensor of ER Ca^{2+} levels, and its two homologs STIM1 and STIM2 have different Ca^{2+} affinities and ability to activate Orai. STIM1 is thought to be the major ER Ca^{2+} sensor and mediator of SOCE, sensing Ca^{2+} in the range of 100–400 μM through a pair of lumenal EF-hand motifs (Gudlur et al. 2018). The role of STIM2 is more unclear, and is believed to act in a supporting role to promote STIM1 coupling with Orai (Ong et al. 2015). STIM is expressed almost solely in the ER membrane and has one

transmembrane helix anchoring the protein in the membrane, a C-terminal cytosolic region, and a N-terminal lumenal region which contains the ER sensor domains. The C-terminal cytosolic region contains a polybasic tail that enables STIM to interact with lipids on the inner leaflet of the PM and a CRAC-activation domain (CAD) through which STIM interacts with Orai. There are three Orai genes (Orai-1, -2, and -3) which can form homo or heterohexameric channels in the PM (Hou et al. 2012; Yen, Lokteva, and R. Lewis 2016), although the activity of each channel depends on the exact isoforms present (M. Prakriya and R. Lewis 2015). The STIM1-Orai interaction occurs at ER-PM junctions that are held apart at 10-20 nm apart by scaffolding proteins (Chang et al. 2013; Fernández-Busnadiego, Saheki, and De Camilli 2015; Giordano et al. 2013; Hogan 2015). Upon activation, Orai channels generate long lasting cell wide Ca^{2+} signals that drive cell proliferation (Deng et al. 2009), as well as local Ca^{2+} microdomains at the ER-PM junctions of 250 nM spanning 450 nm (B.-P. Diercks et al. 2018), allowing the ER to be refilled with Ca^{2+} via SERCA. SERCA is thought to be the major Ca^{2+} uptake pathway into the ER, using ATP hydrolysis to pump two Ca^{2+} ions per ATP hydrolyzed (Guerrero-Hernandez, Dagnino-Acosta, and Verkhratsky 2010). The connection between ER lumenal Ca^{2+} concentrations and capacitative calcium entry is a delicate balance, as some Ca^{2+} is required in the ER lumen to ensure proper protein folding (Lodish, Kong, and Wikström 1992).

In the cytosol, Ca^{2+} diffusion is sharply limited by the existence of Ca^{2+} buffers and sensors (Figure 1), dropping off sharply with distance when compared to simple diffusion (Shimomura, F. H. Johnson, and Saiga 1962). Ca^{2+}-binding proteins such as parvalbumin, calbindin D-28k, and calretinin, soak up elevated Ca^{2+} concentrations as Ca^{2+} buffers (Schwaller 2009). In addition to the presence of the cytosolic Ca^{2+} buffers, Ca^{2+} sensors bind to Ca^{2+} through Ca^{2+} binding domains to propagate the second messenger signal. The first type of Ca^{2+} binding site identified was the EF-hand domain, comprised of a helix-turn-helix motif (Kretsinger and Nockolds 1973). Ca^{2+} binding sites were subsequently described as being either continuous or noncontinuous sequences, and either EF-hand or non-EF-hand type (Kirberger and J. J. Yang 2013). Over the decades, Ca^{2+} binding sites have been further classified into three major classes (Pidcock and G. R. Moore 2001; McPhalen, Strynadka, and James 1991). Class I sites consist of a continuous stretch of amino acids in the protein's primary sequence. Examples of class I Ca^{2+}-binding sites include: calmod-

ulin (a canonical EF-hand domain), calpain (a non-canonical EF-hand domain), and S100 proteins (pseudo-EF-hand domains). Class II binding sites combine a continuous amino acid sequence with a coordinating ligand from a separate part of the sequence, for example, copper amide oxidase (Parsons et al. 1995). Class III binding sites are the least common of the three, with multiple sequences from different regions of the primary amino acid sequence coming together in the tertiary structure to form the binding site as in the C2 domain of protein kinase C (PKC) (Kohout et al. 2002) or the binding site in adamalysin (Gomis-Rüth, Kress, and Bode 1993). Ca^{2+} can either directly or indirectly influence cellular processes by stimulating downstream signaling pathways. For example, Ca^{2+} can bind to synaptotagmins to directly influence exocytosis and troponin C can directly stimulate the interaction between actin and myosin in contracting myocytes (Xue et al. 2021; Korte et al. 2012). Ca^{2+} also works to both directly sensitize the Na^{+}, K^{+}, and Cl^{-} channels that regulate cell excitability and secretion and to indirectly influence their behaviour through calmodulin (Ambudkar 2014; Gamper and Shapiro 2003). Ca^{2+} indirectly works to influence other cellular processes by recruiting Ca^{2+} sensitive enzymes, such as the Ca^{2+}/calmodulin-dependent protein kinase class of enzymes (CamK) (Dupont, Houart, and De Koninck 2003), Myosin light-chain kinase (MLCK) (Tansey et al. 1994), and phosphorylase kinase (Cohen et al. 1980). Ca^{2+} can regulate long term cellular processes such as transcription and chromatin remodeling. Oscillating Ca^{2+} signals activate transcription factors (Dolmetsch, K. Xu, and R. S. Lewis 1998), with the frequency of the Ca^{2+} oscillations critical for activation of NFAT and NF-KB dependent transcription (W. Li et al. 1998).

Ca^{2+} signaling through the numerous Ca^{2+} effectors, buffers, channels, and pumps is thus both incredibly complex and critical for the cell's internal signaling. Ca^{2+} as an ion, is a more multi-purpose ion than its close relatives (Na^{+}, K^{+}, and Mg^{2+}) due in large part to Ca^{2+} ions' flexible binding geometries, which enables binding to a larger range of protein binding sites (Fedrizzi, Lim, and Ernesto Carafoli 2008). Ca^{2+} can act as both a first and second messenger, and can be regulated by controlling the transcription and translation of components of the Ca^{2+} signaling toolkit. While Ca^{2+} is critical for cell survival, if the Ca^{2+} signal is not carefully controlled and decoded properly into the correct cellular response, the resulting Ca^{2+} signaling dysfunction may ultimately contribute to the pathogenesis of a number of conditions.

5.1.1 Calcium signalling at ER-mitochondrial contact sites

Intracellular calcium signals are a critical component in regulating a multitude of cellular processes. Calcium signals are precisely and spatiotemporaly controlled by components of the cell's Ca^{2+} signaling toolbox, which includes Ca^{2+} binding proteins, channels, pumps, and buffers. These Ca^{2+} signaling components are localized mostly to the cytosol, ER, PM, and mitochondria (Berridge, Lipp, and Bootman 2000). While the importance of the ER as the cell's major intracellular calcium store had been accepted since the 1970s, the role of the mitochondria in calcium signaling took longer to elucidate. Mitochondria were known to uptake Ca^{2+}, but the precise mechanism and physiological role of this activity was unknown (DeLuca and Engstrom 1961; Frank D. Vasington and Murphy 1962). Experimental evidence on isolated mitochondria suggested a low-affinity uptake mechanism driven by the electron transport chain and ATP hydrolysis, leading to the tentative conclusion that mitochondria only uptake calcium in pathophysiological conditions of substantially elevated cytosolic calcium levels (Ernesto Carafoli 2003; Rosario Rizzuto, Duchen, and Tullio Pozzan 2004). The energetic basis of Ca^{2+} uptake by the mitochondria remained enigmatic until the chemiosmotic hypothesis was detailed in 1967 (Mitchell and Moyle 1967). Ca^{2+} uptake by pumps or transporters was ruled out in favor of a uniporter complex that would allow Ca^{2+} to enter the matrix by moving down its electrochemical potential gradient (Nicholls and Crompton 1980), although the identify of the mitochondrial calcium uniporter (MCU) would not be confirmed until years later (Baughman et al. 2011). In the 1990s, mitochondria were shown to uptake calcium in physiological conditions by showing that Ca^{2+} signals originating from IP_3Rs could enter the mitochondrial matrix using matrix-targeted aequorin (Rosario Rizzuto, Brini, et al. 1993). Calcium concentrations, originating from IP_3Rs, at these microdomains between the ER and mitochondria can reach upwards of 16 μM (Csordás, A. P. Thomas, and Hajnóczky 1999), allowing the low-affinity MCU to import Ca^{2+} into the matrix (Figure 2). In the matrix, Ca^{2+} binds to α-ketoglutaric dehydrogenase and NAD^+-isocitric dehydrogenase in the citric acid cycle and to the phosphatase that dephosphorytates pyruvate-dehydrogenase (McCormack, Halestrap, and Denton 1990). As such, maintenance of physiological matrix Ca^{2+} levels is critical for TCA cycle function, specifically the production of reducing compounds to the electron transport chain and to the synthesis of ATP.

If matrix calcium levels were solely determined on thermodynamic principles, matrix calcium levels would be about a million-fold higher than levels in the cytosol (Rosario Rizzuto, Duchen, and Tullio Pozzan 2004). The existence of the low-affinity MCU and of Ca^{2+} antiporters in the IMM prevent this scenario. The existence of Ca^{2+} efflux mechanisms in the IMM was first determined in experiments using Ruthinium Red or La^{3+}, which blocked Ca^{2+} influx through the MCU and monitoring the gradual release of the accumulated Ca^{2+} (C. S. Rossi, F. D. Vasington, and E. Carafoli 1973; T. Pozzan and Azzone 1976). The Ca^{2+} efflux mechanism was then discovered to be mediated by either Na^+ or H^+ antiporters (Nicholls and Crompton 1980). In the 1970s, the Na^+/Ca^{2+} and the H^+/Ca^{2+} exchangers were characterized (Ernesto Carafoli 2003). In contrast to the Na^+/Ca^{2+} exchanger on the PM, NCX, the mitochondrial $Na^+/Ca^{2+}/Li^+$ exchanger (NCLX) is able to substitue Li^+ for Na^+ to drive Ca^{2+} efflux. This characteristic of the mitochondrial NCLX allowed for its identification and cloning (Palty et al. 2010). Whether NCLX Na^+/Ca^{2+} exchange was electrogenic or electroneutral was debated, with experimental evidence initially supporting an electroneutral 2 Na^+/Ca^{2+} (Affolter and E. Carafoli 1980; Brand 1985b; Brand 1985a), and an electrogenic 3-4 Na^+/Ca^{2+} exchange (Jung, Baysal, and Brierley 1995; Kim and Matsuoka 2008; Dash and Beard 2008). The most recent evidence supports an electrogenic 3 Na^+/Ca^{2+} exchange mode for NCLX. The H^+/Ca^{2+} exchanger was identified as Leucine zipper/EF-hand-containing transmembrane protein 1 (Letm1), a contributor to the neuromuscular features of Wolf-Hirschhorn syndrome (McQuibban et al. 2010; South, Bleyl, and Carey 2007; Zollino et al. 2003). Letm1 can work bidirectionally, exchanging matrix H^+ for Ca^{2+} to extrude Ca^{2+} during elevated Ca^{2+} events alongside NCLX (Santo-Domingo and Demaurex 2010). Experimental evidence shows Letm1 exchange is electroneutral, extruding 1 Ca^{2+} for two H^+ (Tsai et al. 2014). In addition to the Ca^{2+} efflux transporters, Ca^{2+} in the matrix can be buffered by inorganic phosphate (Ernesto Carafoli and Roman 1980).

While Ca^{2+} transport across the IMM is complex, involving multiple exchangers and the MCU, Ca^{2+} movement through the outer mitochondrial membrane (OMM) occurs primarily through the voltage-dependent anion channel (VDAC) (Gincel, Zaid, and Shoshan-Barmatz 2001) (Figure 2). In humans, there are three VDAC isoforms, with VDAC1 being the most abundantly expressed in most cell types. X-ray crystallography and NMR studies show VDAC is a β-barrel with a pore

diameter of 1.5 nm (Varda Shoshan-Barmatz et al. 2010). While VDAC was originally considered an inert pore (Colombini 1979), allowing all substrates 5 kDa or below free access to the intermitochondrial space (IMS), current research describes multiple pore states. An open state with a pore diameter of approximately 3 nm that allows unencumbered transport of ATP, metabolites, and anions into the IMS. A closed state with a pore diameter of approximately 1.8 nm is impermeable to ATP, but shows a preference for cations (Colombini 2009). VDAC1 also plays a role in mediating Ca^{2+} transfer to the mitochondria, forming a interaction with IP_3R via glucose-regulated protein 75 (grp75) (Szabadkai et al. 2006), also known as mortalin or mthsp70 (Wadhwa, Taira, and Kaul 2002; Kaul, Deocaris, and Wadhwa 2007). IP_3R-3 has been shown to be the predominant isoform present at ER-mitochondrial contact sites and is the major isoform responsible for Ca^{2+} transfer to the mitochondria (Mendes et al. 2005).

IP_3R-mediated Ca^{2+} transfer to the mitochondria is precisely controlled as matrix Ca^{2+} overload leads to the initiation of apoptosis (Figure 3), and impaired Ca^{2+} transfer leads to an autophagic response to restore cell bioenergetics (Figure 4). When matrix Ca^{2+} is high, the permeability transition pore (PTP) forms in the IMM (Rasola and Bernardi 2007; Azzolin et al. 2010). Once formed, the PTP has a pore diameter of approximately 3 nm, allowing for the rapid release of ions and metabolites from the matrix into the IMS. This destroys the membrane potential across the IMM, which normally stands at -180 mV with the build up of positive charge on the IMS side (A. L. Moore and Bonner 1982). The IMM is remodeled as the matrix swells due to osmotic forces and the OMM ruptures at the end, releasing cytochrome c into the cytosol (Rasola, Sciacovelli, et al. 2010). In addition to the release of cytochrome c, other pro-apoptotic factors Smac/Diablo, HtrA2/Omi and endonuclease G are released from the IMS (Tait and Green 2010). The host of pro-apoptotic factors then activate executioner caspases 3 and 7, leading to apoptosis where the cell undergoes chromosome condensation, cytoplasm shrinkage, DNA fragmentation, and membrane blebbing (He, N. Lu, and Z. Zhou 2009; Elmore 2007). After the Ca^{2+} signal from IP_3R terminates, the PTP can close so that ATP production can facilitate the latter stages of apoptosis (Szalai, Krishnamurthy, and Hajnóczky 1999). Once the PTP opens cell death is eminent (Kroemer, Galluzzi, and Brenner 2007), although the cell can choose to undergo necrosis instead of apoptosis (Armstrong 2006). IP_3Rs are critical for initiating the high Ca^{2+} matrix load required

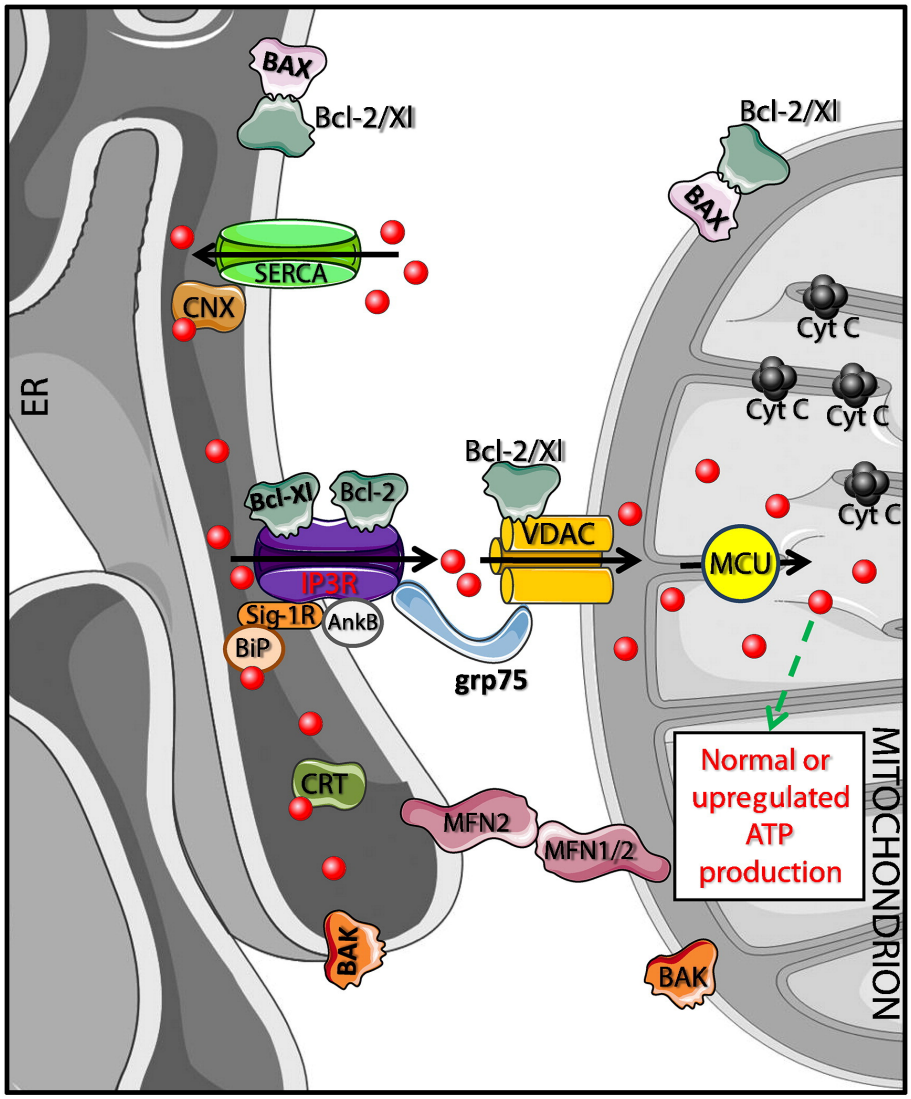

Figure 2: **IP_3R-mediated Ca^{2+} from the ER lumen to the mitochondria.** IP_3R-mediated Ca^{2+} transfer to the mitochondria during homeostasis. Physical interaction between IP_3R on the ER membrane and VDAC on the outer mitochondrial membrane via grp75 promotes mitochondrial Ca^{2+} (red circles) uptake upon IP_3R activation. The transferred Ca^{2+} ions are critical for cell bioenergetics by their regulation of ATP production, via their binding to dehydrogenases in the citric acid cycle. The thick black arrows show movement of the Ca^{2+} ions, dashed green arrows indicate the physiological result of the Ca^{2+} transfer. Image from (Decuypere et al. 2011).

for apoptosis initiation. This matrix Ca^{2+} overload, in the context of IP_3R dysregulation, is seen in cardiac ischemia–reperfusion injury (Giorgi, Romagnoli, et al. 2008), polio infection (Brisac et al. 2010), and in neurodenerative diseases such as amyloid lateral schlerosis (Martorana et al. 2012).

The link between IP_3Rs and autophagy has only recently been fleshed out. Under normal, physiological conditions, autophagy is used by the cell to transfer long-lasting proteins, damaged organelles, and foreign particles to the lysosome for degradation (Yim and Mizushima 2020). Under conditions of nutrient deprivation, cells utilize autophagy to disassemble these materials to meet immediate energy requirements, thus providing the cell with a pro-survival mechanism for stressful situations (Klionsky 2007). Although autophagy can promote cell survival in the short term, long-term reliance on autophagy can still ultimately lead to cell death if the underlying causes of autophagy fail to be resolved (Kroemer and Levine 2008). Initially the role of IP_3Rs in autophagy was unclear. Some studies reported that an increase in cytosolic Ca^{2+}, caused by either inhibition of SERCA with thapsigargin or GPCR/RTK stimulation with agonists, triggered autophagy (Høyer-Hansen et al. 2007; Grotemeier et al. 2010). Other studies reported that autophagy was initiated by inhibition of IP_3Rs (Criollo et al. 2007; Khan and Suresh K. Joseph 2010), blockage of L-type Ca^{2+} channels (A. Williams et al. 2008), and reduction of IP_3 levels in the cytoplasm (Sarkar et al. 2005). This contradiction was explained in part in 2010, where it was shown that there is a basal IP_3R activity required for controlling mitochondrial bioenergetics through Ca^{2+} binding to dehydrogenases in the TCA cycle (Cárdenas et al. 2010). By either inhibiting IP_3R, or downregulating its translation, the Ca^{2+} transfer to the mitochondria is lessened, leading to impaired ATP production through oxidative phosphorylation. As the AMP/ATP ratio increases, autophagy is initiated via the AMP-activated protein kinase (AMPK) pathway (Figure 4). IP_3Rs may provide a scaffold, on which binding proteins compete to initate either apoptosis or autophagy. In particular, when both Beclin-1 and Bcl2 bind hP_3R, the close proximity of the two proteins results in an anti-apoptotic interaction (Vicencio et al. 2009). In one experiment, inhibition of IP_3R with Xestospongin-B resulted in the dissociation of Beclin-1 from IP_3R, resulting in autophagy (Cárdenas et al. 2010). The exact role of IP_3R scaffold proteins and of post-translational modifications on autophagy initiation still requires further investigation.

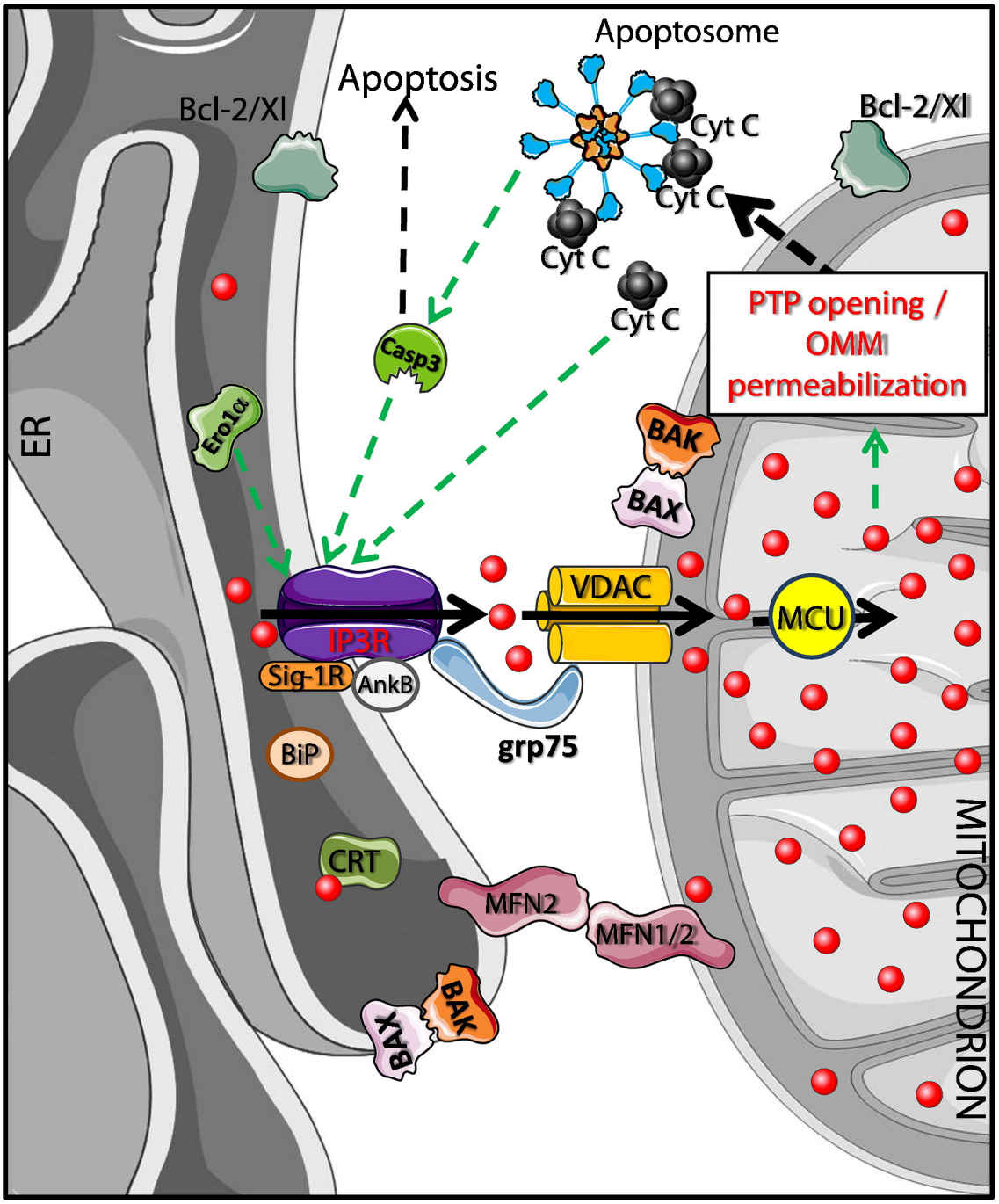

Figure 3: **IP$_3$R-mediated Ca^{2+} from the ER lumen to the mitochondria during apoptosis.** An increase in IP3R-mediated transfer of Ca^{2+} ions from the ER lumen towards the mitochondria triggers the initiation of apoptosis. Mitochondrial matrix Ca^{2+} overload leads to both the formation and opening of the permeability transition pore (PTP), which leads to the permeabilization of both the IMM and OMM, and the consequent elimination of the potential across the IMM. This leads to the release of several apoptogenic factors in the IMS, including cytochrome C (Cyt C), which culminates with the activation of caspase-3 (Casp3). This pathway then further promotes caspase activation and apoptosis. The increased width of the black arrows indicate the increased strength of the Ca^{2+} transfer. Image from (Decuypere et al. 2011).

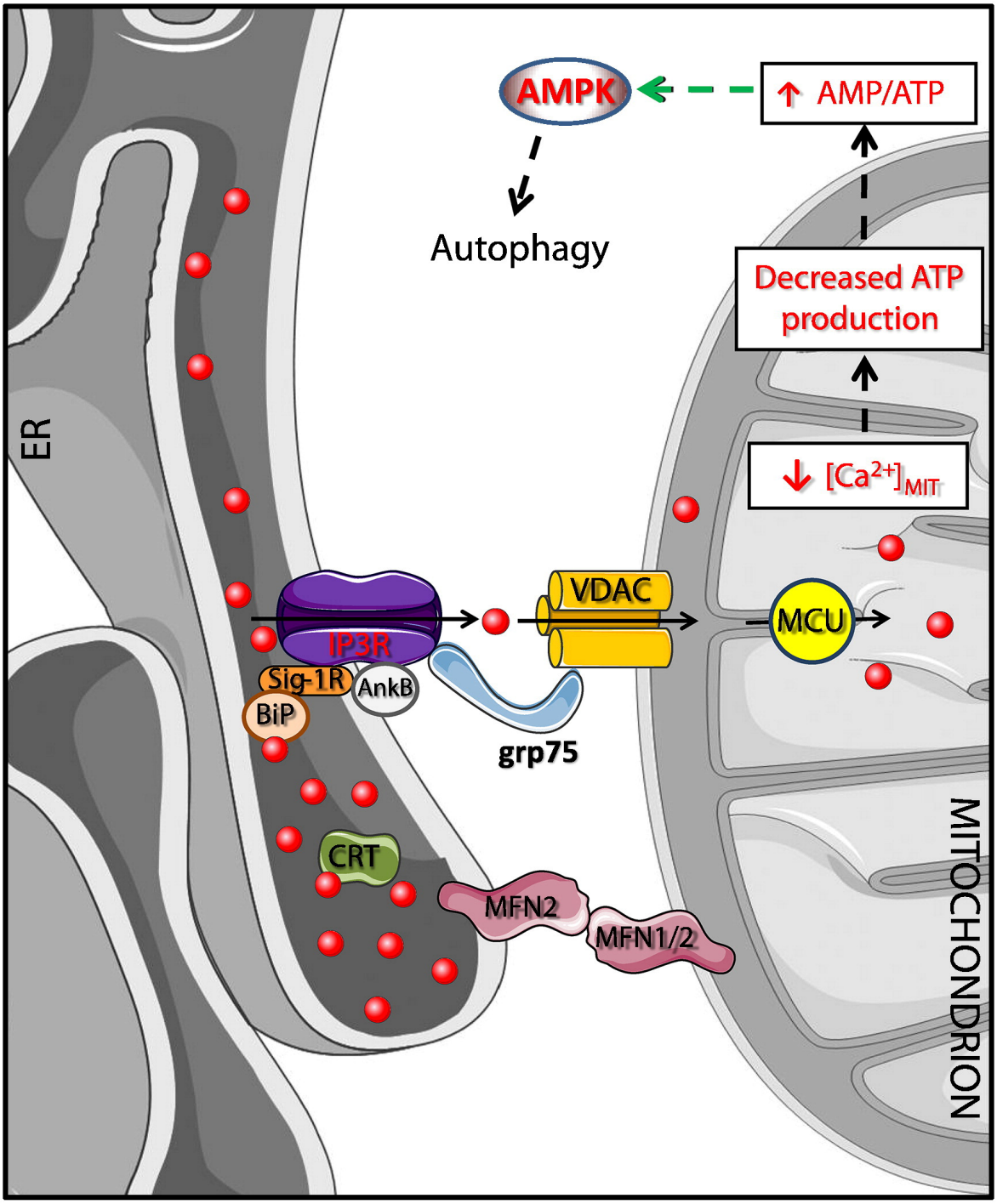

Figure 4: **IP_3R-mediated Ca^{2+} from the ER lumen to the mitochondria during autophagy.** A decrease in the IP_3R-mediated Ca^{2+} transfer from the ER lumen to the mitochondria triggers the initiation of autophagy. In situations where IP_3R activity is impaired, Ca^{2+} transfer from the ER to the mitochondria is staunchly decreased. This leads to a decrease in ATP production, which results in an increase in the cytosolic AMP/ATP ratio, leading to activation of the AMPK (AMP-activated protein kinase) pathway and ultimately autophagy. The decreased width of the black arrow indicates the weakened strength of the Ca^{2+} transfer. Image from (Decuypere et al. 2011).

5.1.2 IP_3Rs

IP_3Rs are one of the two major intracellular, ligand-gated Ca^{2+}-release channels located primarily on the ER or sarcoplasmic reticulum (SR), the other being the closely related RyRs. IP_3Rs are ubiquitously expressed in all eukaryotes and have been for the past 800 million years since the divergence from the last common invertebrate ancestor gene version, (Figure 5), (Alzayady, Sebé-Pedrós, et al. 2015). Notably, the unicellular *C. owczarzaki* IP_3R-A bears remarkable similarity to mammalian IP_3Rs, responding to IP_3 and exhibiting familiar Ca^{2+}-release activity. This indicates the *C. owczarzaki* IP_3R-A gene provides a good model of an ancestral IP_3R from which all modern vertebrate versions descend from. Although IP_3Rs are ubiquitous across most of Eukarya, being found from Drosophila (Hasan and Rosbash 1992) to humans, evidence for their presence in plant cells is debatable (Krinke et al. 2006), and there is less information available on the role of IP_3Rs in unicellular organisms (I. Bezprozvanny 2005; D. Zhang et al. 2007).

In mammals, there are three isoforms that share approximately 70% amino acid sequence identity, with higher sequence similarity at the more conserved regions at the IP_3-binding site and in the ion-conduction pathway in the transmembrane domain. Each isoform differs in its affinity for IP_3, Ca^{2+} release properties, response to regulatory molecules and proteins, and tissue distribution (Figure 6). Type-1 IP_3R (IP_3R-1) is the predominant isoform in Purkinje cells, which is why IP_3R was historically purified from cerebella. Type-2 IP_3R (IP_3R-2) is the predominant isoform in cardiac muscle tissue, while type-3 IP_3R (IP_3R-3) dominates in many cultured cell lines such as HEK, HeLa, and HBE (H. De Smedt et al. 1994; De Smedt et al. 1997; Richard J. H. Wojcikiewicz 1995). IP_3Rs can either exist as homo- or heterotetramers, with additional diversity arising from the splice variants of IP_3R-1 (C.W. Taylor, Genazzani, and S. Morris 1999) or from post-translational modifications such as phosphorylation (Jayaraman et al. 1996; R. J. Wojcikiewicz and S. G. Luo 1998; T.-S. Tang et al. 2003) or N-linked glycosylation (Michikawa et al. 1999). Each subunit is comprised of approximately 2700 residues, resulting in a tetramer mass close to 1.2 MDa. The large cytosolic domain represents 89 % of the protein's mass and includes both the N- and C-termini, while the transmembrane domain represents the remaining 11 % of the mass, with a minimal number of residues accessible from the ER lumen (S. Ludtke et al. 2011). IP_3R can be divided into five func-

tional domains: the suppressor domain (IP_3R-1: 1-225), the IP_3-binding core (IP_3R-1: 226-578), the central modulatory domain (IP_3R-1: 579-2275), the transmembrane domain (IP_3R-1: 2276-2589), and the C-terminal tail (IP_3R-1: 2590-2749) (Keiko Uchida et al. 2003). Cryo-EM studies of IP_3R-1 showed that the protein is composed of nine distinct domains: the suppressor domain (SD) comprising a beta-trefoil fold (residues 1-229), a second beta-trefoil domain comprising the β half of the IP_3-binding core (IBC) (residues 230-435), a solenoid armadillo domain comprising the half of the IBC and extending into the central modulatory domain (residues 436-788), two additional solenoid armadillo domains (residues 1101-1587, and 1717-2121 respectively) that are separated by the central lateral domain (CLD), the juxtamembrane domain that lays almost parallel to the ER membrane (residues 2122-2191 and 2538-2611), the transmembrane domain comprising six alpha helices (2273-2600), and a C-terminal tail that forms a coiled-coil (residues 2681-2731) (Fan, M. L. Baker, et al. 2015).

There is consensus among different groups that IP_3R-2 has the highest affinity to IP_3, followed by IP_3R-1, then IP_3R-3 (C. Taylor and Tovey 2010; Iwai, Michikawa, et al. 2007; Tu, Zhengnan Wang, Nosyreva, et al. 2005), although some older studies reported IP_3R-1 having the highest IP_3 affinity with a K_d of 1 nM, compared with 2 nM for IP_3R-2, and 40 nM for IP_3R-3 (Richard J. H. Wojcikiewicz and Su Ge Luo 1998). The different conclusions may likely have been the result of differences in the purification techniques with studies that used purified, recombinant IP_3R converging to the above IP_3 affinity schema and studies using receptor purified from native tissue sometimes reporting diverging results, likely due to the presence of heterotetramers in the sample. This difference in IP_3 binding affinity is believed to result from isoform specific differences in the SD. The IP_3R-1 SD was determined to reduce the IP_3 affinity to the receptor by 10 fold compared to a truncated construct lacking the SD, and removing the IP_3R-3 SD increased IP_3 binding affinity (Szlufcik et al. 2006). A study a year later quantified these finding in IP_3R-2 and IP_3R-3, showing that SD truncated N-terminal domain constructs had indistinguishable IP_3 affinities of approximately 2 nM (Iwai, Michikawa, et al. 2007). This same study reported specific residues in the flexible loop regions between beta strands in the IP_3R-3 SD that are responsible for the relatively low IP_3 affinity compared with the other isoforms: E39, A41, D46, M127, A154, T155, L162, W168, N173, N176, and V179 (Figure 7).

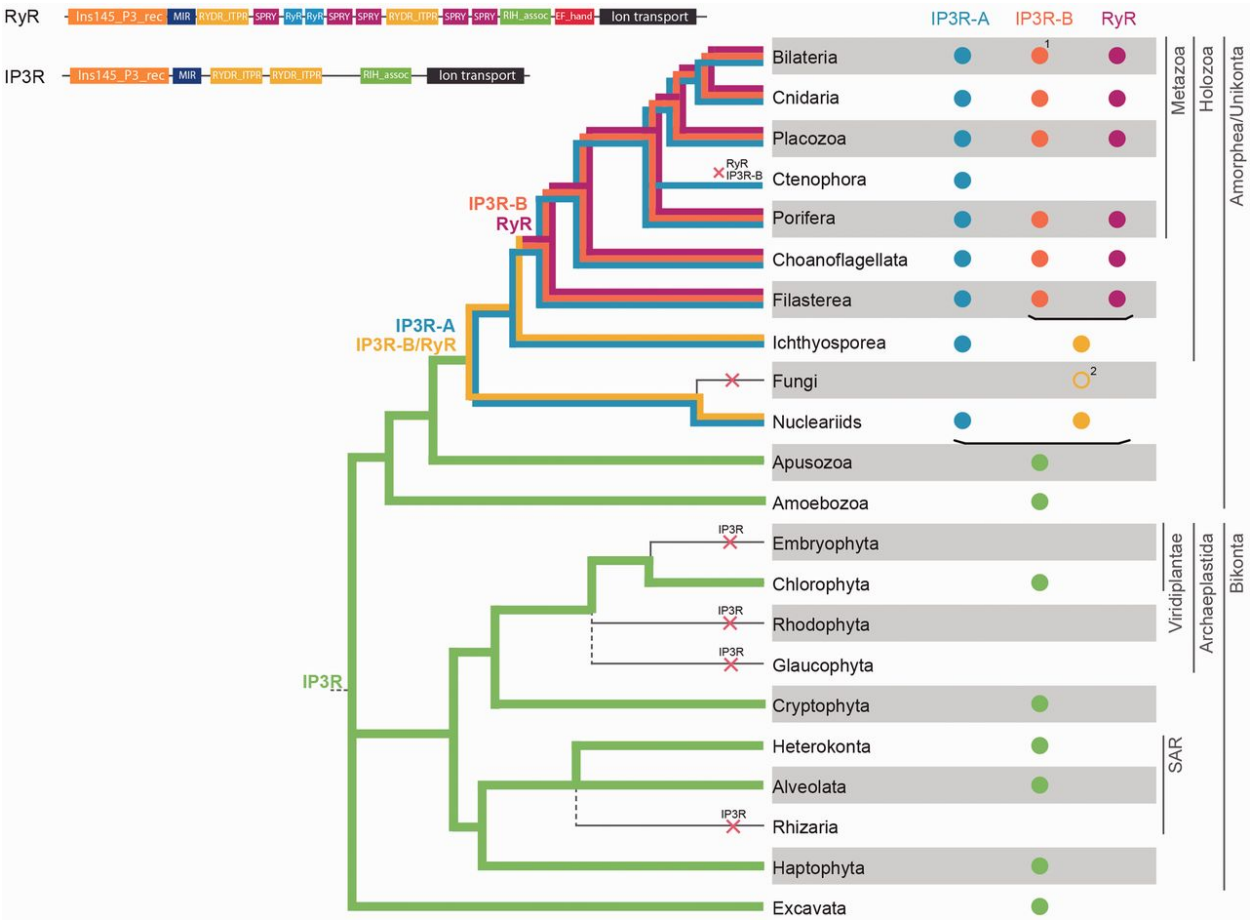

Figure 5: **Phylogenetic tree of both IP$_3$R and RyR.** The colored lines represent the origins and further genetic divergence into related paralog families of the ancestral IP$_3$R gene (green), the ancestral IP$_3$R-B/Ryr gene (orange), IP$_3$R-A (blue), IP$_3$R-B (dark orange), and RyR (magenta). Red crosses show multiple lineage independent losses of IP$_3$R-A. In the upper left are the linearized domain representations of consensus IP$_3$R and Ryr across multiple branches. The phylogenetic tree represents an eukaryotic consensus of the following studies (Derelle and Lang 2012; He, et al. 2014). Image from (Alzayady, Sebé-Pedrós, et al. 2015).

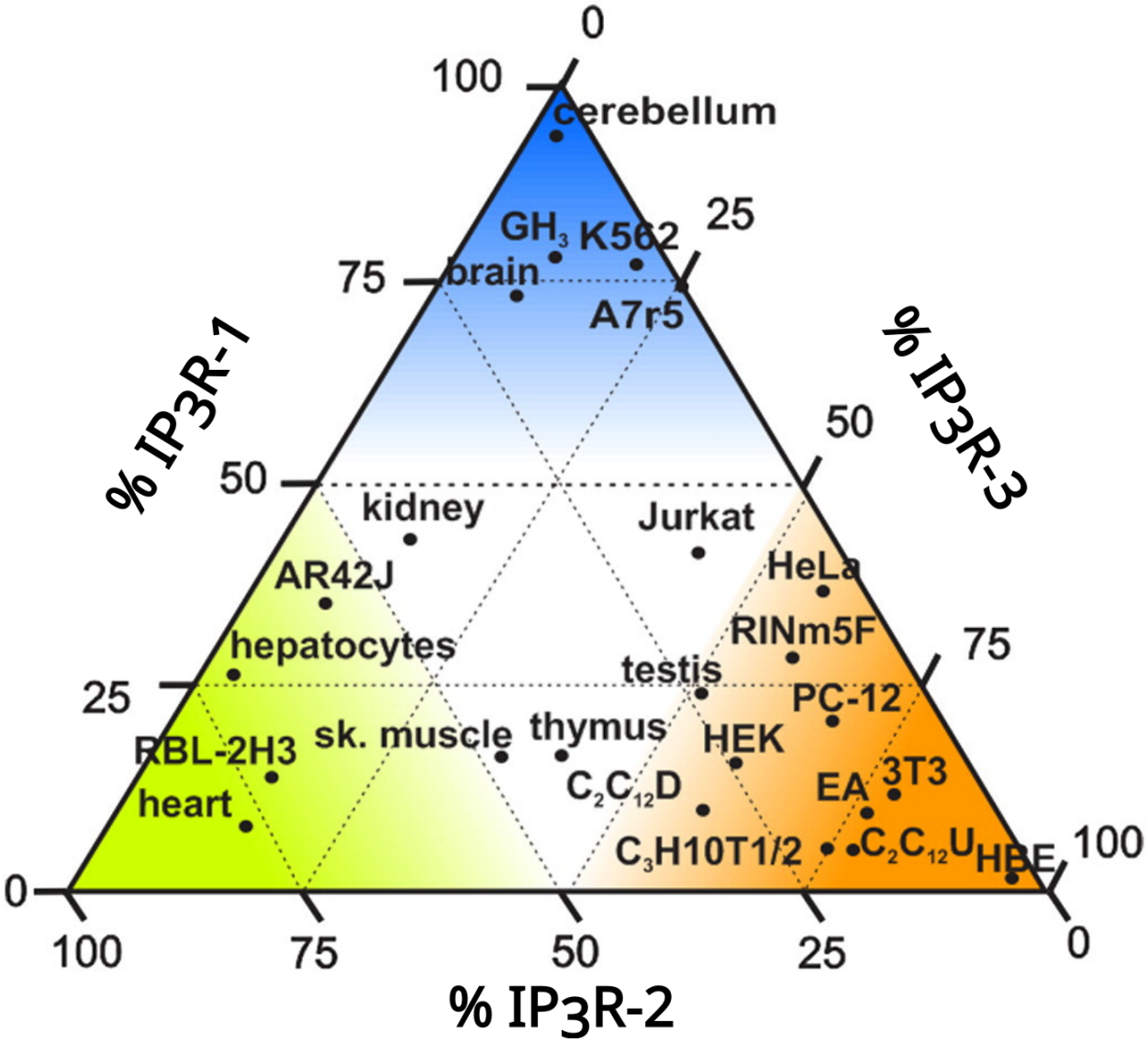

Figure 6: **A triangle-diagram representation of the mRNA expression levels of IP_3R isoforms across multiple cell lines and tissues.** The majority of cells express more than one IP_3R isoform. IP3R-1 is predominantly expressed in the cerebellum and in neurons, IP3R-2 in the liver, and IP3R-3 in many common laboratory cell lines. Levels of mRNA, measured from RT-PCR using the methods described in (H. De Smedt et al. 1994; De Smedt et al. 1997), were compared with protein level measurements done using isoform specific antibodies (Richard J. H. Wojcikiewicz 1995). The numerical values on the triangle's sides represent the percentage of each isoform in each listed cell type. Image adapted from (Ivanova et al. 2014).

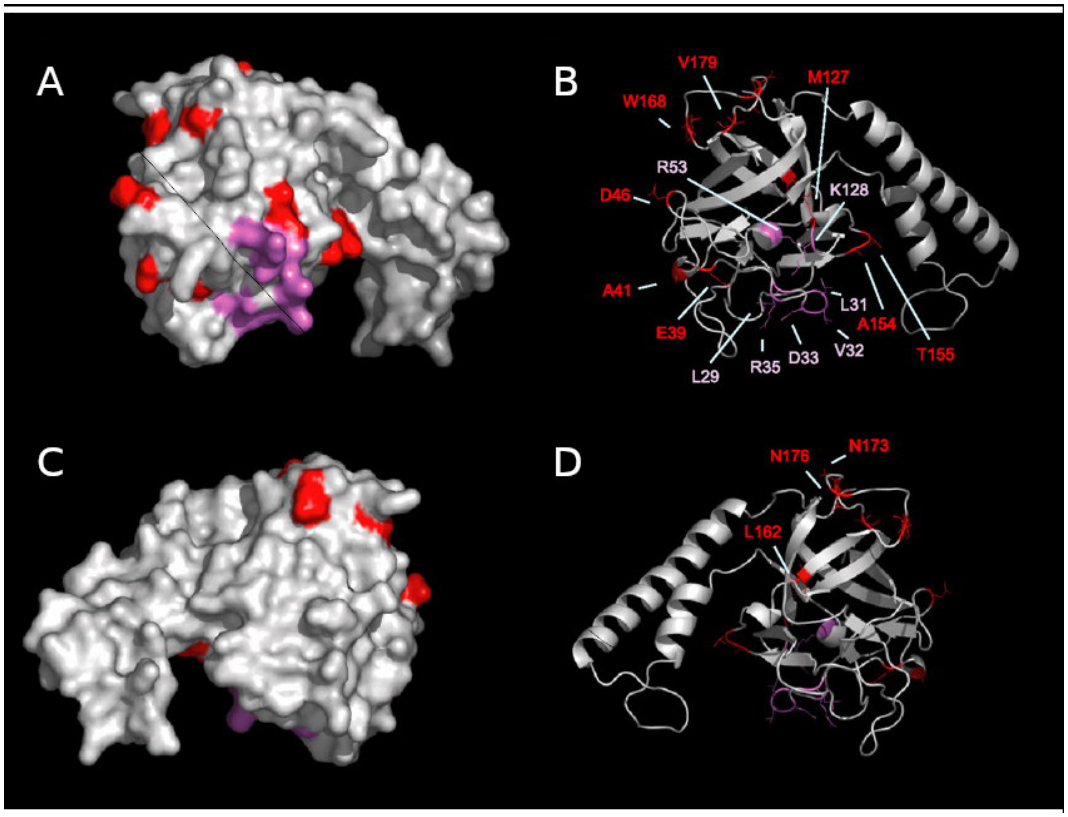

Figure 7: **3D representations of important residues for suppression of IP_3 binding.** Mouse IP_3R-3 suppressor domain shown in surface diagrams (A and C) and in ribbon diagrams (B and D). In red are the important amino acid residues in the SD that are critical for the IP_3R-3 specific binding suppression. In pink are conserved residues critical for binding suppression in all isoforms (Bosanac, Yamazaki, et al. 2005). Panel A is rotated by 180° in C. B is also rotated by 180° in D. Image adapted from (Iwai, Michikawa, et al. 2007).

Initially, the number of bound IP_3 molecules required to promote receptor gating and Ca^{2+} flux was unknown (Alzayady, L. Wang, et al. 2016). Reports conflicted over whether IP_3 binding was positively cooperative, where the binding of IP_3 to one subunit would promote IP_3 binding to additional subunits (Marchant and C. W. Taylor 1997; Meyer, Holowka, and Stryer 1988), or if IP_3 molecules bound in an agnostic manner (Iwai, Tateishi, et al. 2005; Iwai, Michikawa, et al. 2007). Some reports suggested that three IP_3s bound to the tetramer were sufficient to promote activation (Marchant and C. W. Taylor 1997; Dufour, Arias, and T. Turner 1997), while another report using IP_3Rs with only two intact binding sites reported that two bound IP_3s were sufficient (Boehning and S. K. Joseph 2000). A quantitative study from 2016, where the amount of functional binding sites was controlled using concatenated receptors definitively showed that all four IP_3 binding sites

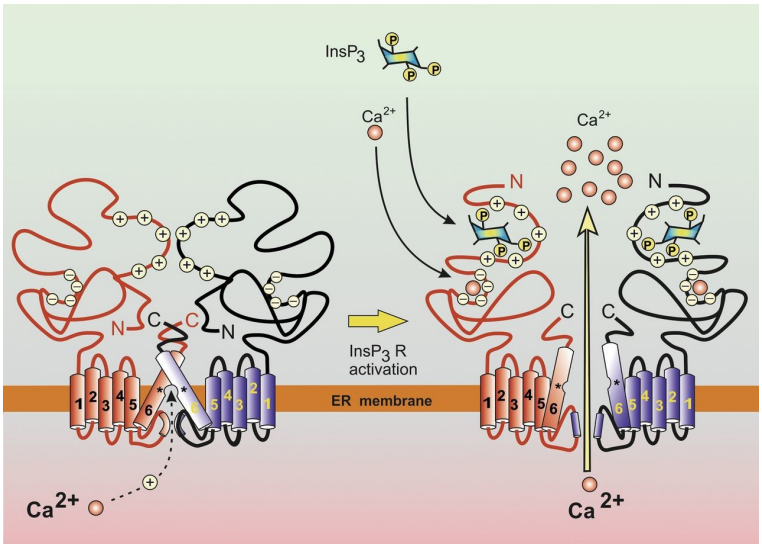

Figure 8: **IP_3R activation by its co-agonists.** IP_3R is a tetramer. Here, two subunits are shown for clarity. The transmembrane domain consists of six helices, with TMD6 the pore lining helix. The selectivity filter and pore loop are located on the ER lumenal loop between TMD5 and TMD6. The large N-terminal cytoplasmic region contains the IP_3 and Ca^{2+} binding sites. Upon both ligands binding, a conformation change is propogated down the large central modulatory domain towards the pore to allow Ca^{2+} to pass through the pore. This cartoon depiction was drawn based on the information in (C. Taylor, Fonseca, and E. Morris 2004). Image from (Berridge 2016).

need to be occupied to promote IP_3R-mediated Calcium flux (Alzayady, L. Wang, et al. 2016). This conclusion was further supported with an ensemble of IP_3R-3 pre-active cryo-EM structures, showing IP_3 binding promotes the independent transition of each subunit from a looser to a more compact state as the tetramer proceeds towards activation (Paknejad and Hite 2018).

In addition to IP_3, Ca^{2+} is required as an essential co-agonist for IP_3R activation (Figure 8). In patch-clamp experiments, the receptor's open probability in saturating IP_3 conditions is low in 50 nM $[Ca^{2+}]$, which is within the normal $[Ca^{2+}]$ cytosolic concentration range (J. Kevin Foskett and Mak 2010). As the $[Ca^{2+}]$ is raised through the nanomolar range towards 1 μM, the IP_3R open probability reaches to a maximum of approximately 80%. Using a different electrophysiology method, nuclear patch-clamp, IP_3R activity increases towards maximal open probability, maintaining this probability over a broader micromolar range of $[Ca^{2+}]$ before activity starts to decrease at 10 µM $[Ca^{2+}]$, demonstrating the characteristic biphasic regulation by Ca^{2+} that is tightly linked to receptor function. Even though all three isoforms demonstrate the same broad-shaped activity curves over increasing $[Ca^{2+}]$, differences exist. IP_3R-1 activity has been determined to

demonstrate positive Ca^{2+} cooperativity (Hirota et al. 1995), which would enable IP_3R-1 to rapidly activate and reach maximum open probability through calcium-induced-calcium-release (CICR). In contrast, IP_3R-3 does not demonstrate cooperativity, instead increasing the open probability over a broader range of $[Ca^{2+}]$, allowing the receptor to activate in response to low IP_3 concentrations. The properties of the bell-shaped IP_3R activity curve appears to depend on the IP_3 concentration used. IP_3Rs under saturating IP_3 conditions deactivate quickly in high $[Ca^{2+}]$, producing narrow curves (Marchenko et al. 2005; Ramos-Franco, Caenepeel, et al. 1998; Ramos-Franco, Fill, and G A Mignery 1998; Striggow and B. E. Ehrlich 1996; Tu, Tomoya Miyakawa, et al. 2002; Tu, Nosyreva, et al. 2003; Tu, Zhengnan Wang, and I. Bezprozvanny 2005), or fail to respond to Ca^{2+} inhibition in some cases (Hagar et al. 1998; Mak, S. M. McBride, et al. 2003; Ramos-Franco, D. Bare, et al. 2000; Ramos-Franco, Fill, and G A Mignery 1998). The biphasic calcium dependency can be modeled with a biphasic hill equation (J. Kevin Foskett and Mak 2010):

$$P_o = P_{hill}\left(1 + \left(\frac{K_{act}}{[Ca^{2+}]_i}\right)^{H_{act}}\right)^{-1}\left(1 + \left(\frac{[Ca^{2+}]_i}{K_{inh}}\right)^{H_{inh}}\right)^{-1} \quad (1)$$

where P_{hill} is the maximum open probability the IP_3Rs can reach if there was no Ca^{2+} inhibition, K_{act} is EC_{50} for Ca^{2+}, K_{inh} is the IC_{50} for Ca^{2+}, H_{act} is the level of Ca^{2+} cooperativity in activation, and H_{inh} is the level of Ca^{2+} cooperativity in IP_3R inhibition (J. K. Foskett et al. 2007).

The structural basis for Ca^{2+}-mediated regulation of IP_3R activity has remained hotly debated in the field for decades. Initially, two competing ideas seemed plausable: Ca^{2+} binding to intrinsic Ca^{2+} binding sites on IP_3R, or Ca^{2+} binds to an accessory protein like calmodulin to modulate IP_3R function (C. Taylor, Fonseca, and E. Morris 2004). Seven Ca^{2+} binding sites were identified by structure function analyses using $^{45}Ca^{2+}$ and ruthenium red overlay procedures in IP_3R1 (I. Sienaert et al. 1996; Ilse Sienaert et al. 1997), with two sites positioned in the IP_3 binding core itself at positions 304-381 and 378-450. At the time the dissertation project began, there was no consensus on what any of these Ca^{2+} binding sites' purposes were, with minimal evidence linking one of these sites to the biphasic regulation of IP_3R by Ca^{2+}. The only piece of evidence came from mutational studies where a highly conserved glutamate residue (2100 in IP_3R-1, which forms part of what we now term the 'activitory' Ca^{2+}-binding site) was changed to alanine, resulting in a 5-10

fold decrease in Ca^{2+} sensitivity to activation (Tomoya Miyakawa et al. 2001; Tu, Nosyreva, et al. 2003). Through patch clamp recordings of single channel activity, two Ca^{2+} binding sites, one activitory and one inhibitory were identified (Mak, S. McBride, and J. Kevin Foskett 1998) and were confirmed using cryo-EM 20 years later (Paknejad and Hite 2018). Calcium ions are the primary source of IP_3R conductance in vivo, as there is no K^+ gradient across the ER membrane (Lam and Galione 2013). IP_3R can conduct both mono and divalent cations, with a $P_{divalent}/P_{monovalent}$ of between 3.2–11, and can pass Cl^- ions, albeit not efficiently (J. K. Foskett et al. 2007; Mak, S. McBride, Raghuram, et al. 2000).

The open probability of IP_3R can be increased through ATP binding to the receptor in a subtype specific manner (Hogan 2015; C. D. Ferris, Huganir, and S H Snyder 1990; Iino 1990). IP_3R-1 was originally reported to respond to micromolar concentrations of ATP (0.13 mM), IP_3R-3 responded to millimolar concentrations (2 mM) (I. Bezprozvanny 2005), while IP_3R-2 appeared unresponsive to ATP modulation in both Ca^{2+} release assays and single-channel bilayer electrophysiology recordings under maximal IP_3 concentrations (Miyakawa et al. 1999; Tu, Zhengnan Wang, Nosyreva, et al. 2005) (Figure 9). IP_3R-1 is modulated by ATP in a non-cooperative manner, while IP_3R-3 is modulated in a highly cooperative manner. The molecular basis underlying these differences in sensitivity was proposed to be different ATP binding sites, which would presumably have different ATP binding affinities. These potential binding sites were identified by searching for glycine-rich sequences (Karlien Maes et al. 2001; Wierenga and Hol 1983), similar to those found in Walker A motifs in the nucleotide binding sites in ATPases and GTPases. Of the three identified potential ATP binding sites, the ATPA site is unique to IP_3R-1 and was proposed as the reason why this isoform is the most sensitive to ATP modulation (Tu, Tomoya Miyakawa, et al. 2002; K. Maes et al. 2000). The ATPA site was later ruled out as an ATP binding site after mutations in the site designed to inhibit ATP binding failed to abrogate ATP modulation of IP_3R activity (Betzenhauser et al. 2009). The ATPB site (LGLLG) was originally discovered in IP_3R-2 spanning residues 1969-1974, and was proposed as the ATP binding site through abrogation of ATP binding in a mutagenesis experiment that exchanged the glycines for alanines (Vervloessem et al. 2015). The ATPC site was later found to contain a PKA phosphorylation site, and was ruled out as an ATP binding site (Wagner, Betzenhauser, and Yule 2006). Prior to the onset of this dissertation,

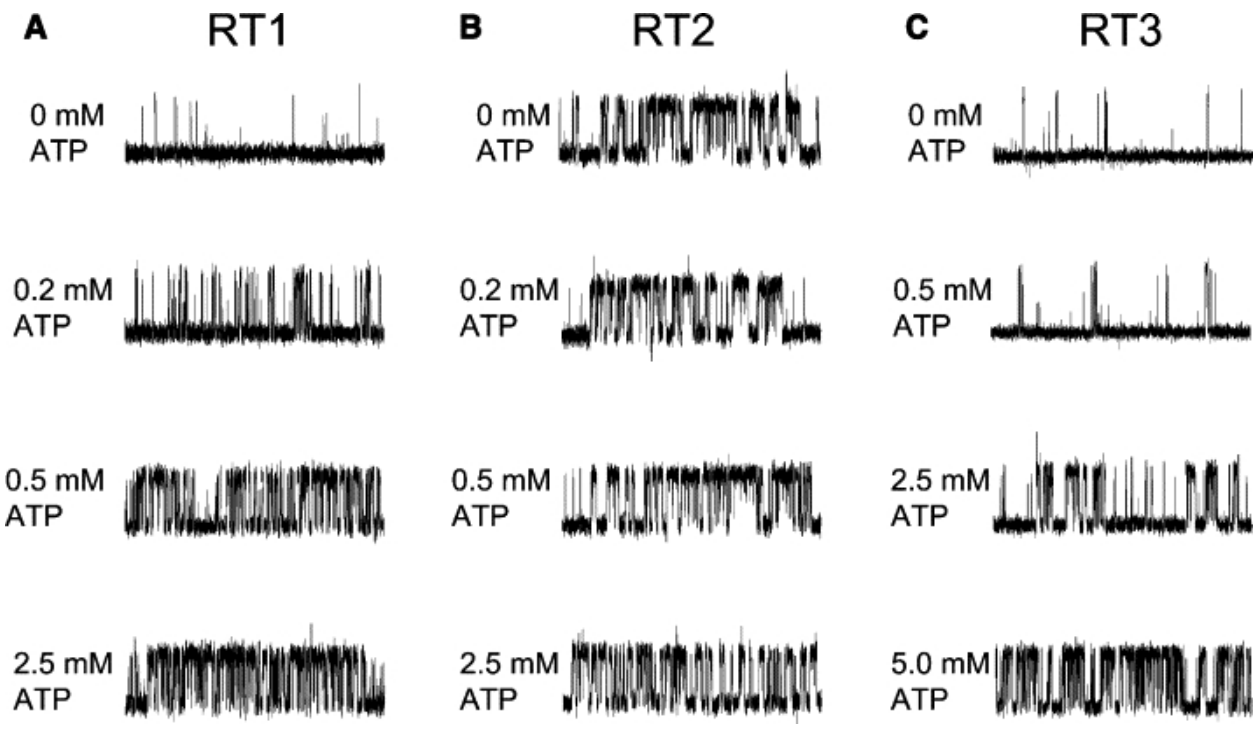

Figure 9: **Rat IP_3R isoforms sensitivity to varying ATP levels.**Representative bilayer electrophysiological recordings of rat IP_3R-1 (A), rat IP_3R-2 (B), and rat IP_3R-3 (C) in the presence of 2 μM IP_3, pCa 6.7, and Na_2ATP as listed above. Image from (Tu, Zhengnan Wang, Nosyreva, et al. 2005).

there was no available structure showing the ATP binding modality or confirming the location of ATP binding in IP_3R.

5.1.3 A historical perspective on the identification of the IP_3R and the search for structures

The discovery of IP_3R has its origins in the 1970s, although in the decade prior ER-resident ion channels were proposed (Franzini-Armstrong 1963). The connection between IP_3 as a second messenger and Ca^{2+} release from an intracellular store was under intense investigation. The ER and SR connection to muscle contraction through calcium signaling was observed (Endo, Tanaka, and Ogawa 1970), calcium-induced calcium release was first identified, and the concept of depolarization originating from calcium release became mainstream (Franzini-Armstrong and Jorgensen 1994). Simultaneously, the first accounts of calcium release from ligand-gated ion channels linked to second messengers were reported (Case and Clausen 1973; Nielsen and Petersen 1972), and the field began

to narrow focus on IP_3, and other inositol phosphates, as a possible candidate for activating these unknown receptors (Michell 1975). IP_3 was directly linked to calcium release from an "IP_3 receptor" located on a non-mitochondrial intracellular calcium store in 1983 (Streb et al. 1983). This 'IP_3 receptor' was found in high concentrations in mouse cerebella (P. Worley, Baraban, and S. Snyder 1989; P. F. Worley et al. 1987), which enabled the first purification of the IP_3-binding protein from the native source (Supattapone et al. 1988). Following this first purification, the IP_3-binding protein was reconstituted into liposomes, where IP_3R was clarified to be one protein that was both capable of binding IP_3 and mediating Ca^{2+} release, instead of existing as a heterogenous complex of two or more distinct proteins (C. Ferris et al. 1989).

While this cohort of studies focused on identifying the IP_3 binding protein and confirming its function as a calcium release channel, the IP_3R was independently being characterized as a membrane protein capable of being both glycosylated and phosphorylated. The IP_3R was independently referred to as P400 (Mallet et al. 1976; K. Mikoshiba, Huchet, and Changeux 1979; Katsuhiko Mikoshiba, Okano, and Tsukada 1985), PCPP-260 (Walaas, Nairn, and Greengard 1986), and GP-A (Groswald and Kelly 1984) by different groups. The P400 protein was linked to the staggerer phenotype in mouse models of hereditary cerebellar ataxia. The P400 proteins were purified (N. Maeda et al. 1988), and used to raise anti-P400 monoclonal antibodies, the first mIP_3R specific antibodies (Nobuaki Maeda et al. 1989). These P400 monoclonal antibodies were used to immunoscreen cDNA libraries from mouse cerebellum in order to clone the IP_3R gene for the first time (Furuichi et al. 1989). Simultaneously, other groups cloned the IP_3R gene from differential subtractional analysis of cDNA from mouse cerebellum libraries of both wild-type and staggerer mice (Nordquist, Kozak, and Orr 1988; Gregory A. Mignery et al. 1989). In 1990, the IP_3R cDNA was expressed in a mouse fibroblast L cell line, where the IP_3R's identity was confirmed through H-IP_3 radioligand binding assays and Ca^{2+} release experiments from membrane fractions (Atsushi Miyawaki et al. 1990). The following year, IP_3R was identified as a non-covalently linked tetramer via agarose gel electrophoresis through bis(sulfosuccinimidy1)suberate cross-linking experiments (Maeda, Kawasaki, et al. 1991). Following the initial cloning of IP_3R-1 cDNA from mouse in 1989, IP_3R-1 cDNA was cloned from rats in 1990 (G. Mignery and T. Südhof 1990), and three groups published the human IP_3R-1 sequence in 1994 and 1995 (Yamada et al. 1994; Harnick et al. 1995;

Nucifora et al. 1995). In a similar manner and timescale, IP_3R-2 was cloned from mouse (Iwai, Tateishi, et al. 2005), rat (T. C. Südhof et al. 1991), and humans (Yamamoto-Hino et al. 1994). IP_3R-3 cDNA was similarly cloned from mouse (Iwai, Tateishi, et al. 2005), rat (Blondel et al. 1993), and human (Maranto 1994; Yamamoto-Hino et al. 1994).

After the IP_3R-1 gene was sequenced, efforts began to predict the receptor's morphology through sequence analyses and structure-function studies. Through truncation experiments, the three major functional domains were identified: the ∼600 residue N-terminal IP_3-binding domain, a ∼400 residue C-terminal channel forming domain, and a large ∼1700 residue central modulatory domain (G. Mignery and T. Südhof 1990). This same study identified that the transmembrane domain was critical for successful tetramerization, and observed large conformational changes upon IP_3 binding as measured through gel filtration. Concurrently, another group confirmed the transmembrane domain, or the C-terminal tail, controlled tetramer formation and that the first 605 residues of the N-terminus, which were highly conserved with Drosophilia IP_3R-1, contained the IP_3 binding site (Miyawaki et al. 1991). The IP_3R-1 transmembrane domain (residues 2275–2593) was predicted to have either eight (Mignery et al. 1990) or six (S. Yoshikawa et al. 1992) transmembrane helices using hydropathy analysis. Dozens of structure-functional analyses were critical for discovering IP_3R functions as a molecular scaffold and that IP_3Rs could synthesize signals from multiple sources into spatiotemporally controlled Ca^{2+} signals (Sipma et al. 1999; Patel et al. 1997; Cardy and C W Taylor 1998; Keiko Uchida et al. 2003).

Historically, it has been very difficult to obtain structures of the IP_3R due to its large size (1.2 MDa), its nature as a membrane protein, and its dynamic flexibility. IP_3R's naturally low expression across different cell types has also thwarted crystallization attempts and both solution and solid-state NMR approaches (Bosanac, Michikawa, et al. 2004). Purkinje cells were an excellent early source for IP_3R, since the protein expresses at relatively high levels, compared to other tissues, in ER cisternae stacks (Herndon 1963). Initially, the first glimpses at the receptor were obtained using negative stain electron microscopy on isolated cisternae stacks (Maeda, Niinobe, and Mikoshiba 1990; Chadwick, Saito, and Fleischer 1990) and 2-D crystalline EM arrays (Katayama et al. 1996; Takei et al. 1994. From the crystalline arrays imaged from cisternae isolated from cere-

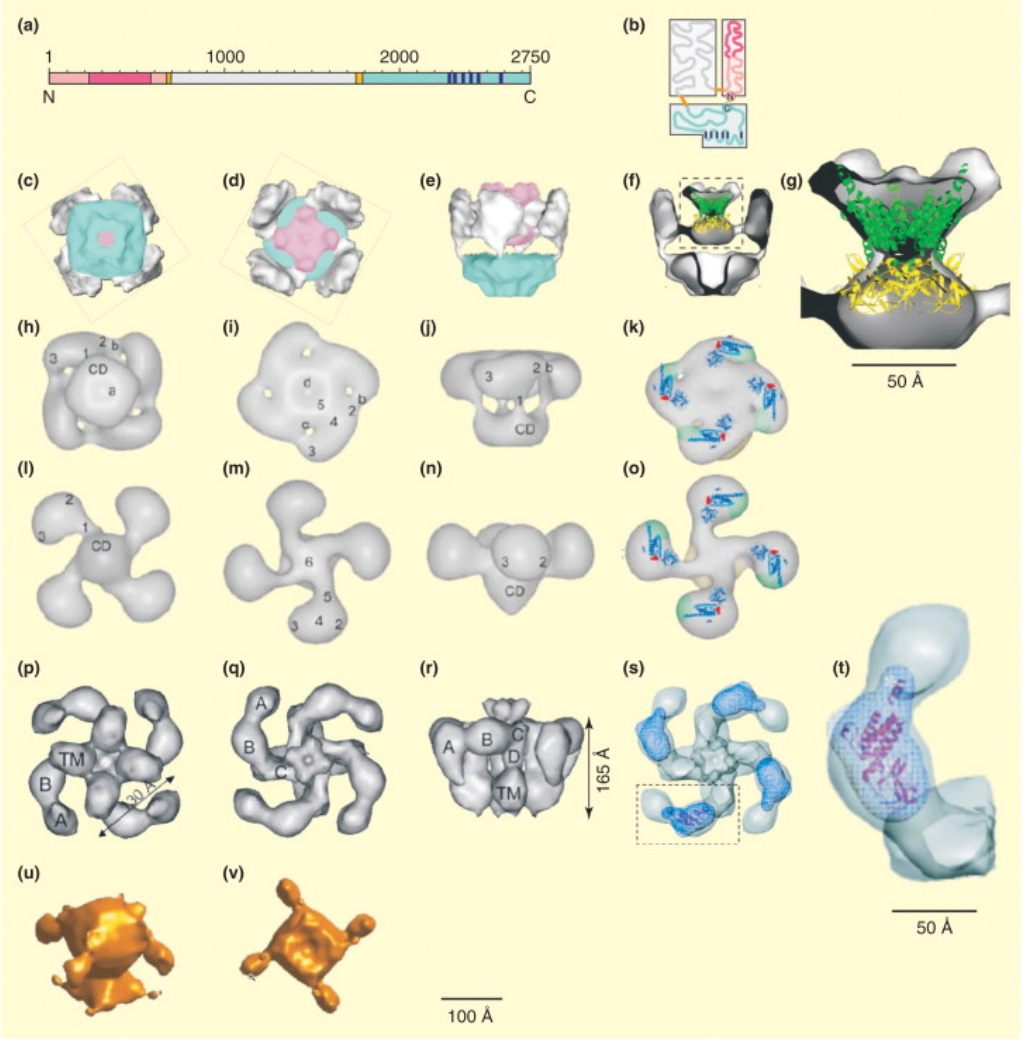

Figure 10: **Five electron microscopy structures of IP_3R-1 at intermediate resolution.** A simplistic linear representation of IP3R domains in one subunit (A, B) and the proposed orientation of the N-terminal SD (pink), the IP_3 binding core (magenta), the 'petal domain' (white), and the transmembrane domain (blue) with the individual six transmembrane alpha helices colored dark blue. The negative stain EM structure determined by (Fonseca et al. 2003) is colored as in (A) and is shown in a variety of orientations from the ER lumen (C), the cytoplasm (D), perpendicular to the ER membrane (E), and the same orientation as in (E) but with one subunit cut away to show the interior of the protein. (G) shows the Cryo-EM structure with the X-ray crystal structure of the IP_3 binding core (Bosanac, Alattia, et al. 2002) docked into the N-terminal part of the structure. (H-O) The negative stain EM structure determined by (Kozo Hamada, Terauchi, and Katsuhiko Mikoshiba 2003) in the absence of Ca^{2+} (H-K) or the presence of 1 mM $CaCl_2$ and viewed from the ER lumen (H, L), cytoplasm (I, M), or perpendicular to the ER membrane (J, N). The crystal structure of the IP_3 binding core was docked into the N-terminal domain (K, O) to match where the authors suggested the domain lay. (P-T) The Cryo-EM structure determined by (Serysheva, D. J. Bare, et al. 2003) is shown from the ER lumen (P), the cytoplasm (Q), perpendicular to the ER membrane (R), and with the IBC crystal structure docked into the N-terminal where they suspected its location to be (S-T). The first reported Cryo-EM structure, which was reported by (Q.-X. Jiang et al. 2002) shown from a downward angle in the cytoplasm (U) and from the ER lumen (V). Image from (C. Taylor, Fonseca, and E. Morris 2004).

bellar Purkinje cells, individual IP_3R proteins can be seen as electron rich regions. Measurements of individual proteins from these 2D arrays suggested IP_3Rs formed square, compact particles with dimensions of 12 nm by 12 nm.

Initial attempts at building 3D models of IP_3R-1, purified from native sources, using single particle analysis from negative stain images could only reveal minimal information due to low resolution. The proteins demonstrated four-fold symmetry when viewed from the cytoplasm, and adopted either a tightly-bound square or a looser-pinwheel conformation with dimensions of either 190 x 190 Å (Kozo Hamada, Miyata, et al. 2002; Maeda, Niinobe, and Mikoshiba 1990) or 250 x 250 Å respectively (Chadwick, Saito, and Fleischer 1990; Kozo Hamada, Miyata, et al. 2002) (Figure 10h-o). In the early 2000s, five EM structures of IP_3R-1 at 20-40 Å resolution were published back to back, three cryo-EM structures and two EM negative stain structures, and ignited a fierce debate over the protein's true quartenary structure (Kozo Hamada, Terauchi, and Katsuhiko Mikoshiba 2003; Fonseca et al. 2003; Serysheva, Hamilton, et al. 2005; Q.-X. Jiang et al. 2002; C. Sato, K. Hamada, et al. 2004) (Figure 10). The only means of validating the structures were through personal experience, and comparison with previously published structure-function experiments such as cross-linking. This lack of clarity over which of the reported structures correctly represented IP_3R-1 was not resolved until almost a decade later (S. Ludtke et al. 2011). This period of uncertainty ultimately resulted in a 2010 meeting of the International Electron Microscopy Data Bank Task force to develop validation tools and cutoff criteria for assessing cryo-EM models (R. Henderson, Sali, et al. 2012). The reported structures confirmed only the basic topology of the receptor, that there is a large cytosolic domain and a much smaller transmembrane domain. Despite the groups imaging IP_3R-1 under similar buffer conditions and in the absence of both IP_3 and added Ca^{2+}, the structures begin to diverge at moderate resolution. The divergence was due to high levels of noise in the raw micrographs, which when combined with the low contrast and incorrect starting models led to over interpretation of the data and both artifacts and parts of the final maps missing (Stewart and N. Grigorieff 2004).

The first cryo-EM structure of IP_3R-1 (Q.-X. Jiang et al. 2002) was obtained using protein from mouse cerebellum, resolved to 24 Å and calculated to be 1.2 MDa assuming $0.81\frac{Da}{A^3}$ (Dobson 1999). This structure appeared as an uneven dumbbell 170 Å in length, with the smaller end a compact

100 Å x 100 Å square-shaped domain (Figure 10u-v). The larger end contained four 50 Å long arms protruding laterally outwards to form a 155 Å x 155 Å cytosolic domain. On the lumenal side of the transmembrane domain, an internal cavity was observed, which the authors attributed to the ion conduction pathway, that decreased to 20 Å in diameter at the smallest point in the dumbell on the cytoplasmic side. Based on this large internal cavity, and the location of the constriction point in the cytoplasm, the authors proposed the selectivity filter and gate were located on the cytoplasmic side of the transmembrane domain, in contrast to the KcsA potassium channel's architecture, which had previously been the model for IP_3R-1 (A. J. Williams, West, and Sitsapesan 2001). Instead, the authors proposed the transmembrane domain's architecture was more similar in lateral and longitudinal size to the transmembrane domains of voltage-gated sodium (C. Sato, M. Sato, et al. 1998) and potassium channels (Sokolova, Kolmakova-Partensky, and N. Grigorieff 2001). This IP_3R-1 structure is very compact when compared to the IP_3R-1 structures published by the other groups, or to contemporary Ryanodine receptor structures (Serysheva and Steven J. Ludtke 2010)

A competing cryo-EM structure published one year later, using protein obtained from bovine cerebella, and resolved to 30 Å revealed a completely different quartenary structure (Serysheva, D. J. Bare, et al. 2003). This structure was notably larger than the first cryo-EM structure, with the cytosolic domain forming a pinwheel-like structure with dimensions of 250 Å x 250 Å and a square-shaped transmembrane domain with dimensions of 150 Å x 150 Å (Figure 10p-t). Similarly to the first structure, the receptor's height was also determined to be 170 Å. Instead of the transmembrane domain connecting to the cytosolic domain through a narrow, centralized bridging density, the second structure reported the cytosolic domain itself was formed from four curved spokes that connected to the transmembrane domain through thin 'bridging densities'. Although this structure was determined in the absense of IP_3 and in low Ca^{2+} conditions, the cytosolic domain's pinwheel shape was not in line with previous EM structures determined from negative stain in the above conditions, which formed more compact, square shaped structures (Fonseca et al. 2003; Kozo Hamada, Miyata, et al. 2002; Kozo Hamada, Terauchi, and Katsuhiko Mikoshiba 2003). Although this structure was collected in apo conditions, the central pore in the transmembrane domain was larger than expected for a closed structure. Despite these drawbacks, this was the first structure in which the ligand binding domain (Bosanac, Alattia, et al. 2002) was docked into the N-terminal domain to

begin to connect previous structure-function data to a cryo-EM model. This crystal structure of the IBC bound to IP_3 (Bosanac, Alattia, et al. 2002) was resolved to 2.2 Å and showed IP_3 binding to the βTF-2 and ARM1 domains. The structure of the βTF-1, or the suppressor, domain would be determined to 1.8 Å resolution in 2005 (Bosanac, Yamazaki, et al. 2005). Prior to this IP_3R-1 structure, and the previous cryo-EM structure, the IP_3 binding domain had been predicted to be localized close to the beginning of the N-terminus using heparin-gold labeling during negative stain data collection. (Kozo Hamada, Miyata, et al. 2002).

Of the three early cryo-EM structures, the last structure published in the cohort reported the highest resolution at 20 Å (C. Sato, K. Hamada, et al. 2004). This third structure reported IP_3R-1 as having a 175 Å x 175 Å cytosolic domain shaped like a 'hot-air balloon', taller than both of the two previously reported structures at 231 Å (Q.-X. Jiang et al. 2002; Serysheva, D. J. Bare, et al. 2003) (Figure 11c). The cytosolic domain contains four prominant L-shaped densities at the N-termini, which the authors docked the ligand-binding domain crystal structure into, in line with (Serysheva, D. J. Bare, et al. 2003) (Figure 11d, e). The porous cytosolic domain is continuously connected to the transmembrane domain, with no clearly defined constriction point as in (Q.-X. Jiang et al. 2002). The morphology of this connection differed from the slender, connecting column densities reported in one later ∼1 nm resolution type-1 RyR structure (Steven J. Ludtke et al. 2005), and from the thinner bridging densities observed in crystallized tetrameric K^+ channels (Y. Jiang et al. 2002a; Kuo et al. 2003; Long, Campbell, and Mackinnon 2005; Tao et al. 2009). The observed transmembrane domain was mostly hollow, and the authors could not observe any density near the central four-fold axis which could make up the ion conduction pathway.

In contrast to the three early cryo-EM structures of IP_3R-1, the early structures derived from negative stain data were consistent with each other, and with prior structure-function experiments (Fonseca et al. 2003; Kozo Hamada, Terauchi, and Katsuhiko Mikoshiba 2003). Both structures had considerably lower resolution (34 Å and 30 Å) than the three cryo-EM structures (Kozo Hamada, Terauchi, and Katsuhiko Mikoshiba 2003; Fonseca et al. 2003). The 3 nm structure (Fonseca et al. 2003) is shaped like a flower, with clearly separate 180 Å x 180 Å x 110 Å cytosolic and 126 Å x 126 Å x 70 Å transmembrane domains, unlike in C. Sato, K. Hamada, et al. 2004. One critical divergence in this structure was the larger than expected transmembrane domain, which made up

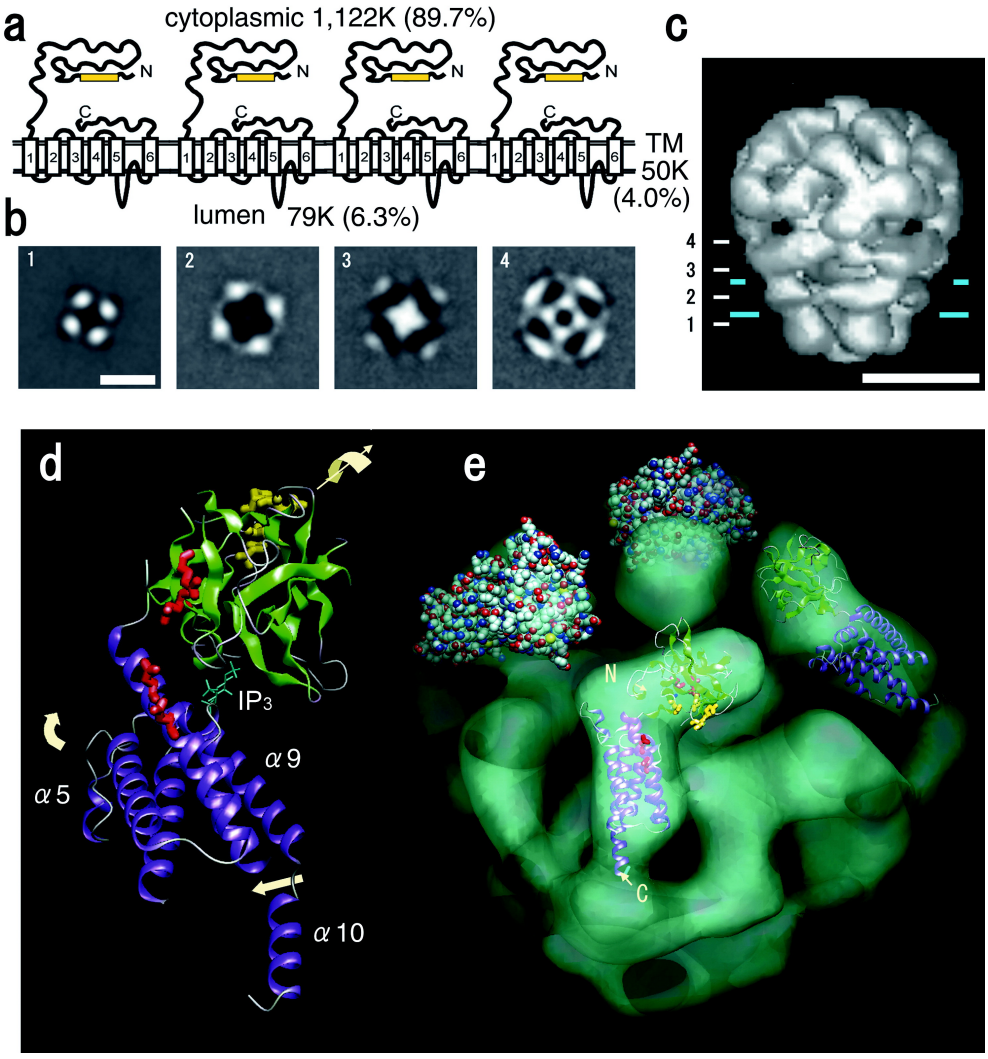

Figure 11: **Cryo-EM IP_3R-1 structure with four N-terminal 'L-shaped' densities.** (A) predicted topology of the IP_3R-1 tetrameric transmembrane domain. (B) Cross sections through the IP_3R-1 map at different Z-heights starting from the transmembrane domain and ending in the cytoplasmic N-terminal domain. (C) the full density map for IP_3R-1 with the Z-heights in (B) shown as cyan lines and the transmembrane domain cordoned off by two blue lines 30 Å apart to signify the ER membrane. The white scale bar at the bottom represents 100 Å. (D) ribbon structure of the IBC bound to IP_3 (1N4K). To fit this IBC crystal structure into the L-shaped N-terminal domains (E) in the Cryo-EM structure, the IBC was modified according to the arrows present in (D). The crystal structure in (D) is colored according to domain with the IBC-α (blue), IBC-β (green), and IP_3 (light blue). Yellow residues indicate the proposed Ca-I site while red residues indicate the Ca-II site. Image from (C. Sato, K. Hamada, et al. 2004).

approximately 35 % of the structure's mass as opposed to the approximately 11 % reported in the cryo-EM structures (Q.-X. Jiang et al. 2002; Serysheva, D. J. Bare, et al. 2003; C. Sato, K. Hamada, et al. 2004) and in prior hydropathy analyses (Mignery et al. 1990; S. Yoshikawa et al. 1992). The structure with 34 Å resolution (Kozo Hamada, Terauchi, and Katsuhiko Mikoshiba 2003) revealed a similar overall architecture, with four-fold symmetry clearly seen in the cytosolic domain. The transmembrane domain made up 25 % of the structure's mass, which the authors justified based on the assumption that their transmembrane domain also included the C-terminal tail. This would increase the transmembrane domain's mass to approximately 90 kDa, which is the size the C-terminal trypsinized fragment seen previously by three groups (S K Joseph, Pierson, and S. Samanta 1995; Boehning and S. K. Joseph 2000; F. Yoshikawa, Iwasaki, et al. 1999).

In 2011, a 10 Å structure in the closed conformation was published that verified IP_3R-1's quartenary structure using better evaluation metrics, settling the debate at long last (S. Ludtke et al. 2011), (Figure 12). The transmembrane domain was more clearly defined, showing a four helical bundle of transmembrane helices along the ion conduction pathway, with one helix originating from each subunit. This architecture, in conjunction with observed 'windows' in the cytosolic domain directly adjacent to the transmembrane domain, is very similar to the reported architecture of K^+ channels (Doyle et al. 1998; Kuo et al. 2003; Tao et al. 2009). Due to the low resolution, the purpose of these observed 'windows' could only be speculated and was hypothesized to facilitate transport of Ca^{2+} ions laterally from the mouth of the transmembrane pore to the cytosol. This validated cryo-EM structure of IP_3R-1 was similar to the two earlier negative stain EM structures (Fonseca et al. 2003; Kozo Hamada, Terauchi, and Katsuhiko Mikoshiba 2003), but bore little to no resemblance to the earlier three cryo-EM structures (Q.-X. Jiang et al. 2002; Serysheva, D. J. Bare, et al. 2003; C. Sato, K. Hamada, et al. 2004). The four subunits were found to connect via a central plug in the cytosolic domain, which was not observed previously in any of the IP_3R or RyR structures. Critically from this study, the central pore-lining helix was identified as TMD6, based on animo acid sequence alignments and comparison with K^+ channel crystal structures, with a conserved glycine residue at position 2587 forming the proposed hinge region by which the helix would bend and open the gate in a similar manner to the *Methanobacterium thermoautotrophicum* Calcium-gated potassium (MthK) channel (Y. Jiang et al. 2002b). Lumenal turrets formed by the

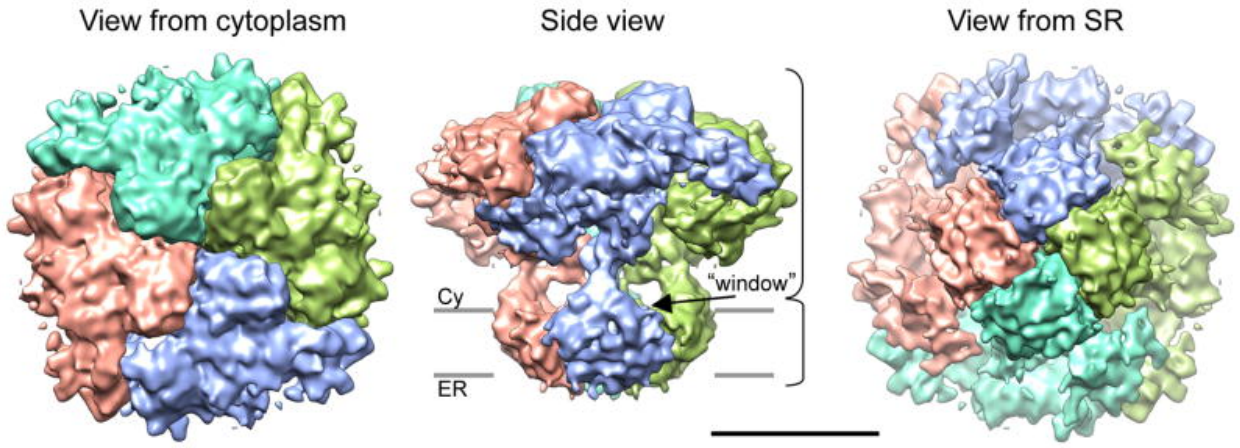

Figure 12: **Surface representation of the cryo-EM density map of IP_3R-1 that determined the quaternary structure.** The 3D surface representation of IP_3R-1 is represented as viewed from the cytoplasmic side, through the membrane plane, and from the lumenal side. In each view, subunits are colored individually to show the quaternary structure more clearly. The contour level for the surface representation was determined by assuming a protein density of 0.81 Da/Å^3, which amounts to ∼330 kDa per subunit. The gray bars show the relative dimension of the ER membrane and the scale bar represents 100 Å. Image from (S. Ludtke et al. 2011)

extended loops between TMD5-6 (residues 2464–2529)) were observed for the first time in IP_3R-1, forming a structural divergence from the RyR (S. Ludtke et al. 2011), that were similar to those seen previously in the inwardly-rectifying potassium (Kir) channel (Tao et al. 2009).

The field would leap forward in 2015 with the publication of a near-atomic resolution (4.7 A) structure of rat IP_3R-1 in the apo conformation (Fan, M. L. Baker, et al. 2015) (Figure 13). At this resolution, 85 % of the protein's backbone, or 2,327 out of 2,750 residues, was modeled allowing for the demarcation of the boundaries between individual domains: two contiguous beta-trefoil domains (1-436), three consecutive armadillo domains (437-2192), an intervening lateral domain (2193-2272), the six alpha helical transmembrane domain (2273-2600), the linker domain (2601-2680), and the C-terminal tail (2681-2731). The jump in resolution can be attributed to both the 'resolution revolution' in cryo-EM with leaps forward in direct CMOS detectors and new data processing methods. However, this structure contained a few modeling errors within the armadillo domains in the central modulatory domain, possibly as a result of limited resolution of the cryo-EM maps for these regions. The transmembrane domain was shown to contain six alpha helices from each subunit in a right-handed helical bundle while the C-terminal tail, formerly described as a

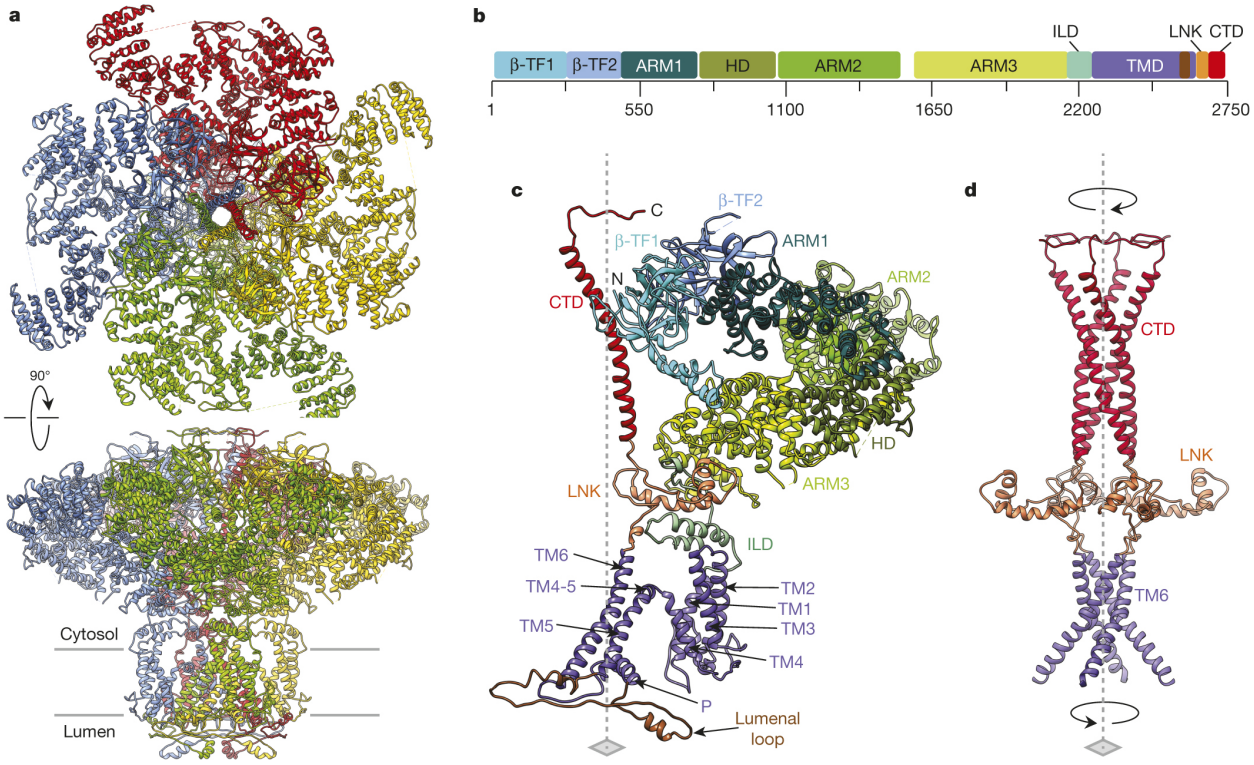

Figure 13: **The first high-resolution IP$_3$R-1 structure.** (A) Cryo-EM structure of full-length IP$_3$R-1 shown looking down from the cytoplasm and from within the ER membrane. Individual subunits are color coded. (B) linear IP$_3$3R-1 representation colored according by domain (GI accession 17380349). (C) one individual IP$_3$R-1 subunit, color coded according to the domains indicated in (B). (D) the IP$_3$R-1 core comprised of the pore lining helices in the TMD and terminating with the C-terminal coiled-coil tail. The dashed-line indicates the four-fold axis while the arrows indicate the structure's handedness. Image from (Fan, M. L. Baker, et al. 2015).

channel plug, forms a left handed coiled-coil. From this structure, the side chains of the residues lining the ion conduction pathway in the transmembrane domain were resolved and modeled, allowing for the identification of both pore helices and the selectivity filter's position on a highly conserved lumenal loop between TMD5 and TMD6 (residues 2546–2552). Finally, the structure proposed that the IP$_3$R-1 gate is located at the hydrophobic constriction point of the central TMD6 helical bundle where L2582, F2586 and I2590 constrict the ion conduction pathway to a diameter of approximately 5 Å. This provided convincing evidence that the channel was in the closed, non-conducting, conformation since hydrated Ca^{2+} ions are 8-10 Å in diameter (Fulton et al. 2003).

Up until this point, all of the published IP$_3$R structures were both of type 1, and in either apo or Ca^{2+} inhibiting conditions. In 2018, a 4.1 Å structure of IP$_3$R-1 bound to the agonist

adenophostin-A (AdA) in activating Ca^{2+} concentrations (Fan, M. R. Baker, Zhao Wang, et al. 2018) (Figure 14) and an ensemble of recombinant IP_3R-3 structures in pre-active and inhibited confornations were published (Paknejad and Hite 2018). Although the AdA-bound structure was not open based on the architecture of the transmembrane domain, this structure provided one of the first full-structure glimpses at ligand-induced conformation changes in the cytosolic domain. AdA binding resulted in the clam-shell closure of the IBC, which propagated to the three ARM domains culminating in changes in JD. This interface then exerts force on the transmembrane domain through their connecting linkers. However, the force exerted by AdA binding was not sufficient to dilate the hydrophobic constriction point, formed by residues F2586 and I2590, sufficiently to allow hydrated Ca^{2+} ions to pass through. This structure can thus be considered an intermediate gating conformation. The ensemble of IP_3R-3 structures, provided a fundamental understanding into the mechanisms underlying these long-range conformational changes that occur upon IP_3 binding and revealed two Ca^{2+} binding sites under high calcium concentrations (2 mM) (Figure 16). The five structures of IP_3R-3 bound to IP_3 show a subunit by subunit transition from a Class 1 state, where the IP_3-induced changes are localized to the IBC, to a Class 2 state, where the IP_3-induced changes propagate downwards through the ARM domains to rotate the JD domain (Figure 15). The Class 2 state indicates an IP_3R-3 on the path to channel activation prior to Ca^{2+} binding to the activatory site. The inhibited IP_3R-3 structure obtained in the presence of 2 mM $CaCl_2$ contained two observed Ca^{2+} ions bound to two Ca^{2+} binding sites, with one binding site located at the ARM2/CLD interface in the cytosolic domain and another site lower in the cytosolic domain at the interface formed by residues and backbone carbonyls from the ARM3 and the JD. Since both Ca^{2+} binding sites were occupied under high Ca^{2+} concentrations, it is impossible to definitively tell from the structures which binding site is responsible for Ca^{2+}-mediated channel activation and which is responsible for mediating Ca^{2+}-mediated IP_3R inhibition. Only a structure of an IP_3R isoform in the active conformation would provide the final pieces of evidence for assigning functionality to the two Ca^{2+} binding sites, and for describing the exact mechanisms of channel gating.

5.1.4 Techniques to measure IP_3 binding affinity

The first evidence for the existence of IP_3Rs came from radioligand binding assays demonstrating the presence of high-affinity, saturable IP_3 binding sites in permeabilized hepatocytes and neu-

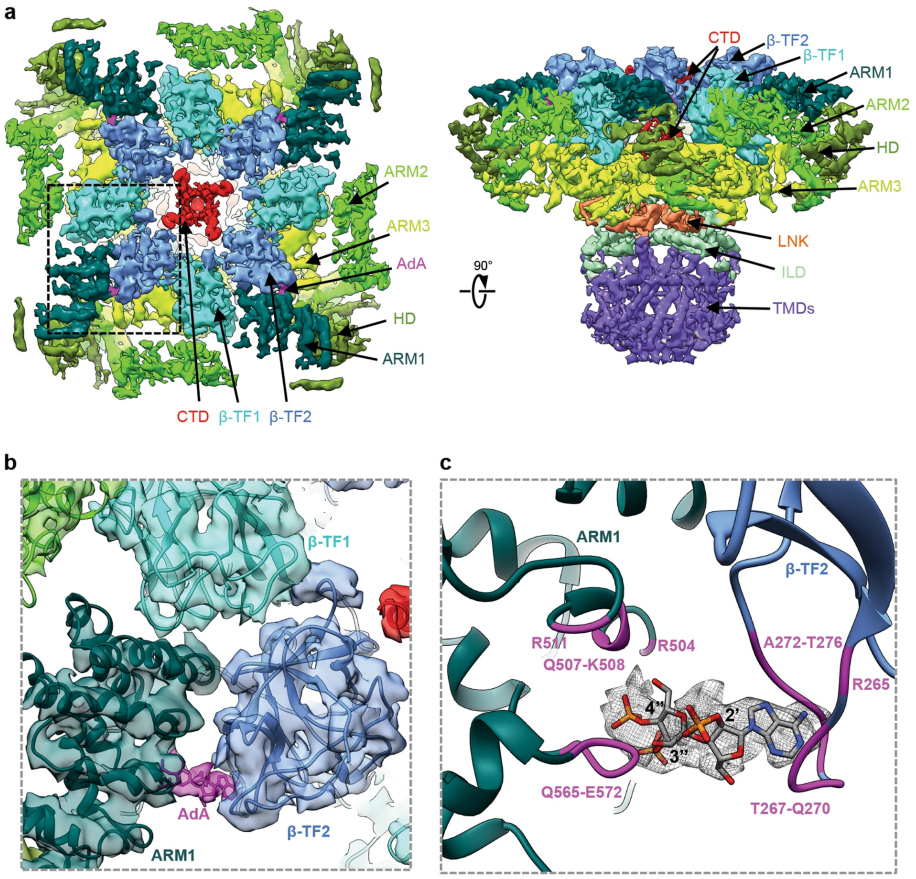

Figure 14: **Cryo-EM structure of IP_3 R-1 receptor bound to Adenophostin A.** (A) The cryo-EM density map of the IP_3R-1-AdA structure viewed from the cytosoplasm (left) and from the side through ER membrane (right). The map is filtered to 4.1 Å and corrected with a B factor of 100 $Å^2$. Each subunit's domains are colored individually. Densities in the structure attributed to AdA are colored magenta. (B) Closer view of the AdA density present in the IBC. AdA-IP_3R-1 structure is superimposed on its density map and color-coded by domain; the AdA compound is fit among the IP_3R-1 density connecting the two parts of the IBC. (C) AdA compound in the IP3-binding pocket overlaid with densities from the (4σ) difference map. Amino acids within 5 Å from the bound AdA are labeled and colored magenta. Image from (Fan, M. R. Baker, Zhao Wang, et al. 2018).

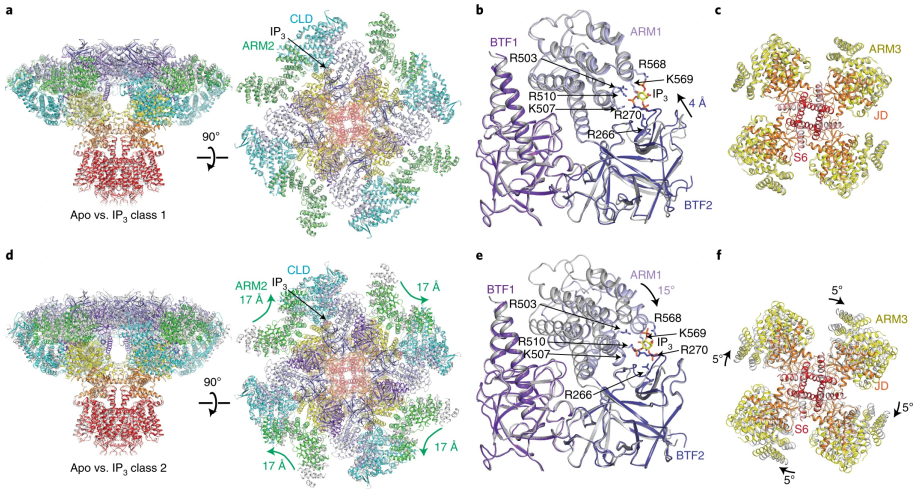

Figure 15: **Comparison of the IBC in two IP_3-bound conformations.** (A) Superposition of apo IP_3R-3 (gray) with the class 1 IP_3-bound pre-active conformation (colored by domain) viewed from the cytoplasm and from the side. (B) Zoomed-in superposition of the IBC of apo and class 1 IP_3R-3. (C) Zoomed-in superposition of the ARM3, JD, and TMD6 of both apo and class 1 IP_3R-3. (D) Superposition of apo (gray) and class 2 IP_3-bound pre-active IP_3R-3 (colored by domain) in the same views as in (A). (E) Zoomed-in superposition of the IBC of apo and class 2 IP_3R-3. (F) Superposition of the ARM3, JD, and TMD6 of apo and class 2 IP_3R-3. Image from (Paknejad and Hite 2018)

trophils (Michell 1975), as well as in membrane fractions from the anterior pituatory (Guillemette et al. 1987), liver (Spät, Fabiato, and Rubin 1986), adrenal cortex (Baukal et al. 1985), and rat cerebellum (Paul F. Worley et al. 1987; P. F. Worley et al. 1987). From these initial studies, it was determined that IP_3Rs had high specificity to IP_3 over other inositol phosphates and that IP_3 binding is approximately 100-fold higher in the cerebellum compared to the peripheral tissues. The first purification of IP_3R was done starting from rat cerebellum, and utilized radioligand binding assays to optimize the solubilization strategy (Supattapone et al. 1988). IP_3 binding was markedly decreased upon addition of trypsin, providing confirmation that IP_3R was a protein, and was unaffected by high sodium concentration in the buffer, providing evidence that IP_3R was likely an integral membrane protein. During the cloning and initial characterization of IP_3R, radioligand binding assays were used to confirm the recombinant protein produced from the cloned genes could bind IP_3 (Furuichi et al. 1989).

The identification of residues in the IBC were derived from structure-activity analyses that measured IP_3 binding to truncated IP_3R constructs. Residues 224 –579 of mIP_3R-1 were found to be the minimum region capable of binding IP_3, and described as the IP_3 binding core. This conclu-

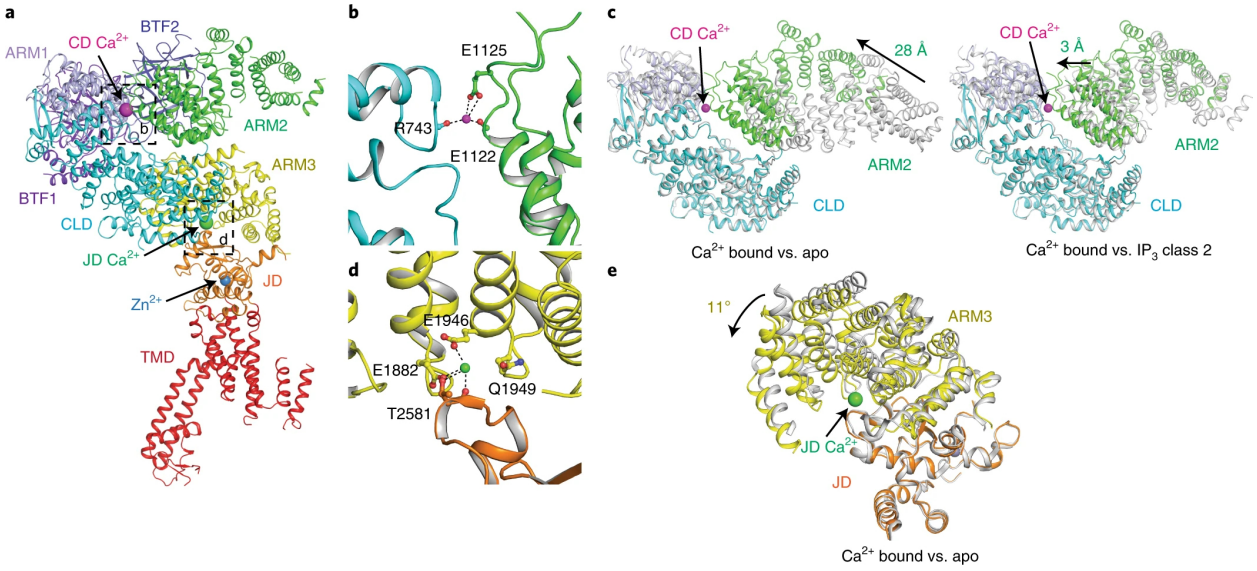

Figure 16: **Location of the two occupied Ca^{2+} binding sites in one IP_3R-3 subunit.** (A) One IP_3R-3 subunit colored by domain viewed from the side through the ER membrane. Bound Ca^{2+} (green at the activitory site or magenta at the inhibitory site) and Zn^{2+} (blue) ions are shown as spheres. (B) The proposed inhibitory Ca^{2+} binding site formed by residues at the ARM2-CLD interface. (C) Superposition of the inhibitory Ca^{2+} binding site in both the apo (gray) and high Ca^{2+} IP_3R-3 (colored by domain) conditions, and the high Ca^{2+} condition (gray) and the class 2 IP_3-bound pre-active (colored by domains) IP_3R-3 structures. (D) The proposed stimulatory Ca^{2+} binding site formed by residues at the ARM3-CLD interface. (E) Superposition of the stimulatory binding Ca^{2+} site in the apo (gray) and high Ca^{2+} IP_3R-3 conditions. Image from (Paknejad and Hite 2018).

sion was reached from measuring H-IP_3 binding to a N-terminal mIP_3R-1 fragment encompassing the first 734 residues (F. Yoshikawa, Morita, et al. 1996). The construct was gradually truncated residue by residue from both ends, until IP_3 binding was abolished.

Key steps in IP_3R activation were determined by taking advantage of partial agonist binding curves. Ligand-gated ion channels transition from the inactive to active state upon agonist binding, through a sequence of short-lived, unstable, transition states (Rees, E. Johnson, and Lewinson 2009). The exact mechanism can range from an ensemble of incremental snapshots to one concerted motion opening the channel. The energy for these transitions come from the agonist binding to the receptor. The agonist's efficacy is the degree to which the agonist can induce the receptor to adopt the open conformation, whereas the agonist's affinity speaks to the strength of the binding interaction. Partial agonists then may have lower affinity, efficacy, or both. This decreases the amount of energy they impart to the structure upon binding. In addition to these characteristics, partial agonists may also stabilize unique conformations compared to the full agonist. The Taylor group synthesized 2-O-modified IP_3 analogs, partial agonists, and used the calculated K_d values to determine the free energy changes upon binding (A. M. Rossi et al. 2009). The partial agonists and IP_3 bound with the same affinity, leading to the conclusion that IP_3-derived partial agonists function not by decreasing contacts with the binding site, but by impairing the transmission of the conformational changes induced by binding. The comparison of the ΔGs of IP_3 and the partial agonists binding to both the full-length and truncated IP_3Rs allowed for the definition of key steps in IP_3R activation which included the IBC clamshell closure upon IP_3 binding, and the critical role of the SD in transmitting conformation changes to the pore.

Calorimetry as a technique dates back to the earliest scientific literature. In the 1760s, Joseph Black measured the heat capacity and the latent heat of water, marking the beginning of the study of thermodynamics (Partington 1960). Shortly after Black, Laviosier designed the first ice calorimeter to measure the metabolic heat produced by a guinea pig at rest (R. J. Morris 1972). Current calorimetry techniques collect data in three broad ways: through temperature changes, via heat conduction, or via power compensation (Freyer and E. A. Lewis 2008). In instruments that measure binding through temperature changes, the ligand binding to its target produces a temperature change in the measuring cell. The resulting raw output is a function of temperature versus

time. In adiabatic instruments, temperature changes in the measuring cell can be converted into heat changes, measured in joules or kcals, by multiplying the energy equivalent of the calorimeter by the temperature changes. In heat conduction instruments, any heat produced or consumed in the reaction is transmitted to a jacket surrounding the cell, which functions as a heat sink and is kept at a constant temperature. Measuring the heat flow between the measuring cell and the heat sink relies on the Seebeck-effect (Maekawa et al. 2004; K. Uchida et al. 2008), which involves the conversion of temperature differences between the two locations into an electrical potential. The resulting raw output of this technique is voltage as a measure of time, since the voltage produced is proportional to the temperature differences across the connecting sensors. The final calorimetry method is power compensation, which is often referred to as isothermal. In isothermal instruments, the measuring cell is kept at a constant, cooled temperature, via a coordinated heater. As a binding experiment proceeds, heat changes in the measuring cell are sensed, and power flow is reduced to the heater in order to return the cell back to the baseline. As a result, heat released from binding is coupled to the drop in the heater's output. The raw data is thus the power supplied to the heater, in joules/sec or kcal/sec, as a function of time forming the 'thermogram' characteristic of isothermal calorimetry (ITC) experiments. The heat changes in the measuring cell are calculated by integrating over the amount of time the heater takes to return the cell to the baseline temperature. The binding assays shown in section six were performed using an isothermal calorimeter.

ITC has been used to measure protein-protein interactions, protein-DNA binding, metal ion binding to proteins, and small molecule binding to proteins. In the context of protein-ligand binding, the simplest schematic involves equilibria between three species: free-ligand, protein with an empty binding pocket, and the bound complex. ITC has an advantage over other techniques in that the reaction can occur with buffers at physiologically relevant pH and salt concentration, and the proteins do not require labeling or chemical dyes (Brown 2009). At the beginning of the ITC experiment, the unbound protein is the only species in the measuring cell. As free-ligand is injected into the measuring cell via a controlled titration, the amount of bound protein progressively increases. This leads to progressively smaller and smaller peaks in the thermogram as the protein population becomes fully saturated with ligand. The heat consumed or released during each titration (q_i) is proportional to the amount of ligand that binds. This can be calculated in the following formula:

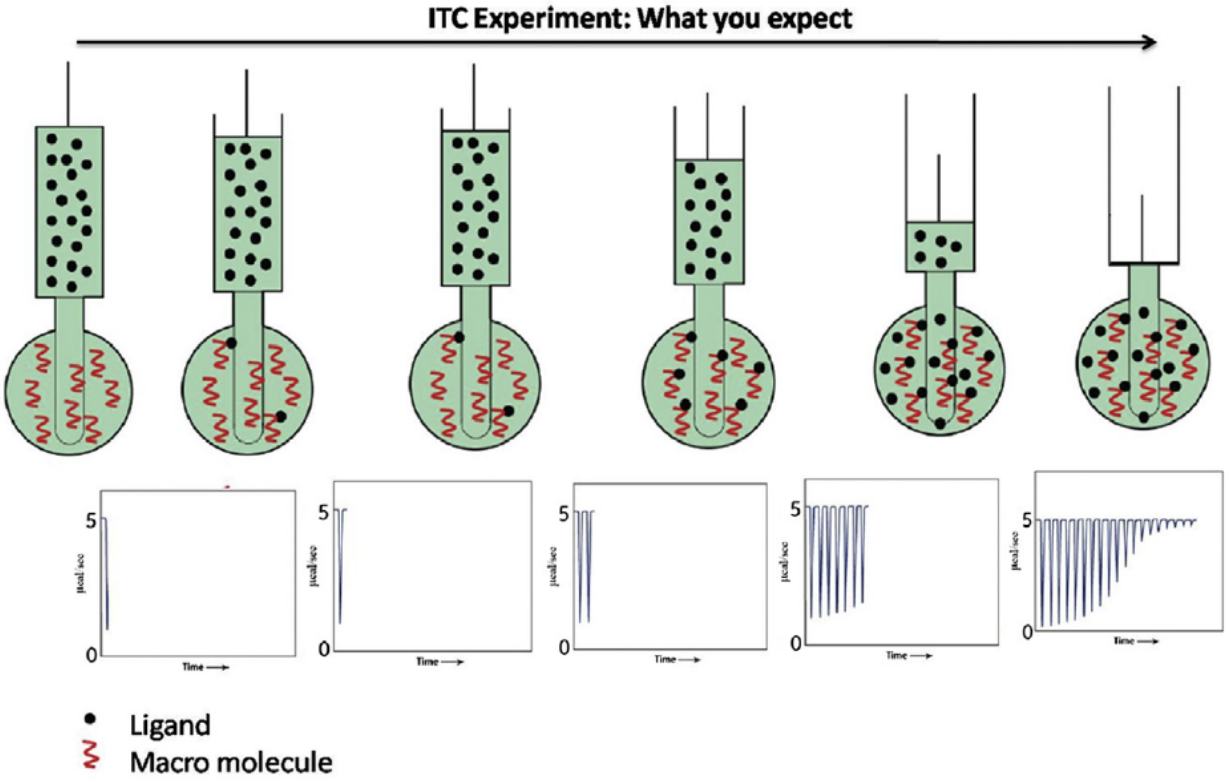

Figure 17: **An illustrated depiction of a typical ITC titration experiment.** As increasing amounts of the ligand species is injected in to the sample cell containing the protein, eventually leading to full occupation of the proteins' binding sites (top image). Each titration of ligand produces a heat change in the sample chamber, leading to each peak in the thermogram. As more binding sites become occupied, less heat change is produced from each subsequent titration. Image from (Srivastava and Yadav 2019).

$$q_i = v\Delta H \Delta L_i \tag{2}$$

where v is the total volume of the measuring cell, ΔH is the enthalpy change upon binding, and ΔL_i is the change in ligand concentration upon the i^{th} titration. Enthalpy describes the heat flow of a reaction. Exothermic binding reactions release heat as a product upon ligand binding, while endothermic reactions consume heat from their surroundings as a reactant during the binding process. After the binding reaction reaches saturation, thermogram peaks past that point represent the heat of ligand dilution in combination with the mechanical effects of mixing the measuring cell's contents. These post-saturation peaks can be subtracted from earlier pre-saturated peaks as a baseline correction for the above mentioned effects as shown in the following formula (Srivastava and Yadav 2019):

$$Q = V_o \Delta H_b [M]_t \left(\frac{K_a[L]}{x} \right) \tag{3}$$

where ΔH_b is the change in enthalpy per mole of ligand binding, $[M]_t$ is the total concentration of protein in the measuring cell, and K_a is the binding constant. ITC has the capability to assign the binding stoichiometry (n) separately from the ligand's binding affinity. The binding stoichiometry is determined from the titration equivalence point of the binding curve, the point at which the slope is the steepest. More complicated binding modes may involve multiple ligand binding sites on the protein. Proteins with two (Buczek and Horvath 2006; L. N. Lin et al. 1993; Gorshkova et al. 1995; Deka et al. 2007) and three (Freire, Schön, and Velazquez-Campoy 2009; Le et al. 2013; Osawa et al. 2005; Gustchina et al. 2013) distinct ligand binding sites have been successfully studied using ITC, representing the formation of multi-protein complexes (Rickert et al. 2004) and the binding of multi-valent ligands (Dam et al. 2000). The equation above can be adapted for second and higher order binding modalities by rewriting the equation using total ligand concentration, instead of the free ligand concentration, since the total ligand concentration is the known quantity (Brautigam 2015). These higher order binding models can be conceptually treated as either microscopic or macroscopic. Microscopic models treat each binding site individually, assuming no cooperativity of

multiple ligands binding the target, and when there is no specific order in which the binding sites must be occupied. Macroscopic binding models assume cooperativity, or step-wise occupation of the binding sites and adjust the model equations to account for co-dependent Ka values (Freire, Schön, and Velazquez-Campoy 2009).

One important experimental factor for a successful ITC experiment, involves optimizing the unitless Wiseman c-parameter (Wiseman et al. 1989):

$$c = \frac{nP_t}{K_d} \tag{4}$$

where n is the binding stoichiometry, P_t is the protein concentration in the measuring cell, and K_d is the binding affinity of the ligand. A infinitesimally tightly binding ligand produces a c-parameter that approaches infinity. A c-parameter this high produces a rectangular binding isotherm instead of the characteristic sigmoidal curve, as no ligands will dissociate from the complex under these conditions. Estimation of K_d from this rectangular isoform is difficult, although the binding stoichiometry and reaction enthalpy can be calculated. Ligands with low c-parameters, $c < 5$, form flat binding isotherms that result in similar difficulties in estimating K_d, unless the binding stoichiometry is previously known (Wiseman et al. 1989). These flat binding isotherms lack an inflection point, resulting in correlation between the enthalpy, stoichiometry, and binding affinity terms. Moderately tightly binding ligands should have c-parameters in the range of 20-100 to produce an optimal (Srivastava and Yadav 2019), sigmoidal binding isotherm. From the isotherm, the K_d is estimated from the least-squares analysis of the binding isotherm. Moderately tightly binding ligands are very sensitive to small changes in c due to minute changes in protein concentration in the measuring cell. Hence, tightly binding ligands with a low K_d value require lower protein concentrations in the measuring cell than weakly binding ligands. The K_d for very weakly binding ligands may be hard to estimate if the isotherm never reaches saturation under the experimental conditions, and if the protein concentration cannot be further increased.

To determine the ΔG, ΔH, and ΔS, in addition to n and K_d, ITC analysis software first conducts baseline correction and subtracts for the heat of dilution, typically by subtracting a blank dataset in which ligand is titrated into buffer. A binding model is chosen from the available options which

in the NanoITC analysis software can include: One Set of Sites, Two Sets of Sites, Sequential Binding Sites, Competitive Binding, Dissociation and Enzyme Assays. After choosing the one set of sites model, the program plots an initial curve, taking into account N, K (binding constant in M-1), and H (heat change in cal/mole). Next, the model is fit to the data through running 100-1000 iterations of fitting, with the goal of minimizing the sum of the residuals, meaning the calculated binding curve would follow the data points closely. The change in Gibbs Free Binding energy can be calculated as follows:

$$\Delta G = -RTlnK \tag{5}$$

The change in entropy and enthalpy can be calculated from:

$$\Delta G = \Delta H - T\Delta S \tag{6}$$

Microscale thermophoresis (MST) is a newer, powerful technique to measuring binding interactions that takes advantage of the principles underlying thermophoresis. Thermophoresis, also known as thermodiffusion, the Soret effect, or the Ludwig-Soret effect is the concerted, targeted movement of molecules in a temperature gradient. The Soret effect is observed in liquids, solids, and gases (Köhler and Morozov 2016).Thermophoresis was first described in liquids 1856 by the German physician Carl Friedrich Wilhelm Ludwig when he filled a rubber u-shaped tube with 8.98 % sodiumm sulfate solution and placed each end in either boiling or ice-water. He observed that the solute concentrated at the cold end of the tube (Ludwig 1856). The Swiss physician Charles Soret built on Ludwig's diffusion experiments, observing that solutes in a straight rubber tube, with the ends kept at 80 °C and room temperature respectively, did not remain uniformly distributed instead congregated at the cooler end (Platten and Costesèque 2004). The Soret effect can be conceptually described in the below equation (Kempers 2001):

$$\Delta X_i = -X_i(1 - X_i)\alpha_{Ti}\frac{\Delta T}{T} \qquad (i = 1, ..., N) \tag{7}$$

where X_i is the mole fraction of component i,T the absolute temperature, N the number of components, and α_{Ti} the thermal diffusion factor of component i. This equation is mostly used for calculation of Soret coefficients for different gaseous and liquid mixtures by experimental techniques such as: thermogravitational Clusius-Dickel columns (Clusius and Dickel 1938; Farber and Libby 1940), membrane cells (Saxton, Dougherty, and Drickamer 1954; Rassoul and Bott 1970), flow cells (Butler and J. C. R. Turner 1966), thermal lenses (Giglio and Vendramini 1974; K. J. Zhang et al. 1996), thermal diffusion Rayleigh scattering (Thyagarajan and Lallemand 1978; Braun and Libchaber 2002), beam deflection, ratio-cells (Agar, J. C. R. Turner, and Norrish 1960; Payton and J. C. R. Turner 1962; Longsworth 1957), and the optical transient method (Bobrova and Rabinovich 1967; Bobrova and Bukhtilova 1972). Despite the decades of investigation into the Soret effect, a comprehensive theoretical explanations for molecules moving along a temperature gradient has not been yet realized.

Current research efforts into thermophoresis focus on the local thermodynamic equilibrium for individual molecules in the temperature gradient. In 2005, Duhr and Braun studied the movement of nanoscale polystyrene spheres along a temperature gradient, produced by a infrared laser, and described the results as an exponential steady state Boltzman distribution (Duhr and Braun 2006a). The concentration of beads along the temperature gradient was exponentially dependent on the local temperature, with molecules moving away from higher temperature areas into cooler areas. Assuming the chamber was divided into small subdivisions, the local equilibria of molecules in each subdivision could be concatenated with the molecules' diffusion to produce the steady state distribution. The result of this study suggested the Soret coefficient scaled with particle or molecule size, likely due to increased solvation energy as the surface area increases. A competing camp instead aims to understand thermophoresis as a non-local equilibrium effect that relies on fluid dynamics, local force-fields around individual molecules, and particle-solvent potentials (Emery and Drickamer 1955; Voit et al. 2005). One year later after their work on local equilibrium underlying thermophoresis, Duhr and Braun expanded their work through thermodiffusion experiments on small DNA segments under multiple salt conditions, temperature gradients, and DNA sizes (Duhr and Braun 2006b). The data from this study provided further support to solvation energy of the molecules providing the underlying basis for thermophoresis where:

$$S_T = \frac{D_T}{D} \tag{8}$$

where S_T is the Soret coefficient, D_T is the thermodiffusion coefficient, and D is the constant diffusion coefficient. Building on their conclusions one year prior, Duhr and Braun extended their claim that thermophoresis can be modeled by a steady state Boltzman distribution of particles under local equilibrium and used this to build a thermodynamic foundation for estimating the Soret coefficient by taking the temperature dependent derivation of Gibbs Free energy:

$$S_T = \frac{D_T}{D} = (kT)^{-1} \left(\frac{\delta G}{\delta T} \right) \tag{9}$$

Ultimately, Duhr and Braun were able to determine the relationship between DNA and polystyrene beads' characteristics and their thermophoresis. Longer DNA segments resulted in slower thermophoresis, as did molecule hydrodynamic area. Molecule charge had a quadratic relationship with thermophoresis, suggesting hydrophobic molecules migrate at a slower rate. Finally, molecule movement had a linear relationship with temperature, showing that thermophoresis increases with increasing temperature. The work of Duhr and Braun would ultimately go on to form the theoretical basis underlying MST.

The most well known MST instruments are made by Nanotemper and include the Monolith NT.115 for the measurement of fluorescently-tagged proteins, and the Monolith NT.LabelFree for tracking unlabled proteins through tryptophan fluorescence. The basis for the technique relies on measuring the differences in thermophoresis between free protein and ligand-bound protein. Proteins can be labeled using covalently attached GFP-derivatives, or by using chemical dyes that bind with high-affinity to histidine tags (Bartoschik et al. 2018), so long as the labeling method has an excitation and emission wavelengths that falls within the three LED-filter combinations available: blue (exitation 460–480 nm, emission 515–530 nm), green (excitation 515–525 nm, emission 560–585 nm), or red (excitation 605-645 nm, emission 680–685 nm) (Seidel et al. 2013). The Monolith NT.115 requires 10-16 capillaries per experiment, each 50 μm diameter capillary tube holding a maximum volume of 4 μL. Capillary tubes are loaded with sample through dipping the tubes into the samples,

then allowing capillary action to take place. Determination of K_d, and other thermodynamic constants, requires a serial dilution of the non-labeled ligand titrated against a constant concentration of labeled protein. Since each capillary should have identical protein concentrations, the fluorescence scans of each individual capillary provide a quality control metric, allowing for identification of pipetting errors, aggregation, and adsorption to the capillary walls (Rainard, Pandarakalam, and McElroy 2018). This pre-scan can also be used to optimize the LED power if the capillaries' fluorescent profiles are either too low or greater than the detection threshold (Tso and Brautigam 2021). A temperature gradient of 2-6 °C is created sequentially for each capillary using an infrared laser with an emission wavelength of 1480 nm using a dichroic mirror, to target localized heating to the middle of the capillary with a spread of 200 μm (Jerabek-Willemsen, Chistoph J. Wienken, et al. 2011). Before the IR laser activates, initial fluorescence is recorded. The applying the IR laser induces a rapid change, on the order of 100 ms, in the fluorescence intensity, referred to at the temperature jump (T-jump), as the fluorescently-labeled proteins diffuse away from the laser's epicenter towards the ends of the capillary. The T-jump property of the fluorescently-labeled protein is dependent on its local environment, with conformational changes due to ligand binding and changes in the solvation shell slowing, or speeding up this portion of the MST trace (Royer 2006). The third region of the MST trace is a slower diffusion-limited movement of the fluorescently-labeled proteins, lasting several seconds, as the proteins form a concentration gradient along the temperature gradient. Eventually, the fluorescent signal plateaus as the thermodiffusion of the proteins is counterbalanced by the mass diffusion. The laser is turned off, and the proteins reverse course to rapidly thermodiffuse back towards the capillary's center in an inverse T-jump. The MST trace ends with the proteins approaching a new steady-state, driven purely by mass diffusion in the direction of the reversed, thermodiffusion. In principle, this backdiffusion of the labeled-proteins is reminiscent of the underlying basis of fluorescence recovery after photobleaching (FRAP) experiments (Axelrod et al. 1976).

To convert the raw MST trace data into a binding curve, the normalized fluorescence is calculated for each capillary in the serial dilution as follows:

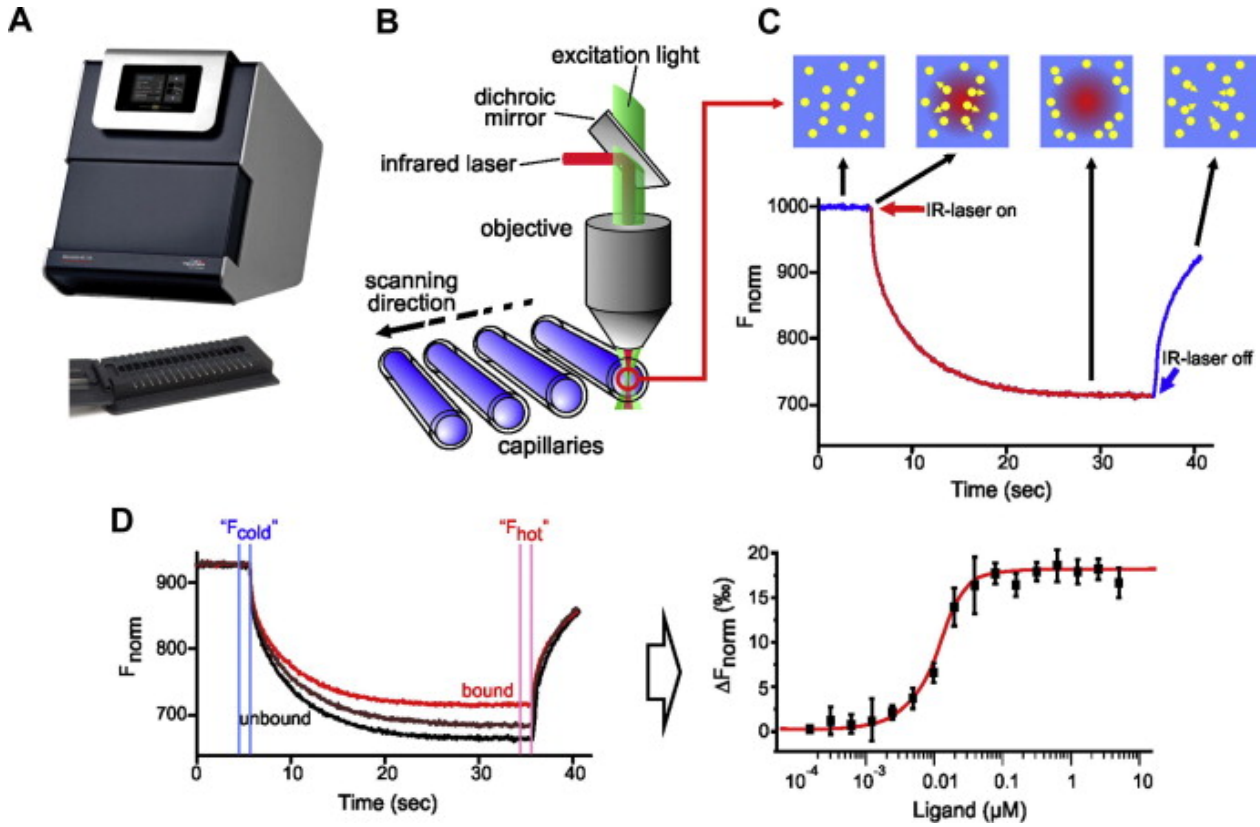

Figure 18: **A typical MST instrument setup and experimental procedure.** (A) A Monolith NT.115 instrument produced by NanoTemper Technologies. Shown underneath is the capillary tray which can hold a maximum of 16 capillaries. (B) When imaging each ~4 μL volume per capillary, the MST optics setup utilizes both a focused-IR laser to head the middle of the capillary and objective lens which allows for both excitation and detection of fluorescent proteins' movements. (C) A sample MST experiment. First, an initial fluorescence measurement is taken to ensure the proteins are homogeneously distributed in the capillaries. The IR laser is turned on, and the proteins immediately move out of the affected area, producing the 'T-Jump". After this initial fast thermodiffusion, proteins continue to thermodiffuse towards the cooler areas of the capillary. The IR-laser is turned off, and proteins rapidly thermodiffuse back into the previously heated area, producing the inverse T-Jump and further diffusion of the proteins back into the middle of the capillary. (D) A sample MST binding experimental result. The black trace line measures an unbound protein's movements and the red trace indicates the changes in thermophoresis upon ligand binding. The data is viewed as time versus the change in normalized fluorescence. Titrating in the ligand produces differences in the thermophoresis traces, which produces a binding curve. Image from (Jerabek-Willemsen, André, et al. 2014).

$$F_{norm} = \frac{F_1}{F_0} \tag{10}$$

where F_0 is the initial fluorescence before the infrared laser activates, and F_1 is the fluorescent measurement a few seconds into the thermodiffusion. The F_0 value usually requires little variation from the default selection, but the F_1 point can be adjusted to increase the signal-to-noise ratio as needed. The F_{norm} is calculated for each capillary, and plotted on the y-axis as a percent change versus the log ligand concentration on the x-axis. According to Nanotemper, the K_d model should be fit to the data unless there is observed or known cooperativity, in which case the Hill model should be chosen. The K_d curve can be fitted to the data points using three parameters in the following equation:

$$F_n = \left(\frac{B^*}{B^*_{tot}} F_{n,B*}\right) + \left(\frac{AB^*}{B^*_{tot}} F_{n,AB*}\right) \tag{11}$$

where B concentration of unbound labeled protein, B^*_{tot} is the total concentration of unlabeled protein, $F_{n,B*}$ is the F_{norm} of unbound protein, AB is the concentration of bound protein, and $F_{n,AB*}$ is the F_{norm} of the bound protein complex. The fit of the binding curve is optimized through several iterations of a Monte Carlo algorithm where, in brief, random noise from a Gaussian distribution with the same variance as the fitted model is added to the model, non-linear least squares minimization is performed, measuring the values of the three parameters with each iteration to estimate the residuals (M. L. Johnson 2008; Buckland 1984). The high and low ranges for this parameter set are used to denote the confidence interval of the fitted curve (Scheuermann et al. 2016). On the sigmoidal curve, the K_d value is equal to the inflection point and denotes the concentration at which half of the ligand occupies binding sites on the protein.

5.1.5 IP_3R Inhibitors and Agonists

Deregulated calcium signaling and alteration of IP_3R activity has been implicated in a host of pathophysiological states, involving both metabolic and neurodegenerative disorders, as well as in

several cancers. Currently, detailed knowledge of IP_3Rs' role in the disease state is lacking due to the dearth of pharmacological tools to effectively modulate their behaviour in vivo and in vitro. What limited agonists and antagonists exist are imperfect, lacking isoform specificity or having low potency and, in the case of the antagonists, lacking specificity to IP_3R itself. In the search for and development of isoform specific agonists and antagonists, co-ligand structures are an invaluable starting point for structure-based drug design of therapeutics which ultimately can be used to restore physiological IP_3R-mediated calcium signaling in the clinical setting, such as using an IP_3R-3 specific antagonist to prevent motor neuron death in ALS patients (E. F. Smith, Shaw, and De Vos 2019).

The natural agonist of all IP_3R isoforms and variants across all cell types, tissues, and organisms is IP_3. IP_3 is a water-soluble compound created through the hydrolysis of PIP_2 by PLC in the PM into both IP_3 and the membrane-bound diacylglycerol. IP_3 has a molecular weight of 420.10 g/mol, with three phosphate groups attached to the 1, 4 and 5 positions on the central inositol ring. Positions 2, 3, and 6 are occupied by hydroxyl groups. Ultimately, the three phosphate groups give IP_3 a net-negative charge, allowing the compound to bind to positively charged residues in the IBC of rIP_3R-1: R265, T266, T267, G268, R269, R568, R504, K508, R511, Y567, and K569 (Bosanac, Alattia, et al. 2002). The P4 phosphate group primarily coordinates residues on the βTF-2 domain (R265, T266, T267, G268, R269 with K569 as the exception) while the P5 phosphate group primarily coordinates residues on the ARM1 domain (R504, K508, R511 and Y567, with R265 and R269 the exceptions). IP_3 binding results in a clamshell-like closing of the IBC. Of the basic residues in the IBC, R265, K508 and R511 have been identified through mutational analysis as critical for IP_3 binding (F. Yoshikawa, Morita, et al. 1996) Through structure-functional analyses, the P4, P5, and hydroxyl group at the 6th position of IP_3 were deemed critical for receptor activation (Robert A Wilcox et al. 1998).

The first category of IP_3R agonists discovered and categorized were the Adenophostins. Adenophostins A (AdA) (Figure 19) and B (AdB) were first identified from *Penicillium brevicompactum* SANK 11991 and SANK 12177 fungal cultures, originally harvested from soil samples from the Hokkaido and Nagasaki prefectures in Japan in 1993. AdA and AdB were produced under fermentation condi-

tions and subjected to multiple rounds of acetone extraction from 680 L culture broths. Afterwards, both compounds were determined through radioligand binding assays to have Ki values of 0.18 nm, compared to 15 nm for the endogenous ligand IP_3. AdA was also found to be 10-fold more potent than IP_3 at inducing channel activation(M. Takahashi et al. 1993). These compounds would go on to serve as the basis for designing more specific IP_3R agonists. One natural question that arose was which parts of the adenophostin compounds were most responsible for their function and binding, including specifically the purpose of the adenine moiety. One of the first SAR studies of synthetic AdA analogs demonstrated that the adenine ring, or an equivalent aromatic substitute, was critical for high affinity binding (Correa et al. 2001). The adenine ring was proposed to have either a direct interaction with the IBC by participating in supplementary binding interactions with residues near the binding site (Riley et al. 2001), or indirectly through repositioning the 2'-phosphate group in order to strengthen its coordination (R. A. Wilcox et al. 1995). One group from the University of Bath synthesized all possible biphosphate analogs of AdA, which itself contains two phosphate groups, in order to test the SAR of the phosphates and adenine moieties (Sureshan et al. 2009) . They found that removing the 2'-adenine group reduced the binding affinity by 400-fold compared to IP_3. Two phosphates at the 3" and 4" positions of AdA, comparable to phosphates at the P-4 and P-5 positions on IP_3, were found to be critical for high affinity binding with the IBC, but compounds with phosphates at different positions could also activate IP_3R, albeit with much lower potency. From this study, it was determined that the 4' phosphate on IP_3 was critical for the interaction with the βTF-2 domain, but the 5' phosphate could be replaced with a cation-pi interaction between the adenine on AdA and R504 (Sureshan et al. 2009).

In study published in 2015, AdA was modified by replacing the adenine with a triazole ring in order to simplify the synthesis of AdA analogs utilizing azide-alkane click-chemistry, which would theoretically speed up the time from synthesis to SAR determination (Vibhute, Konieczny, et al. 2015) (Figure 19). Importantly, the replacement of the adenine with the triazole ring did not affect the AdA analog's potency. This study was used as the basis for another strategy for making a more potent IP_3R agonist, which involved synthesizing a tetrameric ligand, thinking this may improve activity since all four IP_3 binding sites must be occupied to stimulate channel gating (Alzayady, Wagner, et al. 2013). The same group behind the 2015 study tested this hypothesis

by designing dimer compounds of their AdA-triazole analogs containing oligoethylene glycol chains of four different lengths (Vibhute, Pushpanandan, et al. 2016). The dimerized agonists failed to increase their potency compared to either original AdA or parent AdA-triazole analog, and interest in this strategy waned (Vibhute, Pushpanandan, et al. 2016). In addition to the dimerized triazole strategy, other groups have made inroads starting from the original AdA compound, and synthesizing AdA-analogs in unexplored synthesis spaces. These new modifications of the original AdA compound involved varying the sugar compounds, nucleobase motif, the positions of the phosphates, and progressively trimming the compound to determine the essential moieties (Correa et al. 2001). Most of the compounds produced in this study had potencies equivalent to AdA and provided excellent characterization of moieties critical for AdA and IP_3 coordination to the binding pocket, but could not improve upon them. In 2019, progress was made in the synthesis of a new compound more potent than AdA while investigating the effects of different inositol sterioisomers on IP_3R activation. D-myo inositol derivates are common in regulating ion channel biology, with IP_3 belonging to this sterioisomer class (M. P. Thomas, Mills, and B. V. L. Potter 2016). The D-chiro-inositol sterioisomer derivatives (Figure 22) are rarer in Eukarya by comparison and are typically isolated from plants (Horbowicz, Brenac, and Obendorf 1998). In this SAR study, the alpha-glucopyranosyl unit in AdA was replaced with a D-chiro-inositol cyclitol biphosphate, which increased this compounds potency relative to AdA, with an EC_{50} value of 21 nM compared to EC_{50} value of 35 nM for AdA (Dohle et al. 2019).

Very recently in 2020, one group successfully synthesized an agonist that is both more stable than IP_3 and more resistant to the cell's degradation machinary (Mills et al. 2020). This was done starting from glucopyranoside 2,3,4-triphosphate, which is considered to be the simplest glucose-based mimic of AdA and a great starting space for novel synthesis strategies (Jenkins and B. V. Potter 1996). Glucopyranoside 2,3,4-triphosphate is 10-fold less potent than IP_3, indicating the importance of the adenine and ribose sections in the derivative compound (Correa et al. 2001) but is resistant to degradation by 5-phosphatase and 3-kinase (R. A. Wilcox et al. 1995). Thus, d-chiro-Inositol Ribophostin was synthesized applying the glucose-substitution and D-chiro inositol approaches. This compound was more potent than IP_3, and only 2-fold less potent than AdA. More groups are now building on the successful synthesis of d-chiro-Inositol Ribophostin by starting the synthesis using D-glucose or L-glucose templates in the hopes of improving potency while keeping

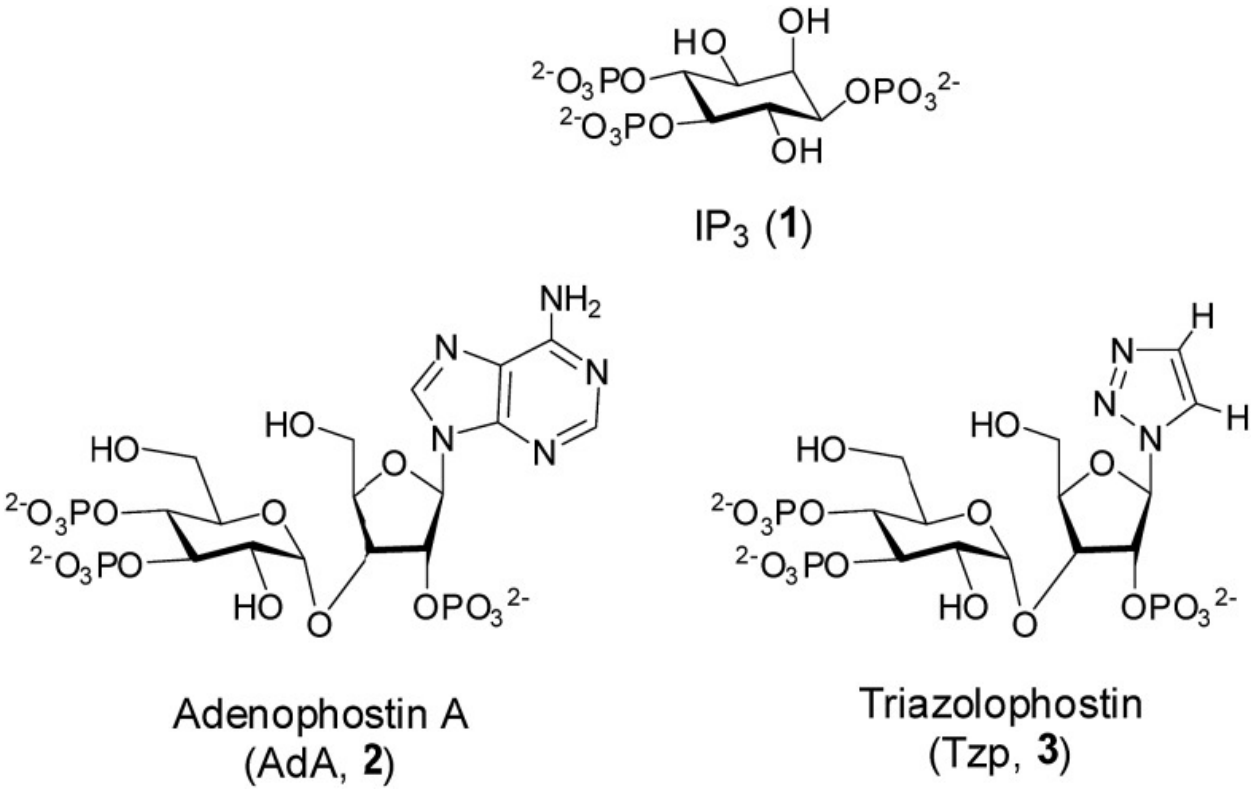

Figure 19: **Comparison of IP_3, Adenophostin A, and triazolophostin chemical structures.** The chemical structures of IP_3 (top), adenophostin A (AdA) (left), and triazolophostin (Tzp) (right). Ada and Tzp contain phosphate motifs similar to those in IP_3. Image from (Vibhute, Pushpanandan, et al. 2016).

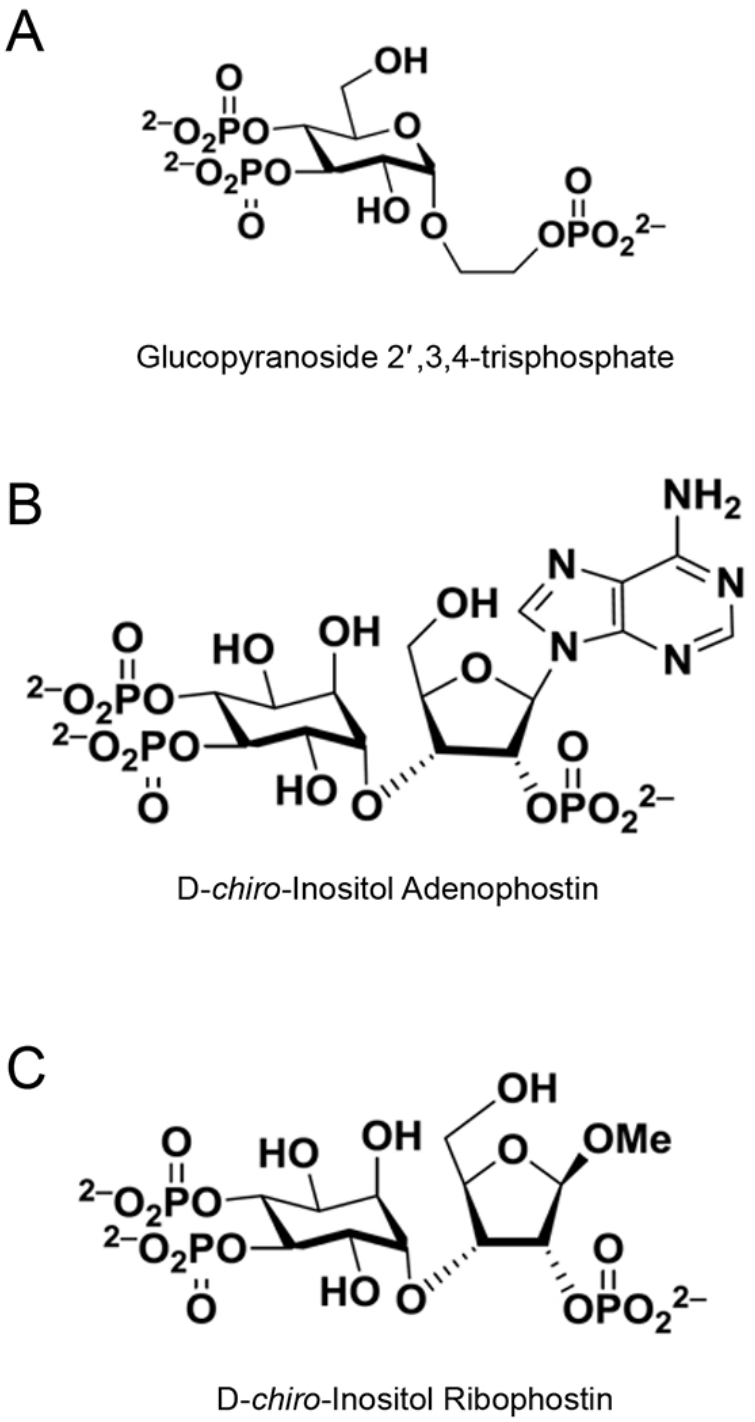

Figure 20: **D-Chiro AdA derivative compounds produced as potential IP_3R agonists.** Chemical structures of Glucopyranoside 2,3,4-trisphosphate (A) an IP3R agonist 10-fold less potent than IP3, D-chiro-Inositol Adenophostin (B) and D-chiro-Inositol Ribophostin (C) which is 2-fold less potent than AdA. Image from (Gambardella, Morelli, et al. 2021).

the resistance to IP_3-specific degradation (Shipton et al. 2020). The problem with all of these efforts, is that none of these agonists are isoform specific. Some SAR studies have suggested that the 2' and 3' positions on IP_3 are key determinants of subtype specificity (Nerou et al. 2001; Mochizuki et al. 2010), but more work is required apply this knowledge towards making the existing agonists isoform specific. Complicating structure-based drug design approaches to create isoform specific agonists is the one existing cryo-EM structure of rIP_3R-1, purified from rat cerebellum, in complex with AdA (Fan, M. R. Baker, Zhao Wang, et al. 2018). In this structure, the AdA compound is modeled incorrectly, with the sugar represented as a xylose instead of a ribose, and AdA's density in the IBC is poorly resolved despite the higher binding affinity compared to IP_3 (Gambardella, Morelli, et al. 2021). Atomic resolution structures of each IP_3R isoform with either AdA or derived analogs will greatly improve current efforts to create potent, isoform specific compounds that could be used as effective pharmacological tools in studying IP_3R activity.

Synthesis and development of IP_3R specific inhibitors has been less straightforward and more exploratory than the search for IP_3R specific agonists, due largely in part to the lack of a good staring template. The majority of the commercially available IP_3R antagonists function by competing against IP_3 for the IBC. To achieve a better binding affinity towards the IBC, the antagonists would have to have similar chemical moieties to those found in IP_3. However, if the antagonists' structure are too chemically similar to IP_3 then the compound risks having partial-agonist action. A few antagonist classes have different chemical structures from IP_3, but with these classes often have an unclear mechanism of action. The glycosamninoglycan heparin is a membrane-impermeable competitive antagonist of IP_3R-mediated Ca^{2+} release (Ghosh et al. 1988). Although heparin can exist in multiple oligimer states, only heparin of 4-6 kDa has been shown to act as an IP_3R antagonist since it is a polycation and may partially mimic the three phosphate groups of IP_3. In one of the original studies on heparin as a competitive angatonist in the 1980s, heparin was determined to have a K_i of 2.7 nM and could inhibit fully active IP_3Rs within 20 seconds (Ghosh et al. 1988). This high affinity of heparin binding towards the IP_3 binding site is the major reason why early affinity purification efforts of IP_3Rs from native tissue utilized heparin columns (Supattapone et al. 1988). While heparin binds to IP_3R with high affinity, there are many off-target affects due to non-specific binding to other protein targets such as: the uncoupling of GPCRs from the G-proteins (Willuweit

and Aktories 1988; Dasso and C W Taylor 1991), activation of RyR (I. B. Bezprozvanny et al. 1993), and inhibition of IP_3-kinase (G. Guillemette et al. 1989). To assess the affect of heparin on each of the three IP_3R isoforms, IP_3-evoked Ca^{2+} release was measured through fluorescence-based assays with the fluorescence indicator 20 μM Mag-fluo-4AM in the ER lumen in a DT40 knock-out cell line for all IP_3R isoforms. Experiments in DT40 cells expressing any of the IP_3R isoforms showed a competitive antagonist mechanism for heparin (Saleem et al. 2014). Radioligand binding assays in the same study measured heparin's binding affinity to each isoform, and determined the order of binding affinity as being highest to type 3, followed by type 1, then type 2. One of the conclusions of this study was that IP_3R-3 was the most susceptible to inhibition by heparin in native cells due to the combination of lower innate binding affinity to IP_3 and higher heparin affinity compared to the other two isoforms.

A group of well known IP_3R inhibitors named Xestospongin A, B, C, and D (Figure 21) were isolated from the Australian marine sponge *Neopetrosia exigua*, formerly known as *Xestospongia exigua*, in 1984 and their chemical structures characterized through X-ray diffraction of crystallized samples (M. Nakagawa et al. 1984; Hoye, North, and Yao 1994). In vivo, these macrocyclic bis-1-oxaquinolizidines were found to be vasodilative, relaxing blood vessels in the same mechanism as related vasodilative compounds araguspongine B, C, and demehylxestospongin B which were also extracted from marine sponges *Xestospongia exigua* and *Xestosponginia muta* (Kobayashi, Kawazoe, and Kitagawa 1989; Althagbi et al. 2020). The first report of the Xestospongin compounds' activities came in 1997 when it was demonstrated that A, C, D, and modified B could block IP_3R-mediated Ca^{2+} release from microsomes (Gafni et al. 1997). In the same study, the binding affinity of each Xestospongin compound was measured through radioligand binding assay, showing that Xestogponsin C (XeC) bound to IP_3Rs purified from rabbit cerebella with the highest binding affinity (IC_{50} = 358 nM) and could inhibit Ca^{2+} flux from IP_3-sensitive store, but not ryanodine sensitive calcium stores. Demehylxestospongin B in the same study demonstrated the lowest potency of the xestospongin compounds, with an IC_{50} of 5865 nM, 16-fold less potent than xestospongin C. This study was the foundation for other research groups investigating the binding affinities and potencies of xestospongin derivative compounds. In the same vein, two derivatives of the demehylxestospongin B compound, 7-OH-XeA and araguspongin C (ArC), confirmed the inhibitory properties of the xestospongin class of compounds on IP_3R-mediated calcium release. Both

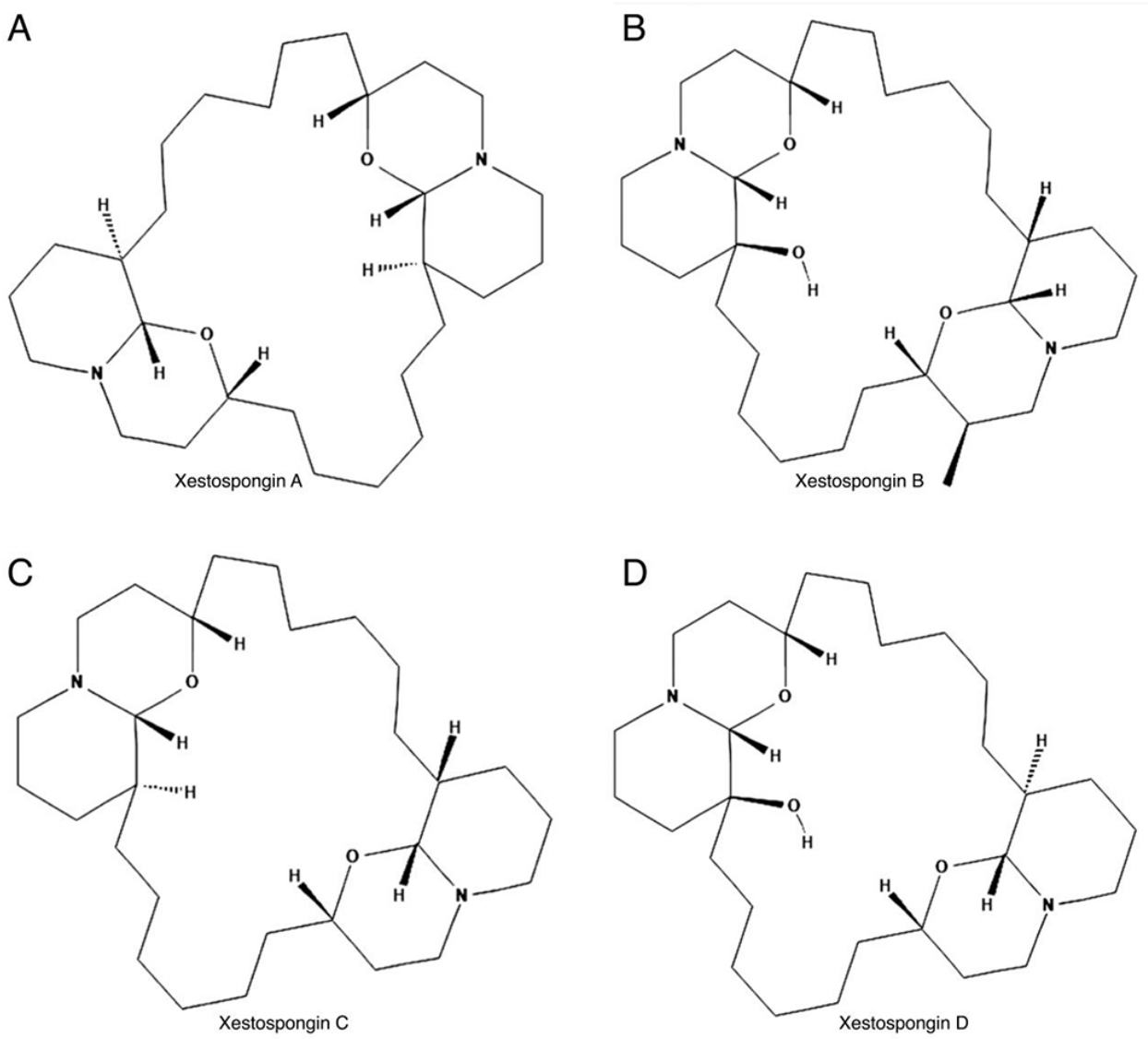

Figure 21: **The four original Xestospongin IP_3R inhibitors.** Chemical structures of the four Xestospongin (Xe) compounds originally described in (M. Nakagawa et al. 1984; Hoye, North, and Yao 1994). XeA (A), XeB (B), XeC (C), and XeD (D). Image from (Gambardella, Morelli, et al. 2021).

compounds demonstrated 10 to 15-fold less potency than XeC (Ta et al. 2006). The xestospongin C mechanism of action to block IP_3R-mediated Ca^{2+} flux has remained elusive. The original study on xestospongin C showed that the compound was capable of blocking IP_3R activity without binding to the IP_3 binding site, but the location of its proposed binding site has not been identified. In the early 2000s, experiments were done to confirm that XeC was not only truly membrane-permeable, but also capable of competing against IP_3 to block IP_3-mediated calcium flux in permeabilized cells (Oka et al. 2002). A similar study, conducted in guinea-pig smooth muscle cells, confirmed that 3 μM XeC could block IP_3R-mediated calcium flux, but upon further investigation the inhibitor was determined to actually block voltage-dependent calcium channels with an IC_{50} value of 0.63 μM (H. Ozaki et al. 2002). The authors then propose a functional mechanism by which XeC can non-specifically inhibit IP_3R: the elongated lipophilic core of the compound, surrounded by charged nitrogen groups on the exterior, may fit inside the IP_3R channel pore. This hypothesis may explain how XeC can selectively inhibit IP_3Rs in permeabilized cells, but not in whole cells. Additional studies suggest that XeC can also inhibit SERCA, L-type Ca^{2+} channels, Ca^{2+} activated K^+ channels, and Ca^{2+} store/capacitative calcium entry (Smet et al. 1999; Castonguay and Robitaille 2002; Solovyova et al. 2002). Even though many different groups use XeC as an IP_3R inhibitor, inhibition of IP_3-mediated calcium flux is not consistent between groups (Solovyova et al. 2002). Another group also attempted to use XeD to inhibit IP_3R in the HT22 neuronal cell line, but reported only partial blocking of the channel (Duncan, Hwang, and Koulen 2007). One study attempted to resolve the basis for the inconsistent inhibitory effects of the Xestospongin class on IP_3R activity. This group used the original concentrations of XeC and XeD (Gafni et al. 1997) to block IP_3R Ca^{2+} flow in both permeabilized and intact cells, and they found that XeC and XeD are capable of inhibiting a small fraction of IP_3R-activity, but true pharmacological inhibition occurred at the maximal used concentrations in the study, which was 20 μM for both compounds(Saleem et al. 2014). The ultimate downside to using Xestospongins is that they are weak inhibitors and have multiple off-target effects in whole cells.

2-Aminoethoxydiphenyl borate (2-APB) was first synthesized in 1954 by Ronderstvent from triphenylboranes and ethanol amine (Rondestvedt, Scribner, and Wulfman 1954). In 1997, the Ozaki group was the first to show that 2-APB can inhibit IP_3R, located in rat cerebellar microso-

mal preparations, with an IC_{50} of 42 μM without competing against IP_3 for the IBC (Maruyama et al. 1997). Although they did not conduct experiments in that study to test the specificity of 2-APB to IP_3R, they postulated that the compound had potential as the first membrane-permeable IP_3R inhibitor. In 2001, the non-specificity of 2-APB to IP_3R was confirmed, as 2-APB was shown to block capacitative calcium entry in cells lacking IP_3R, indicating that 2-APB can inhibit proteins involved in Store-operated calcium entry (Iwasaki et al. 2001), although the identity of these proteins was not confirmed until 2005 and 2006, respectively for STIM1 and Orai1 (Liou et al. 2005; Feske et al. 2006). Since these initial reports, 2-APB has been used by many different groups as a membrane permeable IP_3R inhibitor (Missiaen et al. 2001; Maruyama et al. 1997), even though the compound can also bind to and inhibit SERCA (Bilmen et al. 2002) and store-operated Ca^{2+} entry (Goto et al. 2010). 2-ABP at 50 μM appears to bind to and inhibit the IP_3R-1 isoform without preventing IP_3 binding (Saleem et al. 2014). IP_3R-3 activity was inhibited at higher 2-APB concentrations (100-300 uM), but the mechanism of inhibition seemed to be blockage of the ER calcium uptake through SERCA instead of specific inhibition of IP_3R. In this study, IP_3R-2 did not respond to treatment with 2-APB, which replicated findings from other groups (Gregory, Rychkov, and Barritt 2001; Hauser et al. 2001; Kukkonen, Lund, and Åkerman 2001; Bootman et al. 2002; Soulsby and R. J. H Wojcikiewicz 2002). Several groups have used 2-APB as the basis for design of inhibitors that can selectively target SOCE, while avoiding off target effects from binding to SERCA and IP_3R. The Mikoshiba group tried to improve the specificity and potency of 2-APB for SOCE, and examined two structurally isomeric analogs from their library of over 600 2-APB derivatives: DPB162-AE and DPB163-AE(Goto et al. 2010). Both analogs contained similar diphenylborate motif, with the linker being the only difference between the analogs. Both compounds were approximately 100-fold more potent than 2-APB and could inhibit SOCE, although DPB163-AE activated SOCE at low concentrations in a similar manner to 2-APB. The current most potent 2-APB analog came from this group that has previously synthesized 493 2-APB analogues (H. Zhou et al. 2007; Suzuki et al. 2010; S. Ozaki, Ebisui, et al. 2010). From this ensemble of compounds, inhibitor-911 was found to have an IC_{50} measurement of 0.2 mM as measured by SOCE and IP_3 IP_3-induced calcium release assays. (S. Ozaki 2014). Ultimately, 2-APB derivatives have yet to achieve specificity to either IP_3R or Orai1, and broadly inhibit cytosolic calcium flux.

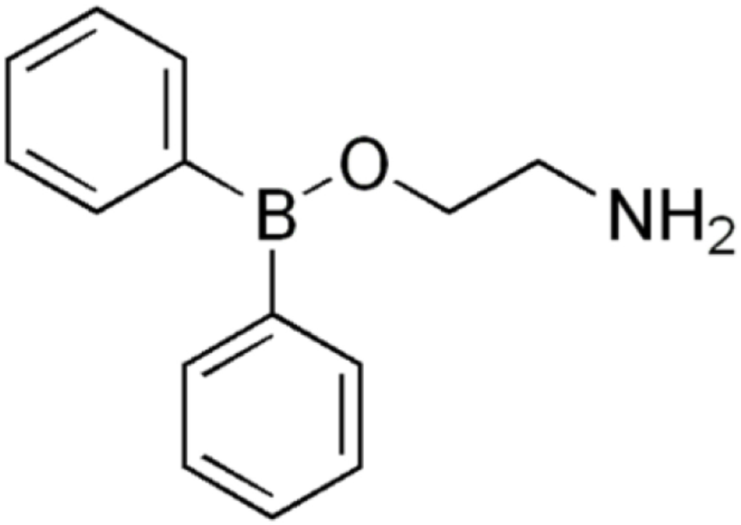

Figure 22: **Chemical structure of the non-specific IP_3R inhibitor 2-Aminoethoxydiphenyl Borate (2-APB).** A membrane-permeable IP_3R antagonist with an IC_{50} value of 42 μM. Image from (Gambardella, Morelli, et al. 2021).

5.2 The Cryo-EM Resolution Revolution

5.2.1 A historical perspective

Electron microscopy has its origins in the 1930s with the work of Ernst Ruska and and Max Knoll. In 1931, the first prototype of a transmission electron microscope was capable of 400x magnification and relied on short-focus magnetic coils to act as lenses to focus the electron beam (Ruska 1987). This was the theoretical basis for future generations of electron microscopes, relying on magnetic fields to deflect electrons and lens systems to focus the beam onto the sample. Ruska improved upon the initial design two years later in 1933, increasing the magnification to 12,000x by using a thin slice of metal to remove divergent electrons from the central beam. This improved version was optimized and mass produced starting in 1938 by the firm of Siemans and Haske (Big 1956). Hardware advancements for the transmission electron microscope came in the 1960s via the work of DeRosier and Klug in their work characterizing the T4 bacteriophage tail (De Rosier and A. Klug 1968). The duo aimed to solve three major bottlenecks: preservation of the sample under high vacuum conditions, mitigating the radiation damage caused by electrons hitting the sample, and the inherent low contrast of biological samples. Their solution was soaking their bacteriophage samples in heavy atom salts, primarily uranyl acetate, to create an electron dense cast around the

sample. This strategy increased sample contrast, allowed for the preservation of the sample in the vacuum chamber, and mitigated radiation damage as the heavy atom cast was imaged rather than the delicate sample. This was the birth of negative stain electron microscopy, named such because the heavy atom cast scattered electrons more strongly compared to the weaker scattering by the interior protein (Eva Nogales 2016). However, negative stain microscopy was limited to about 15 Å resolution due to the nature of the technique. A jump in possible resolution occurred through the efforts of Taylor and Glaeser in the 1970s, where cryopreservation methods were developed to preserve high-resolution information in the biological samples (K. A. Taylor and R. M. Glaeser 1974). However, the biological samples used by Taylor and Glaeser were frozen, hydrated catalase crystals, and since not all samples readily crystallize improvements in cryopreservation needed to occur in order to launch cryo-EM as a technique. The first attempt of preparing non-crystalline samples for cryo-EM was pioneered by Dubochet and his colleagues, where cryo-plunging samples into liquid cyrogens ethane or propane propelled cryo-EM into more popular use among biologists (Dubochet et al. 1982).

Initial targets of single particle cryo-EM were helical samples, viral capsids, and 2D crystals since 3D reconstruction techniques lagged behind advances in both hardware and sample preparation. Henderson and colleagues used 2D crystalline arrays of bacteriorhodopsin in 1990 to generate an atomic resolution structure (R. Henderson, J. M. Baldwin, et al. 1990), which was used as the basis for GPCR structure determination via homology modeling for years afterwards. In determining the bacteriorhodopsin structure, both micrograph images and electron diffraction patterns were combined. However, 2D electron crystallography relies on both tilting the sample to generate more views of the protein and the sample producing a nicely ordered, perfectly flat 2D crystals. Nevertheless, 2D electron crystallography produced several atomic resolution models, including tubulin (E. Nogales, S. G. Wolf, and Downing 1998), the plant light-harvesting complex (W and Dn 1991), and aquaporin at 1.9 Å resolution (Gonen et al. 2005). Icosahedral viruses were the first non-crystalline structures to generate nanometer resolution with single particle electron microscopy due to their inherent high symmetry, allowing secondary structures to be visualized (Böttcher, Wynne, and R. A. Crowther 1997; Conway et al. 1997). These highly symmetrical viral capsids would produce atomic resolution maps in the late 2000s (Xing Zhang et al. 2008). In 1991, the Frank

group determined the structure of the 70S Escherichia coli ribosome, the first non-symmetrical protein structure to be determined with single-particle EM (Frank et al. 1991).

5.2.2 Recent Hardware Developments

By the 1990s, structure determination via electron microscopy remained in the minority compared to more established techniques such as X-ray crystallography and NMR, with EM structures earning the infamous moniker 'blobology' (Saibil 2017). In the period of 10 years, starting from the first sub-nanometer viral capsid structures, research labs across the globe began using cryo-EM in earnest to investigate the quartenary and tertiary structures of a variety of targets, including the IP_3R (Kozo Hamada, Terauchi, and Katsuhiko Mikoshiba 2003; Serysheva, Hamilton, et al. 2005; Q.-X. Jiang et al. 2002; C. Sato, K. Hamada, et al. 2004). Two major categories of EM hardware allowed for the genesis of the cryo-EM 'resolution revolution': advances in microscope hardware and the availability of direct electron detectors. In terms of hardware developments, improvements have been made in the electron source moving from older generation lanthanum hexaboride crystals (LaB6) and tungsten filaments to both cold and hot field emission guns (FEGs). LaB6 and tungsten filaments work though heating the materials until the voltage potential is greater than the work function of the material, allowing electrons to break free of the material and enter the microscope column as part of the beam (Thompson et al. 2016). Operating voltages for microscopes with these electron sources is typically 80-200 kV. FEGs operate at higher voltages, typically 200-300 kV, and form brighter, more coherent beams that allow for a higher, final theoretical resolution of the sample (Z. H. Zhou and Wah Chiu 1993). Although higher operating voltage can increase the final resolution, there is a corresponding increase in radiation damage in the sample and a decrease in image contrast.

In addition to the FEGs and higher acceleration voltages, hardware advancements came in the form of improved vacuums, more stable cryo stages, and improvements in lens systems. More precise adjustments in the lens systems allowed for minimization of phase errors due to axial coma, an abberation that occurs when the microscope's illumination is not perfectly parallel with the optical axis of the objective lens system (Robert M. Glaeser et al. 2011). Modern microscopes are

also fully computerized, allowing for precise microscope alignment, defocus, and controlling data collection conditions. For example, a common method of data collection is 'low-dose mode', which aims to reduce radiation damage by having the first electrons that hit the sample be used in image formation (Unwin and R. Henderson 1975; R. C. Williams and Fisher 1970; Ohtsuki and Zeitler 1975; Fujiyoshi et al. 1980). Both the Titan Krios by Thermo Fisher and the JOEL 3200 by JOEL implemented the above advances to reduce specimen drift and perturbances from the environment in addition to switching from side entry sample loading to autogrids.

Arguably, the most important hardware advancement has been the direct electron detector (DED). The type of detector used is critical for the quality of data collected. The two parameters used to evaluate detector performance are: the modulation transfer function (MTF), and the detective quantum efficiency (DQE). The MTF measures the response of the detector in the frequency range of the microscope, while the DQE is the ratio of input to output signal-to-noise ratio, which is itself a measure of signal and noise variance (Ruskin, Z. Yu, and Nikolaus Grigorieff 2013). Historically film was the preferred method to record data, as the DQE was approximately 0.3 and large areas of the grid could be imaged (McMullan, S. Chen, et al. 2009). Between 2002-2012, several structures that broke the 14 Å threshold were collected on film and stored in the electron microscope database (EMDB) (Xing Zhang et al. 2008; X. Yu et al. 2011; M. Wolf et al. 2010; Xinzheng Zhang et al. 2012; Liu et al. 2010; Estrozi and Navaza 2010; Settembre et al. 2011; D.-H. Chen et al. 2011). In spite of the excellent DQE, imaging using film was not time-effective as the data had to be collected on film, digitized, then processed. This prevented automation since users could not adjust on the fly. One of the first alternatives to film was the charge-coupled device (CCD) cameras. The DQE for CCDs was lower than that of film at approximately 0.1 DQE, but eventually supplanted film due to their ability to easily integrate with software for automated data collection (Faruqi 1998; Sander, Golas, and Stark 2005). CCDs have recently been supplanted by the advent of direct electron detectors (DEDs), which record electron hits directly instead of utilizing the CCD strategy, which was to first digitize the electrons as they hit a scintillator. DEDs can improve the signal-to-noise ratio of images by directly counting the electrons in low-dose mode (McMullan, Clark, et al. 2009), although this can still saturate the detector. To prevent this, modern microscopes allow for data collection in 'movie-mode', which allows for the electron dose

to be fractionated among a multi-second exposure, collecting images at a frame rate of about 0.2 s/frame. The 20-30 movie frames each contain low-contrast images due to the 1-2 electrons that hit per image, but the images can be combined computationally during data processing (Binshtein and Ohi 2015).

5.2.3 Recent Software Developments

While the hardware advancements detailed previously were instrumental in initiating the cryo-EM resolution revolution, complementary advancements in both image processing software and computation were critical components. The basis for single particle analysis has been the breath of algorithms to correctly center and align 2D projections, or Fourier transforms, of particles in order to build the 3D reconstruction. The major challenges in building the 3D reconstruction has been the noisiness of the underlying micrographs and the need to precisely align the different particle orientations. Before the DEDs became commercially available, millions of particles needed to be collected and averaged in order to overcome the inherent noise. With DEDs improving the DQE, the required particles for a successful 3D reconstruction dropped on the order of thousands.

One of the first methods developed to match the relative orientations of the 2D projection images was the projection matching approach by Joachim Frank's group in 1994 (Penczek, Grassucci, and Joachim Frank 1994). In this approach, every image of the particle is compared to a low-resolution 3D reference and the angle of each particle is assigned based on cross-correlation. The initial 3D reference can be computationally generated from the micrographs, or from collecting data at different tilt angles such as the random conical tilt method (Radermacher et al. 1987). An alternative to the random conical tilt is to determine the relative orientation of the 2D projections using the 'common line' approach in either Fourier space (Richard Anthony Crowther, Huxley, and Aaron Klug 1971) or real space (Van Heel 1987). However, neither common lines approach will solve the handedness of the protein. Early image processing software incorporated the aforementioned image-alignment methods in Spider (Joachim Frank et al. 1996) and Imagic (Heel et al. 1996). The next generation of image processing software EMAN (S. J. Ludtke, P. R. Baldwin, and W. Chiu 1999) and EMAN2 (G. Tang et al. 2007) were developed in the late 1990s by Wah Chiu and Steven Ludtke in an attempt to make data processing available to non-experts. In 2007, Frealign improved

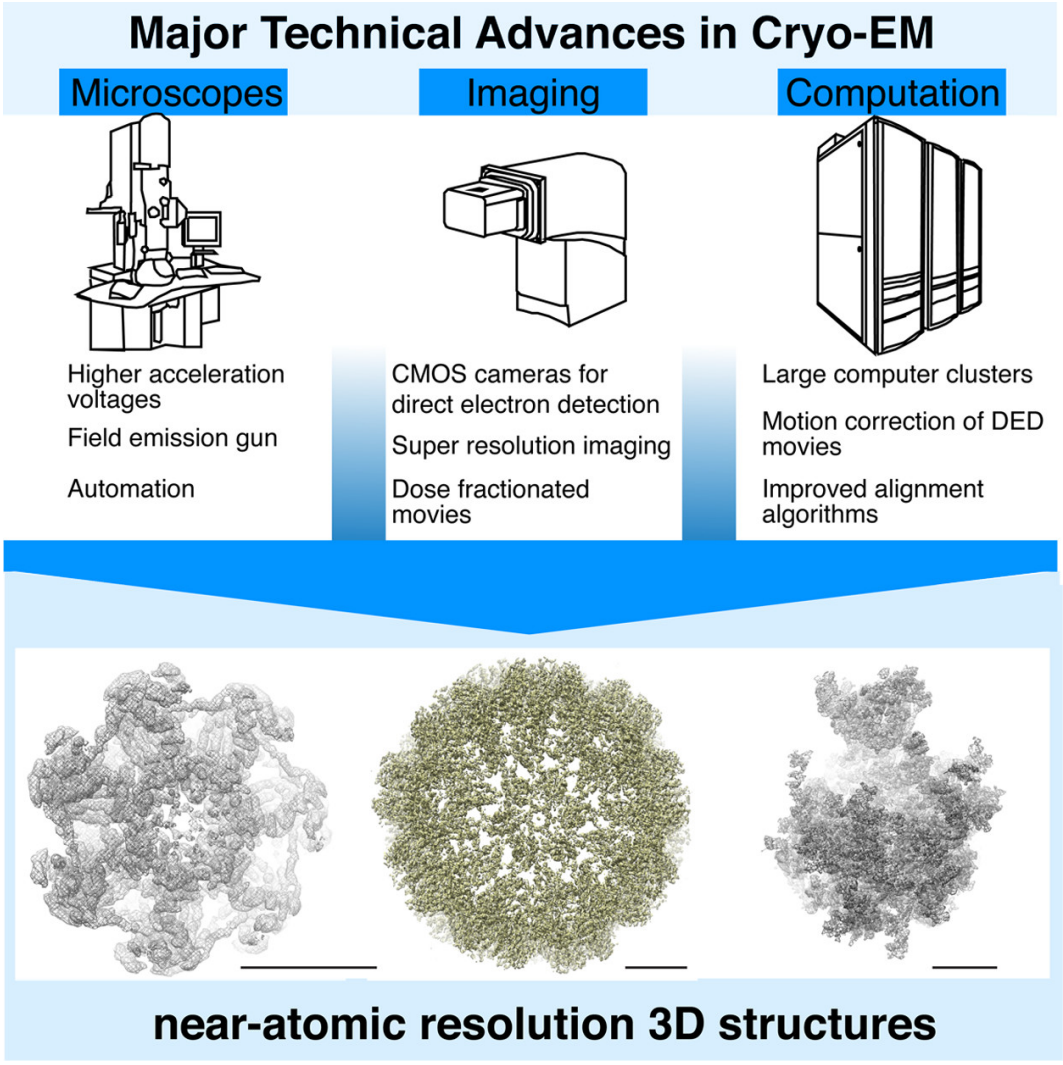

Figure 23: **The major technological advances that have led to Cryo-EM's 'resolution revolution'.** Example high resolution cryo-EM structures that have benefited from the shown technological advances in microscope equipment. These include the 3.3 Å 20S proteasome (EMDB-562370), the 3.8 Å Brome Mosaic Virus (EMDB-6000107), and the 3.2 Å yeast mitochondrial large ribosomal subunit (EMDB-256683). The scale bars in the three structures each represent 50 Å. Image from (Binshtein and Ohi 2015).

contrast transfer function correction and advanced 3D refinement through iteratively improving the density and reassigning the 2D projection images' angles (Nikolaus Grigorieff 2007).

The most popular image processing software suites are Relion (Sjors H. W. Scheres 2012), cisTEM (Grant, Rohou, and Nikolaus Grigorieff 2018), and cryoSPARC (Punjani et al. 2017). All three enable users to separate particles based on structural heterogeneity, in the form of both conformational heterogeneity and differences in the makeup of protein complexes (Fernández, Bai, Hussain, et al. 2013; Fernández, Bai, Murshudov, et al. 2014). The with the advent of the resolution revolution came the rising popularity of using a maximum likelihood approach (F. J. Sigworth 1998; S. H. Scheres 2010) and stochastic gradient descent to optimize 3D classification of particles (Punjani et al. 2017). After the EMDB Task Force met at the 2010 meeting of the International Electron Microscopy Data Bank to discuss the lack of validation metrics and criteria for the field, the 'gold-standard' Fourier shell correlation (FSC) began to gain popularity. The FSC validation involves separating the data into two half-sets, processing each independently, and comparing the final maps using cross-correlation to assess resolution variances. The point in which the FSC curve drops below 0.143 is now the accepted resolution cutoff for cryo-EM structures. The 0.143 cutoff was proposed in 2002 for structures with resolutions greater than 10 Å (Rosenthal and Richard Henderson 2003), as opposed to the earlier, more conservative 0.5 FSC cutoff which is more applicable to lower-resolution structures (Spahn et al. 2004). In conjunction with the above improvements in image processing software, the development of automatic image acquisition software SerialEM and EPU have allowed for much larger data collections, and has correspondingly increased the computational requirements for data processing (Mastronarde 2003). New and faster GPU-based imaging software has increased computationally heavy 2D and 3D classfication steps (Kimanius, Forsberg, et al. 2016), but larger jobs still require massive amounts of computational time to complete and quickly fill up data storage, as most datasets are now multiple terabytes. Thermofisher's new EPU software aims to solve the data storage problem with its newest .EER filetype, which saves individual electron counts on Falcon cameras instead of collecting multiple image frames for movies, allowing the data to be orders of magnitude more compressed than data saved in traditional .mrc or .tiff file formats (H. Guo et al. 2020).

Relion 4.0, the latest release at the moment, has implemented an improved classification algorithm called VDAM (Variable-metric gradient Descent), which is a modified stochastic gradient descent algorithm that is an alternative to the older Expectation–Maximization algorithm that Relion 3.0 used (Kimanius, Dong, et al. 2021). In addition to the improved 3D classification algorithm, Relion 4.0 also offers a convolutional neural network for 2D classification that aims to prevent wasting computational resources on 2D classes that converge to very few particles. This is done by structuring the neural network in the vein of self-organizing maps and neural gases (Fritzke 1994), where in each iteration the 2D class with the smallest likelihood probability is substituted with a 2D class that exhibits high variability.

6 Cryo-EM structure of human type-3 inositol triphosphate receptor reveals the presence of a self-binding peptide that acts as an antagonist[1]

6.1 Introduction

Inositol 1,4,5-triphosphate receptors (IP_3Rs)3 are ligand-gated calcium (Ca^{2+}) release channels localized predominantly in the endoplasmic reticulum (ER) membrane of all cell types (J. K. Foskett et al. 2007). Inositol 1,4,5-triphosphate (IP_3) generated by phospholipase C upon G protein- or tyrosine kinase-coupled receptor activation binds to IP_3Rs and opens the channel, leading to transfer of Ca^{2+} from the ER lumen to the cytoplasm (J. K. Foskett et al. 2007). Ca^{2+} released by IP_3Rs act as universal messengers required to regulate diverse physiological processes including fertilization, muscle contraction, apoptosis, secretion, and synaptic plasticity (Parys and H. De Smedt 2012; Berridge 2016). Deregulation of IP_3Rs results in abnormal Ca^{2+} signaling, leading to a broad spectrum of pathologies including cancer, neurodegenerative, autoimmune, and metabolic diseases (Katsuhiko Mikoshiba 2015).

In mammals, there are three different subtypes (J. K. Foskett et al. 2007; Parys and H. De Smedt 2012; Berridge 2016) of IP_3Rs, which share 60–70% sequence identity, can form homo- or heterotetramers, exhibit different spatial expression profiles, and are involved in diverse signaling pathways. The type 3 receptors (IP_3R-3s) are predominantly expressed in rapidly proliferating cells and are involved in taste perception and hair growth (Sato-Miyaoka et al. 2012; Miura et al. 2007; Hisatsune, Yasumatsu, et al. 2007). Additionally, deregulation of IP_3R-3 is implicated in diseases with deficiencies in cell fate decisions such as cancer and degenerative diseases (Mendes et al. 2005; Hayashi and Su 2007; Kuchay et al. 2017). For example, the expression of the IP_3R-3 is up-regulated in several cancer types including glioblastoma, breast, gastric, and colorectal cancer (Mound et al. 2017; Kang et al. 2010; Sakakura et al. 2003; Shibao et al. 2010). Furthermore, many tumor suppressors and oncoproteins such as protein kinase B, protein phosphatase 2A, promyelocytic leukemia protein, phosphatase and tensin homolog (PTEN), and BRCA1-associated protein 1

[1]This chapter is adapted from the article "Cryo-EM structure of human type-3 inositol triphosphate receptor reveals the presence of a self-binding peptide that acts as an antagonist."
Emily A. Schmitz contributed to experiment conceptualization, data curation, data analysis, investigation, and both writing and editing.

tightly regulate the stability and activity of IP_3R-3s (Kuchay et al. 2017; Bononi et al. 2017; Giorgi, Ito, et al. 2010; Szado et al. 2008). Inhibiting IP_3R-3 degradation in PTEN-regulated cancers was shown to be a valid therapeutic strategy (Bononi et al. 2017). Although IP_3R-3s are responsible for regulating distinct biological processes compared with types 1 and 2, it is unclear whether there is any mechanistic difference in their operation.

IP_3Rs function as signaling hubs where signals from different pathways and metabolic states are integrated to allosterically modulate IP_3R gating. Receptor activity is tightly controlled by many factors including second messengers (e.g. IP_3, Ca^{2+}), other small molecules (e.g. ATP), modulatory proteins, and posttranslational modifications such as phosphorylation and ubiquitination. Despite recent advances in the structural studies of IP_3Rs, molecular understanding of receptor gating and regulation remains largely unknown.

Structural investigation of IP_3Rs was pioneered by using the IP_3R-1 obtained from native tissues, due to its abundant expression in the cerebellum and well-established purification strategy (Fan, M. L. Baker, et al. 2015; Fonseca et al. 2003; Kozo Hamada, Terauchi, and Katsuhiko Mikoshiba 2003; Q.-X. Jiang et al. 2002; C. Sato, K. Hamada, et al. 2004; Serysheva, D. J. Bare, et al. 2003; Nakade et al. 1994; Supattapone et al. 1988; Fan, M. R. Baker, Zhao Wang, et al. 2018). Recently, cryo-EM structures of recombinant IP_3R-3 have been reported and the global architectures of both IP_3R-1 and IP_3R-3 share common features (Paknejad and Hite 2018). Due to the large size of the IP_3Rs, different structures contain nonoverlapping information resulting, primarily, from variations of local resolution within the 3D map. In fact, the atomic view of the complex is still incomplete. Published structures in the unliganded (apo) and liganded states provide a basis to develop mechanistic hypotheses on the channel gating. However, the current conformational ensemble falls short in revealing the full gating cycle, modulation, as well as mechanism of inhibition by known chemical reagents.

Here we present a cryo-EM structure of the human IP_3R-3 (hIP_3R-3) in a ligand-free conformation revealing a loop extending from the regulatory ARM2 domain that occupies the IP_3-binding site and thus may function as a regulator of IP_3 binding. In addition, our structure identified previously unresolved local structures of the complex, and the location of lipid-binding sites in the transmembrane domain. Collectively, our structural characterization of the hIP_3R-3 provides novel insight into the mechanistic function of IP_3Rs.

6.2 Results

6.2.1 Structure of hIP$_3$R-3

We expressed recombinant hIP$_3$R-3 using the Sf9 insect cell/baculovirus expression system and purified detergent-solubilized protein in the absence of any known ligands (Figure 42). After initial analysis of the protein sample using negative-stain EM, we solved its structure using cryo-EM to an overall resolution of 3.8 Å (Figure 24 and Figs. S2–S4). We used high resolution crystal structures for the ligand-binding core (PDB IDs 3JRR and 3UJ4) to interpret the map and modeled the rest of the structure manually (Chan et al. 2010; Seo et al. 2012). The overall structure of the hIP$_3$R-3 expressed in Sf9 cells is consistent with the structures of hIP$_3$R-3 expressed in HEK GnTI() cells, and very similar to the structure of rat IP$_3$R-1 purified from native tissues (Fan, M. L. Baker, et al. 2015; Fan, M. R. Baker, Zhao Wang, et al. 2018; Paknejad and Hite 2018).

Subunits that form the tetrameric ion channel can be divided into 3 regions: the large, N-terminal cytoplasmic domain (CD), the channel-forming transmembrane domain (TMD), and the C-terminal cytoplasmic domain (CTD) (Figure 24 C). The CD of each subunit resembles a tripod with a hinge-like central linker domain (CLD) (residues 790–1100 and 1587–1697) connected to 3 Armadillo solenoid domains (ARM1–3) (Figure 24 C). The CLD is located at the outer perimeter of the tetrameric receptor. The N-terminal domain (ARM1) extends toward the central 4-fold symmetry axis and connects to 2 contiguous β-trefoil domains (β-TF1 and β-TF2), forming the ligand-binding domain (LBD). β-TF1 of one subunit interacts with βTF2 of the neighboring subunit forming a rim around the 4-fold symmetry axis. The second ARM domain (ARM2) bulges from the CLD and is oriented parallel to the membrane surface. It interacts with ARM1 of the neighboring subunit and forms the outer periphery of the receptor together with the CLD. The third ARM domain (ARM3) connects the cytoplasmic domains to a juxtamembrane domain (JD) positioned at the cytoplasmic face of the TMD. The JD is formed by assembly of two fragments separated by the TMD. A U-motif composed of a β-hairpin and a helix-turn-helix motif located at the C-terminal end of the ARM3 domain encapsulates a latch-like domain extending from the C-terminal end of the TMD. The JD is further stabilized by a H2C2 zinc finger domain formed by the residues Cys-2538, Cys-2541, His-2558, His-2563, and a zinc ion (Figure 24 C).

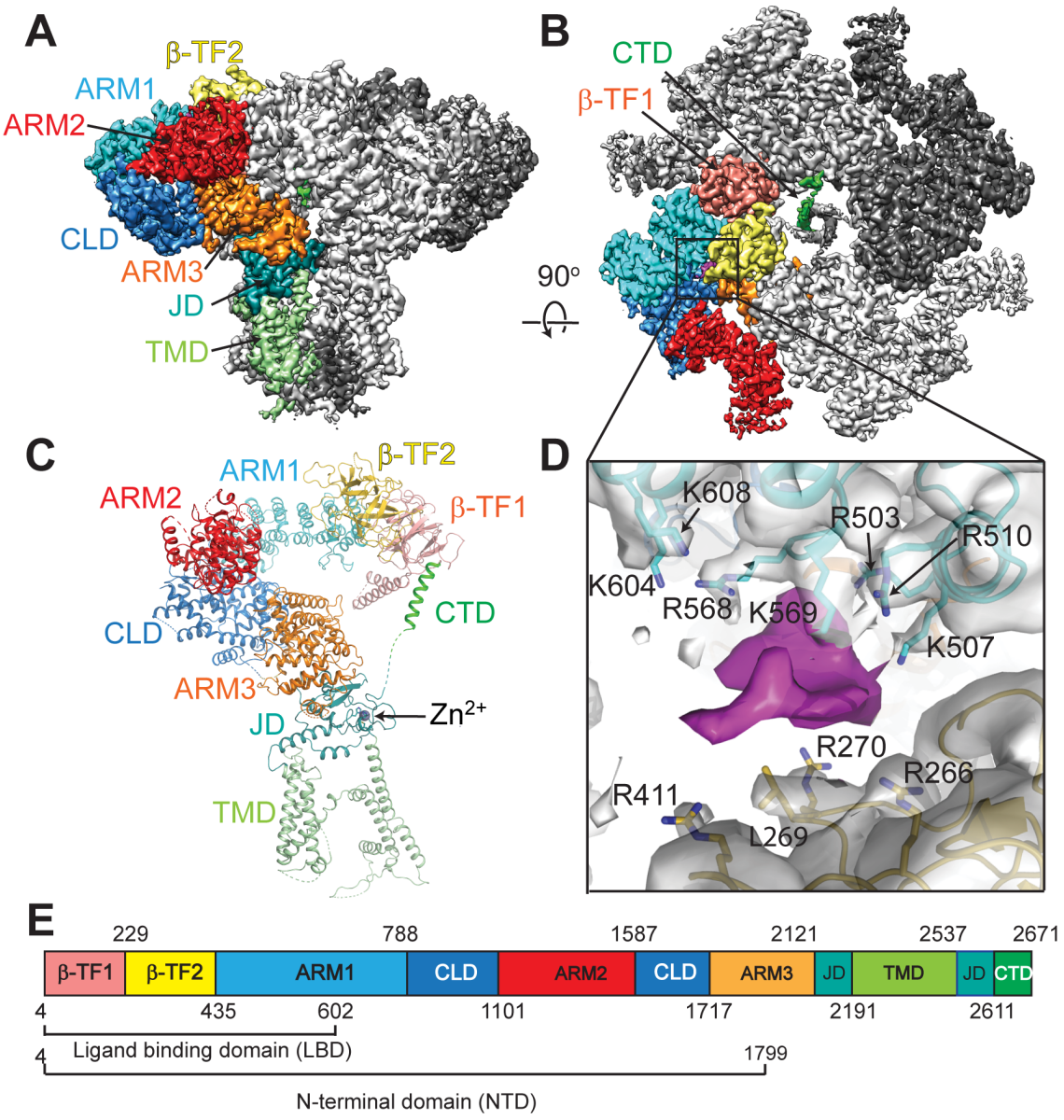

Figure 24: **Cryo-EM structure of hIP$_3$R-3.** (a) and (b), density map of the hIP$_3$R-3 viewed along the membrane plane (a) and from cytosol (b). Each domain in one of the subunits is colored differently. The other subunits are colored in different shades of gray. Additional density occupying the IP$_3$ binding. (c), ribbon representation of the hIP$_3$R-3 subunit highlighting the domain architecture. Zinc ion is shown as gray sphere. (d), density map around the IP$_3$-binding site is shown in gray (transparent) along with the additional density colored in magenta. The residues forming the pocket are shown in sticks. (e), domain boundaries of hIP$_3$R-3 subunits. Domains are colored as in panels a–c.

6.2.2 IP_3-binding site is occupied by a loop extending from ARM2

We observed substantive density at the IP_3-binding site, despite our initial intention to obtain the structure in a ligand-free conformation (Figure 24, A–D). The density for the residues forming the binding pocket was well-resolved indicating that the additional density is from a potential ligand that occupies the IP_3-binding site; hereafter we will refer to this density as "ligand-like" density (Figure 24 D). To improve the quality of the density at the IP_3-binding site, we first treated each individual subunit as a single particle and artificially expanded the dataset by symmetry expansion around the C4 symmetry axis that increased the number of particles 4-fold from 82,511 to 330,044 (Figure 44) (S. H. W. Scheres 2016). Then, we performed partial signal subtraction from the experimental images to reduce the signal to a region that would only cover the first approximately 1,800 residues (IP_3R-3 NTD) including the LBD as well as ARM1, ARM2, CLD, and part of ARM3 domains of a single protomer (Figure 44) (S. H. W. Scheres 2016. The subtracted particles were then classified into six 3D classes using a mask that covers the IP_3R-3 NTD without performing angular or translational alignment (Figure 44). Although all six maps from this classification scheme contained the ligand-like density at the IP_3-binding site, two of the classes revealed continuous density connecting the "ligand-like" to the first and second helices of ARM2 (αARM2–1 and αARM2–2) (Figure 25 A and Figure 46 , A and B). We observed similar results from the 3D classifications performed using different strategies as discussed under "Experimental procedures." Further investigation of the surrounding area in the model led us to surmise this extended, connecting ligand-like density could, in fact, be an unmodeled loop of the ARM2 domain. In our model, based on the 3D reconstruction of the intact receptor, residues connecting αARM2–1 to αARM2–2 are not modeled due to lack of interpretable density potentially resulting from the intrinsic flexibility of this loop (Figure 25 B and C). This loop was also left unmodeled, presumably due to flexibility, from previously published IP_3R-3 structures (Paknejad and Hite 2018). Within this region there are two patches enriched in acidic residues (Figure 25 E). Therefore, it is plausible that this loop forms a self-binding peptide (SBP) extending toward the IP_3-binding site and bringing one or both of these patches in close proximity to basic residues in the pocket of the IP_3-binding site (Figure 25 B–D). SBPs are peptide segments that specifically recognize and interact with their cognate targets, while being incorporated to the target in the primary sequence via a flexible polypeptide

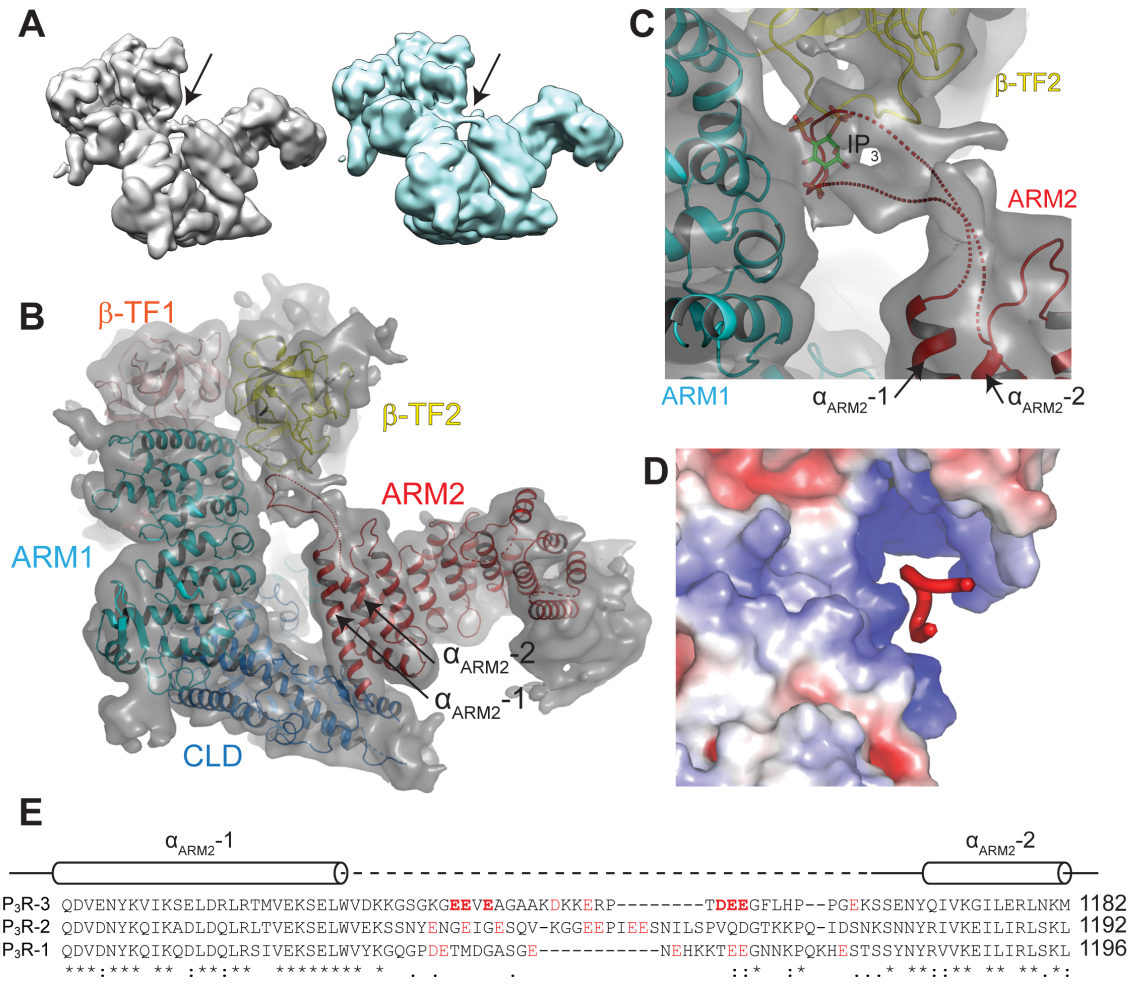

Figure 25: **IP$_3$-binding site is occupied by a loop extending from ARM2.** (a), density maps of hIP$_3$R-3 NTD class 5 (left) and class 3 (right) after focused 3D classification. Arrows point to the density extending from ARM2 domain. (b), ribbon representation of hIP$_3$R-3 NTD along with transparent surface rendering of the density map of hIP$_3$R-3 NTD- class 5. Dashed lines represent the putative path for the Cα atoms of the residues forming the loop between αARM2–1 and αARM2–2. (c), close up view of the IP$_3$-binding site of the SBP-bound hIP$_3$R-3 along with a docking pose of IP$_3$, placed based on the alignment of the LBDs of IP$_3$- and SBP-bound hIP$_3$R-3s. (d), electrostatic surface representation of the IP$_3$-binding site with a modeled loop in red. (e), sequence alignment of hIP$_3$R subtypes around the sequence covering αARM2–1 and αARM2–2. Cylinders represent α-helices. Dashed lines indicate the disordered region in the reconstruction of entire receptor with C4 symmetry. Acidic residues within the loop are colored red.

linker (Z. Li et al. 2019).

Although the presence of a density representing a loop extending from the ARM2 domain is unambiguous, modeling of specific amino acids forming the loop was not possible due to weak features observed resulting from the flexibility of the loop and ARM2. Each 3D class had a different ARM2 arrangement relative to the rest of the CD through a rigid body rotation on a pivotal point where ARM2 is connected to the CLD (Figure 46 C). In addition, density at the IP_3-binding site is not uniform among different 3D classes implying a dynamic interaction between the SBP and the IP_3-binding site (Figure 46 , A and B).

6.2.3 IP_3R-3 SBP competes against IP_3 binding

We reasoned the SBP loop would compete against IP_3 binding if it is interacting with the IP_3-binding site. To test this hypothesis, we took two approaches. In the first approach, we expressed and purified the hIP_3R LBD (residues 4–602) and a larger N-terminal domain (NTD; residues 4–1799), containing ARM2, as GFP fusion proteins and performed microscale thermophoresis (MST) experiments to measure the binding affinity of IP_3 (Figure 26, A and B). IP_3 affinity for the NTD was over 7-fold lower than for the LBD alone (K_d = 1.31 ± 0.46 and 0.18 ± 0.028 μM, respectively) (Figure 26 B). Deletion of the putative SBP (residues 1133–1155) from the NTD construct increased the affinity for IP_3 (K_d = 0.25 ± 0.09 μM), not significantly different from that of the LBD alone (Figure 26 B). Furthermore, mutagenesis of the four glutamate residues at both acidic patches to alanine (E1136A, E1137A, E1153A, and E1154A) in the putative SBP of the full-length NTD protein caused a similar increase in the IP_3 affinity (K_d = 0.44 ± 0.20 μM). Taken together, these observations support the hypothesis that residues 1133–1155 of hIP_3R-3 form a SBP that competes for binding of the major agonist, soluble IP_3.

In the second approach to test this hypothesis, we prepared a construct where the SBP was fused via a flexible linker to the C-terminal end of the LBD so it would be in close spatial proximity to the IP_3-binding site (Figure 26 A). We hypothesized this would behave like a gain-of-function construct, where the LBD-SBP fusion would have lower affinity for IP_3, similar to the NTD construct used above. We performed ITC experiments to test if the presence of the SBP affects the protein's

affinity for IP_3. Similar to the MST experiments, the LBD's affinity for IP_3 decreased nearly three fold in the presence of the SBP (K_d = 0.19 ± 0.02 to 0.52 ± 0.02 μM) (Figure 26 C). This effect was again abolished when the acidic residues in the SBP were mutated to alanines (Figure 26 , A–C). These results further support the hypotheses that the SBP competes against IP_3 binding and that the acidic residues are important for this effect, as suggested by the models of our IP_3R-3 structure.

6.2.4 IP_3R-3 SBP binding

When compared with the apo-LBD (PDB ID 6DQJ) (Paknejad and Hite 2018), with no visible density at the IP_3-binding site, the LBD of the SBP-bound hIP_3R-3 adopts a very similar overall conformation with a few local differences at the loops forming the IP_3-binding site at the β-TF2 domain (Figure 27 A). The most apparent difference involves the loop formed by Leu-269 and Arg-270, which is positioned closer to the SBP density, and the side chain of Leu-269, which points in the opposite direction (Figure 27 A). This slight movement does not seem to affect the overall arrangement of the IP_3R-3 CD, as the whole CD can be superimposed with an r.m.s.d value of 1.1 Å over 1,728 aligned residues. However, there is a subtle but noticeable counter-clockwise rotation (approximately 3°) of the entire tetrameric CD relative to the TMD in the SBP-bound hIP_3R-3 compared with the apo-hIP_3R-3, when the TMDs of both structures are aligned (Figure 27 C).

Previous structures of hIP_3R-3 in complex with IP_3 revealed two different LBD conformations; apo-like class 1 and class 2 with substantial conformational changes (Paknejad and Hite 2018). The LBD in SBP-bound conformation is more similar to the apo-like class-1 structure (PDB ID 6DQN, Figure 27 B). Orientation of the loop formed by Leu-269 and Arg-270 is highly similar in both structures suggesting that conformational changes of this loop are coupled to ligand binding (Figure 27 B). The arrangement of the tetrameric CD relative to the TMD is also comparable in both structures (Figure 27 D). In contrast, when compared with the ARM1 domain in the SBP-bound structure, the class 2 IP_3-bound structure (PDB ID 6DQV) ARM1 domain is rotated by approximately 20° toward to the β-TF2 domain (Figure 47). This rotation leads to overlap of residues in the ARM1 domain of the class 2 structure with our SBP density. Therefore, it is not possible for the LBD to adopt a similar conformation when the SBP occupies the IP_3-binding site

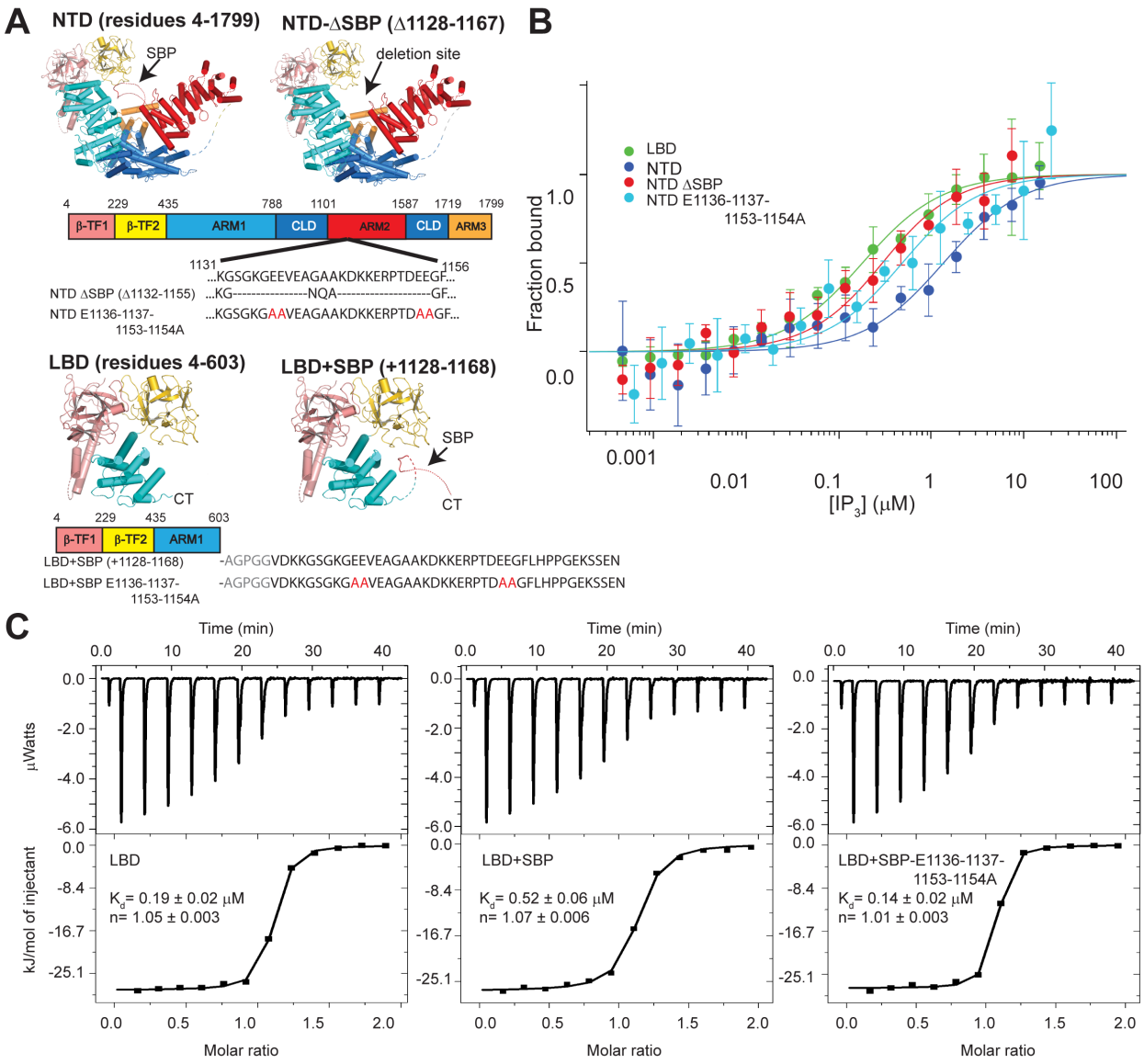

Figure 26: **The SBP competes against IP_3 binding.** (a), structural and schematic representation of the proteins used for binding assays. Changes in the SBP sequence was shown using dashes for deletion construct and in red for glutamate to alanine mutations. (b), MST analysis of IP_3 interaction with hIP$_3$R-3-LBD (green), hIP$_3$R-3-NTD (blue), hIP$_3$R-3-NTD-ΔSBP (red), and hIP$_3$R-3-NTD-E1136–1137-1153–1154A (cyan). Error bars represent standard deviations from three individual repeat measurements. (c), calorimetric titration of IP_3 into hIP$_3$R-3 LBD, hIP$_3$R-3 LBD + SBP, and hIP$_3$R-3 LBD + SBP-E1136–1137-1153–1154A (upper panels) and integrated heat as a function of IP_3/protein ratio (lower panels). Calculated K_d values are shown for each panel.

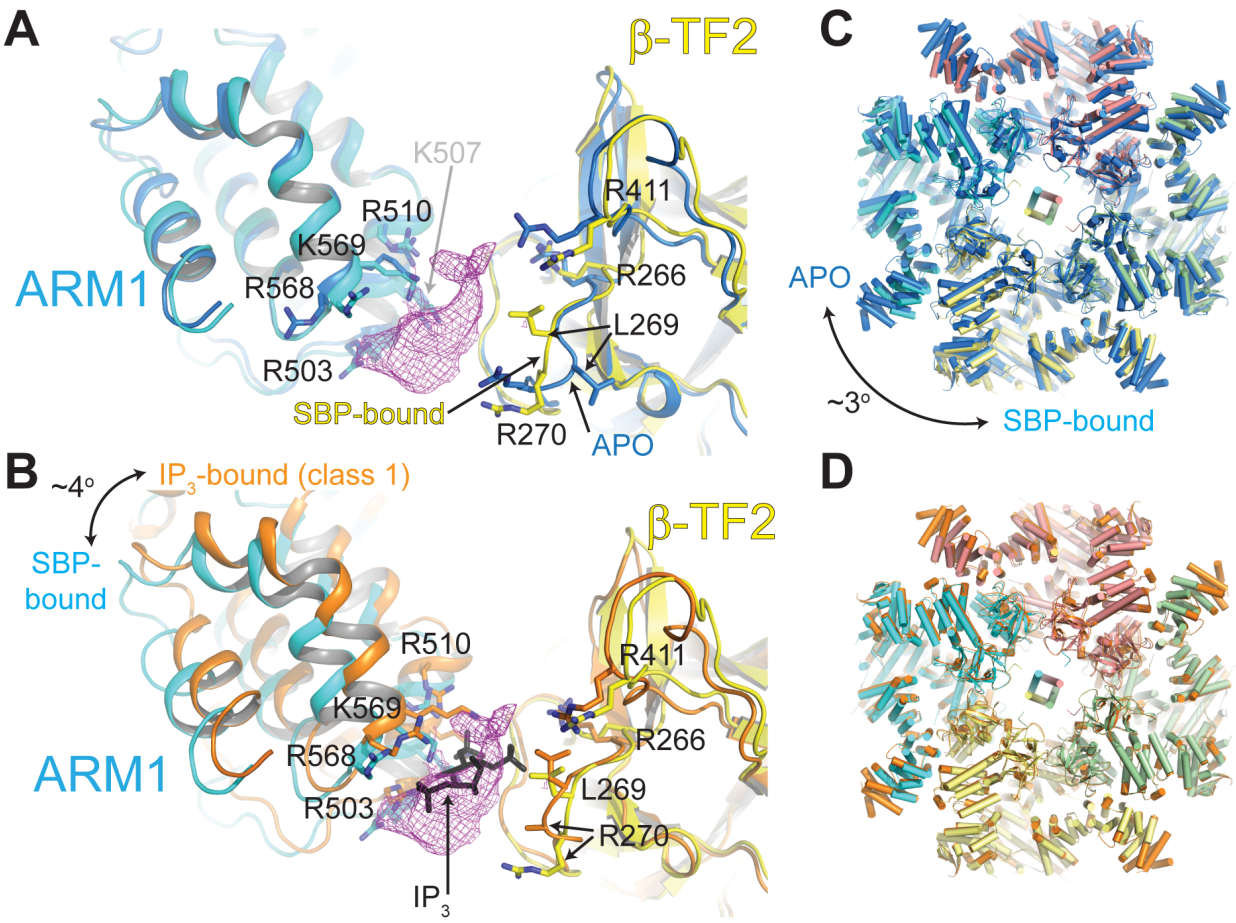

Figure 27: **Structural comparison of SBP-bound IP$_3$R-3 with apo and IP$_3$-bound hIP$_3$Rs.** (a) and (b), β-TF1 and β-TF2 domains of the SBP-bound hIP$_3$R LBD are superposed onto β-TF1 and β-TF2 domains of (a) apo hIP$_3$R-3 (PDB ID 6DQJ, shown in blue) and (b) IP$_3$-bound -hIP$_3$R-3 (PDB ID 6DQN, shown in orange). β-TF2 and ARM1 domains of the SBP-bound hIP$_3$R LBD are colored in yellow and cyan, respectively. β-TF1 domains are not shown in the figure for clarity. Residues forming the IP$_3$-binding pocket are shown in stick representation. IP$_3$ is colored black and magenta mesh represents the SBP density. c and d, comparison of the CDs of SBP-bound hIP$_3$R-3 with (c) apo-hIP$_3$R-3 (blue) and (d) IP$_3$-bound -hIP$_3$R-3 (orange) after superposing the TMDs. Subunits of the SBP-bound hIP$_3$R-3 are colored in cyan, salmon, green, and yellow.

due to steric hindrance, suggesting that the SBP would act as an antagonist.

6.2.5 Transmembrane domain

The TMD structure is consistent with previous IP_3R structures and has the overall architecture of voltage-gated ion channels with a central pore domain surrounded by voltage sensor-like domains at the periphery (Figs. 1C and 5). Unlike voltage-gated ion channels, we observe two additional helices (S1′ and S1″) per subunit penetrating through the membrane from the luminal side, similar to those observed in the previous cryo-EM studies of hIP_3R-3s as well as rabbit type-1 ryanodine receptors (RyR-1s) (Paknejad and Hite 2018; Georges et al. 2016). Thus, these auxiliary TM helices seem to be a common feature of intracellular calcium release channels. Primary sequences of these two helices are the most diverse region within the TMD among 3 subtypes of IP_3Rs and could potentially be involved in subtype-specific regulation and/or localization of the IP_3Rs.

Through the ion permeation path of the channel, from the cytoplasmic side, there is an upper vestibule, the narrowest constriction of the channel, and a lower vestibule followed by an architecture similar to the selectivity filter seen in potassium channels (Figure 48). In agreement with a closed channel conformation in the resting state, the shortest pore diameter along the channel was 1.1 Å where residues Phe-2513 and Ile-2522 are located (Smart et al. 1996; Marcus 1988; Figure 48). At the lower vestibule side of this constriction, there is a π-helix (residues 2501–2509) located at the middle of the S6 helix (Figure 48). As suggested previously, transition from π- to α-helix within this region is potentially coupled to gating similar to TRPV6 channels where channel opening is accompanied by a local α- to π-helical transition in S6 (Paknejad and Hite 2018; McGoldrick et al. 2018).

We observed two strong, nonprotein densities per subunit at the TMD. The true identity of the molecules occupying these positions cannot be determined with certainty from the current data, but they potentially derive from either nonannular lipid molecules co-purified with the receptor or well-ordered detergent molecules (Figure 27). In either case, these sites are likely to be occupied by lipids in biological membranes, as they are embedded in the TMD core and form extensive interface with the protein residues. The density located in the cytoplasmic leaflet of the bilayer

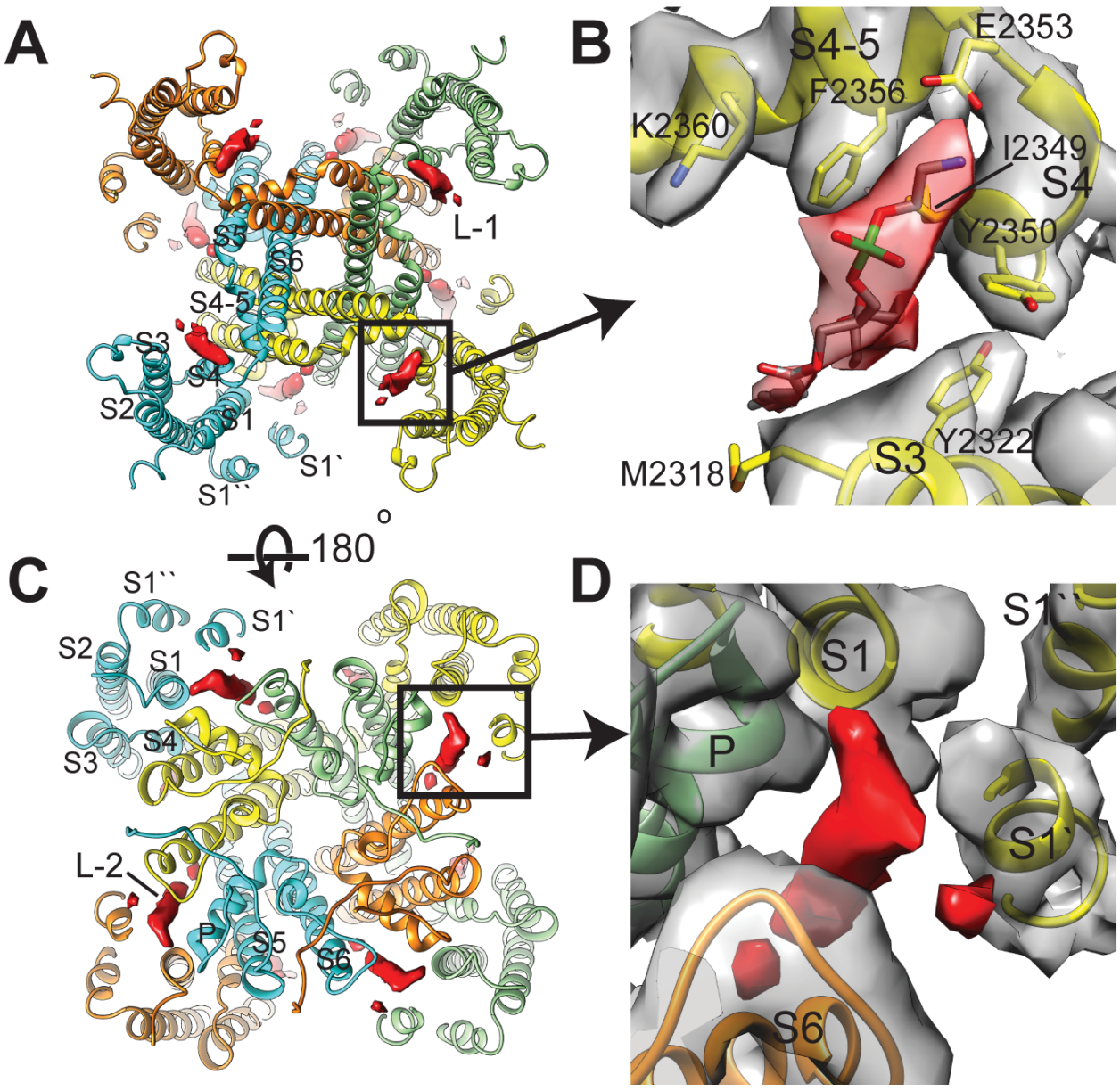

Figure 28: **Structure of the TMD.** (a) and (c), ribbon diagram of the hIP$_3$R-3 TMD viewed from the cytoplasm (a) and ER lumen (c) with nonprotein density countered at 4 σ representing bound-lipid molecules. b and d, the binding site for L-1 (b) and L-2 (d) viewed in the same orientation as in panels a and c, respectively. Density for the protein and the lipid molecules are shown in gray and red, respectively. Residues that are involved in L-1 binding are shown as sticks. A putative phosphatidylethanolamine molecule in stick representation was placed into the L-1 density for illustrative purposes, although it was not built in the actual structural model.

is located at the cavity formed by the S3, S4, and S4–5 helices and is in the vicinity of residues Tyr-2322, Ile-2349, Tyr-2350, and Phe-2356 (Figure 27 , A and B). The tip of the density facing the cytoplasmic side extends toward Glu-2353, suggesting that the lipid molecule contains a positively charged head group that can form a salt bridge with the side chain of Glu-2353. The second lipid density is located at the interface of three subunits in the luminal leaflet of the bilayer and could be critical for proper assembly (Figure 27 , C and D). The binding site is formed by S1 and S1′ of one subunit together with the P helix and S6 helix of two neighboring subunits (Figure 27 D).

6.2.6 C-terminal cytoplasmic domain

Unlike RyRs, the C-terminal ends of IP_3Rs extend through the central four fold axis and form a left-handed helical bundle at the core of the receptor (Fan, M. L. Baker, et al. 2015). In our structure, density for the CTD is less resolved compared with the rest of the receptor, but in sufficient quality to model a polyalanine peptide that forms a left-handed coiled-coil motif (Figure 29 , A and B). Connection of the coiled-coiled motif to the JD is only visible at very low threshold levels, and was not built into the model. The C-terminal side of the helices forming the coiled-coiled domain extend toward the β-TF ring and interact with the β-TF2 domain of the neighboring subunit (Figure 29). The interaction is mediated through a hydrophobic patch formed by Val-287, Val-288, Leu-303, Ile-363, Leu-366, and Leu-392 on the surface of the β-TF2 domain and potentially involves residues Leu-2660, Gly-2661, Phe-2662, Val-2663, Asp-2664, and Val-2665 at the C-terminal end of the receptor (Figure 29 , C and D).

6.3 Discussion

The identified direct interaction between the SBP and the ligand-binding site may have a critical physiological role in IP_3R-3 activity and regulation. By occupying the IP_3-binding site, the SBP reduces the sensitivity of the IP_3R-3 to its physiological agonist IP_3. Similar mechanisms of receptor regulation were observed for other protein families as well. For example, fibroblast growth factor receptor autoinhibition is mediated by electrostatic interaction of a subregion rich in acidic residues, known as an acid box, with the heparin-binding site of the same subunit, reducing receptor affinity for heparin and fibroblast growth factor (Kalinina et al. 2012). Of note, heparin is an antagonist

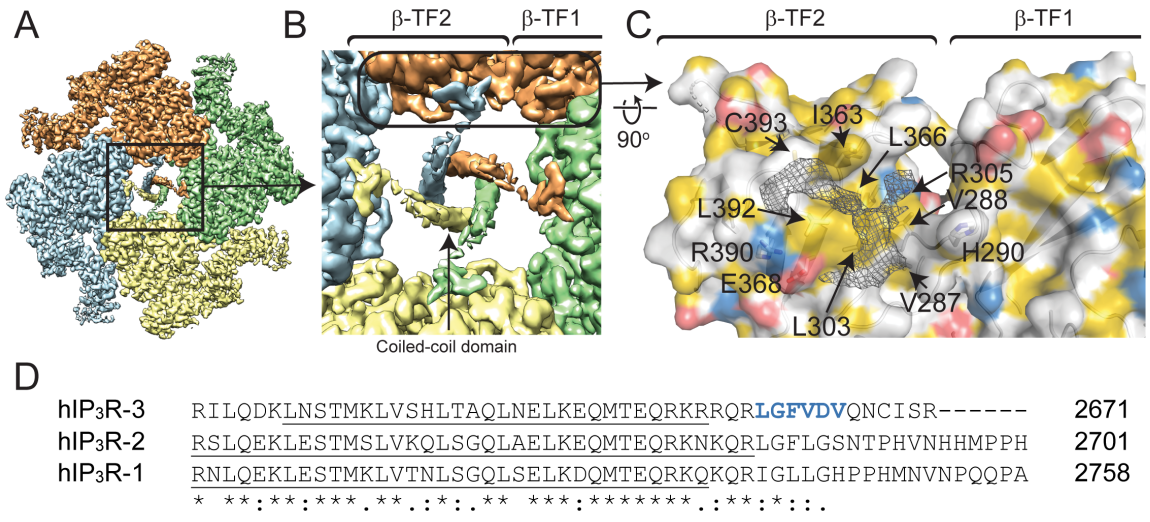

Figure 29: **Coupling between the N- and C-terminal domains of hIP$_3$R-3.** (a), density map of hIP$_3$R-3 viewed from the cytoplasmic side. Density for each subunit is colored differently. (b), close up view of the map in panel a focusing on the C-terminal coiled-coil domain. (c), surface representation of the of the β-TF1 and β-TF2 domains colored using the YRB coloring scheme (Hagemans et al. 2015) (yellow, carbon atoms not connected to nitrogen and oxygen atoms; red, negatively charged atoms; blue, positively charged atoms; and gray, remaining atoms) along with the cryo-EM map (gray mesh) of the C-terminal end of the neighboring subunit to emphasize the hydrophobic nature of the interaction. The residues of the β-TF2 domain in close distance to the C-terminal end of the neighboring subunit are shown in sticks and labeled. (d), sequence alignment of hIP$_3$R subtypes around the C-terminal end of the proteins. Underlined sequences represent the predicted coiled-coil motifs. Residues shown in blue form the hydrophobic patch proposed to interact with the hydrophobic surface of the β-TF2 domain of the neighboring subunit.

of IP_3Rs and interacts with the IP_3-binding site.

Among the IP_3R subtypes, IP_3R-3 has the lowest affinity to IP_3. The subtype differences in IP_3 affinity are mainly attributed to sequence variations at the β-TF1 domain (also known as the suppressor domain) (Iwai, Michikawa, et al. 2007). However, the current data indicate that the SBP also has a role in modulating binding affinity because of sequence variability within the SBP among the IP_3R subtypes, especially in the number and positioning of the acidic residues (Figure 25 E). In addition, we speculate that the SBP is a plausible target for many proteins that are known to modulate the sensitivity to IP_3. For example, phosphorylation of the Ser/Thr residues within the SBP would increase the net negative charge on the SBP and potentially lead to tighter binding to the IP_3-binding site reducing the receptor sensitivity to IP_3. Moreover, any protein that interacts with the SBP may restrict its interaction with the IP_3-binding site, sensitizing the IP_3R to IP_3.

In addition to a potential physiological role in regulation of IP_3R activity, identification of the SBP as a competitive inhibitor of IP_3 binding opens potential avenues in development of pharmacological agents targeting these important families of proteins. Further research to identify the structural determinants of the SBP interaction with the IP_3-binding site will pave the road for development of novel inhibitors of IP_3Rs.

One puzzling question is why the additional density from the SBP at the IP_3-binding site was not observed in a previously reported ligand-free hIP_3R-3 structure. One plausible explanation is that the larger number of particles used in our study (82,511 compared with 26,325) provided additional information that permitted the resolution of the SBP. In addition, this could arise from technical differences, such as the protein expression system (mammalian versus insect cells), purification methods, and/or sample preparation for cryo-EM analysis. Furthermore, cryo-EM studies of large macromolecular complexes provide opportunities to identify novel features through different image-processing strategies even with samples prepared in similar conditions. IP_3Rs are regulated by numerous factors, some of which are not well-understood at the moment, and exhibit multiple conformational rearrangements. Thus, it is likely that further structural studies of IP_3Rs will continue to uncover additional features providing further functional insights.

In conclusion, the data presented here reveal a previously unanticipated regulatory mechanism of IP_3R where a loop distantly located from the LBD in the primary sequence occupies the IP_3-

binding site and competitively inhibits IP_3 binding. Regulation by the SBP is likely to confer subtype-specific biological function to IP_3-mediated calcium signaling due to divergence in the loop sequence among members of the IP_3R family. Our structural data will facilitate design of modifications on the SBP of the intact receptors to functionally test their effect in channel activity to determine the molecular mechanism of the SBP regulation and its physiological role.

6.4 Materials and methods

6.4.1 Expression and purification of hIP$_3$R-3

The gene encoding hIP$_3$R-3 (accession number BC172406) was purchased from Dharmacon (Strausberg et al. 2002), subcloned (residues 4–2671) with C-terminal OneStrep tag into pFL vector, and incorporated into baculovirus using the Multibac expression system (Fitzgerald et al. 2006). Sf9 cells (4 × 106 cells/ml) infected with the baculovirus were harvested by centrifugation (4,000 × g) 48 hours after infection. Cells were resuspended in a lysis buffer consisting of 200 mM NaCl, 40 mM Tris-HCl, pH 8.0, 2 mM EDTA, pH 8.0, 10 mM β-mercaptoethanol (βME), 1 mm phenylmethylsulfonyl fluoride were lysed using an Avastin EmulsiFlex-C3. The cell lysate was centrifuged at 6,000 × g for 20 minutes, and the membrane was pelleted by centrifugation at 40,000 rpm (Ti45 rotor) for 1 hour. The membrane pellets were resuspended and homogenized in ice-cold resuspension buffer (200 mM NaCl, 40 mM Tris-HCl, pH 8.0, 2 mM EDTA, pH 8.0, 10 mM βME), and solubilized using 0.5% lauryl maltose neopentyl glycol (LMNG) and 0.1% glyco-diosgenin (GDN) at a membrane concentration of 100 mg/ml. After 4 hours of stirring, the insoluble material was separated by centrifugation at 40,000 rpm (Ti45 rotor) for 1 hour and the supernatant was passed through Strep-XT-Superflow resin (IBA Biotagnology). The resin was washed with wash buffer composed of 200 mM NaCl, 20 mM Tris-HCl, pH 8.0, 1 mM EDTA, 10 mM β-ME, 0.005% LMN, 0.005% GDN, and the protein was eluted using the wash buffer supplemented with 100 mM d-biotin, pH 8.2. The protein was further purified by size exclusion chromatography using a Superose 6 column (10/300 GL, GE Healthcare) equilibrated with 200 mM NaCl, 20 mM Tris-HCl, pH 8.0, 1 mM EDTA, pH 8.0, 2 mM TCEP, 0.005% LMN, and 0.005% GDN. Fractions corresponding to hIP$_3$R-3 were concentrated to 2.3 mg/ml, centrifuged at 70,000 rpm using a S110-AT rotor (Thermo Scientific) for 10 minutes, and used immediately for cryo-EM imaging. After centrifugation, concentration of

the protein decreased to 1.3 mg/ml.

6.4.2 Negative stain data collection and analysis for hIP$_3$R-3

Four hundred mesh copper grids were coated with carbon. 4 μL of 0.05 mg/ml of hIP$_3$R-3 was applied to each glow discharged grid (2 minutes on a Quorum K1000X) and allowed to absorb for 30 seconds. The grid was blotted on filter paper, washed twice in MilliQ water, and negatively stained with 0.75% (w/v) uranyl formate. Images were recorded on a 4k $\times$ 4k CCD camera (Gatan) using an FEI TF20 transmission electron microscope operated at 200 keV. All images were collected at 50,000 magnification in low dose mode using SerialEM automated collection mode at a defocus of -1.5μm (Mastronarde 2005). Image processing was performed using the RELION software package (Sjors H. W. Scheres 2012). The particles were automatically picked using templates generated from 822 manually picked particles. 100 2D class averages were generated from 12,227 particles using 25 iterations of 2D classification and alignment in RELION (Figure 43 A).

6.4.3 Cryo-EM sample preparation and data collection for hIP$_3$R-3

2.0 μL of 1.3 mg/mL of hIP$_3$R-3 was applied to a 200-mesh C-flat holey carbon 2/1 grid (Protochips) that was glow discharged for 2 minutes at 25 mA. The grid was blotted for 3 seconds at force 1 before being plunged into liquid ethane using an FEI MarkIV Vitrobot at 8 °C and 100% humidity. Micrographs were collected using an FEI Polara F30 microscope operated at 300 keV in counting mode on a K2 Summit direct electron detector (Gatan). Data were collected at a nominal magnification of $\times$31,000 at a defocus range of 1.4 to 3.5 μm under low dose conditions. Specimens were exposed for 10 seconds at approximately 11 e^-/pix/s over 50 frames resulting in a total dose of approximately 70 $e^-/\text{Å}^2$ using SerialEM automated data collection (Mastronarde 2005). The pixel size of the image was 1.247 Å.

6.4.4 Cryo-EM image processing for hIP$_3$R-3

Motion correction and CTF parameter determination was done using the on-the-fly processing software Focus (Biyani et al. 2017). All images were motion corrected from frames 0–44 using motioncor2 (Zheng et al. 2017) with a dose weighting parameter of 1.4 $e/\text{Å}$/frame. CTF parameters for each image were calculated using Gctf (K. Zhang 2016) and used to remove micrographs with

low maximum resolution or high astigmatism. Motion-corrected images were then imported into RELION-2 (Sjors H. W. Scheres 2012). RELION-3 was used as the new version became available (Zivanov, Nakane, Forsberg, et al. 2018). Autopicking was done using representative class averages obtained from 757 manual picked particles as templates. Particles were extracted at a box size of 350 × 350 pixels and binned to 64 × 64 pixels. 2D class averages were determined using 25 iterations of classification. Particles that generated class averages showing well-defined domain structure were re-extracted at 340 × 340 pixels without binning and were subject to 2D classification. Particles that generated 2D class averages showing clear secondary structure subparticle features were subject to 3D classification. The EM density map of the IP_3R-1 (EMD-6369) was scaled and clipped, using e2proc3d.py (EMAN) (G. Tang et al. 2007), to match our pixel and box size, filtered to 60 Å, and used as an initial model for 3D classification into 6 classes with no symmetry imposed. Two classes had impaired density for one of the subunits and excluded from further analysis. Refinement and reconstruction of the particles belonging to the other four classes were performed using cisTEM by imposing C4 symmetry (Grant, Rohou, and Nikolaus Grigorieff 2018) (Table 1). The resulting map was sharpened by applying a B-factor of $90\mathring{A}^2 2$ using Rosenthal and Henderson's method (Rosenthal and Richard Henderson 2003). The final average resolution at the "gold standard" 0.143 cutoff was 3.8 Å. Half-maps were generated using the 3D-generated module in cisTEM. Local resolution was also calculated in ResMap (Kucukelbir, Fred J. Sigworth, and Tagare 2014) (Figure 45). Chimera (Pettersen, Goddard, Huang, Couch, et al. 2004), COOT (Emsley et al. 2010) and The PyMOL Molecular Graphics System (Version 2.0, Schrödinger, LLC) were used for visualization and figure preparation.

Cryo-EM data collection, refinement, and validation statistics

Data collection and processing	
Microscope	FEI Polara TF30
Detector	Gatan K2 summit
Nominal magnification	×31,000
Voltage (kV)	300
Electron exposure (e^{-}/Å^2)	70
Defocus range (μm)	−1.4 to −3.5
Pixel size (Å)	1.247
Symmetry imposed	C4
Number of micrographs	3,899
Initial particle images	110,510
Final particle images	82,511
Map resolution (Å)/FSC threshold	3.8/0.143
Refinement	
Resolution (Å)	3.8
B-factor used for map sharpening (Å^2)	−90
Model composition	
Non-hydrogen atoms	51,564
Protein residues	8,216
Zinc	4
Mean B factors (Å^2)	
Protein	155.0
Zinc	115.7
R.m.s. deviations	
Bond lengths (Å)	0.002
Bond angles (°)	0.532
Validation	
Molprobity score	0.94
Clashscore	0.26
Poor rotamers (%)	0
Ramachandran plot	
Favored (%)	95.13
Allowed (%)	4.87
Disallowed (%)	0.0

Table 1: Chapter 6: Cryo-EM data collection, refinement, and validation statistics.

6.4.5 Symmetry expansion, partial signal subtraction, and focused 3D classification

To resolve the unaccounted density better, we first treated each subunit as a single particle and expanded the dataset by using "$relion_particle_symmetry_expand$" command based on the C4 symmetry and the refined orientation parameters calculated during 3D refinement using RELION-3 for the particles. This process increased the number of particles to 330,044. We created a mask around the hIP$_3$R-3 tetramer using MaskCreate in RELION-3 and removed the part that corresponds to

the IP_3R-3 NTD of one of the subunits using the "volume erase" function of Chimera. The new mask was then used to subtract the signal from the expanded particles using RELION-3 resulting in 330,044 particle images containing a signal for only the IP_3R-3 NTD of one of the subunits. These particles were then subjected to 3D classification using a mask covering the IP_3R-3 NTD, and orientation parameters for the particles from symmetry expansion step. At this stage, we tried several different classification strategies: 3D classification into 4, 6, or 8 classes, 3D classification using a mask excluding the ARM2, and re-classification of the 3D classes into subclasses. The results mostly agreed with each other, and we used the maps from the classification into 6 classes for further analysis (Figure 46 A). Refinement of the particles belonging to Class 5 was performed using cisTEM. The final average resolution at the gold standard 0.143 cutoff was 4.5 Å.

6.4.6 Model building

High resolution crystal structures of the β-TF1 domain of mouse IP_3R-3 (PDB ID 3JRR) (Chan et al. 2010) and β-TF2 and part of the ARM1 domain of the rat IP_3R-1 (PDB ID 3UJ4)(Seo et al. 2012) were docked into the cryo-EM map followed by rigid-body fitting of the individual β-TF1, β-TF2, and ARM1 domains into the cryo-EM map using COOT (Emsley et al. 2010). The resulting model was manually modified to have the correct hIP_3R-3 residue assignment and fit to the cryo-EM map. The rest of the model was built manually using COOT and refined against the cryo-EM map using Phenix real space refinement (Afonine et al. 2013). Residues without clear density for their side chains were built without their side chains (i.e. as alanines), while maintaining their correct labeling for the amino acid type.

6.4.7 Expression and purification of soluble hIP_3R-3 constructs

The gene encoding the hIP_3R-3 LBD (Met-4 to Asn-602) was subcloned into pAceBac1 vector with an N-terminal OneStrep tag followed by a tobacco etch virus protease cleavage site. This construct was modified to prepare the hIP_3R-3 LBD + SBP fusion construct that encodes residues 4 to 603 followed by the Ala-Gly-Pro-Gly-Gly linker and residues 1128 to 1168. For MST experiments, the gene encoding the hIP_3R-3 LBD (residues 4 to 602) and the hIP_3R-3 NTD (residues 4–1799) were subcloned into pAceBac1 vector with an N-terminal OneStrep tag followed by the gene encoding eGFP and tobacco etch virus protease cleavage site. The truncation construct hIP_3R-3 NTD-

ΔSBP was prepared by removing residues between Gly-1132 and Gly-1156 with Asn-Gln-Ala. All constructs were incorporated into baculovirus using the Multibac expression system (Fitzgerald et al. 2006). The constructs were expressed using the Sf9/Baculovirus system (DH10multibac). Sf9 cells (approximately 4.0 × 106 cells/mL) were harvested by centrifugation (1952 × g, 20 minutes) at 48 hours post-infection. The cell pellet was resuspended in lysis buffer composed of 200 mM NaCl, 20 mM Tris-HCl, pH 8.0, 10% glycerol (v/v), 10 mM βME, and 1 mM phenylmethylsulfonyl fluoride. Cells were lysed using Avestin EmulsiFlex-C3 system (greater than 10,000 p.s.i.) and centrifuged at 40,000 rpm (Ti45 rotor) for 45 minutes. The supernatant was recovered and incubated with Strep-XT-Superflow resin (IBA Biotagnology) for 2 hours at 4 °C. The resin was then washed with the wash buffer (200 mM NaCl, 20 mM Tris-HCl, pH 8.0, 10% glycerol, and 10 mM βME) and the protein was eluted with the elution buffer (200 mM NaCl, 50 mM Tris, pH 8.2, 100 mM d-biotin, and 10 mM βME). The proteins used for ITC experiments were further purified by SEC using Superdex 200 column (GE Healthcare) equilibrated with the SEC buffer composed of 200 mM NaCl, 20 mM Tris-HCl, pH 8.0, 10% glycerol (v/v), and 0.5 mM TCEP. SEC for the proteins used in MST experiments were performed using a buffer composed of 200 mM NaCl, 20 mM Tris-HCl, pH 8.0, and 0.5 mM TCEP.

6.4.8 Isothermal titration calorimetry (ITC)

All proteins used in ITC experiments were dialyzed against the same buffer solution composed of 200 mM NaCl, 20 mM Tris-HCl, pH 8.0, 10% glycerol (v/v), and 0.5 mM TCEP to avoid the possible changes in the salt concentration and pH. IP_3 solution was prepared by dissolving the powder in the dialysis solution. ITC experiments were conducted on an Auto ITC 200 instrument at 20 °C by successive injections of 3 μL of 0.8 mM IP_3 to 0.08 mM of the protein solutions at 200 second intervals following an initial injection of 0.2 μL of 0.8 mM IP_3. Data analysis was performed using the software Origin, version 7.0, with the MicroCal ITC analysis module.

6.4.9 Microscale thermophoresis (MST)

MST experiments were conducted on a Monolith NT.115 series (Nanotemper Technologies). Proteins were diluted to 200 nM in 1× MST buffer (50 mM Tris-HCl, 150 mM NaCl, 10 mM MgCl2, 0.05% Tween 20). IP_3 stock solution (2 mM in water) was diluted to 15 μM using 1× MST buffer.

A two fold serial dilution of IP_3 in 18 NT.115 standard capillaries was prepared, with 15 μM IP_3 as the highest concentration and 100 nM protein per capillary. Excitation power was set to 20% and MST laser power was set to medium. Data analysis was performed using the software MO analysis (Nanotemper Technologies).

6.5 Availability

Cryo-EM maps and atomic coordinates have been deposited in the EMDB and PDB under the accession codes EMD-20849 (tetramer with C4 symmetry, PDB ID 6UQK) and EMD-20850 (IP_3R-3 NTD, focused refinement with no imposed symmetry). All other source data are available from the corresponding authors upon request.

7 Structural basis for activation and gating of IP_3 receptors[2]

7.1 Introduction

IP_3Rs are intracellular Ca^{2+} channels, predominantly localized to the ER and activated by the binding of IP_3 generated in response to external stimulation of G-protein coupled receptors (J. K. Foskett et al. 2007; Katsuhiko Mikoshiba 1997; Berridge 2016). Opening of the IP_3Rs results in the rapid release of Ca^{2+} from the ER lumen into the cytoplasm, triggering diverse signaling cascades that regulate physiological processes such as learning, fertilization, gene expression, and apoptosis. Dysfunctional IP_3Rs cause abnormal Ca^{2+} signaling and are associated with many diseases, including diabetes, cancer, and neurological disorders (Terry et al. 2020; Gambardella, Lombardi, et al. 2020). There are three IP_3R subtypes (IP_3R-1, -2, and -3) that share 60–70% sequence identity, form homo- or hetero-tetramers, exhibit different spatial expression profiles, and are involved in different signaling pathways (J. K. Foskett et al. 2007; Katsuhiko Mikoshiba 1997; Berridge 2016). Each IP_3R subunit is about 2700 amino acids in length and contains a transmembrane domain (TMD) and a large cytoplasmic region comprising two β-trefold domains (βTF1 and βTF2), three Armadillo repeat domains (ARM1, ARM2, and ARM3), a central linker domain (CLD), a juxtamembrane domain (JD), and a short C-terminal domain (CTD) (Paknejad and Hite 2018; Fan, M. L. Baker, et al. 2015; Fan, M. R. Baker, Zhao Wang, et al. 2018; M. R. Baker et al. 2021; Azumaya et al. 2020) (Figure 30).

In addition to IP_3, the receptor activation requires Ca^{2+} at nanomolar concentrations, whereas Ca^{2+} at higher concentrations is inhibitory, causing the receptor to be tightly regulated by Ca^{2+} (L. Bezprozvanny, Watras, and Barbara E. Ehrlich 1991; Finch, T. J. Turner, and Goldin 1991a; Finch, T. J. Turner, and Goldin 1991b; Iino 1990). The cryo-EM structure of human IP_3R-3 (hIP_3R-3) in the presence of the inhibitory Ca^{2+} concentrations (2 mM) revealed two binding sites (Paknejad and Hite 2018). However, their role in channel activation and inhibition has remained uncertain. Furthermore, although ATP binding potentiates the receptor by increasing the open probability and duration of the channel openings, the underlying molecular mechanism has not been uncovered (I. Bezprozvanny and Barbara E. Ehrlich 1993; Tu, Zhengnan Wang, Nosyreva, et al. 2005). In

[2]This chapter is adapted from the article "Structural basis for activation and gating of IP_3 receptors."
Emily A. Schmitz optimized and performed the protein expression and purification and contributed to manuscript preparation.

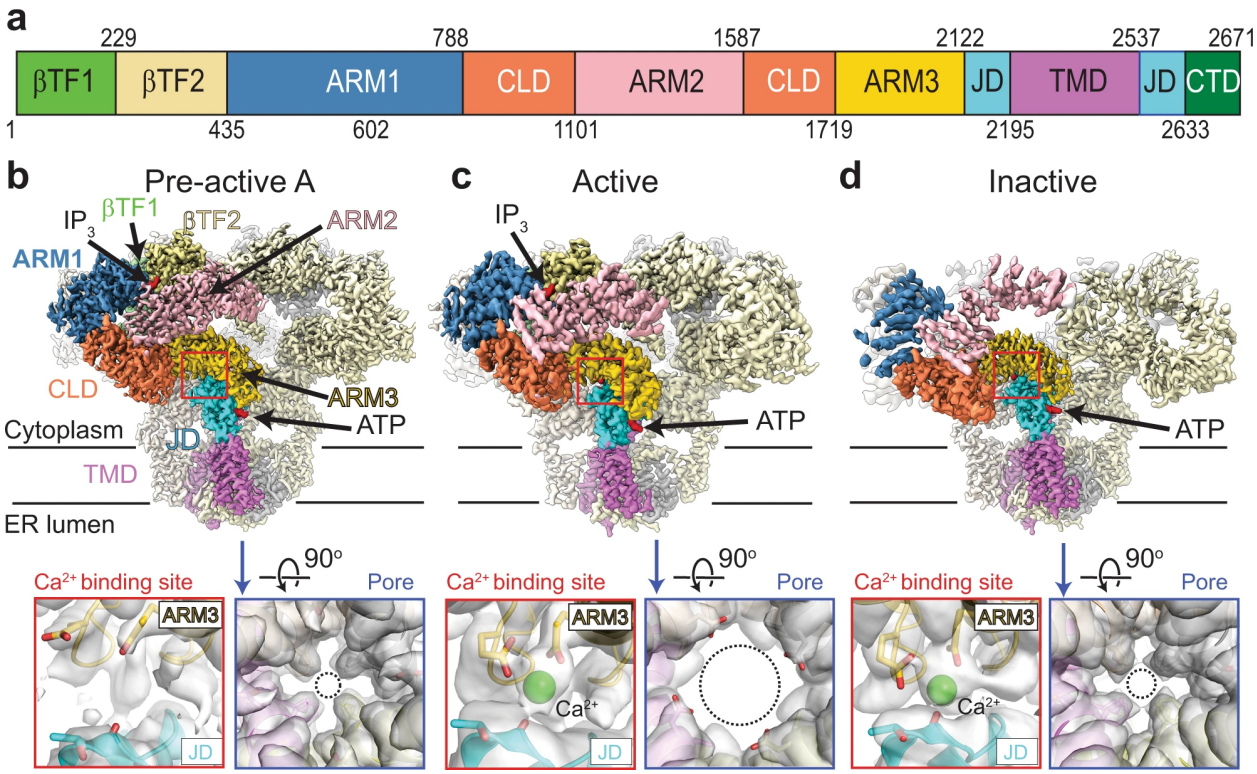

Figure 30: **Cryo-EM structures of hIP$_3$R-3 in multiple conformations.** (a) Domain boundaries of hIP$_3$R-3. b–d Composite maps of hIP$_3$R-3 in pre-active A (b), active (c), inactive (d) conformations. Each domain in one of the subunits is colored as in (a). Maps within the boxes, shown transparent, are close-up views of the Ca^{2+} binding site (red) and the pore (blue) with ribbon representation of hIP$_3$R-3. Select residues are shown in the sticks. Dashed circles indicate opening through the gate.

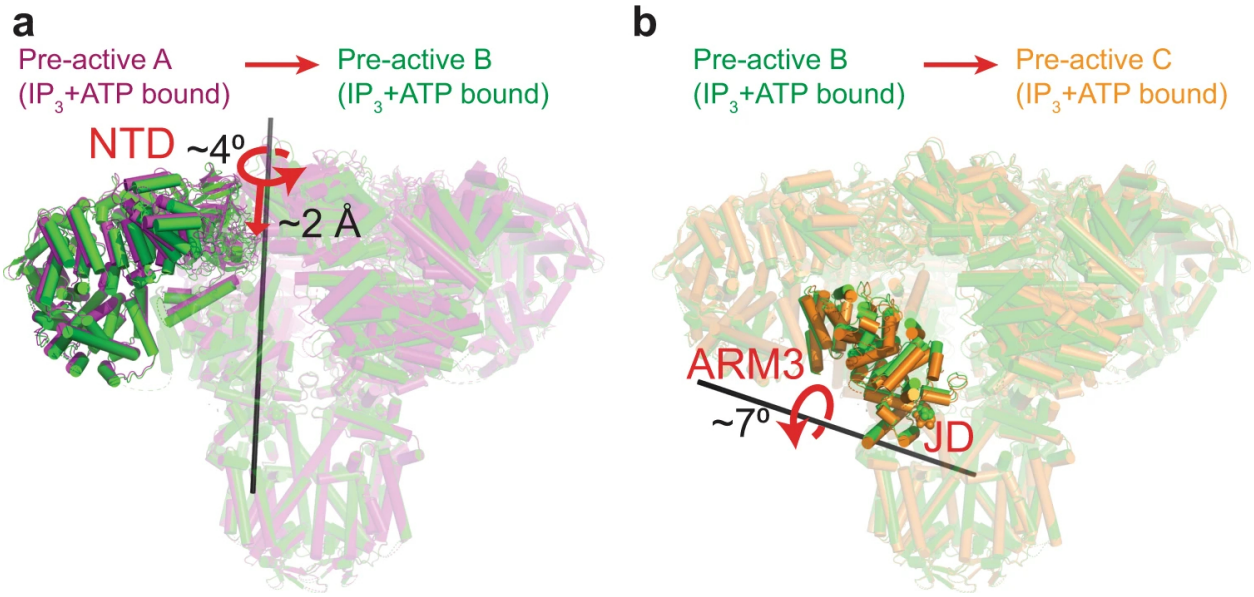

Figure 31: **Conformational changes in the pre-active states.** (a, b) Ribbon representations of hIP$_3$R structures superposed on the residues forming the selectivity filter and P-helix of the TMDs, emphasizing the conformational changes between the states indicated above. Domains with substantial conformational changes are shown in full colors only on one subunit, while the rest of the protein is transparent. Curved and straight red arrows indicate the rotation and translation of the domains with red labels relative to the rotation axis (black bars), respectively.

this study, we illuminate the structural framework of receptor activation and channel opening by analyzing five cryo-EM structures of hIP$_3$R-3 in the closed-pre-activated, open-activated, and closed-inactivated conformations.

7.2 Results

7.2.1 Cryo-EM structures of hIP$_3$R-3 gating conformations

Bimodal regulation of IP$_3$R activity by Ca^{2+} complicates sample preparation because of the requirement for fine adjustment of Ca^{2+} concentration to trap the channel in the open conformation. Although free Ca^{2+} concentrations in solutions can easily be controlled by using Ca^{2+} buffers such as EGTA or BAPTA, it becomes challenging during sample preparation for cryo-EM due to the small volumes used. Typically, a 2–3 μL protein sample is applied to a cryo-grid, but more than 99% of the sample volume is lost during grid preparation due to extensive blotting with filter paper (Arnold et al. 2017). During this time, the samples contact filter paper and cryo-grids, containing various amounts of Ca^{2+}. Small sample volumes and short time frames may reduce these buffers'

efficiency, causing the free Ca^{2+} concentration to increase to inhibitory levels prior to sample freezing. In order to maximize the chances of obtaining particles in the active state, we prepared the sample in: (1) EDTA, which has approximately 200 fold faster binding kinetics to Ca^{2+} than EGTA (Naraghi 1997), a common Ca^{2+} chelator, and is more likely to chelate excess Ca^{2+} and other divalent cations within the short period prior to the sample plunging, (2) ATP, which increases the open probability of IP_3Rs and dampens the inhibitory effect of Ca^{2+}, (I. Bezprozvanny and Barbara E. Ehrlich 1993; Tu, Zhengnan Wang, Nosyreva, et al. 2005), and (3) high concentrations of IP_3.

The final hIP_3R-3 sample was purified in the presence of 1 mM EDTA and supplemented with 0.5 mM IP_3, 5 mM ATP, and 0.1 mM CaCl2 before preparing cryo-grids. Although the free Ca^{2+} concentration was calculated around 100 nM under these conditions using Maxchelator (Bers, Patton, and Nuccitelli 1994), the actual free Ca^{2+} concentration may be higher due to potential leakage of Ca^{2+} during the cryo-grid preparation as mentioned above. We performed a cryo-EM analysis on a large dataset by employing exhaustive 3D classification strategies to separate particles belonging to different functional states resulting in five high resolution (3.2–3.8 Å) structures (Supplementary Figures 51-54; Supplementary Table 2). The pore region in all structures resolved to 3.5 Å or better, allowing us to build side chains and determine if the channel was open or closed (Figure 30; Supplementary Figures 50-54).

Three structures have closed pores with well-resolved densities for IP_3 and ATP and are referred to as pre-active A, B, and C (Figure 30b; Supplementary Figures 51-55). The structure named "active" displays drastic conformational changes at the TMD, leading to pore opening (Figure 30c). In addition to the well-resolved densities for IP_3 and ATP, the active structure reveals substantial density, interpreted as Ca^{2+}, at the ARM3-JD interface, referred to as the activatory Ca^{2+} binding site (Figure 30c; Supplementary Figures 53, 55). In the fifth structure, the channel is closed, the activatory Ca^{2+} binding site is occupied, and the intersubunit interactions of the cytoplasmic domains are lost (Figure 30d; Supplementary Figure 54). The structure is highly similar to the hIP_3R-3 structures obtained in the presence of inhibitory Ca^{2+} concentrations6, except for βTF1, which moves closer to the ARM1 (Supplementary Figure 56). Most notably, ARM2 adopted the same conformation relative to ARM1 and CLD, creating the binding site for the second Ca^{2+} ob-

served at high Ca^{2+} concentrations (Supplementary Figure 56). While these similarities suggest a Ca^{2+} ion occupies this site and the structure represents the Ca^{2+} inhibited state, the quality of the map around the region did not allow accurate inspection of the presence of Ca^{2+} (Supplementary Figure 56). Therefore, we refer to the structure as "inactive" while it remains unclear if it represents a desensitized state that hIP_3R-3 adopts without additional Ca^{2+} binding or an inhibited state forced by binding of additional Ca^{2+} to an inhibitory site.

It is important to note that our initial 3D classification runs resulted in two major classes grouping the pre-active and active structures into one class and the inactive structure into another (Supplementary Figure 30). It was essential to perform another round of 3D classification focusing only on the core of the protein to separate the particles in the active state from the pre-active states, potentially due to subtle differences in the overall structures and the much fewer number of particles in the active state (20,039 particles compared to 346,684 particles in the pre-active states) (Supplementary Figure 30; Supplementary Table 2).

7.2.2 Priming of hIP_3R-3 for activation

To compare the structures presented here, we aligned their selectivity filters and pore helices (residues 2460-2481), which reside at the lumenal side of the TMD and are virtually identical in all classes. The pre-active A structure is almost identical to the previously published IP_3-bound hIP_3R-3 structure (Paknejad and Hite 2018) (Supplementary Figure 57a) and reveals that IP_3 binding causes the ARM1 to rotate about 23° relative to the βTF-2, causing global conformational changes within the cytoplasmic domains, as observed in previous cryo-EM and X-ray crystallography experiments (Paknejad and Hite 2018; Fan, M. R. Baker, Zhao Wang, et al. 2018; Kozo Hamada, Miyatake, et al. 2017; Bosanac, Alattia, et al. 2002; C.-C. Lin, Baek, and Z. Lu 2011; Seo et al. 2012) (Supplementary Figure 57b, c). The pre-active B and C structures adopt distinct conformations that are intermediates between the pre-active A and open state structures. Based on these conformational changes, we propose a sequential transition from pre-active A to B, then C, although the alternative transitions cannot be ruled out entirely. During the transition to the pre-active B state, the N-terminal domain (NTD) of each protomer comprising βTF1, βTF2, ARM1, ARM2, and CLD rotates about 4° counter-clockwise relative to the TMD and moves about 2 Å

closer to the membrane plane (Figure 31 a; Supplementary Movie 1). In the pre-active C state, the NTDs remain primarily unchanged compared to the pre-active B state, while the ARM3 and JD are rotated by 7°, causing mild distortions at the cytoplasmic side of the TMD without opening the channel (Figure 31 b; Supplementary Movie 1). Compared to the ligand-free conformation, the βTFs move about 7 Å closer to the membrane plane, and ARM3-JD rotates about 11° in the pre-active C conformation.

7.2.3 Ca^{2+}-mediated conformational changes leading to pore opening

In the absence of Ca^{2+}, the ARM3 and JD act as a rigid body, where there are no significant conformational changes relative to each other (Figure 31 a, b). When Ca^{2+} is bound, the JD rotates about 11° relative to the ARM3 (Figure 32 a), resembling a clamshell closure, which leads to global conformational changes in the whole receptor, including the movement of the NTD closer to the membrane plane by 2 Å (Figure 32 b; Supplementary Movie 1). In contrast to the limited rotation of the ARM3 (about 5°), the JD rotates about 14° around an axis roughly perpendicular to the membrane plane, leading to conformational changes at the TMD and resulting in pore opening in the active state (Figure 32 b).

Ca^{2+} is coordinated by E1882 and E1946 on the ARM3 and the main-chain carboxyl group of T2581 on the JD (Figure 32 c). H1884 and Q1949 are also close and may interact with Ca^{2+} through water molecules (Figure 32 c). These residues are highly conserved in the homologous ion channel family, ryanodine receptors (RyRs), suggesting a common activation mechanism in IP_3Rs and RyRs (Georges et al. 2016) (Supplementary Figure 58a, b). Mutation of the corresponding residues in RyRs markedly reduced the sensitivity to Ca^{2+}, further supporting this site's involvement in the Ca^{2+} induced activation (W. Guo et al. 2020; Chirasani et al. 2019; L. Xu et al. 2018).

7.2.4 ATP binding site

Within the JD, we observed a well-resolved cryo-EM density for ATP in all the structures (Supplementary Figure 55). The quality of the maps obtained through local refinement allowed unambiguous modeling of ATP, revealing its key interactions with the protein residues (Figure 33 a,

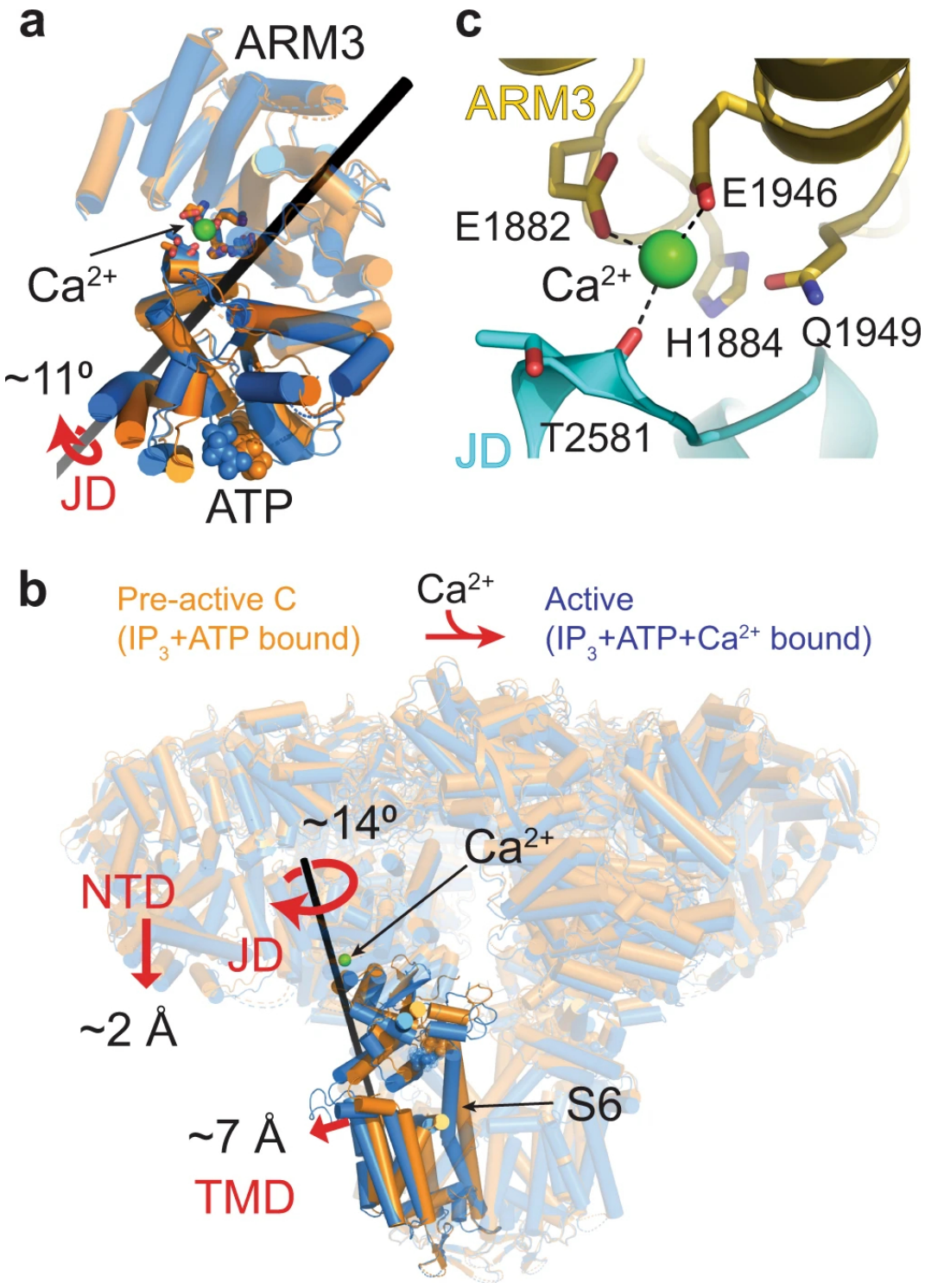

Figure 32: **Conformational changes coupling Ca^{2+} binding to pore opening.** (a) Comparison of the JD (shown in full colors) orientation relative to the ARM3 (shown transparent) in the pre-active-C (orange) and active (blue) structures. The black bar indicates the axis for the rotation of the JD. Ca^{2+} and ATP are shown as spheres. (b) Global conformational changes induced by Ca^{2+} binding are depicted similar to Figure 31. (c) Close-up view of the Ca^{2+} binding site in the active conformation. Domains are colored as in Figure 30.

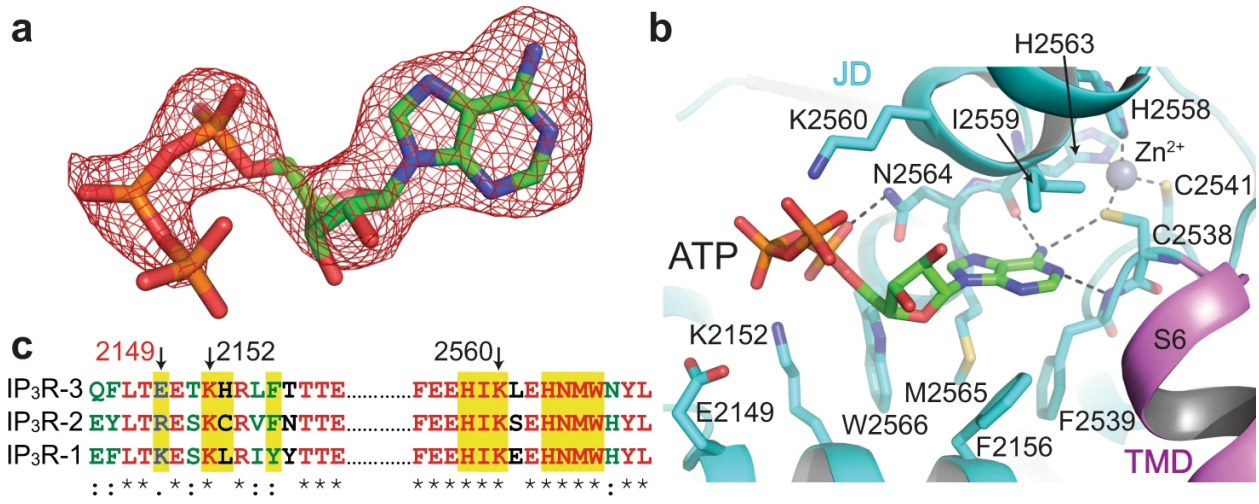

Figure 33: **ATP binds to the JD.** (a) The cryo-EM density of ATP (red mesh) from the composite map of the pre-active A state and the modeled ATP molecule. (b) Close-up view of the ATP binding site in the pre-active A state. Dashed lines indicate hydrogen bonding. (c) Sequence alignment of hIP3R subtypes around the residues forming the ATP binding site. Residues shown in (b) are highlighted. Select residues are indicated by arrows, and E2149 is labeled in red.

b). The adenosine base intercalates into a cavity surrounded by F2156, F2539, I2559, M2565, and W2566 near the zinc finger motif and forms hydrogen bonds with the sulfur of C2538, the backbone amide group of F2539, and the carbonyl groups of H2563 and I2559 (Figure 33 b). The phosphate moieties interact with K2152, K2560, and N2564 (Figure 33 b). There are no apparent structural changes around the binding site upon ATP binding, suggesting that ATP's potentiating effect is likely due to the increased rigidity of the JD (Supplementary Figure 57d). ATP binding site is highly conserved among the subtypes except for E2149 which corresponds to lysine and arginine in IP_3R-1 and IP_3R-2 (Figure 33 c). A positively charged residue instead of E2149 in the proximity of the phosphate moieties may cause tighter interaction of ATP with IP_3R-1 and IP_3R-2, explaining the low binding affinity of ATP to IP_3R-3 compared to IP_3R-1 and IP_3R-2 (Tu, Zhengnan Wang, Nosyreva, et al. 2005).

ATP binds to a similar location near the zinc finger motif in RyRs (Georges et al. 2016; Melville et al. 2022; Ma et al. 2020). However, its binding mode differs, potentially due to the differences in the residues that form the binding pocket, most notably the basic residues interacting with the phosphate moieties (Supplementary Figure 58a, c, d). In RyR-1s, the phosphate moieties interact with K4211, K4214, and R4215, all located on a single helix (Supplementary Figure 58c, d). In

hIP$_3$R-3, there is only a single lysine residue (K2152) on the corresponding helix, and the phosphate moieties interact with K2560, located on the opposite side of the binding pocket. A leucine residue (L4980) occupies this position in RyR-1s. The differences in the number and location of the basic residues likely force the phosphate moieties of ATP to adopt different conformations. Furthermore, F2156 in hIP$_3$R-3 points toward the adenosine binding pocket, prohibiting ATP from adopting the conformations observed in RyR-1s due to steric clash in hIP$_3$R-3s (Supplementary Figure 58c, d).

7.2.5 Structure of the TMD in the open conformation

The TMD of IP$_3$Rs has the same overall architecture of voltage-gated ions channels with a central pore domain, consisting of S5, S6, and pore (P) helix, surrounded by pseudo-voltage-sensor domains (pVSDs), consisting of S1, S2, S3, and S4 helices along with two IP$_3$R/RyR specific TM helices (S1' and S1") (Figure 34). In the closed channel, F2513 and I2517 of the S6 helix form two layers of hydrophobic constriction at the pore, blocking the path for the permeation of hydrated ions (Figure 34). JD's rotation upon Ca^{2+} binding pushes the pVSD's cytoplasmic side away from the pore domain by about 7 Å and tilts the cytoplasmic side of the S6 (S6$_{cyt}$) by 12° (Figure 34 a; Supplementary Movie 1). Concurrently, the S4-5 linker and S5 helix move away from the S6 helix, thereby inducing a distortion of S6 around the constriction site and moving F2513 and I2517 away from the pore. As a result, the diameter of the water-accessible pore increases to 8 Å, large enough to permeate hydrated cations (Figure 34 b). The flexibility introduced by the neighboring glycine residue (G2514), mutation of which to alanine in IP$_3$R-1 is associated with spinocerebellar ataxia (Melville et al. 2022) (SCA29) (Gonzaga-Jauregui et al. 2015), is likely critical to the movement of F2513. The tilting of the S6$_{cyt}$ breaks the salt bridge between D2518 and R2524 of the neighboring subunits, moving D2518 towards the pore while pulling R2524 away, which creates an electronegative path on the cytoplasmic side of the pore (Supplementary Figure 59). In contrast to the prediction of a π- to α-helix transition at the S6$_{lum}$ during channel opening (Paknejad and Hite 2018; Azumaya et al. 2020), the π-helix remains intact, and its tip acts as a pivot for the S6$_{cyt}$ tilting and bulging (Figure 34).

Although the TMDs of IP$_3$Rs and RyRs are highly similar, there are noticeable differences in their pore structures (Supplementary Figure 58e, f). In RyRs, the constriction site is formed by

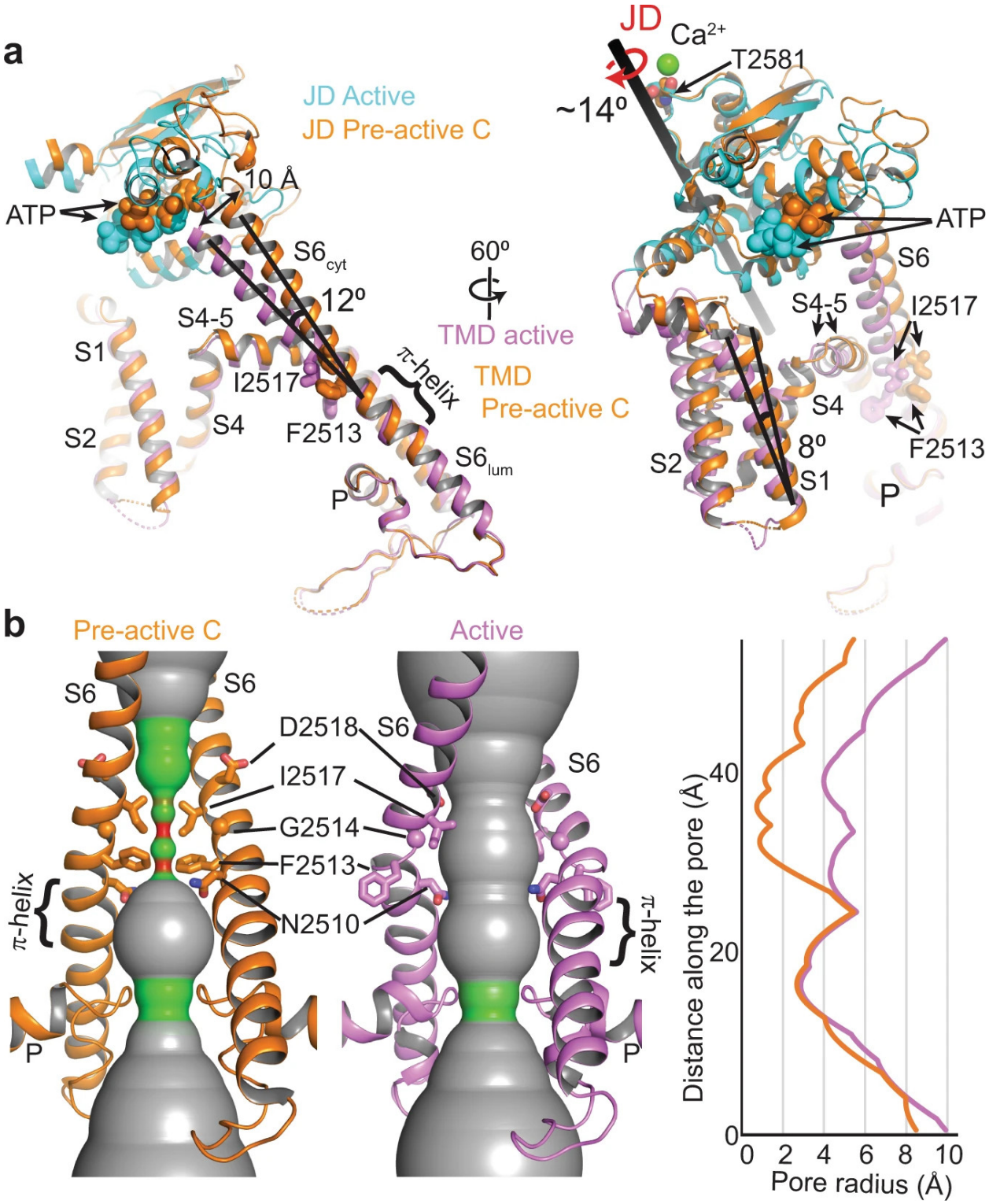

Figure 34: **Structure of the IP$_3$R-3 in the open conformation.** (a) Comparison of the hIP$_3$R-3 structures in the pre-active C and active conformations aligned as in Figure 31. b Ion permeation pathways of hIP$_3$R-3 in pre-active C and active conformations (radii coloring: red, <0.8 Å; green, 0.8-4.0 Å; gray, >4.0 Å) along with the 1D graph of the pore radius. The JD and TMD of the active state are shown in cyan and violet, respectively. The pre-active C structure is colored orange.

glutamine and isoleucine, corresponding to F2513 and I2517 in hIP$_3$R-3, respectively (Woll and Van Petegem 2022). In the open state of RyRs, the isoleucine is positioned similarly to I2517 of hIP$_3$R-3 (Georges et al. 2016; Peng et al. 2016; Wei et al. 2016). On the other hand, the glutamine residue faces the pore in the open state, forming part of the hydrophilic permeation pathway, unlike F2513. Interestingly, N2510 in hIP$_3$R-3, which corresponds to alanine in RyRs, faces the permeation pathway similar to the glutamine of RyRs, suggesting that the amide group plays an important role in the ion permeation. However, since the side chain of N2510 extends from a different position on the S6 helix than the side chain of glutamine in RyRs, the binding pocket for ryanodine (Georges et al. 2016), a RyR-specific inhibitor, is not present in IP$_3$R, potentially causing IP$_3$Rs to be unresponsive to ryanodine (Peng et al. 2016).

Several missense mutations identified in the IP$_3$R subtypes are associated with diseases, including spinocereblar ataxia, Gillespie syndrome, anhidrosis, and neck squamous cell carcinoma (Supplementary Figure 60; reviewed in (Woll and Van Petegem 2022; Kerkhofs et al. 2018; Hisatsune and Katsuhiko Mikoshiba 2017)). Perhaps not surprisingly, most of these mutations are localized around the IP$_3$ binding site and alter IP$_3$ binding affinity (Woll and Van Petegem 2022; Kerkhofs et al. 2018; Hisatsune and Katsuhiko Mikoshiba 2017; Ando, Hirose, and Katsuhiko Mikoshiba 2018). Another hot spot for these mutations is the constriction site of the pore, which undergoes conformational changes during channel opening (Supplementary Figure 60). It is plausible that these mutations either affect the Ca^{2+} permeability (e.g., mutation of N251038 or I251739) or restrict conformational changes required for dilation of the pore (e.g., mutation of G251431). Two of the mutated residues (T251940 and F252041) interact with the residues on the S4-S5 linker, which couples the tilting of the pVSD to the bulging of the constriction site (Supplementary Figure 60b). Mutations of these residues are likely to impair this coupling and thus hinder gating.

7.2.6 The flexibility of the CTD

The CTD, extending from the JD along the symmetry axis, forms a left-handed coiled-coil motif before interacting with the βTF2 of the neighboring subunit. The density for the CTD was poorly resolved in all of the states (Supplementary Figure 61a, b). However, the coiled-coil motifs were visible in the unsharpened maps in the pre-active and active states, enabling us to model poly-alanine peptides without assigned registries (Supplementary Figure 61a, b). The densities for the exten-

sions from the coiled-coil motif towards the βTF2 become visible when viewed at lower thresholds, whereas the linkers between the JD and the coiled-coil motif remain invisible, indicating higher flexibility for this region (Supplementary Figure 61a, b). We did not observe any interpretable density for the CTD in the inactive state (Supplementary Figure 61a, b).

For IP_3R-1, the CTD was proposed to transmit the conformational changes induced by IP_3 at the NTD to the JD (Fan, M. R. Baker, Zhao Wang, et al. 2018). In IP_3R-3, there are no apparent changes on the coiled-coil motif in the pre-active states, but the coiled-coil motif rotates about 20° around the symmetry axis and moves closer to the TMD by 6 Å in the active state (Supplementary Figure 61c, d). However, the linker between the coiled-coil motif and JD remains flexible, suggesting that the structural rearrangements of this domain are not directly enforcing the channel opening (Supplementary Figure 61). In line with these observations, removing CTD residues interacting with the βTF2 or swapping the C-terminal region of IP_3R-1 with the RyRs, which lack the extended CTD, did not diminish receptor activation (Kozo Hamada, Miyatake, et al. 2017; Seo et al. 2012; Schug and Suresh K. Joseph 2006).

7.2.7 Mechanism of hIP$_3$R-3 activation and gating

It has been long recognized that IP_3 binding primes the receptor for activation by Ca^{2+},(Adkins and Colin W. Taylor 1999), but how the priming is achieved has remained elusive. Our structures reveal that IP_3 binding leads to several conformational changes at the NTD, ARM3, and JD, without any apparent structural changes at the activatory Ca^{2+} binding site, and that the ARM3 and JD adopt a new pre-gating conformation relative to the TMD with modest changes at the intersubunit interface between the JDs at the cytoplasmic side of the TMD (Figure 35; Supplementary Figure 62; Supplementary Movie 1). In addition, ARM3s are constrained in their pre-gating conformation by the tetrameric cage-like assembly of the NTDs, forcing the JDs to rotate upon Ca^{2+} binding. The NTD assembly is maintained by the βTF1-βTF2 intersubunit interactions (βTF ring), which remains intact in the pre-active and active states (Figure 35; Supplementary Figure 63; Supplementary Movie 1) and acts as a pivot for the conformational changes that stabilize the ARM3. On the other hand, its disruption in the inactive state leads to the loosening of the tetrameric assembly of the NTDs, relieving the ARM3 constraints and causing the JD and TMD to adopt the closed channel conformation despite the bound Ca^{2+} to the activatory site. Supporting this hypothesis,

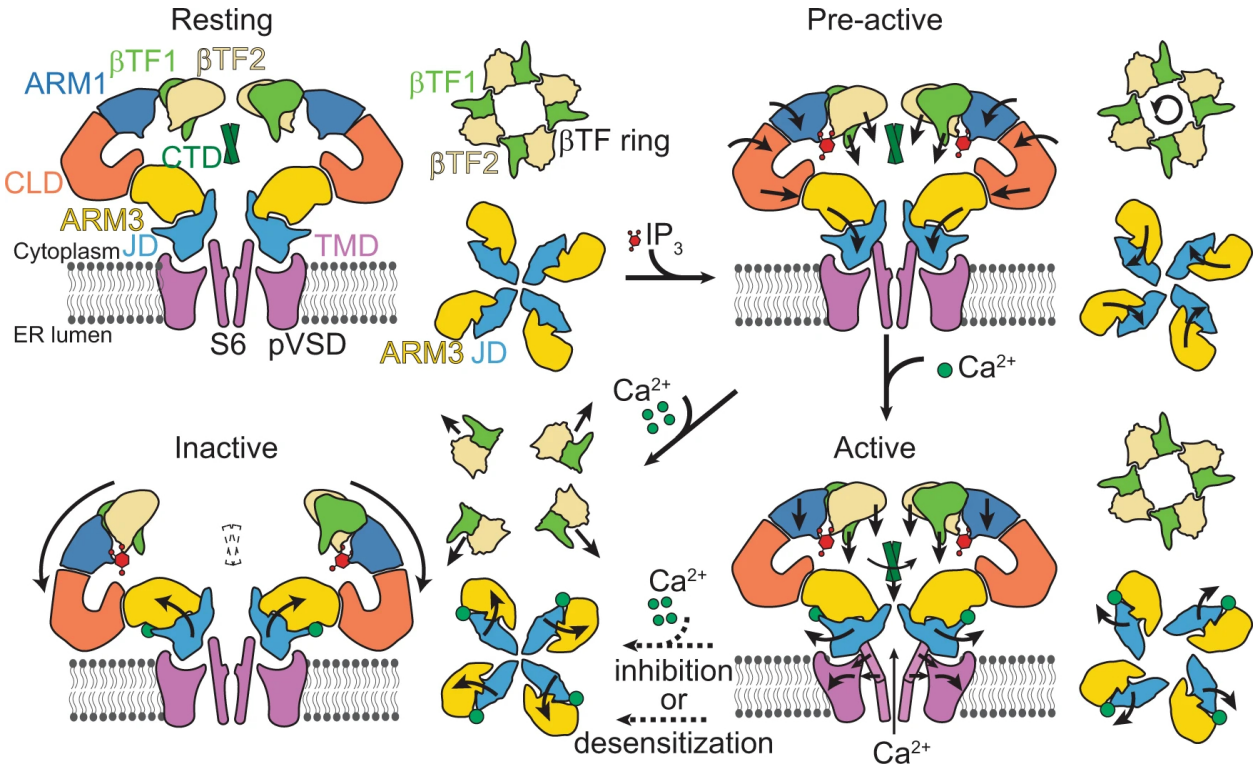

Figure 35: **Schematic representation of the IP$_3$R gating cycle.** (a) side view of the two opposing subunits (left) and cytoplasmic views of the βTFs and ARM3-JD tetramers (right) for each indicated functional state is depicted. The ARM2 and CTD are omitted for clarity. Arrows shown on the domains indicate the direction of the rotation or translation from the previous conformation.

the removal of βTF1 or mutation of W168, which resides at the βTF1-βTF2 interface (Supplementary Figure 63), was shown to abolish IP$_3$R activity (Keiko Uchida et al. 2003; Yamazaki et al. 2010).

In conclusion, the ensemble of structures obtained from the same sample demonstrates structural heterogeneity of IP$_3$Rs in the presence of IP$_3$, ATP, and Ca^{2+}. Our ability to correlate these structures with their plausible functional states allowed us to define the conformational changes at different gating states, revealing the structural features that underpin IP$_3$R activation and gating. These structures will likely serve as foundations for future experiments addressing biophysical and functional questions related to IP$_3$Rs. Furthermore, our study reinforces the power of cryo-EM in analyzing heterogeneous samples and highlights the importance of a thorough investigation of the data to identify physiologically relevant conformations, even when they constitute only a tiny fraction of the sample.

7.3 Materials and methods

7.3.1 Protein expression and purification

Expression and purification of hIP_3R-3 were performed as previously described with minor modifications (Azumaya et al. 2020). Briefly, hIP_3R-3 (residues 4-2671) with a C-terminal OneStrep tag was expressed using the MultiBac expression system (Fitzgerald et al. 2006). Sf9 cells (4×10^6 cells/mL) were harvested by centrifugation (4000 × g) 48h after infection with the baculovirus. Cells resuspended in a lysis buffer of 200 mM NaCl, 40 mM Tris-HCl pH 8.0, 2 mM EDTA pH 8.0, 10 mM β-mercaptoethanol (BME), and 1 mM Phenylmethylsulfonyl fluoride (PMSF) were lysed using Avastin EmulsiFlex-C3. After centrifugation of the lysate at 7000 × g for 20 minutes to remove large debris, the membrane was pelleted by centrifugation at 185,000 × g (Type Ti45 rotor) for 1 hour. Membrane pellets were homogenized in ice-cold resuspension buffer (200 mM NaCl, 40 mM Tris-HCl pH 8.0, 2 mM EDTA pH 8.0, 10 mM BME) using a Dounce homogenizer, and solubilized using 0.5% Lauryl maltose neopentyl glycol (LMNG) and 0.1% glyco-diosgenin (GDN) at a membrane concentration of 100 mg/mL. After 4 hours of gentle mixing in the cold room, the insoluble material was pelleted by centrifugation at 185,000 × g (Type Ti45 rotor) for 1 hour, and the supernatant was passed through Strep-XT resin (IBA Biotagnology) via gravity flow. The resin was washed first with 5 column volume (CV) of wash buffer composed of 200 mM NaCl, 20 mM Tris-HCl pH 8.0, 10 mM BME, 0.005% GDN, 0.005% LMNG, followed by 5 CV of wash buffer supplemented with 5 mM ATP and 20 mM MgCl2 to remove any bound chaperone proteins, and finally with 5CV of wash buffer supplemented with 1 mM EDTA. The protein was eluted using wash buffer supplemented with 1 mM EDTA and 100 mM D-Biotin (pH 8.2). The protein was further purified by size exclusion chromatography (SEC) using a Superose 6 Increase column (10/300 GL, GE Healthcare) equilibrated with the SEC buffer composed of 200 mM NaCl, 20 mM Tris-HCl pH 8.0, 1 mM EDTA pH 8.0, 2 mM TCEP, 0.005% LMNG, and 0.005% GDN. The fractions corresponding to hIP_3R-3 were combined and concentrated to 4 mg/mL using a 100 kDa centrifugal filter (Sartorius). The concentrated sample was then centrifuged at 260,000 × g using an S100AT rotor (ThermoFisher Scientific). The concentration dropped to 1.8 mg/mL.

7.3.2 Cryo-EM sample preparation and data collection

Purified hIP$_3$R-3 in the SEC buffer containing 1 mM EDTA was supplemented with 500 μM IP$_3$ (from 10 mM stock in water), 0.1 mM $CaCl_2$, and 5 mM ATP (from 100 mM stock, pH 7.2). 2.0 μL of the protein sample was applied to 300 mesh Cu Quantifoil 1.2/1.3 grids (Quantifoil Microtools) that were glow discharged for 20 seconds at 25 mA. The grids were blotted for 7 seconds at force 10 using single-layer Whatman ashless filter papers (Cat. : 1442-055, GE Healthcare) and were plunged into liquid ethane using an FEI MarkIV Vitrobot at 8 °C and 100% humidity. The filter papers were not pre-treated with Ca^{2+} chelators or any other chemicals. Four grids prepared using the same sample were imaged using a 300kV FEI Krios G3i microscope equipped with a Gatan K3 direct electron camera in four different data collection sessions at Case Western Reserve University. Movies containing 40–50 frames were collected at a magnification of ×105,000 in super-resolution mode with a physical pixel size of 0.828 Å/pixel and defocus values at a range of 0.8 to 1.6μm using the automated imaging software SerialEM (Mastronarde 2005) and EPU (ThermoFisher Scientific).

7.3.3 Cryo-EM data processing

Datasets from four sessions were initially processed separately using Relion 3.0 (Zivanov, Nakane, Forsberg, et al. 2018). We used MotionCor2 (Zheng et al. 2017) and Gtcf (K. Zhang 2016) to perform beam-induced motion correction and CTF estimations, respectively. We performed auto picking using the Laplacian-of-Gaussian option of Relion, extracted particles binned 4 × 4, and performed 2D class classification. Using the class averages with apparent features, we performed another round of particle picking. We cleaned the particles, extracted as 4 × 4 binned, through 2D classification and performed 3D classification using the hIP$_3$R-3 map (EMD-20849) (Azumaya et al. 2020), which was converted to the appropriate box and pixel size. We observed two predominant conformations. One had a compact NTD and tight interactions between subunits as in previously published IP$_3$R structures in the absence of Ca^{2+}, hereafter called "compact" conformation (Paknejad and Hite 2018; Fan, M. L. Baker, et al. 2015; Fan, M. R. Baker, Zhao Wang, et al. 2018; Azumaya et al. 2020) (Supplementary Figure 51). The other one had the NTD of each subunit tilted away from the central symmetry axis resembling hIP$_3$R-3 structures obtained in the presence of high Ca^{2+} concentrations, hereafter called "loose" conformation (Paknejad and Hite

2018) (Supplementary Figure 51). These particles were separately selected and reextracted using a box size of 480 × 480 pixels at the physical pixel size. After 3D refinements, we performed CTF refinement and Bayesian polishing (Zivanov, Nakane, and Sjors H. W. Scheres 2019).

We combined all the polished particles and performed another round of 3D classification, using one of the compact structures as a reference map. We grouped particles into "compact" and "loose" classes (Supplementary Figure 51). Refinement of the particles in the "compact" conformation yielded a 3D reconstruction with an average resolution of 3.9 Å. Although there were slight changes at the TMD compared to the structure in the closed state, these changes were not significant enough to suggest that the channel was open. To more clearly resolve the density around the TMD, we performed another round of 3D classification using a mask that only covers the ARM3, JD, and TMD and without performing an angular or translational alignment in Relion3 (Supplementary Figure 51) (S. H. W. Scheres 2016). 3D refinements of the particles in each class were performed using non-uniform refinement in CryoSPARC, enforcing C4 symmetry and local CTF refinements (Supplementary Figure 51) (Punjani et al. 2017). Five classes led to four high-resolution (better than 4 Å) 3D reconstructions, whereas the 3D refinement of the other three classes resulted in poorly resolved maps. The particles in the "loose" conformation were processed using non-uniform refinement in CryoSPARC, but without enforcing any symmetry. Local resolution estimates were calculated using CryoSPARC (Punjani et al. 2017) (Supplementary Figure3 50-54). Some of the data processing and refinement software was supported by SBGrid (Morin et al. 2013).

To improve the quality of the maps, we performed local refinements using masks covering parts of the original cryo-EM maps (Supplementary Figure3 50-54). We prepared five masks that cover distinct domains of one of the subunits for the pre-active A, B, C, and active conformations. After symmetry expansion using C4 symmetry, we performed local refinement using CryoSparc (Supplementary Figure 50-53). For the inactive state, we prepared four masks that cover the cytoplasmic domains of each subunit and another mask that covers the tetrameric ARM3, JD, and TMD (Supplementary Figure 54). The local refinements were performed using C1 symmetry for the cytoplasmic domains and C4 symmetry for the tetrameric ARM3, JD, and TMD. The resulting local refinement maps were aligned onto the original maps using Chimera (Pettersen, Goddard, Huang,

Couch, et al. 2004) and merged using the "VOP maximum" command of Chimera (Pettersen, Goddard, Huang, Couch, et al. 2004) to prepare the composite maps (Supplementary Figure 50-54).

7.3.4 Model building

Model building was performed using Coot (Afonine et al. 2013). We first placed the hIP_3R-3 structure in ligand-free conformations (PDB ID: 6UQK) (Azumaya et al. 2020) into the composite map of Pre-active A, and performed rigid-body fitting of individual domains of one of the protomers. We then manually fit the residues into the density and expanded the protomer structure into a tetramer using the C4 symmetry. We performed real-space refinement using Phenix (Afonine et al. 2013). We repeated build-refine iterations till a satisfactory model was obtained. This model was used as a starting model for the other structures following the same workflow. Regions without interpretable densities were not built into the model. Residues without apparent density for their side chains were built without their side chains (i.e., as alanines) while maintaining their correct labeling for the amino acid type. The coiled-coil regions were modeled as poly-alanines without residue assignment using the unsharpened maps. Validations of the structural models were performed using MolProbity (C. J. Williams et al. 2018) implemented in Phenix (Afonine et al. 2013).

7.3.5 Figure preparation

Figures were prepared using Chimera (Pettersen, Goddard, Huang, Couch, et al. 2004), ChimeraX (Pettersen, Goddard, Huang, Meng, et al. 2021), and The PyMOL Molecular Graphics System (Version 2.0, Schrödinger, LLC). Calculation of the pore radii was performed using the software HOLE (Smart et al. 1996).

7.3.6 Data availability

The data that support this study are available from the corresponding author upon reasonable request. Cryo-EM maps and atomic coordinates are deposited to the Electron Microscopy Data Bank (EMDB) and Protein Data Bank (PDB) databases, respectively. The accession codes are EMD-25667 and 7T3P for pre-active A, EMD-25668 and 7T3Q for pre-active B, EMD-25669 and

7T3R for pre-active C, EMD-25670 and 7T3T for active, and EMD-25671 and 7T3U for inactive states, respectively. The following previously published datasets were used: EMD-20849, Cryo-EM structure of type 3 IP_3 receptor revealing presence of a self-binding peptide (Azumaya et al. 2020). 6UQK, Cryo-EM structure of type 3 IP_3 receptor revealing presence of a self-binding peptide (Azumaya et al. 2020). 6DRC, High IP_3 Ca^{2+} human type 3 1,4,5-inositol trisphosphate receptor (Paknejad and Hite 2018). 6DQV Class 2 IP_3-bound human type 3 1,4,5-inositol trisphosphate receptor (Paknejad and Hite 2018). 5TAL, Structure of rabbit RyR1 (Caffeine/ATP/Ca^{2+} dataset, class 1 and 2) (Georges et al. 2016). 7M6A, High resolution structure of the membrane embedded skeletal muscle ryanodine receptor (Melville et al. 2022). Reagents and other materials will be available upon request from E.K. with a completed materials transfer agreement.

8 Structural characterization of antagonist action on hIP$_3$Rs

8.1 Introduction

IP$_3$Rs are ligand-gated calcium ion channels located primarily in the endoplasmic and sarcoplasmic reticulum of almost all eukaryotic cells. IP$_3$Rs are a critical component of the cell's Ca^{2+} signaling system, coupling the extracellular signals that activate GPCRs and RTKs with the effects of intracellular IP$_3$R binding proteins and post-translational modifications to fine tune the Ca^{2+} signal released from the ER lumen. The precisely spatiotemporaly controlled Ca^{2+} signal generated by IP$_3$s exerts its effect through cytosolic Ca^{2+} buffers and Ca^{2+} binding proteins that propagate the signal regulating important cellular functions such as cell division, synaptic transmission, and gene expression (Kozo Hamada and Katsuhiko Mikoshiba 2020; C.-C. Lin, Baek, and Z. Lu 2011). The three IP$_3$R isoforms (IP$_3$R-1, -2, -3) share about 70% sequence similarity, and can form both homo and heterotetramers 1.2 MDa in size. Each monomer is comprised of five functional domains: suppressor domain, IP$_3$-binding core, central modulatory/transducing domain, a transmembrane domain comprising six alpha helices, and a C-terminal left-handed coiled-coiled tail (Gambardella, Lombardi, et al. 2020; Santulli et al. 2017; Fan, M. L. Baker, et al. 2015; Serysheva, M. R. Baker, and Fan 2017; Fan, M. R. Baker, Zhao Wang, et al. 2018; Kozo Hamada, Miyatake, et al. 2017; Chandran et al. 2019).

Understanding the role of IP$_3$R in disease is complicated by the more than 100 different binding proteins (Prole and Colin W. Taylor 2016), IP$_3$R-1 splice variants, and post-translational modifications such as phosphorylation and cleavage by caspases (J. K. Foskett et al. 2007). Investigation into the role of IP$_3$Rs in conditions ranging from the neurological to cancers is complicated by the lack of drugs and compounds that can selectively target the IP$_3$R over other Ca^{2+} transport machinery. The lack of isoform specific pharmacological tools also limits researchers' ability to study the receptor's activity and behavior in the laboratory setting. There has been considerable interest in developing IP$_3$R specific agonists and antagonists, with more success in the agonist search. Partial agonists have been developed to map the key residues in the IP$_3$-binding core that are required for IP$_3$ binding and propagating the initial conformational changes to the central modulatory domain (A. M. Rossi et al. 2009). The X-ray crystal structures of N-terminal sections of the IP$_3$R

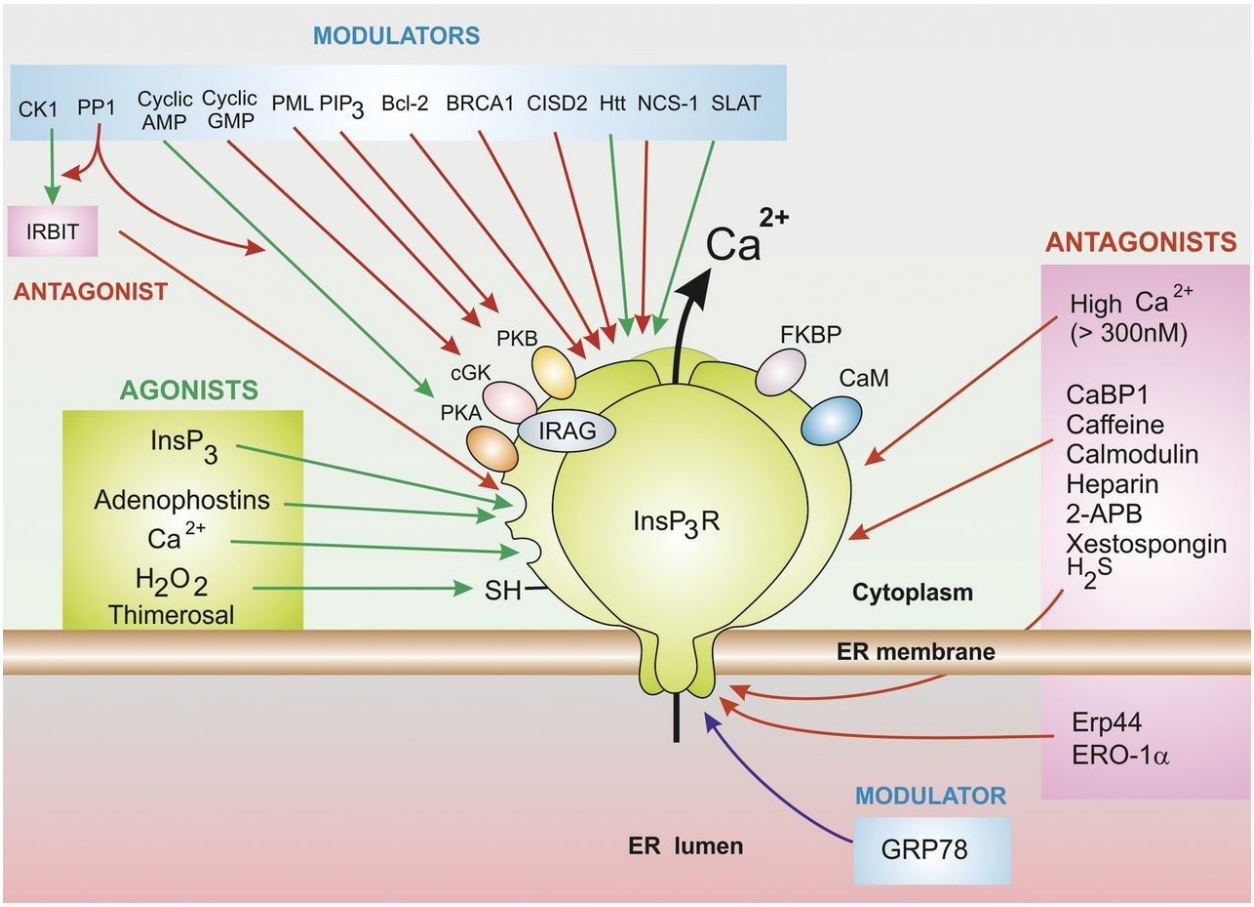

Figure 36: **In addition to its role as a Ca^{2+} channel, the IP_3R is a molecular scaffold whose activity can be modulated by dozens of binding partners.** The required co-agonists for IP_3R are Ca^{2+} and IP_3. Compounds that act as IP3R agonists are shown with green arrows, while compounds and proteins with antagonistic effects are shown with red arrows. In addition to modulatory compounds and proteins, post-translational modificiations, such as phosphorylation modulate IP_3R activity. Image from (Berridge 2016).

(C.-C. Lin, Baek, and Z. Lu 2011; Bosanac, Alattia, et al. 2002), and Cryo-EM structures of the full receptor (Fan, M. R. Baker, Zhao Wang, et al. 2018; Fan, M. L. Baker, et al. 2015; Paknejad and Hite 2018; Azumaya et al. 2020; Schmitz, H. Takahashi, and Karakas 2022) have facilitated the rational design of a host of agonists, described in detail in section 5.2.3. The design of antagonists has been complicated by the lack of structures of IP_3Rs in complex with existing small molecule antagonists, and the dearth of knowledge on where the antagonist binding sites are located on the receptor.

8.2 Results

8.2.1 Cryo-EM structure of IP_3R-3 in the presence of 2-APB

In the search for a co-structure of an IP_3R isoform in complex with an chemical inhibitor, IP_3R-3 was chosen as the initial starting candidate due to its relatively high expression levels compared to the other two isoforms. In addition the purification protocol for IP_3R-3 was already optimized to maximize protein yield and the isoform behaved well in vitrified conditions, showing neither aggregation nor orientation bias. Since there are no IP_3R specific antagonists, a co-structure of IP_3R in complex with a non-specific inhibitor would provide a foundation for future rational drug design of more specific and sensitive compounds. Among the existing non-specific IP_3R inhibitors, 2-APB and XeC are the most widely used to modulate IP_3R activity in the laboratory setting. While both compounds were initially, individually used to generate vitrified conditions with IP_3R-3, the ice quality for grids containing XeC was too poor to allow for data collection. Ice quality for grids containing 2-APB was much better in comparison, and enabled data collection. Although neither the binding affinity nor the exact binding site for 2-APB are known, 5 mM 2-APB was added to produce theoretically saturating conditions since concentrations used in the literature tend to be around 100 μM (Saleem et al. 2014). The Cryo-EM micrographs were processed, with the final map reaching 4.01 Å resolution. Coloring the filtered map according to local resolution shows the core of the protein has higher resolution compared to the more flexible peripheral N-terminal domain (Figure 37). After fitting an apo model of IP_3R-3 into the cryo-EM map, and examining the resulting map carefully, no extra unassigned density could be attributed to 2-APB,

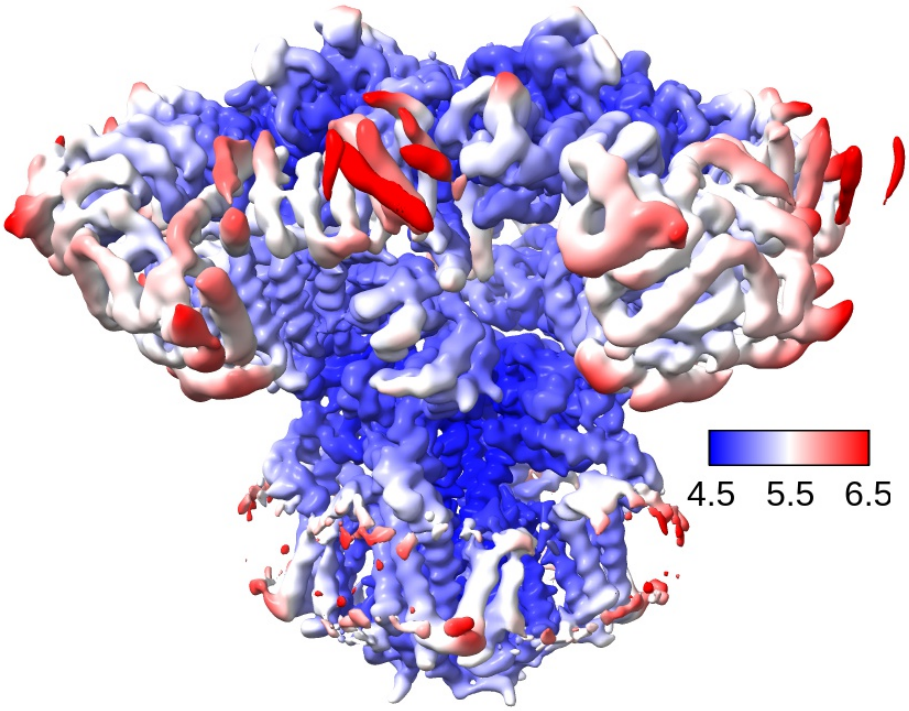

Figure 37: **Local resolution map of hIP$_3$R-3 determined in the presence of 5 mM 2-APB.** Locally filtered map of hIP$_3$R-3 colored by local resolution, calculated using Relion's implementation. Figure was generated using ChimeraX (Pettersen, Goddard, Huang, Meng, et al. 2021).

indicating that the sample conditions were not sufficient for binding, or that the density for the 2-APB binding site was not well-resolved.

8.2.2 Optimization of hIP$_3$R-1 splice variants purification for future structural studies

After the antagonist 2-ABP could not be identified in the Cryo-EM density of the hIP$_3$R-3, we shifted our focus to hIP$_3$R-1. While the exact binding location and affinity of 2-APB towards each isoform remains unknown, the effect of 2-APB on each isoform has been studied (Saleem et al. 2014). In DT-40 cells, 2-APB was shown to inhibit hIP$_3$R-1 in a concentration dependent manner starting at 50 μM, while the same concentration of 2-APB did not effect on hIP$_3$R-2 or hIP$_3$R-3 activity. 2-APB managed to inhibit hIP$_3$R-3 activity at 100 μM, but failed to affect hIP$_3$R-2 (Saleem et al. 2014). From this study, inhibition can potentially be used as a proxy for the strength

of the binding interaction. We reasoned that the chances of having an antagonist bound structure are greater for hIP$_3$R-1 than for hIP$_3$R-3 due to higher 2-APB binding affinity to hIP$_3$R-1. One complication that hIP$_3$R-1 has compared to hIP$_3$R-3 is the number of the splice variants, which may affect expression levels, quality of the purified proteins, and the receptor's affinity to 2-APB and other ligands. Therefore, we first attempted to identify the splice variants that are most suitable for structural studies. The constructs were expressed recombinantly to both improve the expression levels and to increase the samples' homogeneity by controlling which splice variant was expressed. We prepared protein constructs with changes to only one exon at a time using each of the three splice sites (Figure 39). Each hIP$_3$R-1 splice variant construct was expressed separately in small-scale insect cell cultures. Each protein construct's expression level was first assessed via SDS-PAGE, then adequately expressing candidates were moved to FSEC to asses sample homogeneity. In fluorescence-detection size-exclusion chromatography (FSEC), proteins pass through a size-exclusion chromatography (SEC) column coupled to a fluorescence detector. Proteins can be traced as they elute from the SEC column using either the GFP signal if the protein is fused to a GFP, or via tryptophan fluorescence if the protein contains tryptophans and is purified. The resulting fluorescence-based chromatogram allow for analysis of the protein's expression level via the peak height and monodispersity via the symmetry of sharp peaks (Kawate and Gouaux 2006).

The SI splice site is located between residues 318-332, which fall in the IP$_3$-binding core within the βTF-2 domain. The hIP$_3$R-1 SI- splice variant lacks this 14 residue sequence (Figure 38). The hIP$_3$R-1 SIII- splice variant lacks a 9 residue 'VEEETNAEA' insertion between residues 917 and 918 in the CLD. The SII splice site is more complicated, containing three domains (A, B, C), leading to four potential SII subvariants depending on which domains are included (Figure 38).

hIP$_3$R-3, hIP$_3$R-1 with all exons present (SI+,SII+,SIII+), and four hIP$_3$R-1 splice variants (SI-, SII-, SIIC-, and SIII-) were expressed in small scale Sf9 cultures, comparing expression levels and tetramerization through SDS-PAGE and FSEC. hIP$_3$R-1 expression is lower than hIP$_3$R-3, making this construct less optimal for Cryo-EM analysis to generate a co-antagonist structure. The SII-, SIIC-, and SIII- hIP$_3$R-1 splice variants show comparable expression levels with hIP$_3$R-3, making these constructs good candidates for moving on to large scale purification for Cryo-EM

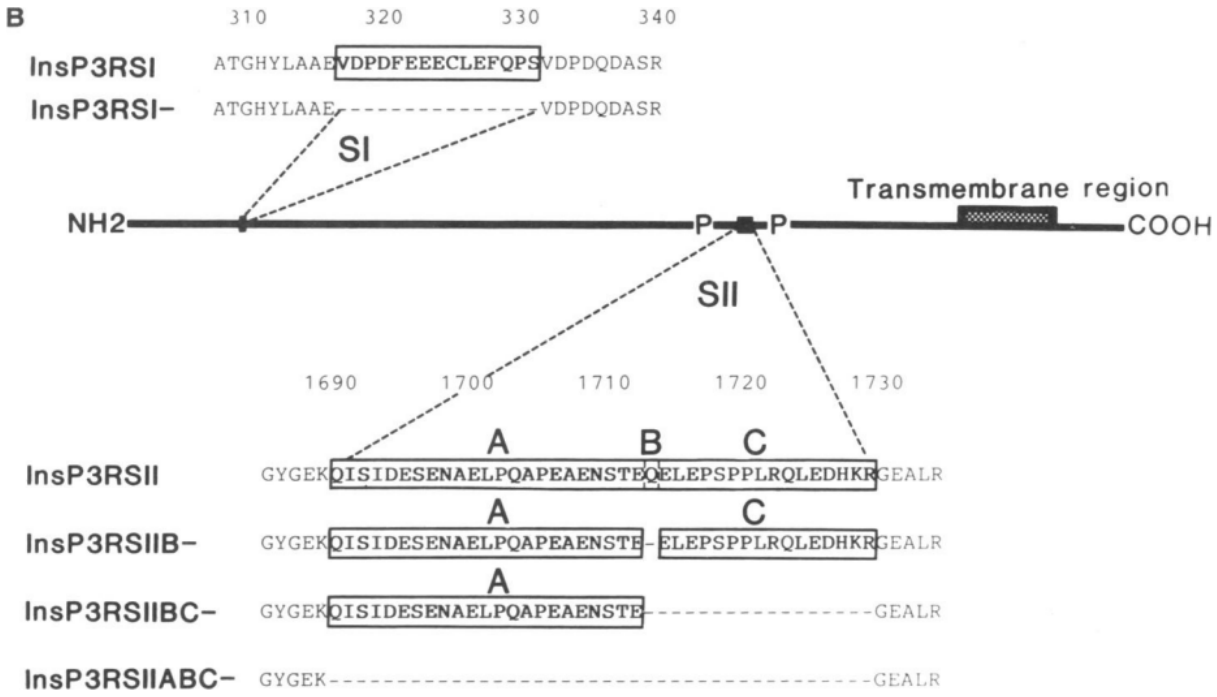

Figure 38: **A linear schematic of the IP_3R-1 SII splice variant sequences and position.** Linearized schematic of IP_3R-1 monomer, showing the location of the SI and SII splice sites. The SI splice site contains an optional 14 residue sequence that is removed in the IP_3R-1-SI- construct. The SII splice site contains three domains (A, B, and C) which can be removed in different combinations to form several splice variant constructs. Relevant SII variants are the SII- variant (lacking all three domains) and the SIIC- variant (lacking the C domain) which were both used in the experiments detailed in this section. The sequences shown were originally published in (Furuichi et al. 1989). The (P) sites indicate potential phosphorylation sites in the sequence. Image from (T. Nakagawa et al. 1991).

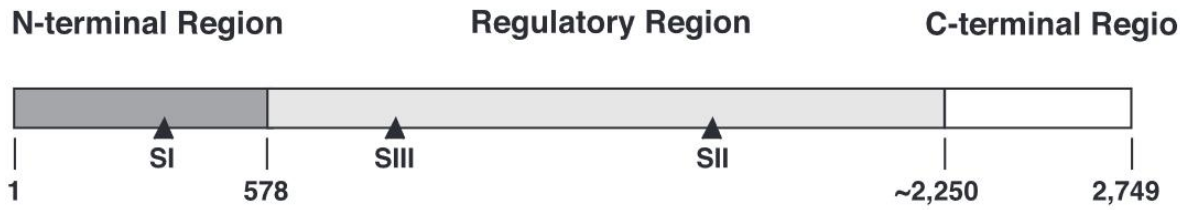

Figure 39: **Linearized schematic of IP_3R-1 domains showing three splice site locations.** Shown in the linear IP_3R-1 schematic are the three broad functional regions (N-terminal domain which includes the IBC), the regulatory domain (also known as the central modulatory domain), and the C-terminal domain (which includes the transmembrane domain and C-terminal tail). The positions of the three splice variants' locations are shown with black arrows. Image from (Bosanac, Michikawa, et al. 2004).

(Figure 41). These three hIP_3R-1 splice variants also elute at the same position from the Superose 6 10/300 GL increase column (GE Healthcare), as measured by tryptophan fluorescence through FSEC. Although the three well expressing splice variants elute at the same position as hIP_3R-3, their peaks have a right shoulder, indicating some level of structural heterogeneity in the sample, which may need to be further examined before using these constructs for the next round of Cryo-EM screening (Figure 40).

8.3 Methods

8.3.1 Purification of splice variants for FSEC

hIP_3R-1 and four splice variants were expressed in small scale 50 mL Sf9 cultures, examined for expression levels and their ability to form stable tetramers using FSEC in comparison to hIP_3R-3. The four splice variants tested were: S1- (lacking a 14 residue in the IBC), SII- (lacking the A, B, and C domains), SIIC- (lacking the C domain), and SIII- (lacking a 9 residue insertion). The Sf9 cultures were pelleted, then resuspended in 5 mL solubilization buffer (200 mM NaCl, 20 mM Tris-pH 8.0, 10 mM βME, 1 mM EDTA, 1 mM PMSF, 0.5% LMNG, and 0.1% GDN. The cells were solubilized at 4 °C for two hours, then centrifuged at 40,000 rpm for 10 minutes at 4 C to pellet cell debris. The proteins were purified by batch binding overnight with Strep XT 4Flow resin (IBA Biotagnology), the eluting with 100 mM D-Biotin. Each construct was run on a 7% SDS-PAGE to compare expression levels and injected onto a Superose 6 Increase 10/300 GL column to examine sample homogeniety and tetremerization (Figure 40). 25 μL of each sample was injected onto the

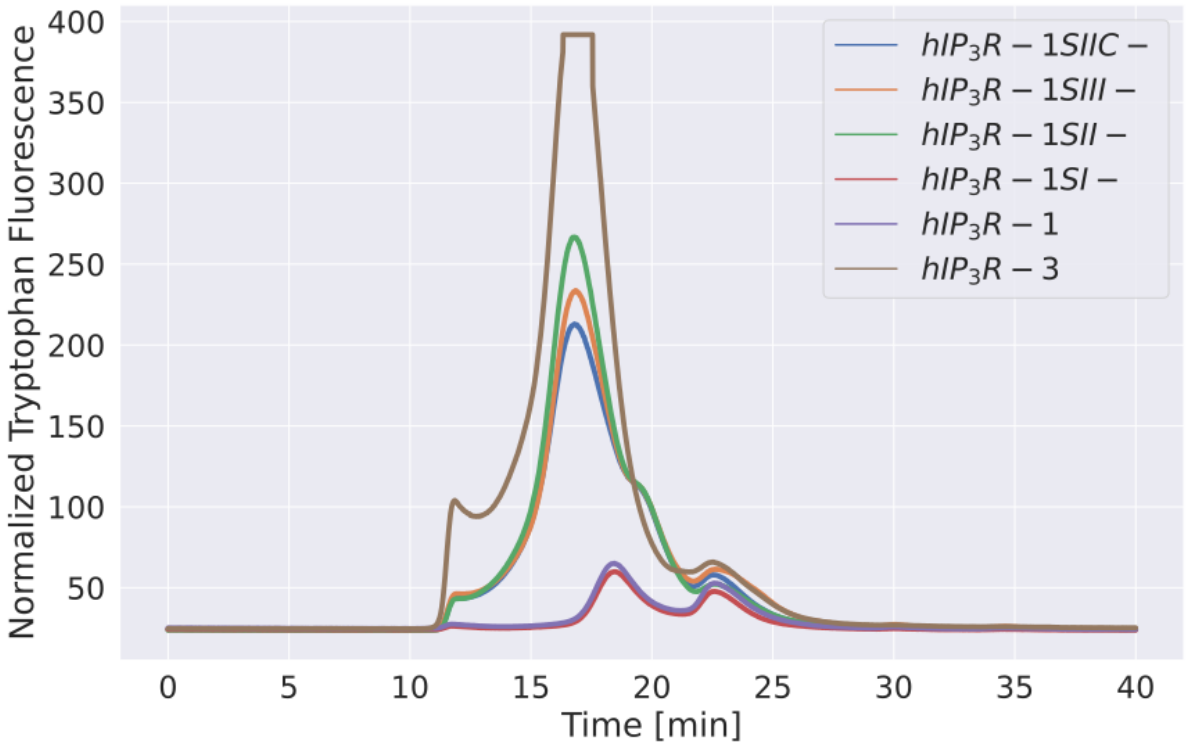

Figure 40: **FSEC screening of hIP$_3$R-1 splice variants.** 25 μL each of six hIP$_3$R constructs were injected onto a Superose 6 Increase 10/300 GL column. The resulting chromatograms were generated from measuring tryptophan fluorescence, and overlaid to compare peak position, height, and width. The flat top of the hIP$_3$R-3 peak is due to saturation of the detector.

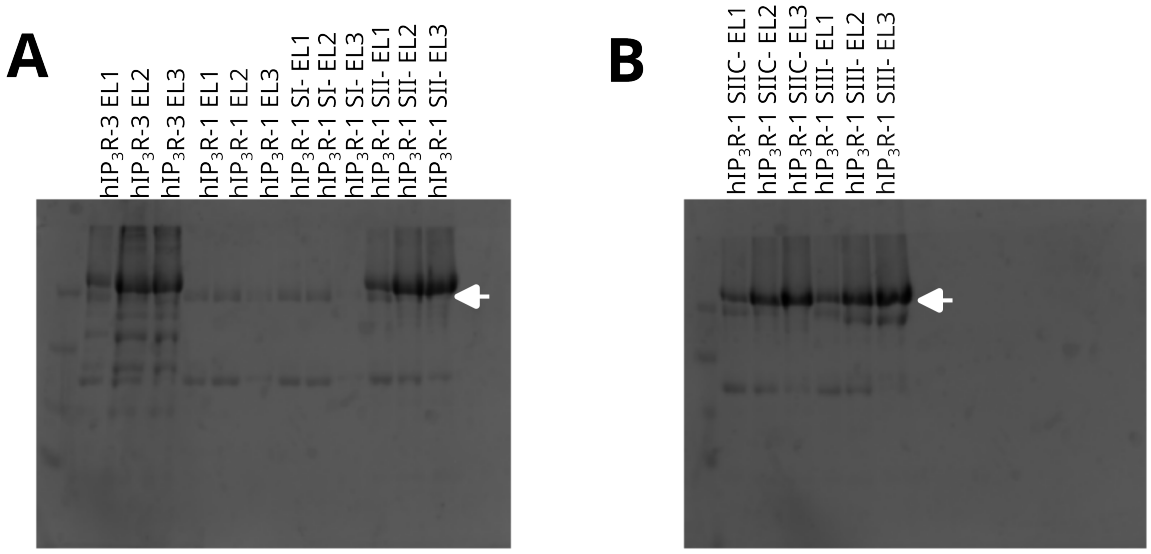

Figure 41: **Expression levels of hIP$_3$R-1 splice variants.** 12 μL from all the first three elution fractions (EL) from each construct's purification were run on a 7% SDS-PAGE.

column, measuring the protein with tryptophan fluorescence.

8.3.2 Cryo-EM Data Processing

hIP$_3$R-3 was expressed in SF9 cells and purified according to the protocol in section 6.4.1 'Expression and purification of hhIP$_3$R-3'. 5 mM 2-APB was added to the sample immediately prior to vitrification with a FEI Mark IV Vitrobot. Copper Quantafoil 300 mesh grids were glow discharged for 20 seconds at 25 mA (Quorum K1000X) to charge the grid surface. Several grids were plunged with varying blotting force and times, keeping the temperature and humidity constant at 8 C and 100% respectively. One grid frozen with this condition was imaged using Vanderbilt's Glacios at 200 kV, producing a pixel size of 0.82 Å.

The data was processed using Relion 4.0 (Kimanius, Dong, et al. 2021). Micrographs were imported and motion corrected using Relion's own implementation of MotionCorr, increasing the patch size to 5 x 5 and setting the B-factor to 150. CTF correction was done using CTFFind-4.1 (Rohou and Nikolaus Grigorieff 2015) using the power spectra from MotionCorr. Afterwards,

corrected micrographs with a maximum predicted resolution of lower than 6 $\AA$ were discarded from the dataset. Initially, Relion's Laplacian of Gaussian (LoG) algorithm was used to pick particles, which were then binned 4 x 4 and used to generate a first round of 2D class averages. A subset of the 2D class averages showing clear particles in a variety of orientations were selected for a round of template-based autopicking. The 1,016,058 particles picked by template-based autopicking were extracted, binned 4 x 4, and used for another round of 2D classification. From this latest round of 2D classification, 8 classes with a total of 929,729 particles were selected for 3D classification. The 165,369 particles belonging to class 5 from the 3D classification were unbinned, extracted and used for another 2D classification. A final round of 3D classification was run using 19 2D classes, with 164,828 particles in total. Class 1 and Class 6 were combined, 3D refined, and post-processed. Relion's own implementation of LocalRes was used to calculate local resolution in the filtered map. The final hIP$_3$R-3 map was 4.01 Å overall resolution.

8.4 Discussion and Outlook

The map of hIP$_3$R-3 in the presence of 5 mM 2-APB reported here at 4.01 $\AA$ did not contain any unassigned densities that could be attributed to bound 2-APB (Figure 37). Due to the low affinity of 2-APB for hIP$_3$R-3, non-ideal conditions for the inhibitor binding, or the limited resolution of the cryo-em maps, the current conditions were not sufficient to capture an antagonist bound state. Perhaps ligands, such as IP$_3$, is required for inhibitor binding. One alternate approach is to repeat the Cryo-EM grid preparation, screening, and data processing pipeline using Inhibitor 911, a more potent 2-APB analog with a measured IC50 of 0.2 μM according to calcium release assays (S. Ozaki, Suzuki, et al. 2013). Inhibitor 911 with its more potent effect on hIP$_3$R activity may prove to be a better candidate for a co-structure since the binding affinity may be higher compared to 2-APB (S. Ozaki, Suzuki, et al. 2013). Since Inhibitor 911 has a effective range at lower concentrations compared to 2-APB, a lower concentration can be added to the sample prior to vitrification and, since the compound is only soluble in organic solvents, it may be easier to screen for ice and and protein quality if the amount of DMSO or methanol is mitigated as much as possible.

It is also worthwhile to screen other small molecule inhibitors such as XeC and XeD, or moving towards small inhibitory binding proteins such as IRBIT or the naturally occurring glycosamino-

glycan heparin. IRBIT is an endogenously expressed hIP_3R antagonist that competes with IP_3 for access to the binding pocket (Ando, Mizutani, Matsu-ura, et al. 2003). The phosphorylation status of IRBIT controls its activity, with phosphorylation required for IRBIT to compete with IP_3 and a dephosphorylated IRBIT having downstream signaling effects (Ando, Mizutani, Kiefer, et al. 2006). IRBIT is thus a good candidate for future drug design efforts to mimic its activity and improve upon it, despite the challenge of stabilizing the binding interaction for structural studies. In the case of heparin, the glycosaminoglycan is membrane impermeable and also affects GPCR activity (Ghosh et al. 1988), the protein acts as a competitive antagonist of hIP_3R-mediated calcium release and elucidating the structural mechanism underlying its regulatory effects may prove fruitful for rational design of more specific, small protein modulators.

While considering the prospect of the above chemical and protein antagonists, switching the isoform under consideration from hIP_3R-3 to hIP_3R-1 is an alternative strategy. From the initial screen of hIP_3R-1 splice variants, hIP_3R-1 SII-, SIIC-, and SII+ have comparable expression levels to the hIP_3R-3 isoform (Figure 41), and elute at the same position with approximately symmetrical peaks, indicating proper tetramerization (Figure 40). The next step is to attempt a large scale purification of each of the three suitable hIP_3R-1 splice variants using the hIP_3R-3 purification protocol as a starting point, then moving into Cryo-EM screening experiments using 2-APB, Inhibitor 911, and XeC. Detergent screens with FSEC may prove useful to confirm the solubilization step in the purification is optimal for these constructs and recovers as much expressed protein as possible.

9 Conclusion and Future Directions

9.1 Modulation of hIP$_3$R activity

In this first part of this work in Chapter 6, an apo, or ligand-free, structure of the hIP$_3$R-3 is reported to 3.8 Å overall resolution via Cryo-EM. Arguably the most critical finding reported in this study was the description of a 27 residue SBP bridging two helices (α_{ARM2}-1 and α_{ARM2}-2) in the ARM2 domain, which lies in the large central modulatory and transducing domain. The SBP was localized in the IP$_3$-binding pocket, hinting at a possible regulatory function. From the binding studies conducted, the SBP was shown to compete against IP$_3$ for access to the binding site, allowing the receptor to both self-inhibit and to fine tune the receptor's affinity for IP$_3$.

SBPs were defined as such in 2015, with a comprehensive molecular dynamics study of eight SBPs and their binding targets (C. Yang et al. 2015). Although, the concept of SPBs in the regulation of protein kinase function as pseudosubstrate autoinhibitory peptides predates the term SBP (M. K. Smith, Colbran, and Soderling 1990). SBPs have been reported in a few systems including, but not limited to: mouse proto-oncogene Vav, human retinoic acid receptor RARγ , fruit fly scaffold module INAD and crypto 14-3-3 protein Cp14b (Z. Li et al. 2019). The hIP$_3$R-3 SBP's inhibitory mechanism of action is similar to that of fibroblast growth factor receptor's self inhibition, where the acid box sequence electrostatically interacts with the heparin binding site to reduce receptor affinity for heparin and fibroblast growth factor (Kalinina et al. 2012). The broad mechanism underlying SBP's mechanisms of action will require further study on the hIP$_3$R-3 and other receptors with similarly acting SBPs. From the reported hIP$_3$R-3 Cryo-EM map in Chapter 6 (Figure 25 C), the SBP appears to be very flexible since the interaction with the residues in the IP$_3$-binding core could not be precisely modeled with atomic resolution, raising the question of whether the hIP$_3$R-3 SBP is an intrinsically disordered sequence or if there are one or more relatively stable conformational states. It would be worthwhile to simulate hIP$_3$R-3 SBP binding using molecular dynamics to investigate whether this SBP demonstrates a folding-upon-binding modality, where an intrinsically disordered peptide would assume a more compact state upon starting the binding process, or whether the peptide would exhibit a binding-upon-folding modality similar to what is found in traditional protein-protein interactions where the peptide needs to assume a

folded conformation prior to being able to bind the target site.

Other questions remain regarding the hIP$_3$R-3 SBP including if the other two isoforms also exhibit this self-inhibitory mechanism and if the presence of isoform specific SBPs contributes to the differing isoform affinities for IP$_3$. Examining existing IP$_3$R-1 published maps for unassigned, ambiguous density in the IP$_3$-binding pocket would be a useful start, but may be complicated by lower particle numbers in previous studies reducing the possible resolution in this region. Collecting new datasets on both hIP$_3$R-1 and hIP$_3$R-2 using the latest microscopes and detectors technology may allow for better resolution of their SBPs. Further mutagenesis and binding assays using chemically synthesized isoform specific SBPs is critical for determining the exact residues required for binding. Swapping the SBPs between isoforms and measuring both IP$_3$ binding affinity and receptor activity would help clarify if the SBPs contribute to isoform specific IP$_3$ affinity and have an appreciable effect on receptor activity.

Another critical, unexplored space in the field of IP$_3$R biology is the role of native lipids in receptor stability and function. In the Cryo-EM maps reported in Chapters 6-8, the same unassigned densities appear in the transmembrane domain, which we attribute to native lipids that remain bound throughout the purification process. The question is then, which lipids are these and what effect do they have on receptor function? Performing mass spectrometry experiments to find these lipids using purified IP$_3$R isoforms may prove difficult due to the receptor's large size. Perhaps introducing cleavage sites to remove the large cytosolic domain while keeping the transmembrane domain intact may be a useful strategy, or designing a minimalistic construct containing as close as possible to an isolated transmembrane domain would allow for easier identification of the ever present lipids. Functional and structural studies in nanodiscs could provide a more 'native-like' ER membrane composition, which may reveal more transiently binding lipids that may potentially play yet undiscovered roles in receptor function. The caveat to using nanodiscs to approximate the native ER membrane environment is that in order to insert the protein into nanodiscs, of which the lipid composition could be controlled, the IP$_3$Rs would need to first be purified using detergents before being reconstituted into the nanodiscs.

In addition to the role of native lipids and the newly discovered SBP on hIP$_3$R-3 activity, the structural mechanisms underlying the modulatory effects of each of the dozens and dozens of IP$_3$R binding proteins provide a variety of future targets for structural studies. The challenging task will be to first determine which IP$_3$R-binding proteins have the strongest and longest lasting binding interactions, which would make them the best candidates for a Cryo-EM co-structure analysis. Additional strategies like chemical or photo-crosslinking may help stabilize the binding interaction to allow the proteins to remain in complex during the vitrification process. Ultimately IP$_3$Rs are incredibly dynamic ion channels, whose activity can be modulated from many fronts, including post-translational modifications. Studies have shown ubiquitination (Wright and R. J. H. Wojcikiewicz 2016), phosphorylation (VANDERHEYDEN et al. 2009), and cleavage by caspases (Assefa et al. 2004) can modulate the receptor's activity. Studying these effects would entail first expressing and purifying the receptor, then applying the post-translational modifications in vitro, confirming them through either mass spectrometry or a Phos-Tag gel, with the ultimate goal of visualizing their effects on IP$_3$R structure using cryo-EM, and combined with functional data to establish structure-functional analyses. Establishing the structural mechanisms underlying these modulatory effects will be critical for understanding the IP$_3$R isoforms' activity in both physiological and pathophysiological environments.

9.2 Structural regulation underlying the IP$_3$R gating cycle

In this second part of this work (Chapter 7), an ensemble of hIP$_3$R-3 structures in multiple conformational states are detailed, ranging from three pre-active states, an active conformation, and an inhibited state. The pre-active structures are ordered from A to C to arrange the domain movements in a logical progression from the top of the N-terminal domain immediately adjacent to the transmembrane domain. The active state details the effects of the conformational changes reaching the transmembrane domain, with the voltage sensor-like domain displaced laterally 7 Å, the central S6 helix bending and rotating to increase the electronegativity of the conduction pathway, and the pore dilating to allow Ca^{2+} ions to pass through.

While the ordering of the pre-active hIP$_3$R-3 structures was primarily determined based on logic, since conformational changes need to propagate from the ligand binding sites to the channel

in order to activate the receptor, concrete evidence for the ordering should eventually be established. One such experiment to establish the order would be to use chemical cross-linking to attempt to lock the receptor in the pre-active states, placing the cross-linkers at sites that would prevent further propagation of the conformational changes, then using the samples to prepare grids and verify the hypothesized structures using Cryo-EM. In addition to this strategy, regions of hIP_3R-3 that were too flexible to model, such as the inhibitory Ca^{2+} site in the high [Ca^{2+}] condition in chapter 7, could also be cross-linked and used to generate amino acid proximity measurements using mass spec to provide distance constraints in homology models, potentially improving these regions of the receptor (Schmidt and Urlaub 2017).

One caveat of the reported inactive structure in Chapter 7 is that based on the low resolution at the inhibitory binding site preventing visualization of density for a Ca^{2+} ion, it cannot be determined whether the receptor is truly inactive or merely desensitized. Collecting additional datasets under the same conditions that allowed for the ensemble to be found, but instead focusing refinement efforts on the particles in which the βTF ring is dissociated could allow for further examination of the desensitized state. A critical gap in the hIP_3R gating cycle is the process of recovering from densitization/inactivation to reinitialize into the apo state. With modern microscopes allowing for collection of larger and larger datasets, and updates to Relion 4.0 (Kimanius, Dong, et al. 2021) and CryoSparc (Punjani et al. 2017) enabling better separation of conformational heterogeneity, intermediate conformations between the densitized state and the apo state can potentially be identified. If this strategy proves fruitless, despite the large amount of expected particles, an alternative strategy would be to collect data on hIP_3Rs in the presence of varying levels of Ca^{2+} and compare the resulting structures in a similar strategy to that employed in Chapter 7. Higher Ca^{2+} concentrations may provide an ensemble of hIP_3R structures in both inhibited and desentitized conditions and provide better resolution of the inhibitory Ca^{2+} binding site.

Early mutagenesis studies predicted over seven Ca^{2+} binding sites per subunit (Ilse Sienaert et al. 1997), but only one binding site was occupied in the active state, and only two sites were occupied in the previously reported inhibited hIP_3R-3 structure (Paknejad and Hite 2018). The previous inhibited structure was determined under high calcium conditions (2 mM), preventing as-

signment of the activitory and inhibitory binding sites. The inactive structure reported in Chapter 7 has the ARM2 in a very similar conformation to the previous inhibited structure, which may indicate this structure is also inhibited. The other Ca^{2+} binding sites that remained unoccupied in all recent IP_3R-3 structures were originally reported from studies using individual, isolated domains that did not confirm proper domain folding. These Ca^{2+} binding sites may simply be Ca^{2+} binding without affecting protein structure. Regardless, mutagenesis studies should confirm which of the two reported binding sites is the activitory site, and which is the inhibitory site. This type of experiment has already been used to validate the activitory Ca^{2+} binding site in IP_3R-1 (Fan, M. R. Baker, Terry, et al. 2022). Another unanswered question is the binding kinetics of Ca^{2+} to both of these binding sites. According to the current model of IP_3R gating, the activitory binding site should have higher Ca^{2+} affinity, as it needs to be occupied in order to gate the channel, while the inhibitory binding site should have lower Ca^{2+} affinity, as it should only be occupied once the local Ca^{2+} concentration increases due to receptor activity. Measuring the Ca^{2+} affinity towards both binding sites could conceiveably be done using either traditional MST, where the IP_3R or IP_3R fragment is labeled with either a covalently attached GFP or using a fluorescent dye that binds to histidine tags, or with label free MST, which tracks protein movement using inherent tryptophan fluorescence. This type of experiment has already been done to measure the affinity of Ca^{2+} ions for calmodulin (Christoph J. Wienken et al. 2010).

One surprising finding is the position of the ATP binding site, and the mechanism by which ATP binding potentiates the receptor. ATP binds to the JD in all reported structures in Chapter 7, with no major conformation changes in this binding site between any of the states except for a bit of movement in the loops in the JD. ATP acts to glue the two sides of the JD together, increasing domain rigidity to provide a means of increasing the force on the S6 during channel gating. To confirm the mechanism underlying ATP's potentiating effect on IP_3Rs the JD can be expressed alone for thermostability assays with and without ATP.

One additional avenue of exploration involves the forces underlying the conformational changes. In the inactive structure from Chapter 7, C1 symmetry was imposed during refinement because each subunit deviated significantly from each other. Forcing C4 symmetry on the inactive particles still

retained good resolution in the TMD, but the densities in the NTD subunits canceled each other out, reducing the structural information available. One source of this conformational heterogeneity is the ARM3 domain. When the channel is open, the competing forces are exerted on the ARM3 domain from the pore opening and from the force holding the βTF ring together. These competing forces ultimately drive the βTF ring to dissociate upon the inhibitory Ca^{2+} binding. When the pore finally closes, the ARM3 transitions into a relaxed state. Quantifying these forces and further examining the tension in the ARM3 during receptor activation could provide links between reported clinically reported hIP_3R mutations and their effects on receptor function. However, experimentally measuring the forces acting on ARM3 may prove to difficult a starting point. Instead, more global forces such as the receptor's large N-terminal domain moving towards the membrane plane could be measured using immobilized IP_3Rs and atomic force microscopy. A similar study on height changes in calmodulin upon Ca^{2+} binding has been done (Trajkovic et al. 2011), but applying this type of experimental setup to a large receptor will prove difficult.

9.3 Structural regulation underlying IP_3R modulation by chemical antagonists

In the third part of this work (Chapter 8), preliminary data describing the initial optimization and attempt at determining an IP_3R structure in complex with a chemical antagonist are detailed. IP_3R-3 was prepared for Cryo-EM analysis in either the presence micromolar amounts of XeC or 5 mM 2-APB. However, the XeC condition proved a more difficult starting point due to the low ice quality in the cryo grids. A cryo map of IP_3R-3 imaged with saturating amounts of 2-APB was determined to 4.01 A resolution, but after careful comparison between this map and the apo map (chapter 6), no density could be attributed to the chemical antagonist. Part of the inherent difficulty in this study is that the binding site for 2-APB is not known. The binding sites for other IP_3R chemical antagonists, such as the xestospongins, have not been identified either although they are proposed to inhibit IP_3R activity by physically blocking the pore (Gafni et al. 1997). Although saturating conditions of 2-APB were used, which would theoretically saturate the binding sites on IP_3R-3, the compound could not be found in the cryo-em map. This may indicate that the conditions prior to vitrification were not sufficient to promote binding. Perhaps 2-APB only binds IP_3R-3 after structural changes resulting from either IP_3 binding to the IBC or Ca^{2+} binding the activitory binding site. A large screen of vitrification conditions containing saturating 2-APB con-

centrations in the presence of one or both of the aforementioned biological agonists would address this question, but would be incredibly time consuming. Since multiple studies have shown that IP_3R-3 has the lowest affinity to both antagonists classes tested here (Saleem et al. 2014), the focus switched to the IP_3R-1 isoform which had the highest measured affinity, and to its many splice variants.

Efforts into finding an isoform-specific antagonist have proven more difficult than the attempts to produce an isoform-specific agonist, due in large part to the fact that the hundreds of synthesized IP_3R agonists have the same starting point: IP_3. Meanwhile, the existing non-specific IP_3R antagonists have unknown binding sites, and thus information on how they influence IP_3R activity through their effects on IP_3R structure is lacking. Since the initial attempts at determining a co-antagonist structure did not prove fruitful, perhaps first narrowing down the potential binding site by attempting to dock the inhibitor into IP_3R using RosettaDock would allow for the targeted refinement of these specific IP_3R regions, allowing for a better chance at recognizing antagonist density in the cryo maps. The initial results detailed in chapter 8 work towards producing a co-antagonist IP_3R structure, starting from either the full length IP_3R-1 or the SII-/SIIC-splice variants, which would then enabled more detailed structure-function analyses to determine the residues critical for antagonist binding, and which motifs on the antagonists are critical for inhibition of IP_3R activity. The ultimate goal is to produce an atomic resolution co-antagonist structure that would enable structure-based drug design, hopefully resulting in novel compound classes that demonstrate isoform-specific selectivity.

10 Appendices

10.1 Cryo-EM structure of human type-3 inositol triphosphate receptor reveals the presence of a self-binding peptide that acts as an antagonist: Data processing and additional data

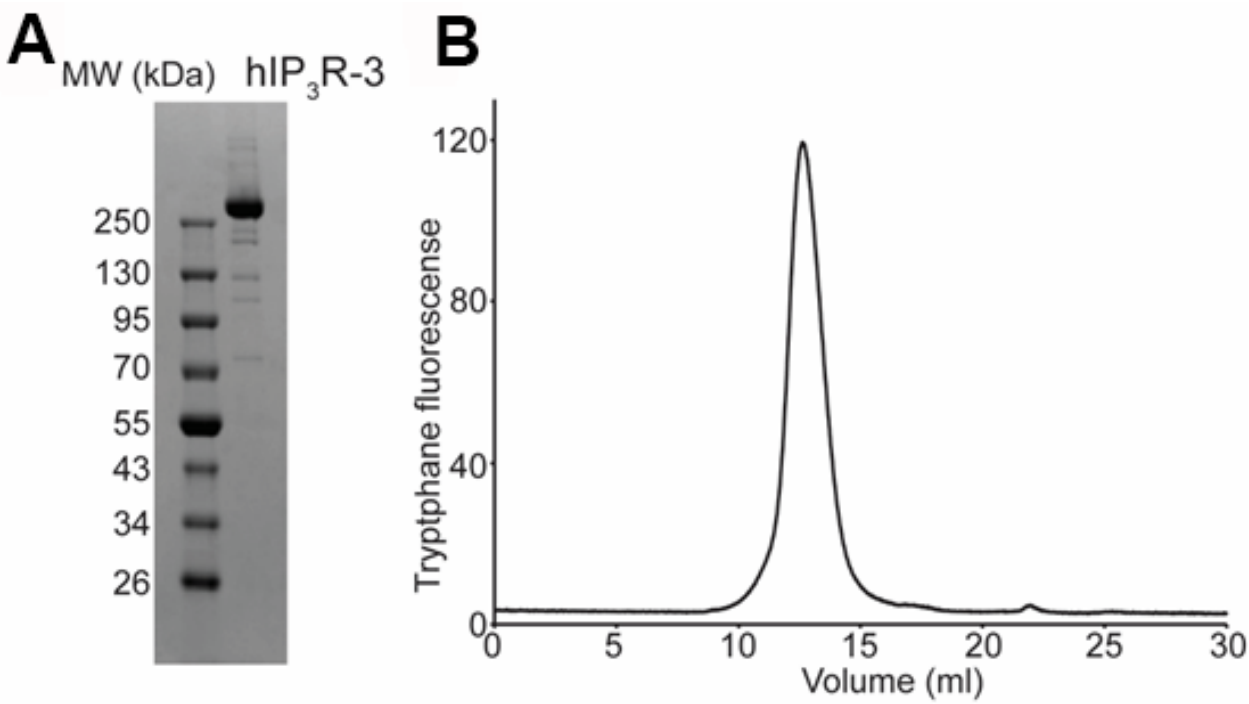

Figure 42: **Purification of recombinant hIP$_3$R-3.** (a) Purification of hIP$_3$R-3 proteins from insect cells using Strep-Tactin-XT Superflow resin followed by SEC. SDS-PAGE showing the final purified protein used in cryo-EM analysis. (b) Size exclusion chromatogram of purified hIP$_3$R-3 proteins detected by intrinsic tryptophan fluorescence (280 nm excitation/330 nm emission).

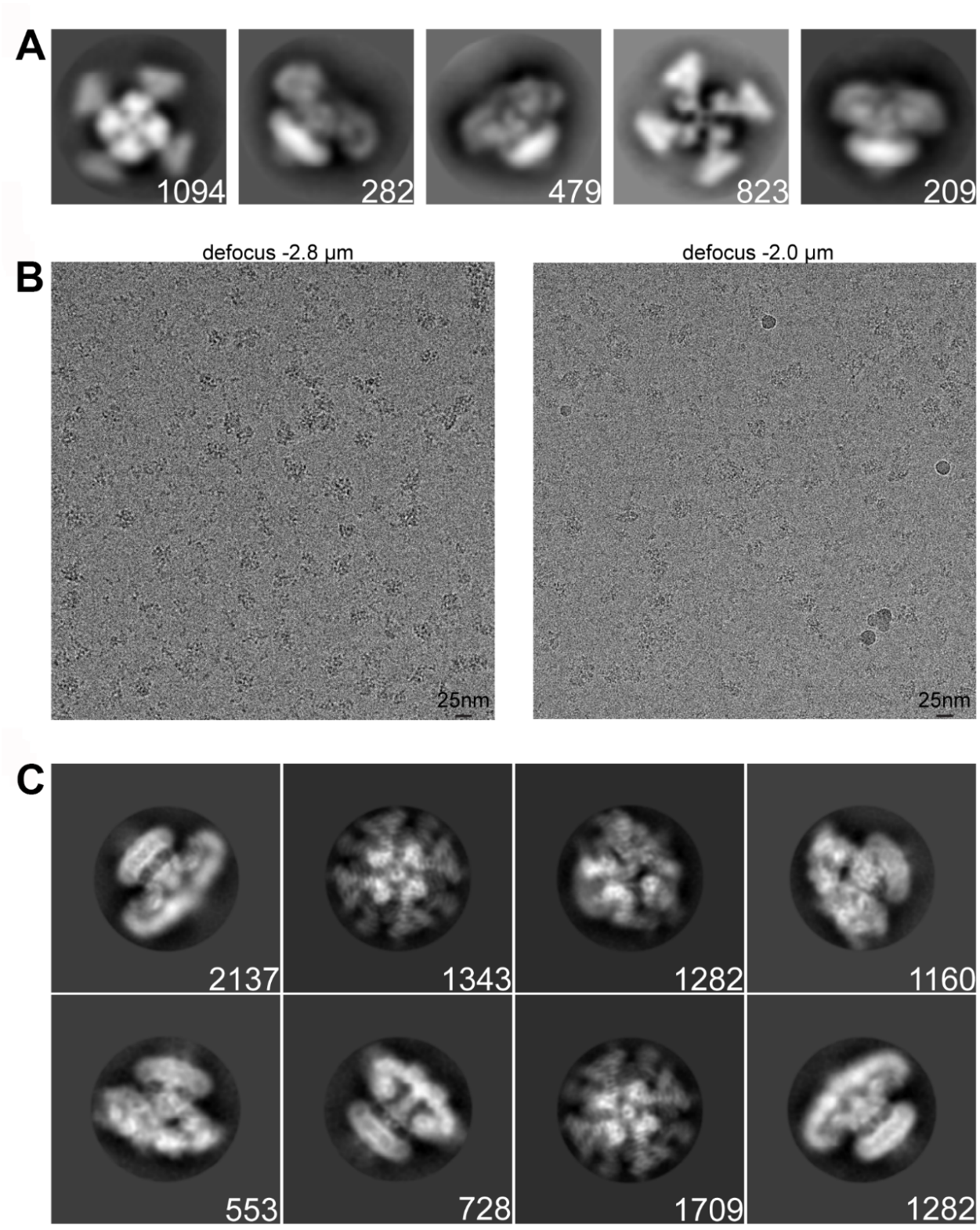

Figure 43: **Raw data and 2D class averages for hIP$_3$R-3.** (a) Representative 2D class averages of the hIP$_3$R-3 calculated from the negative stain data. (b) Representative raw micrographs of the IP$_3$R-3 sample collected at 300kV on a Polara F30 microscope. (c) Representative 2D class averages showing top, side, and orthogonal views of the hIP 3R-3. (a and c) Number of particles in each class is denoted in the bottom right corner.

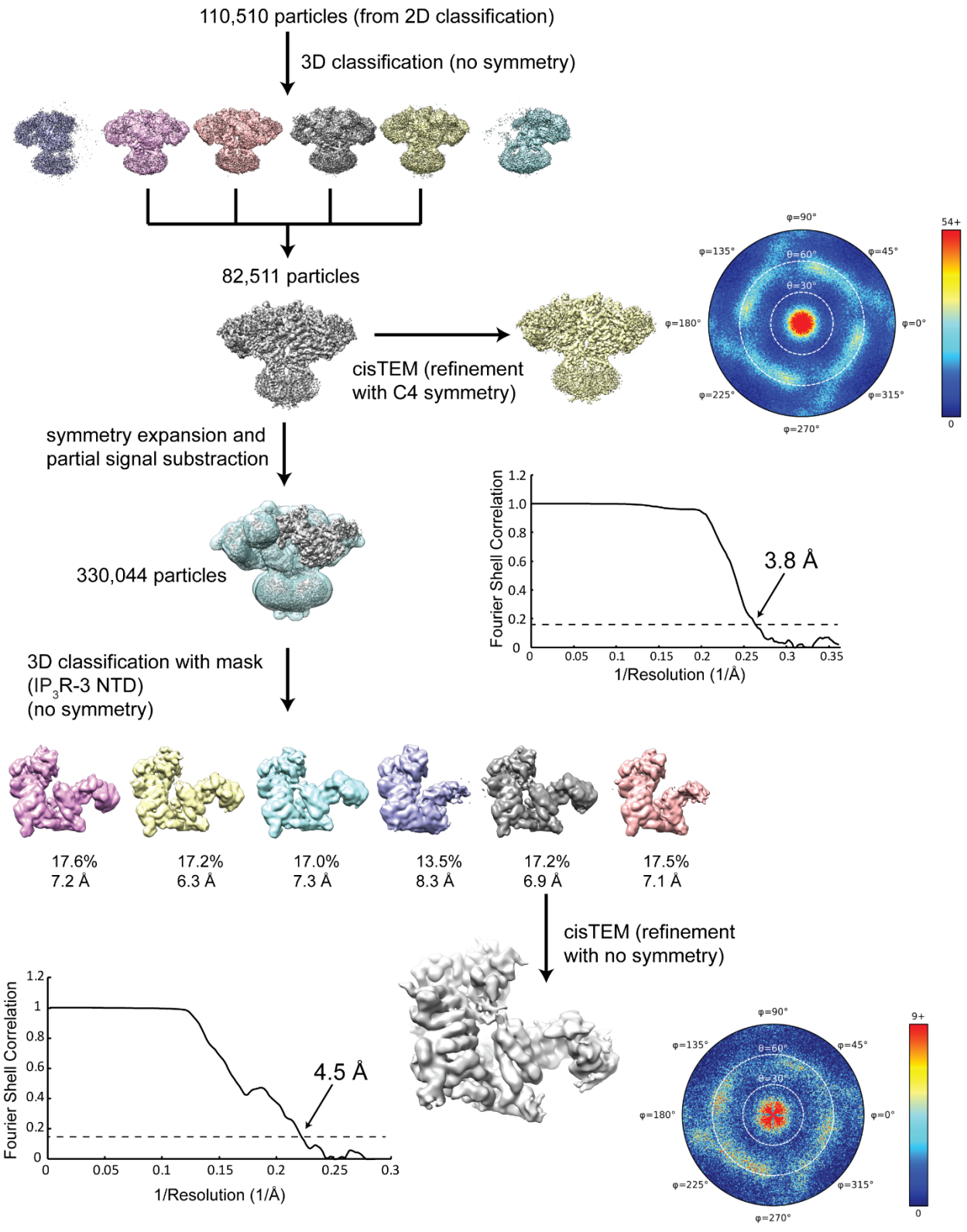

Figure 44: **Cryo-EM analysis of hIP$_3$R-3.** Flowchart detailing the particle selection and refinement procedure to obtain the cryo-EM maps of intact receptor and hIP$_3$R-3 NTD. Angular distribution and FSC curves are shown for both structures.

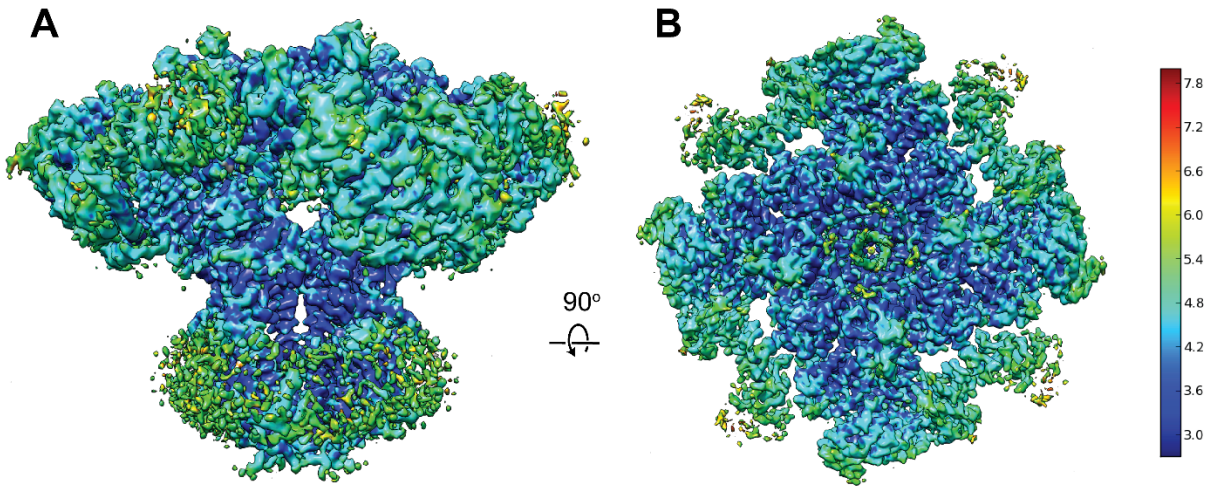

Figure 45: **Local resolution of hIP$_3$R-3.** Local resolution mapped onto final refined 3D reconstruction of hIP$_3$R-3 viewed along the membrane plane (a) and from cytosol (b). Local resolution is mapped from 2.5 $AA – 8.0 $\mathring{A}$ and were calculated using ResMap (Kucukelbir, Fred J. Sigworth, and Tagare 2014).

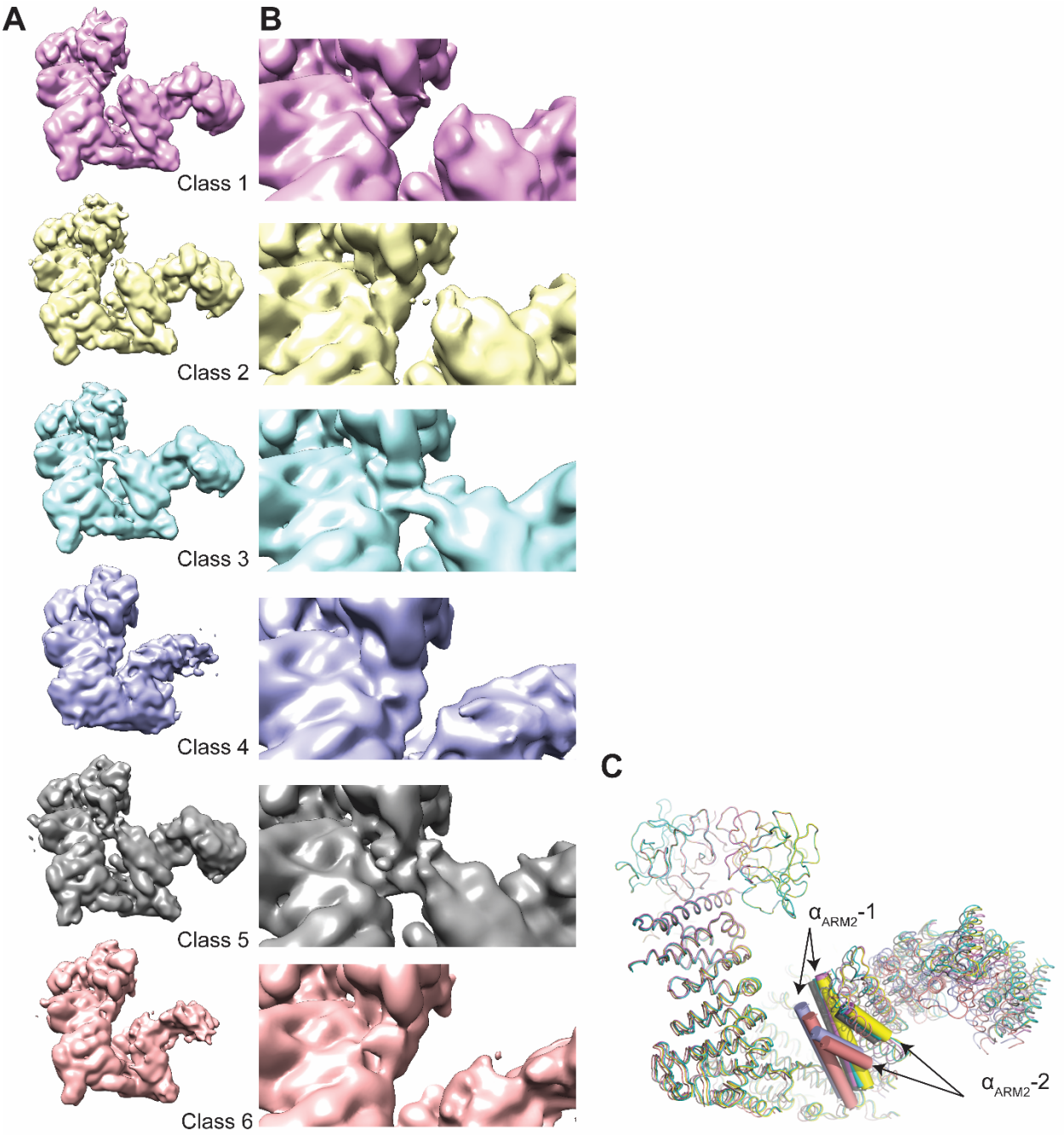

Figure 46: **Focused 3D classification of hIP$_3$R-3 NTD.** (a) Density maps of the six 3D classes resulting from the focused 3D classification of hIP$_3$R-3 NTD. (b) Zoomed view of the IP$_3$ binding site viewed from the same angle as panel a. (c) Structural heterogeneity of ARM2 domain is shown by aligning the β-TF1 and β-TF2 domains of the models prepared by rigid body fitting of individual the β-TF1, β-TF2, ARM1, ARM2, and CLD into the densities shown in panel a. αARM2-1 and αARM2-2 helices are shown as cylinders, while the rest of the protein shown as loops.

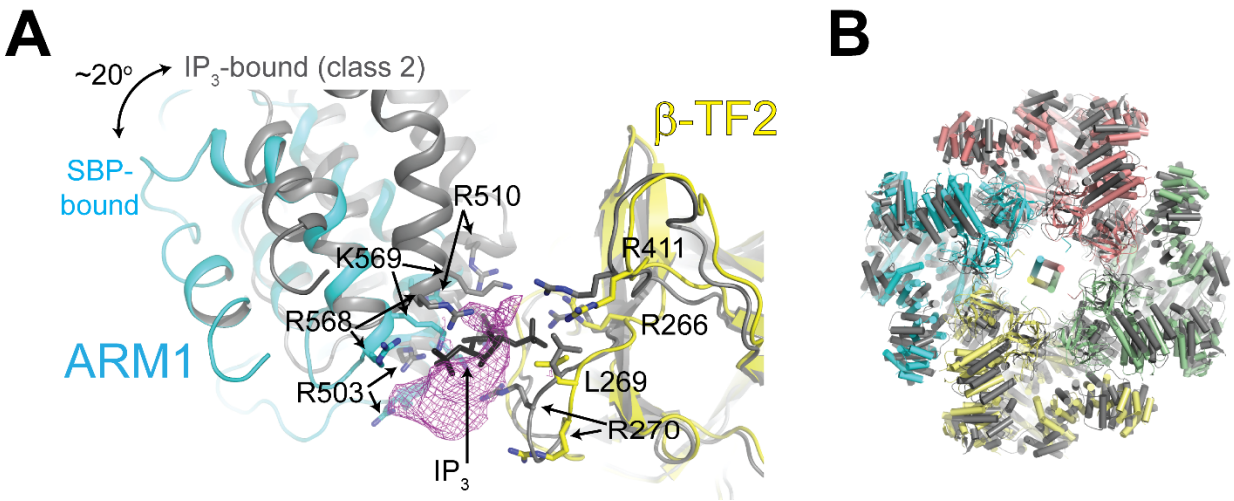

Figure 47: **Structural comparison of SBP-bound IP_3R-3 with IP_3-bound hIP_3Rs (class 2).** (a) β-TF1 and β-TF2 domains of the SBP-bound hIP_3R LBD are superposed onto β-TF1 and β-TF2 domains of IP_3-bound-hIP_3R-3 (class 2, PDB ID: 6DQV, grey) Domains of the SBP-bound hIP_3R-3 is colored as in Figure 27. Residues forming the IP_3 binding pocket are shown in stick representation. IP_3 is colored black. Magenta mesh represents the SBP density. (b) Comparison of the CDs of SBP-bound hIP_3R-3 with IP_3-bound -hIP_3R-3 (class 2) after superposing the TMDs.

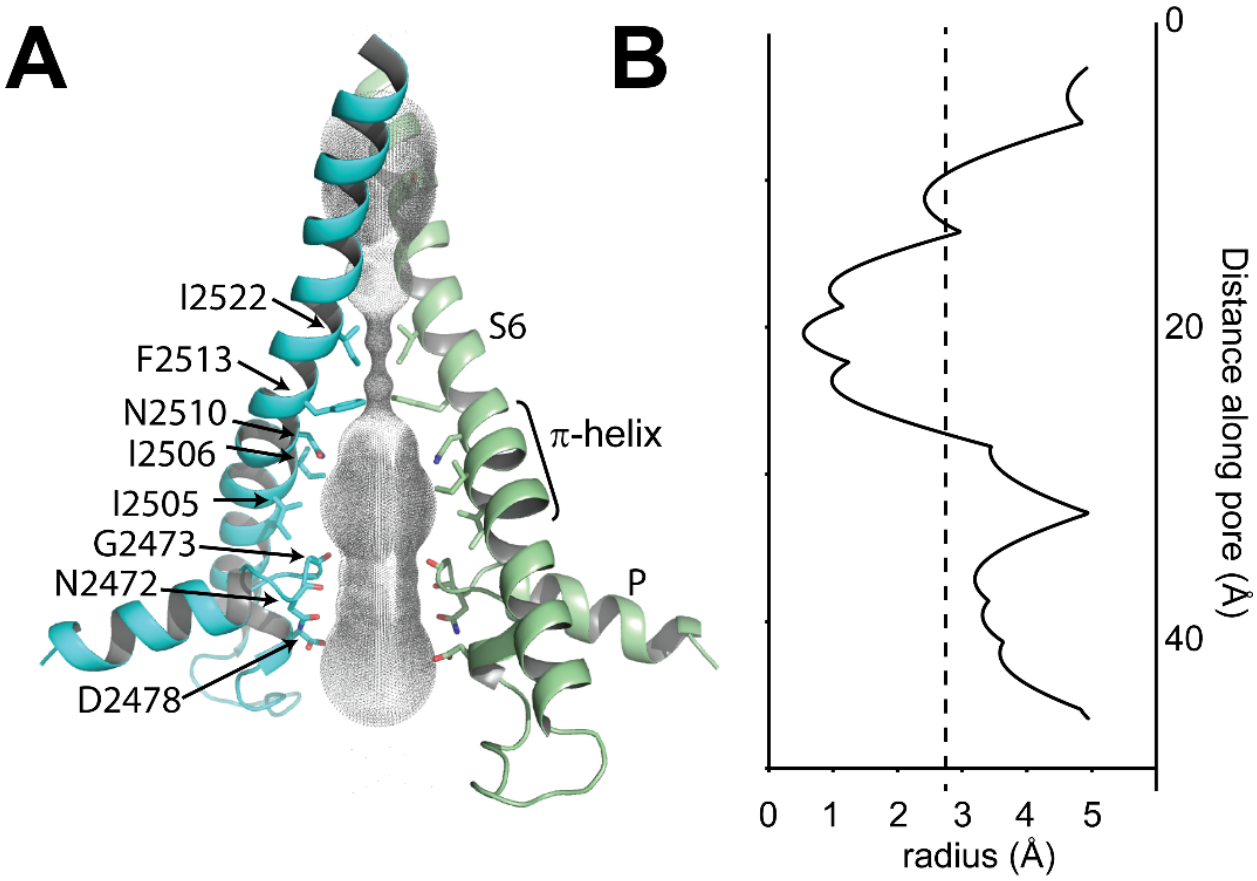

Figure 48: **Ion permeation pathway.** (a) The pore profile generated by the HOLE program (Smart et al. 1996) are shown along with the S6 helix, P helix and P loop. Only two subunits are shown for clarity. Residues that line the ion permeation path are represented as sticks. (b) A representation of pore radius along the permeation pathway. Dashed line indicates an approximate radius of a hydrated Na^+ ion (Marcus 1988).

10.2 Structural basis for activation and gating of IP3 receptors: Data processing and additional data

Data collection and processing					
Microscope	FEI Krios G3i microscope				
Detector	Gatan K3 direct electron camera				
Nominal magnification	105,000 x				
Voltage (kV)	300				
Electron exposure (e/Å^2)	~60				
Defocus range (μm)	-0.8 to -1.6				
Pixel size (Å)	0.828				
Number of Micrographs	42,361				
Particles images (no.)	846,122				
Conformational state	**Pre-active A**	**Pre-active B**	**Pre-active C**	**Active**	**Inactive**
PDB ID	7T3P	7T3Q	7T3R	7T3T	7T3U
EMDB ID	EMD-25667	EMD-25668	EMD-25669	EMD-25670	EMD-25671
Symmetry imposed	C4	C4	C4	C4	C1
Final particles images (no.)	116,925	153,765	75,994	20,039	198,441
Map resolution (Å) (FSC threshold=0.143)	3.2	3.3	3.4	3.8	3.7
Refinement					
Model resolution (Å) (original map, FSC threshold=0.5)	3.7	3.6	3.8	4.1	8.0
Model resolution (Å) (composite map, FSC threshold=0.5)	3.0	3.0	3.1	3.6	3.6
B-factor used for map sharpening (Å^2)	-100	-100	-100	-100	-100
Model composition					
Non-hydrogen atoms	66,992	68,124	68,780	68,516	44,501
Protein residues	8,188	8,336	8,444	8,408	7,269
Zn^{2+}	4	4	4	4	4
IP_3	4	4	4	4	2
ATP	4	4	4	4	4
Ca^{2+}	-	-	-	4	4
Mean B factors (Å^2)					
Protein	46.89	63.80	67.80	113.62	79.55
Ligands	61.05	74.57	83.85	172.47	89.42
R.m.s. deviations					
Bond lengths (Å)	0.004	0.004	0.004	0.003	0.002
Bond angles (°)	0.514	0.519	0.519	0.510	0.434
Molprobity score	1.73	1.73	1.77	1.74	1.63
Clash score	8.24	7.57	8.25	8.16	6.21
Poor rotamers (%)	0.00	0.00	0.00	0.05	0.00
Ramachandran plot					
Favored (%)	95.88	95.48	95.30	95.68	95.77
Allowed (%)	4.12	4.52	4.65	4.32	4.23
Disallowed (%)	0.00	0.00	0.05	0.00	0.00

Table 2: Chapter 7: Cryo-EM data collection, refinement, and validation statistics

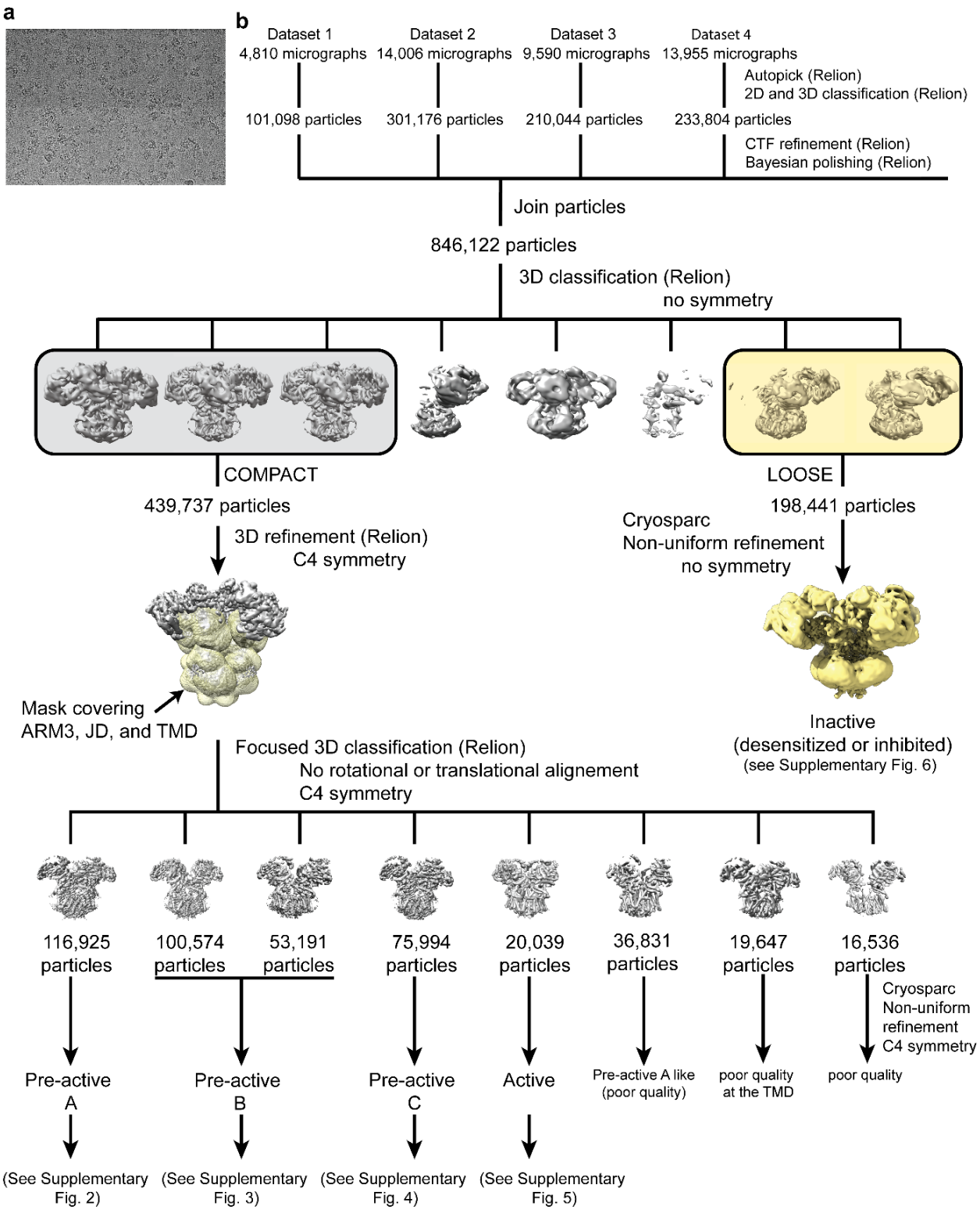

Figure 49: **Cryo-EM analysis of hIP$_3$R-3.** (a) Representative cryo-EM micrograph of the hIP$_3$R-3 dataset. (b) Flowchart detailing the particle selection and refinement procedure to obtain the cryo-EM maps of hIP$_3$R-3 in different gating conformations. The structure in the inactive conformation (yellow) is low-pass filtered using a local resolution map. See methods for details

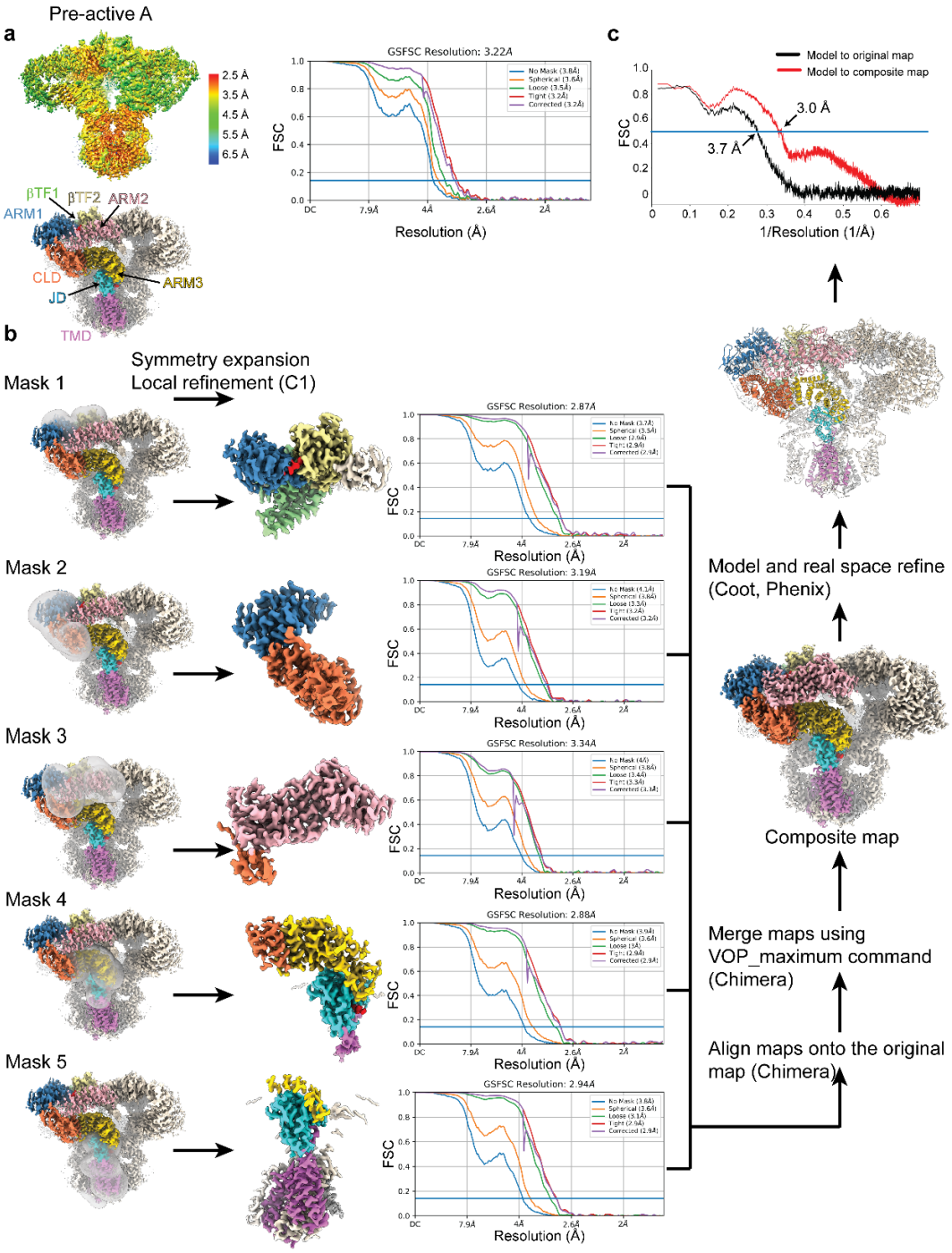

Figure 50: **Cryo-EM analysis of hIP$_3$R-3 in the pre-active A state.** (a) The final refined 3D reconstructions of hIP$_3$R-3 colored by local resolution (top) and individual domains (bottom) as in (Figure 30). FSC curve after Non-uniform refinement in CryoSPARC is shown. (b) Diagram showing the local refinement strategy. Masks are shown transparent, and domains are colored as in (Figure 30). Arrows point to the maps obtained after local refinement. FSC curves after local refinement in CryoSPARC are shown for each mask. See methods for details. (c) FSC curves of the refined model versus the original EM map (black) and the composite map (red) are shown.

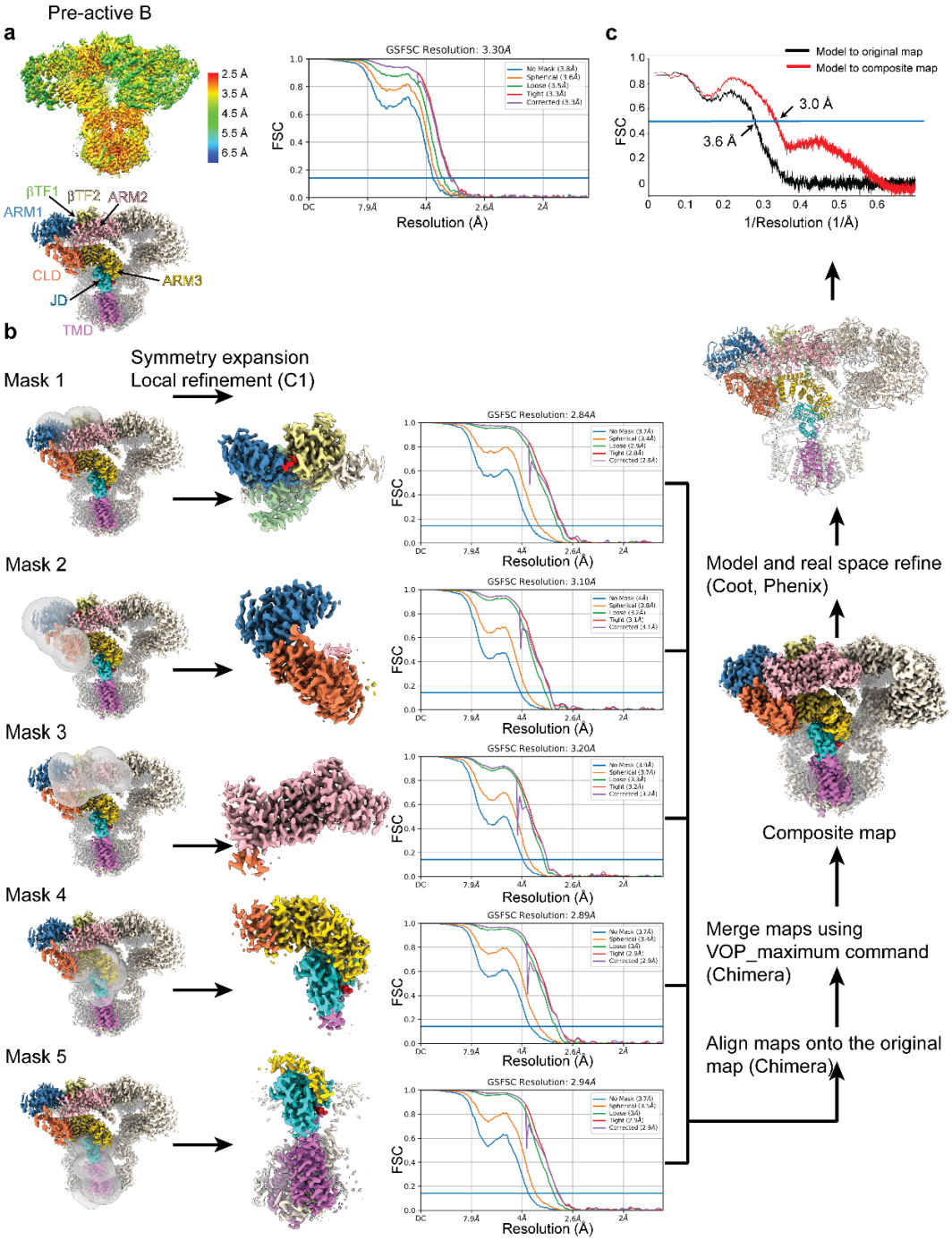

Figure 51: **Cryo-EM analysis of hIP$_3$R-3 in the pre-active B state.** (a) The final refined 3D reconstructions of hIP$_3$R-3 colored by local resolution (top) and individual domains (bottom) as in (Figure 32). FSC curve after Non-uniform refinement in CryoSPARC is shown. (b) Diagram showing the local refinement strategy. Masks are shown transparent, and domains are colored as in (Figure 30). Arrows point to the maps obtained after local refinement. FSC curves after local refinement in CryoSPARC are shown for each mask. See methods for details. (c) FSC curves of the refined model versus the original EM map (black) and the composite map (red) are shown.

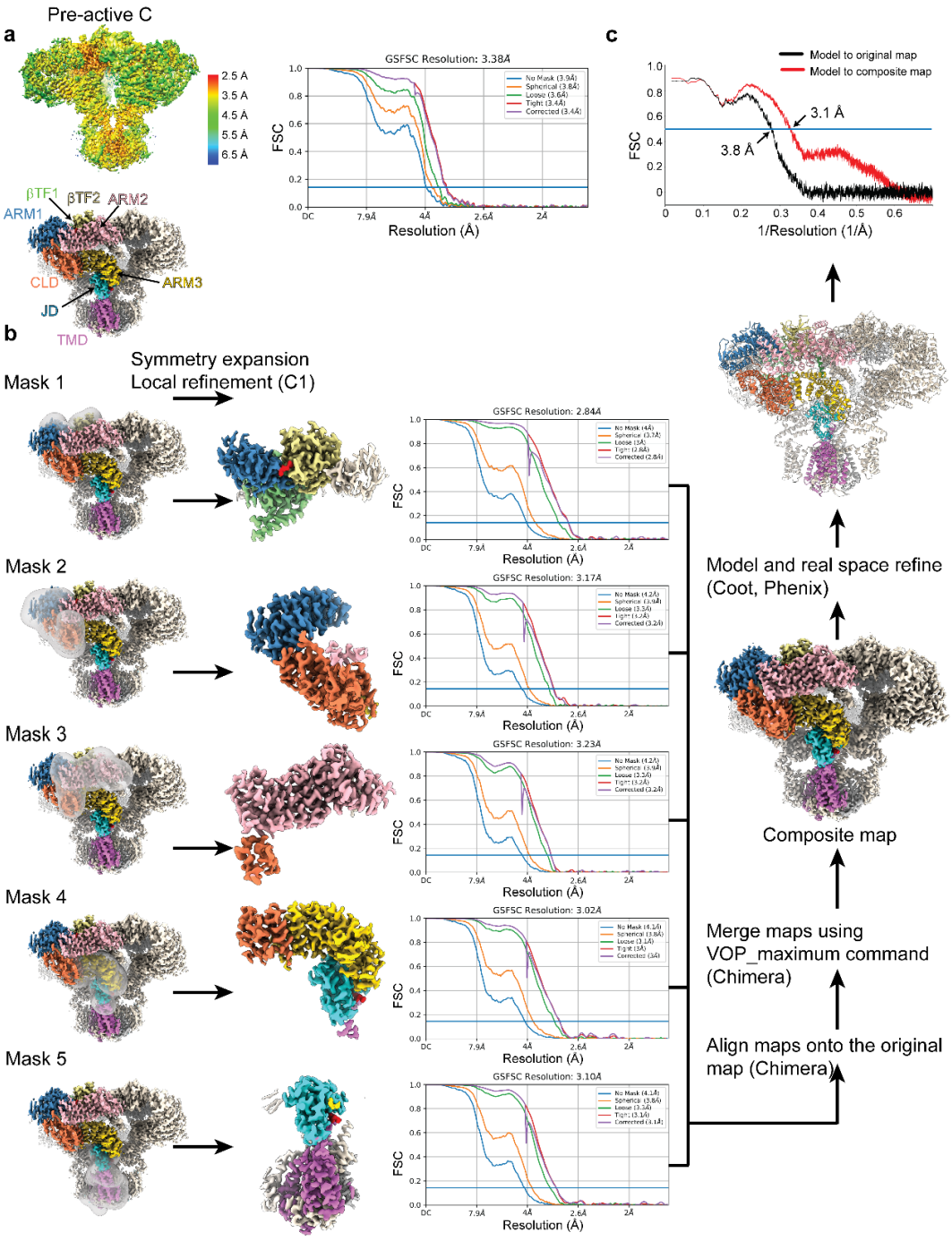

Figure 52: **Cryo-EM analysis of hIP$_3$R-3 in the pre-active C state.** (a) The final refined 3D reconstructions of hIP$_3$R-3 colored by local resolution (top) and individual domains (bottom) as in (Figure 30). FSC curve after Non-uniform refinement in CryoSPARC is shown. (b) Diagram showing the local refinement strategy. Masks are shown transparent, and domains are colored as in (Figure 30). Arrows point to the maps obtained after local refinement. FSC curves after local refinement in CryoSPARC are shown for each mask. See methods for details. (c) FSC curves of the refined model versus the original EM map (black) and the composite map (red) are shown.

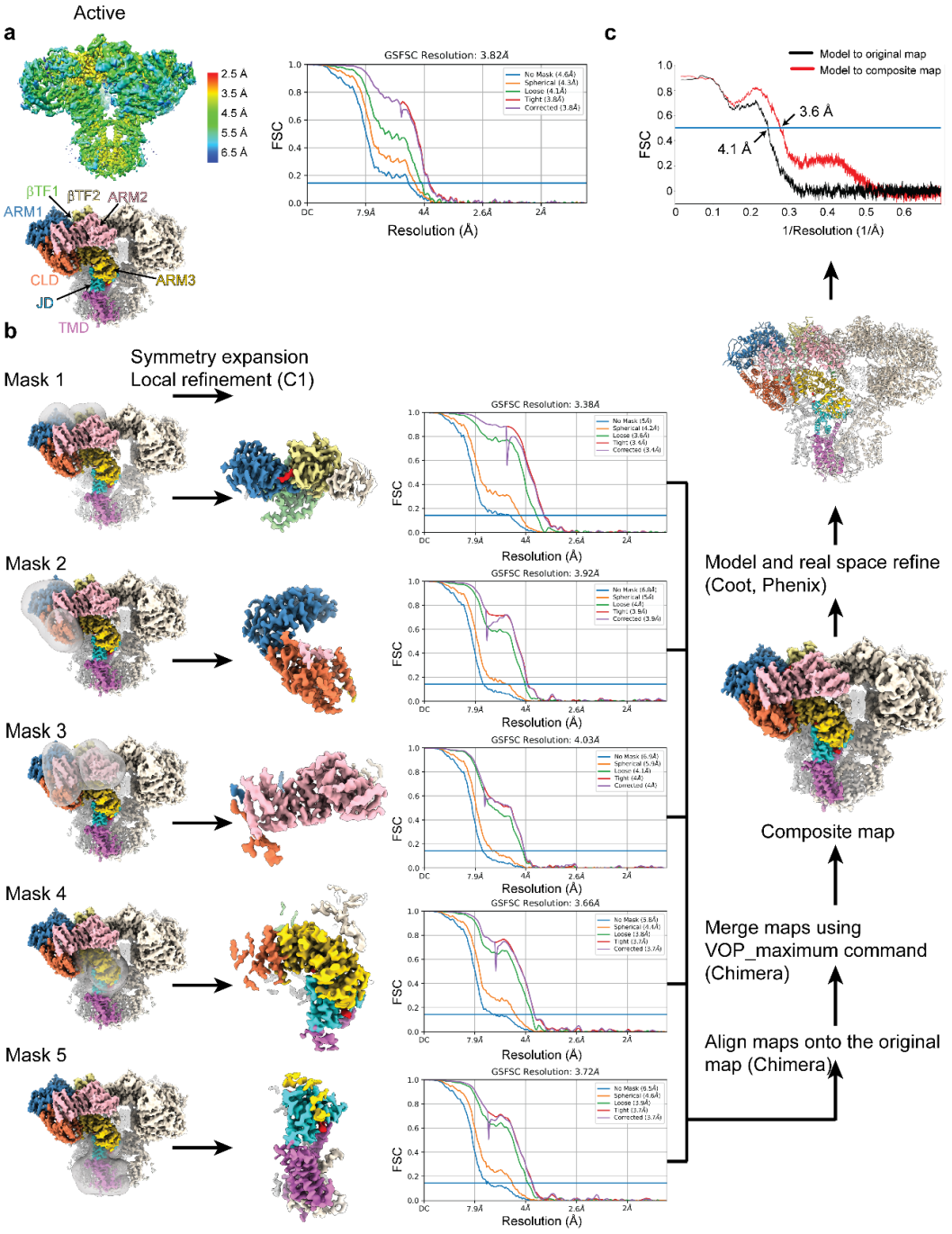

Figure 53: **Cryo-EM analysis of hIP$_3$R-3 in the active state.** (a) The final refined 3D reconstructions of hIP$_3$R-3 colored by local resolution (top) and individual domains (bottom) as in (Figure 30). FSC curve after Non-uniform refinement in CryoSPARC is shown. (b) Diagram showing the local refinement strategy. Masks are shown transparent, and domains are colored as in (Figure 30). Arrows point to the maps obtained after local refinement. FSC curves after local refinement in CryoSPARC are shown for each mask. See methods for details. (c) FSC curves of the refined model versus the original EM map (black) and the composite map (red) are shown.

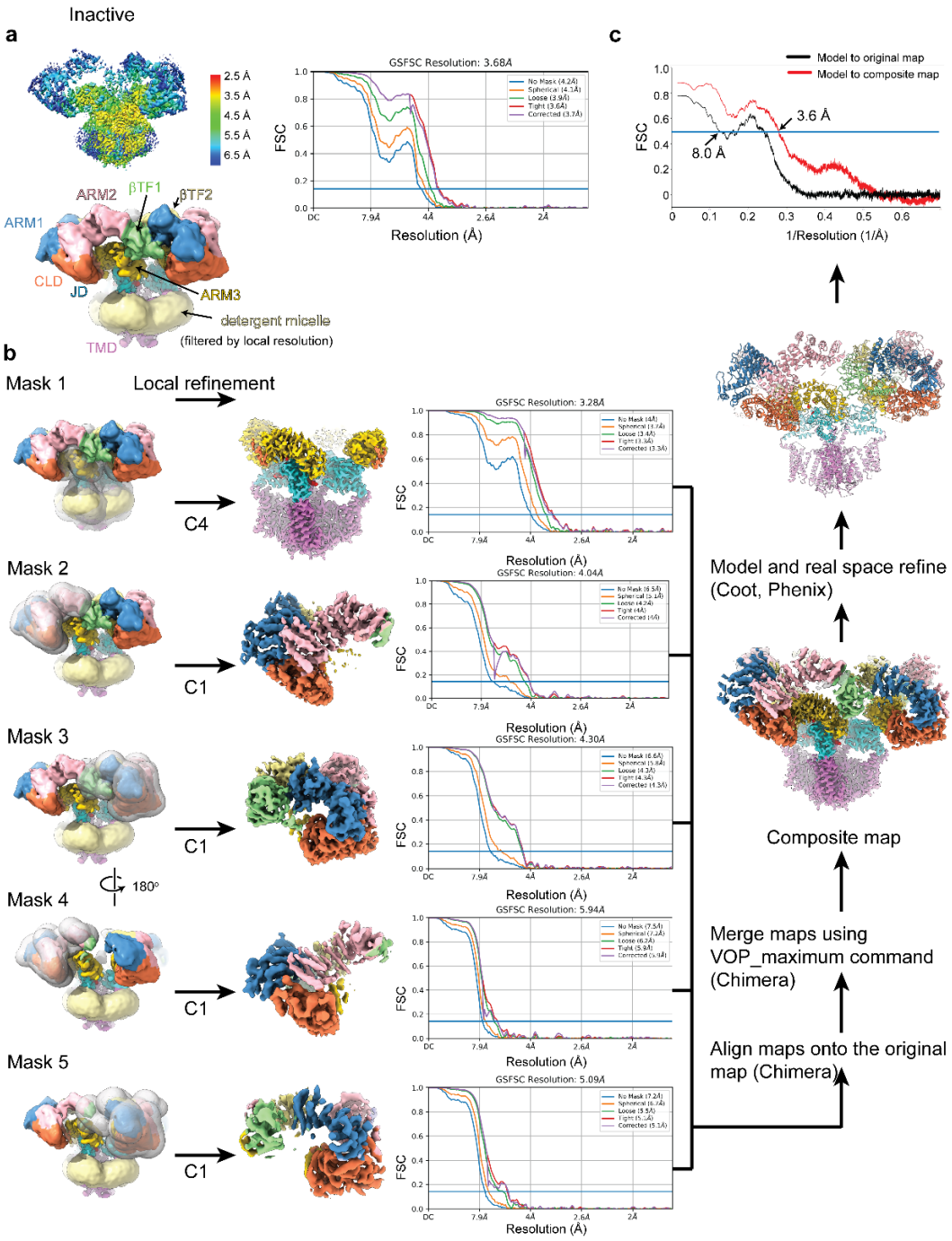

Figure 54: **Cryo-EM analysis of hIP$_3$R-3 in the inactive state.** (a) The final refined 3D reconstructions of hIP$_3$R-3 colored by local resolution (top) and individual domains (bottom) as in (Figure 30). The map colored by individual domains is low-pass filtered using the local resolution map. FSC curve after Non-uniform refinement in CryoSPARC is shown. (b) Diagram showing the local refinement strategy. Masks are shown transparent, and domains are colored as in (Figure 30). Arrows point to the maps obtained after local refinement. FSC curves after local refinement in CryoSPARC are shown for each mask. See methods for details. (c) FSC curves of the refined model versus the original EM map (black) and the composite map (red) are shown.

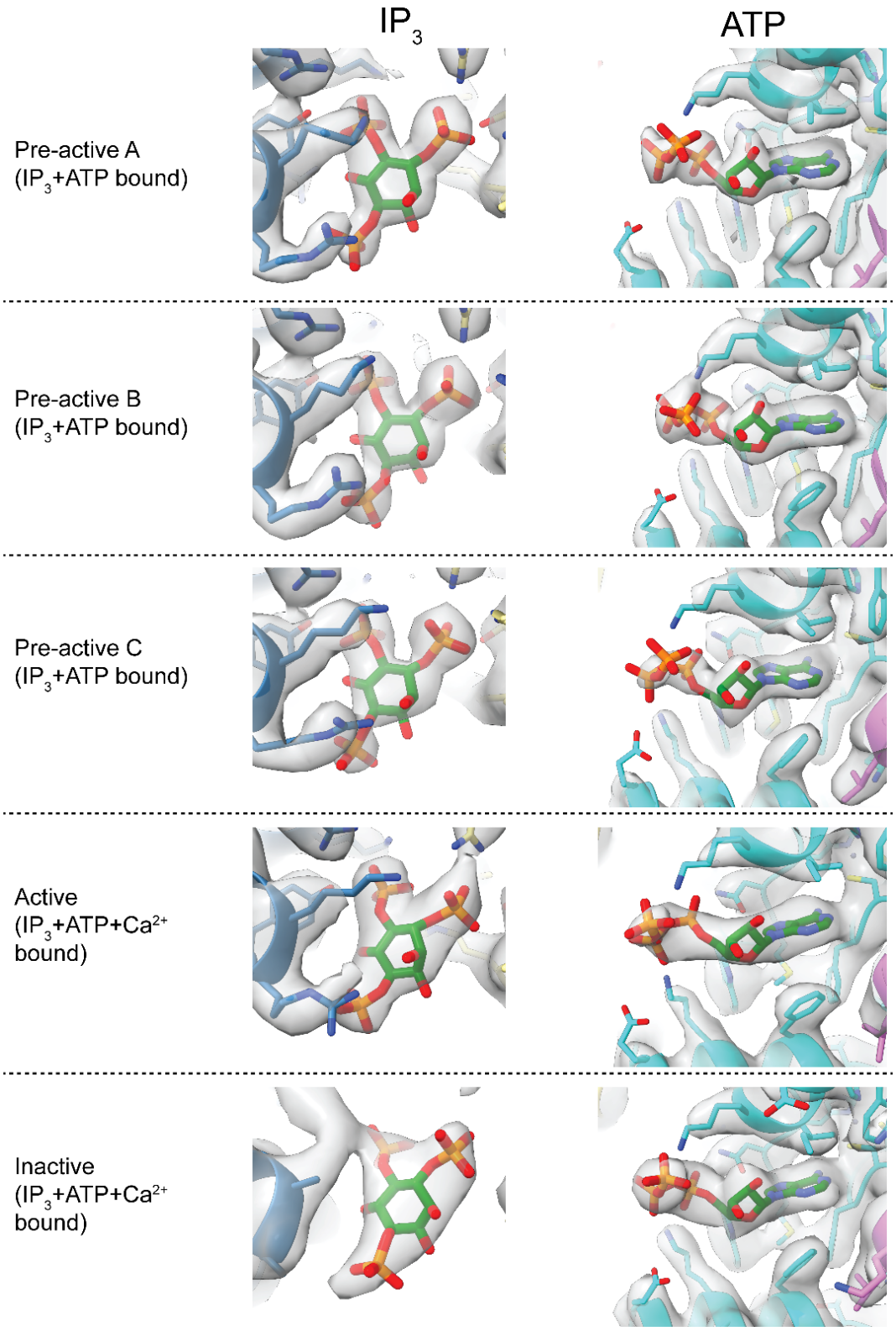

Figure 55: **Ligand binding sites.** Density maps for the IP_3 and ATP binding sites obtained through local refinements are shown as transparent grey surfaces. The ligands and the neighboring residues are represented as sticks.

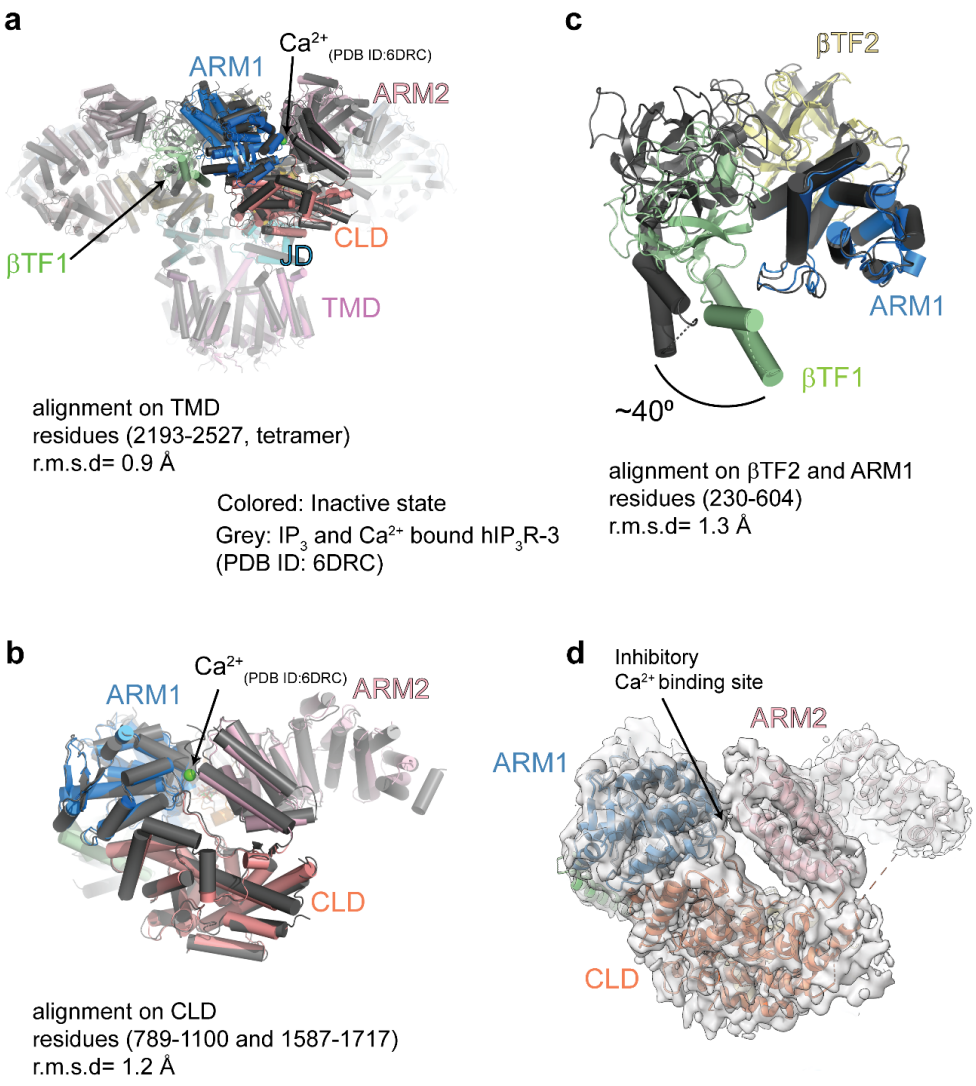

Figure 56: **Structural comparison of the hIP$_3$R-3 structures in the inactive and Ca^{2+} inhibited states.** (a-c) Ribbon representations of hIP$_3$R-3 in the inactive state and the previously published IP$_3$ and Ca^{2+} bound hIP$_3$R-3 structure (colored as in Figure 30) obtained in the presence of inhibitory Ca^{2+} concentrations (grey, PDB ID: 6DRC 1) focusing on similarities in the overall structures (a) and the inhibitory Ca^{2+} binding site (b), and differences in the IP$_3$ binding core and βTF1 orientation (c). The aligned regions and the root mean square deviation (r.m.s.d) values are shown for each panel. The green sphere represents the Ca^{2+} modeled in 6DRC. (d) Cryo-EM map after local refinement (transparent gray) is shown around the ribbon representation of the ARM1, CLD, and ARM2 of the inactive structure. Although the quality of the map allows modeling the domains, the density for the side chains of the residues around the Ca^{2+} binding site is poorly resolved, hampering inspection of the presence of Ca^{2+}.

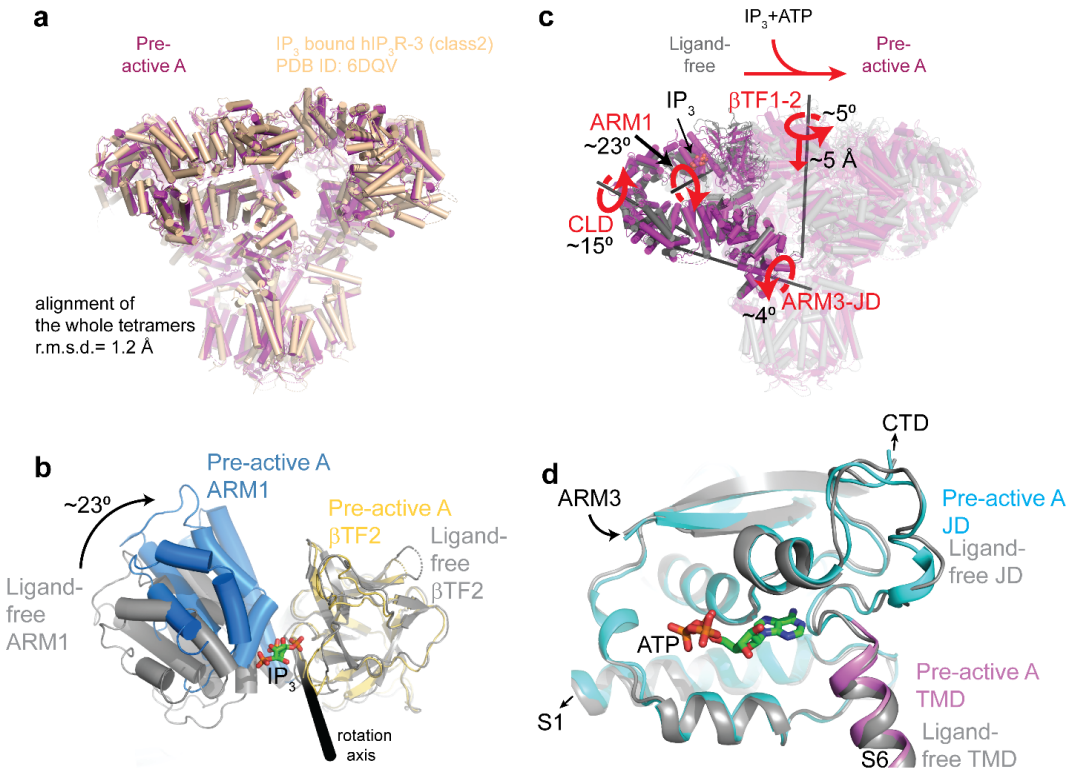

Figure 57: **Structural comparison of the hIP$_3$R-3 structures in the ligand-free and Pre-active A conformations.** (a) Ribbon representations of hIP$_3$R-3 in the pre-active A state and the previously published IP$_3$ bound class 2 state (PDB ID: 6DQV 1). The intact receptors are used for alignment. (b) IP$_3$ induced conformational changes resulting in 23° rotation of the ARM1 relative to βTF2. The structures are aligned on the βTF2. Pre-active A structure is colored as in Figure 30, and Ligand-free structure is colored in grey. IP$_3$ is shown as green sticks. (c) Ribbon representations of hIP$_3$R structures in the resting (PDB ID: 6UQK 2) superposed on the residues forming the selectivity filter and P-helix of the TMDs, emphasizing the conformational changes upon IP$_3$ and ATP binding. Domains with substantial conformational changes are shown in full colors only on one subunit, while the rest of the protein is transparent. Curved and straight red arrows indicate the rotation and translation of the domains with red labels relative to the rotation axis (black bars), respectively. (d) Close-up view of the ATP binding site. Pre-active A structure is colored as in Figure 30, and Ligand-free structure is colored in grey. ATP is shown as green sticks. No major conformational changes around the binding site are observed.

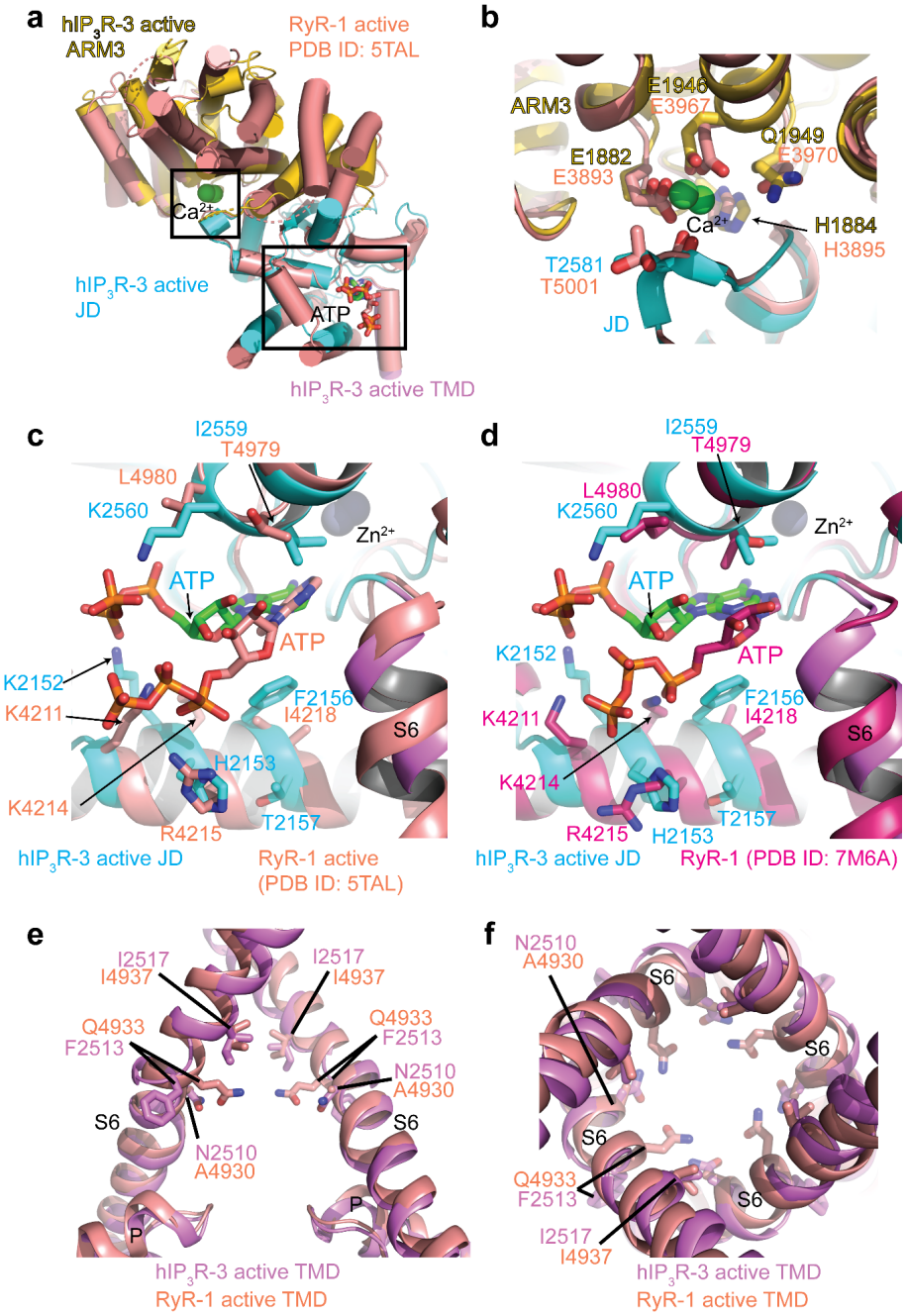

Figure 58: **Structural comparison of hIP$_3$R-3 and RyR1 structures in the active state.** (a) An overlay of the ARM3, JD, and part of S6 of hIP$_3$R-3 with the corresponding domains of rabbit RyR-1 (PDB ID: 5TAL) (Georges et al. 2016). hIP$_3$R-3 is colored as in Figure 30, and RyR1 is colored in salmon. Ca^{2+} and ATP binding sites are boxed. (b) Close-up views of the Ca^{2+}. Residues coordinating Ca^{2+} are shown as sticks and labeled. c-d Close-up view of the ATP binding site of hIP$_3$R-3 aligned onto the corresponding domains of rabbit RyR-1s ((c) PDB ID: 5TAL and (d) PDB ID:7M6A (Melville et al. 2022)). Select residues are shown as sticks and labeled. (e-f) Alignment of the S6 and P helices viewed through the membrane plane (e) and cytoplasm (f). Two of the subunits were not shown in panel (e) for clarity

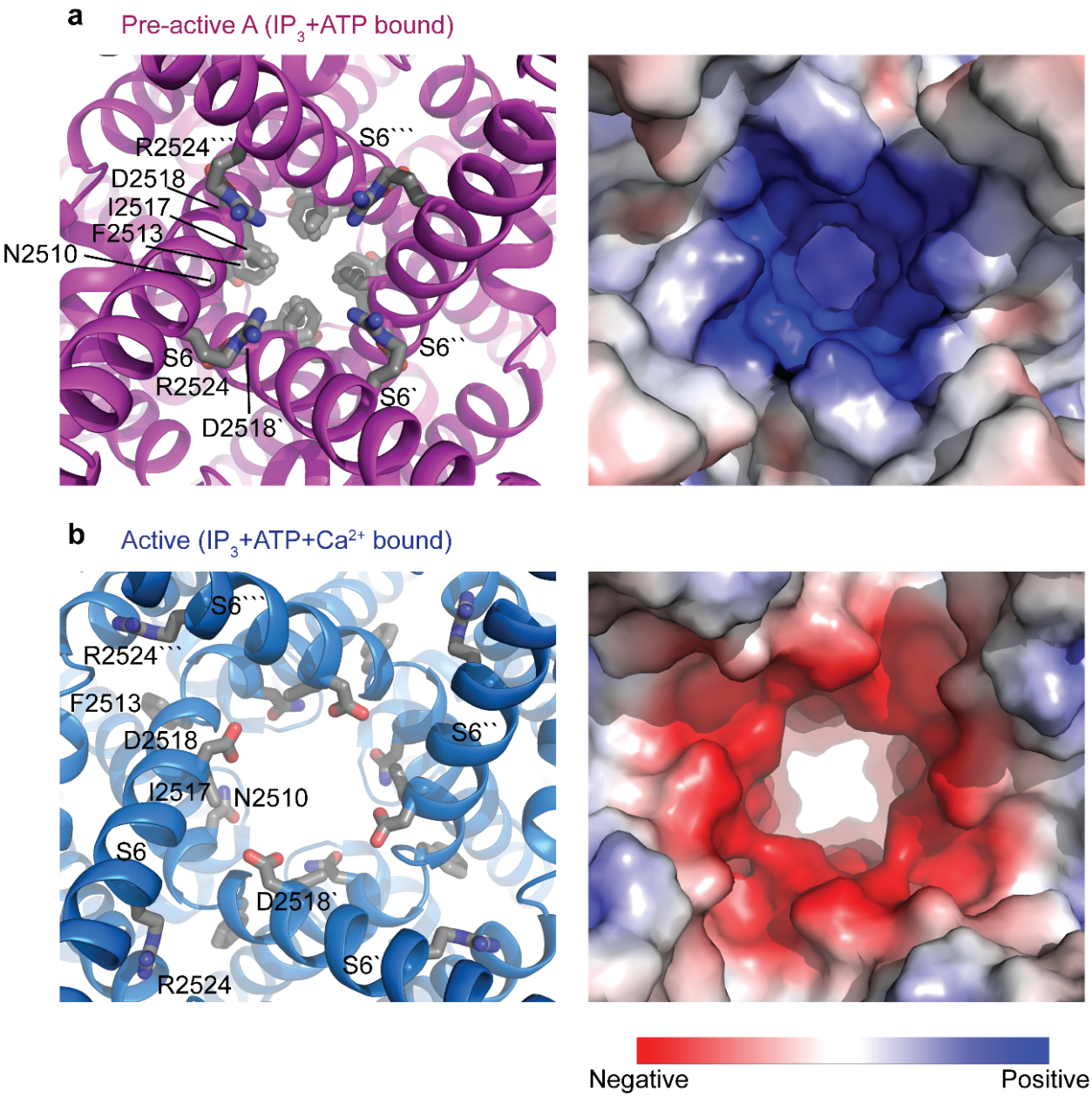

Figure 59: **Structural comparison of hIP$_3$R-3 pores in closed and open conformations.** (a-b) Close up cytoplasmic view of the IP$_3$R-3 pores in the closed (a) and open (b) conformations in ribbon (left) and electrostatic surface representations. Pore lining residues are shown as grey sticks. ‘ is used the differentiate residues in different subunits.

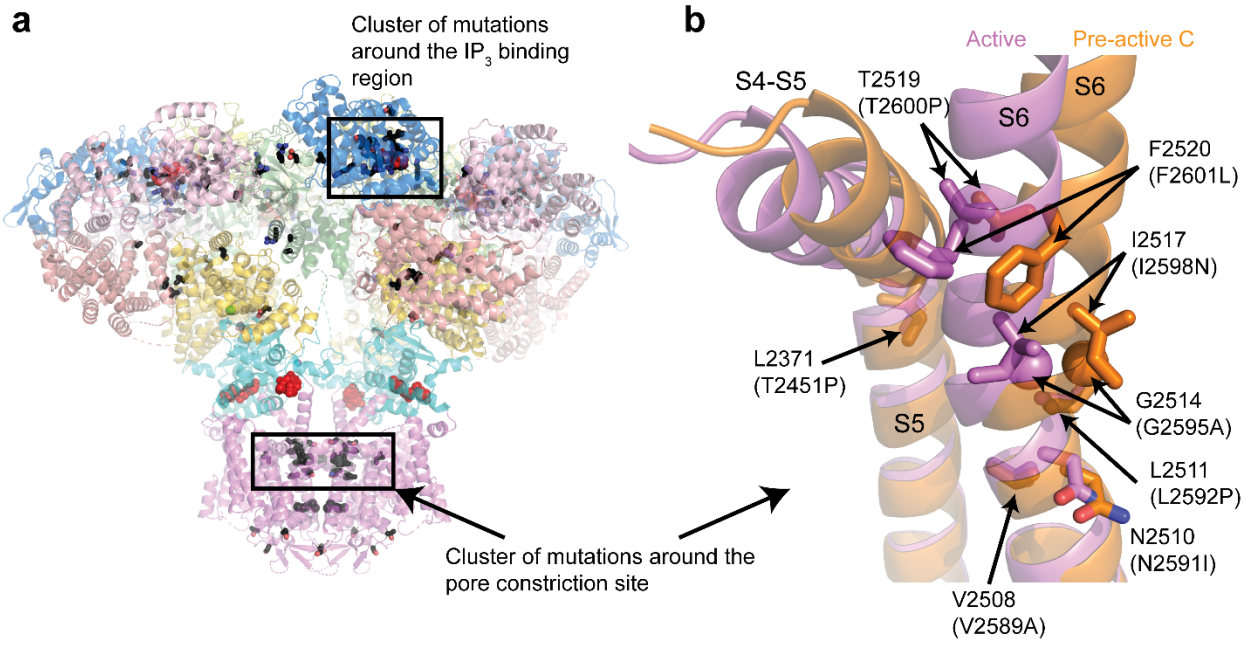

Figure 60: **Mutation hot spots of IP$_3$Rs.** (a) Mutations associated with diseases or annotated as pathogenic or likely pathogenic in ClinVar database (https://www.ncbi.nlm.nih.gov/clinvar/) for all three subtypes of IP$_3$Rs are mapped onto the hIP$_3$R-3 structure in the active conformation. Each domain is colored as in Figure 30, and the mutated residues are shown as black sticks. IP$_3$ and ATP are shown as red spheres, and Ca^{2+} ions are shown as green spheres. Clusters of mutations around the IP$_3$ binding site and the pore constriction site are indicated in black boxes. (b) Close-up view of the mutated residues around the pore constriction site. Only one protomer of pre-active C and active state structures are shown. Structures are aligned as described in Figure 31. Mutated residues are labeled based on IP$_3$R-3 numbering and IP$_3$R-1 numbering with the mutations inside parentheses. The reference sequences used for IP$_3$R-3 are UniProtKB-Q14573 and for IP$_3$R-1 are UniProtKB- Q14643

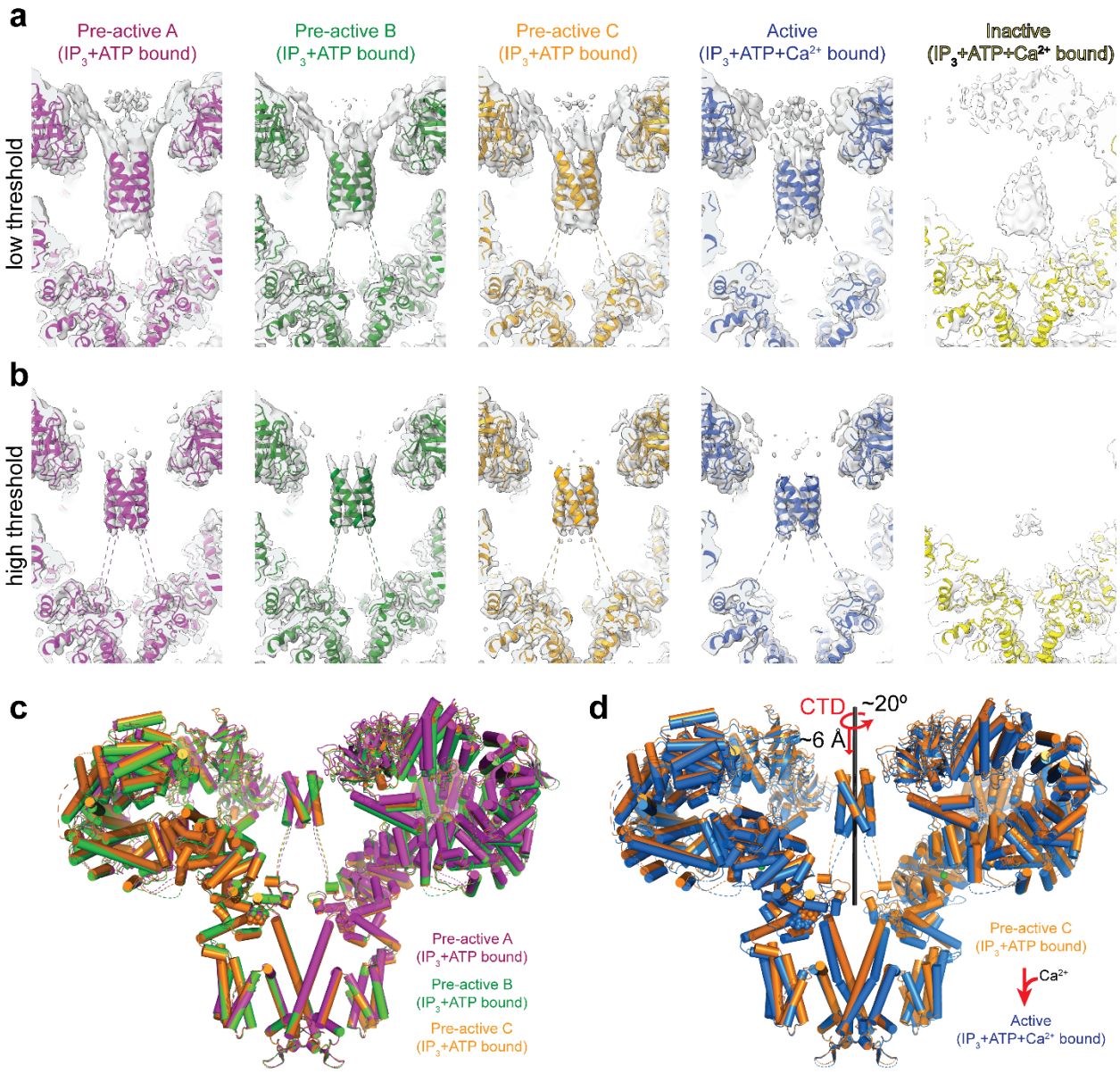

Figure 61: **The flexible architecture of the CTD.** (a-b) Unsharpened Cryo-EM map sections of hIP$_3$R-3 in different gating conformations are shown using lower (a) and higher (b) threshold values to emphasize the variability of the regions connecting the coiled-coil region to the β-TF1 and JDs. Maps are the original maps from the non-uniform refinements and are shown as transparent grey surfaces. The ribbon representations of the fitted models are colored as indicated above each column. (c) There are no noticeable changes for the coiled-coil region of hIP$_3$R-3 in the pre-active conformations. (d) The coiled coil region makes a screw-like motion towards the JD during activation. (c-d) Alignments are performed as in Figure 31. Only two opposing subunits are shown except for the coiled-coil region.

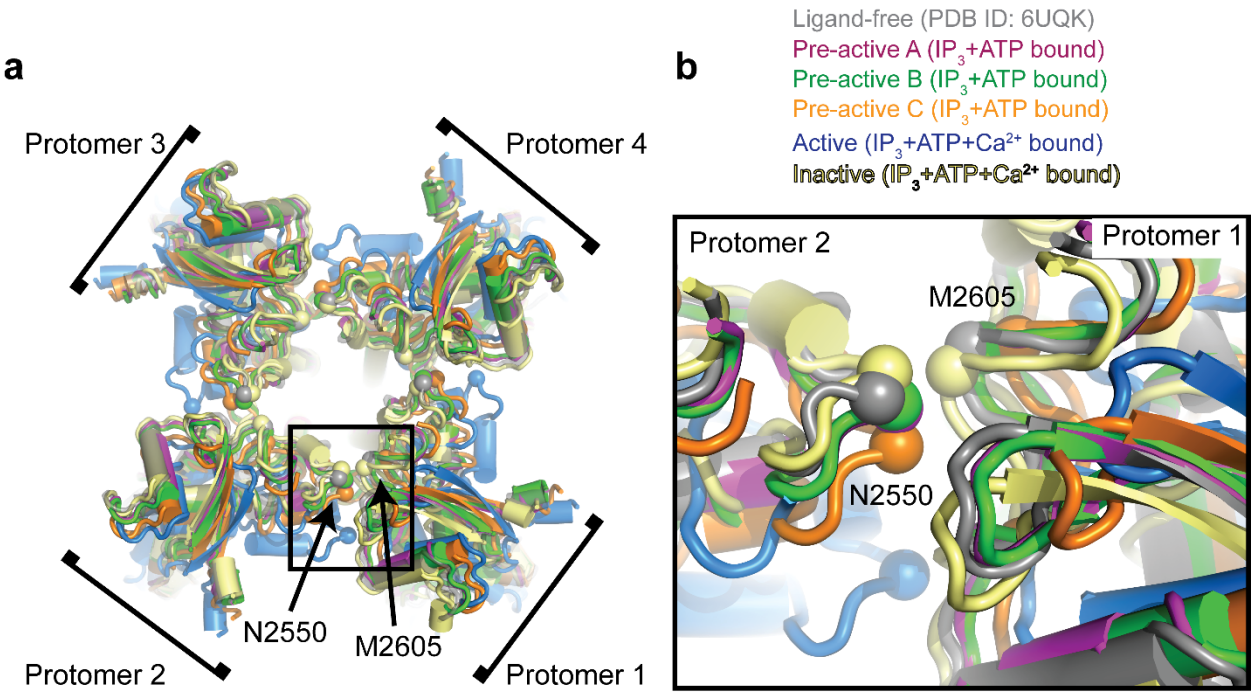

Figure 62: **Structural changes of the JDs.** (a) The tetrameric JDs of hIP$_3$R-3 in multiple gating conformations viewed from cytoplasm through the 4-fold symmetry axis. Structures are superposed on the residues forming the selectivity filter and P-helix of the TMDs. (b) Zoomed view of the boxed area. Structures are colored as in Figure 31. The Cα atoms for the residues N2550 and M2605 are shown as spheres to emphasize the structural differences among different conformations.

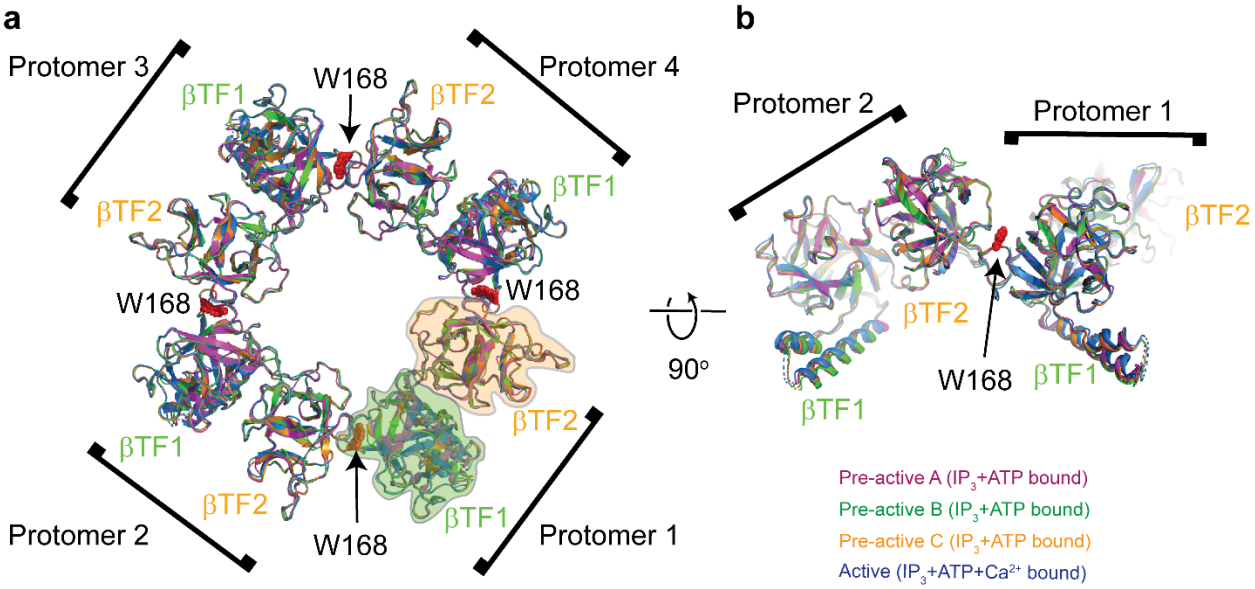

Figure 63: **Structure of the βTF ring.** (a) Aligned structures of the βTF rings of hIP$_3$R-3 in multiple gating conformations viewed from cytoplasm through the 4-fold symmetry axis. (b) 90° rotated view of panel (a). Structures are colored as in Figure 31. The βTF1 and βTF2 of each protomer are labeled, and they are circled for one of the protomers to highlight their boundaries. W168 is shown as red spheres.

References

Adkins, Charles E. and Colin W. Taylor (Oct. 7, 1999). "Lateral inhibition of inositol 1,4,5-trisphosphate receptors by cytosolic Ca2+". In: *Current Biology* 9.19. Publisher: Elsevier, pp. 1115–1118. ISSN: 0960-9822. DOI: 10.1016/S0960-9822(99)80481-3. URL: https://www.cell.com/current-biology/abstract/S0960-9822(99)80481-3 (visited on 04/04/2022).

Affolter, H. and E. Carafoli (July 16, 1980). "The Ca2+-Na+ antiporter of heart mitochondria operates electroneutrally". In: *Biochemical and Biophysical Research Communications* 95.1, pp. 193–196. ISSN: 0006-291X. DOI: 10.1016/0006-291x(80)90723-8.

Afonine, P.V. et al. (Jan. 1, 2013). "New tool: Phenix.real-space-refine". In: *Computational Crystallography Newsletter* 4, pp. 43–44.

Agar, J. N., J. C. R. Turner, and Ronald George Wreyford Norrish (Apr. 19, 1960). "Thermal diffusion in solutions of electrolytes". In: *Proceedings of the Royal Society of London. Series A. Mathematical and Physical Sciences* 255.1282. Publisher: Royal Society, pp. 307–330. DOI: 10.1098/rspa.1960.0070. URL: https://royalsocietypublishing.org/doi/10.1098/rspa.1960.0070 (visited on 05/11/2022).

Allbritton, N. L., T. Meyer, and L. Stryer (Dec. 11, 1992). "Range of messenger action of calcium ion and inositol 1,4,5-trisphosphate". In: *Science* 258.5089. Publisher: American Association for the Advancement of Science Section: Reports, pp. 1812–1815. ISSN: 0036-8075, 1095-9203. DOI: 10.1126/science.1465619. URL: https://science.sciencemag.org/content/258/5089/1812 (visited on 03/23/2020).

Althagbi, Hanan I. et al. (July 17, 2020). "Marine-Derived Macrocyclic Alkaloids (MDMAs): Chemical and Biological Diversity". In: *Marine Drugs* 18.7, p. 368. ISSN: 1660-3397. DOI: 10.3390/md18070368. URL: https://www.ncbi.nlm.nih.gov/pmc/articles/PMC7404069/ (visited on 03/21/2022).

Alvarez, J and M Montero (Nov. 1, 2002). "Measuring [Ca2+] in the endoplasmic reticulum with aequorin". In: *Cell Calcium*. Endoplasmic Reticulum as a Signalling Organelle 32.5, pp. 251–260. ISSN: 0143-4160. DOI: 10.1016/S0143416002001860. URL: https://www.sciencedirect.com/science/article/pii/S0143416002001860 (visited on 06/05/2022).

Alzayady, Kamil J., Arnau Sebé-Pedrós, et al. (Sept. 2015). "Tracing the Evolutionary History of Inositol, 1, 4, 5-Trisphosphate Receptor: Insights from Analyses of Capsaspora owczarzaki Ca2+ Release Channel Orthologs". In: *Molecular Biology and Evolution* 32.9, pp. 2236–2253. ISSN: 0737-4038. DOI: 10.1093/molbev/msv098. URL: https://www.ncbi.nlm.nih.gov/pmc/articles/PMC4540961/ (visited on 08/25/2022).

Alzayady, Kamil J., Larry E. Wagner, et al. (Oct. 11, 2013). "Functional Inositol 1,4,5-Trisphosphate Receptors Assembled from Concatenated Homo- and Heteromeric Subunits". In: *The Journal of Biological Chemistry* 288.41, pp. 29772–29784. ISSN: 0021-9258. DOI: 10.1074/jbc.M113.502203. URL: https://www.ncbi.nlm.nih.gov/pmc/articles/PMC3795275/ (visited on 01/15/2019).

Alzayady, Kamil J., Liwei Wang, et al. (Apr. 5, 2016). "Defining the Stoichiometry of Inositol 1,4,5-Trisphosphate Binding Required to Initiate Ca2+ Release". In: *Science signaling* 9.422, ra35. ISSN: 1937-9145. DOI: 10.1126/scisignal.aad6281. URL: https://www.ncbi.nlm.nih.gov/pmc/articles/PMC4850551/ (visited on 01/15/2019).

Ambudkar, Indu S. (June 2014). "Ca2+ Signaling and Regulation of Fluid Secretion in Salivary Gland Acinar Cells". In: *Cell calcium* 55.6, pp. 297–305. ISSN: 0143-4160. DOI: 10.1016/j.ceca.2014.02.009. URL: https://www.ncbi.nlm.nih.gov/pmc/articles/PMC4059182/ (visited on 06/07/2022).

Ando, Hideaki, Matsumi Hirose, and Katsuhiko Mikoshiba (Nov. 27, 2018). "Aberrant IP3 receptor activities revealed by comprehensive analysis of pathological mutations causing spinocerebellar ataxia 29". In: *Proceedings of the National Academy of Sciences* 115.48. Publisher: Proceedings of the National Academy of Sciences, pp. 12259–12264. DOI: 10.1073/pnas.1811129115. URL: https://www.pnas.org/doi/10.1073/pnas.1811129115 (visited on 04/29/2022).

Ando, Hideaki, Akihiro Mizutani, Hélène Kiefer, et al. (June 23, 2006). "IRBIT suppresses IP3 receptor activity by competing with IP3 for the common binding site on the IP3 receptor". In: *Molecular Cell* 22.6, pp. 795–806. ISSN: 1097-2765. DOI: 10.1016/j.molcel.2006.05.017.

Ando, Hideaki, Akihiro Mizutani, Toru Matsu-ura, et al. (Mar. 21, 2003). "IRBIT, a novel inositol 1,4,5-trisphosphate (IP3) receptor-binding protein, is released from the IP3 receptor upon IP3 binding to the receptor". In: *The Journal of Biological Chemistry* 278.12, pp. 10602–10612. ISSN: 0021-9258. DOI: 10.1074/jbc.M210119200.

Armstrong, Jeffrey S. (Oct. 1, 2006). "The role of the mitochondrial permeability transition in cell death". In: *Mitochondrion* 6.5, pp. 225–234. ISSN: 1567-7249. DOI: 10.1016/j.mito.2006.07.006. URL: https://www.sciencedirect.com/science/article/pii/S1567724906000936 (visited on 06/09/2022).

Arnold, Stefan A. et al. (Mar. 1, 2017). "Blotting-free and lossless cryo-electron microscopy grid preparation from nanoliter-sized protein samples and single-cell extracts". In: *Journal of Structural Biology* 197.3, pp. 220–226. ISSN: 1047-8477. DOI: 10.1016/j.jsb.2016.11.002. URL: https://www.sciencedirect.com/science/article/pii/S104784771630243X (visited on 04/04/2022).

Assefa, Zerihun et al. (Oct. 2004). "Caspase-3-induced Truncation of Type 1 Inositol Trisphosphate Receptor Accelerates Apoptotic Cell Death and Induces Inositol Trisphosphate-independent Calcium Release during Apoptosis". In: *Journal of Biological Chemistry* 279.41, pp. 43227–43236. ISSN: 00219258. DOI: 10.1074/jbc.M403872200. URL: https://linkinghub.elsevier.com/retrieve/pii/S002192582077078X (visited on 09/12/2022).

Axelrod, D et al. (Sept. 1976). "Mobility measurement by analysis of fluorescence photobleaching recovery kinetics." In: *Biophysical Journal* 16.9, pp. 1055–1069. ISSN: 0006-3495. URL: https://www.ncbi.nlm.nih.gov/pmc/articles/PMC1334945/ (visited on 05/12/2022).

Azumaya, Caleigh M. et al. (Feb. 7, 2020). "Cryo-EM structure of human type-3 inositol triphosphate receptor reveals the presence of a self-binding peptide that acts as an antagonist". In: *The Journal of Biological Chemistry* 295.6, pp. 1743–1753. ISSN: 0021-9258. DOI: 10.1074/jbc.RA119.011570. URL: https://www.ncbi.nlm.nih.gov/pmc/articles/PMC7008357/ (visited on 05/16/2022).

Azzolin, Luca et al. (June 18, 2010). "The mitochondrial permeability transition from yeast to mammals". In: *FEBS letters* 584.12, pp. 2504–2509. ISSN: 0014-5793. DOI: 10.1016/j.febslet.2010.04.023. URL: https://www.ncbi.nlm.nih.gov/pmc/articles/PMC2878904/ (visited on 06/08/2022).

Baker, Mariah R. et al. (May 25, 2021). "Cryo-EM structure of type 1 IP3R channel in a lipid bilayer". In: *Communications Biology* 4.1. Number: 1 Publisher: Nature Publishing Group, pp. 1–11. ISSN: 2399-3642. DOI: 10.1038/s42003-021-02156-4. URL: https://www.nature.com/articles/s42003-021-02156-4 (visited on 04/20/2022).

Bartoschik, Tanja et al. (Mar. 21, 2018). "Near-native, site-specific and purification-free protein labeling for quantitative protein interaction analysis by MicroScale Thermophoresis". In: *Scientific Reports* 8, p. 4977. ISSN: 2045-2322. DOI: 10.1038/s41598-018-23154-3. URL: https://www.ncbi.nlm.nih.gov/pmc/articles/PMC5862892/ (visited on 05/12/2022).

Bassik, Michael C et al. (Mar. 10, 2004). "Phosphorylation of BCL-2 regulates ER Ca2+ homeostasis and apoptosis". In: *The EMBO Journal* 23.5, pp. 1207–1216. ISSN: 0261-4189. DOI: 10.1038/sj.emboj.7600104. URL: https://www.ncbi.nlm.nih.gov/pmc/articles/PMC380968/ (visited on 06/05/2022).

Baughman, Joshua M. et al. (Aug. 2011). "Integrative genomics identifies MCU as an essential component of the mitochondrial calcium uniporter". In: *Nature* 476.7360. Number: 7360 Publisher: Nature Publishing Group, pp. 341–345. ISSN: 1476-4687. DOI: 10.1038/nature10234. URL: https://www.nature.com/articles/nature10234 (visited on 06/08/2022).

Baukal, Albert J. et al. (Dec. 17, 1985). "Binding sites for inositol trisphosphate in the bovine adrenal cortex". In: *Biochemical and Biophysical Research Communications* 133.2, pp. 532–538. ISSN: 0006-291X. DOI: 10.1016/0006-291X(85)90939-8. URL: https://www.sciencedirect.com/science/article/pii/0006291X85909398 (visited on 05/04/2022).

Berridge, Michael J. (Apr. 1, 2012). "Calcium signalling remodelling and disease". In: *Biochemical Society Transactions* 40.2, pp. 297–309. ISSN: 0300-5127, 1470-8752. DOI: 10.1042/BST20110766. URL: http://www.biochemsoctrans.org.proxy.library.vanderbilt.edu/content/40/2/297 (visited on 01/15/2019).

— (2016). "The Inositol Trisphosphate/Calcium Signaling Pathway in Health and Disease". In: *Physiological Reviews* 96.4, pp. 1261–1296. ISSN: 1522-1210. DOI: 10.1152/physrev.00006.2016.

Berridge, Michael J., Peter Lipp, and Martin D. Bootman (Oct. 2000). "The versatility and universality of calcium signalling". In: *Nature Reviews Molecular Cell Biology* 1.1, pp. 11–21. ISSN: 1471-0080. DOI: 10.1038/35036035. URL: http://www.nature.com/articles/35036035 (visited on 01/15/2019).

Bers, Donald M., Chris W. Patton, and Richard Nuccitelli (Jan. 1, 1994). "Chapter 1 - A Practical Guide to the Preparation of Ca2+ Buffers". In: *Methods in Cell Biology*. Ed. by Richard Nuccitelli. Vol. 40. A Practical Guide to the Study of Calcium in Living Cells. Academic Press,

pp. 3–29. DOI: 10.1016/S0091-679X(08)61108-5. URL: https://www.sciencedirect.com/science/article/pii/S0091679X08611085 (visited on 04/04/2022).

Betzenhauser, Matthew J. et al. (June 12, 2009). "ATP Regulation of Type-1 Inositol 1,4,5-Trisphosphate Receptor Activity Does Not Require Walker A-type ATP-binding Motifs". In: *The Journal of Biological Chemistry* 284.24, pp. 16156–16163. ISSN: 0021-9258. DOI: 10.1074/jbc.M109.006452. URL: https://www.ncbi.nlm.nih.gov/pmc/articles/PMC2713511/ (visited on 02/02/2022).

Bezprozvanny, I B et al. (Mar. 1993). "Activation of the calcium release channel (ryanodine receptor) by heparin and other polyanions is calcium dependent." In: *Molecular Biology of the Cell* 4.3, pp. 347–352. ISSN: 1059-1524. URL: https://www.ncbi.nlm.nih.gov/pmc/articles/PMC300932/ (visited on 03/21/2022).

Bezprozvanny, Ilya (Sept. 1, 2005). "The inositol 1,4,5-trisphosphate receptors". In: *Cell Calcium*. Frontiers in calcium signalling 38.3, pp. 261–272. ISSN: 0143-4160. DOI: 10.1016/j.ceca.2005.06.030. URL: http://www.sciencedirect.com/science/article/pii/S014341600500117X (visited on 06/28/2019).

Bezprozvanny, Ilya and Barbara E. Ehrlich (June 1, 1993). "ATP modulates the function of inositol 1,4,5-trisphosphate-gated channels at two sites". In: *Neuron* 10.6, pp. 1175–1184. ISSN: 0896-6273. DOI: 10.1016/0896-6273(93)90065-Y. URL: https://www.sciencedirect.com/science/article/pii/089662739390065Y (visited on 04/04/2022).

Bezprozvanny, Llya, James Watras, and Barbara E. Ehrlich (June 1991). "Bell-shaped calcium-response curves of lns(l,4,5)P3- and calcium-gated channels from endoplasmic reticulum of cerebellum". In: *Nature* 351.6329, pp. 751–754. ISSN: 1476-4687. DOI: 10.1038/351751a0. URL: https://www.nature.com/articles/351751a0 (visited on 01/14/2019).

Big, Edward J. (1956). "A Short History of the Electron Microscope". In: *Bios* 27.1. Publisher: Beta Beta Beta Biological Society, pp. 33–37. ISSN: 0005-3155. URL: http://www.jstor.org/stable/4605737 (visited on 06/10/2022).

Bilmen, Jonathan G. et al. (Aug. 2002). "Inhibition of SERCA Ca2+ pumps by 2-aminoethoxydiphenyl borate (2-APB). 2-APB reduces both Ca2+ binding and phosphoryl transfer from ATP, by interfering with the pathway leading to the Ca2+-binding sites". In: *European Journal of Biochemistry* 269.15, pp. 3678–3687. ISSN: 0014-2956. DOI: 10.1046/j.1432-1033.2002.03060.x.

Binshtein, Elad and Melanie D. Ohi (May 26, 2015). "Cryo-Electron Microscopy and the Amazing Race to Atomic Resolution". In: *Biochemistry* 54.20. Publisher: American Chemical Society, pp. 3133–3141. ISSN: 0006-2960. DOI: 10.1021/acs.biochem.5b00114. URL: https://doi.org/10.1021/acs.biochem.5b00114 (visited on 06/10/2022).

Biyani, Nikhil et al. (May 1, 2017). "Focus: The interface between data collection and data processing in cryo-EM". In: *Journal of Structural Biology* 198.2, pp. 124–133. ISSN: 1047-8477. DOI: 10.1016/j.jsb.2017.03.007. URL: https://www.sciencedirect.com/science/article/pii/S1047847717300515 (visited on 06/15/2022).

Blondel, O. et al. (May 25, 1993). "Sequence and functional characterization of a third inositol trisphosphate receptor subtype, IP3R-3, expressed in pancreatic islets, kidney, gastrointestinal tract, and other tissues". In: *The Journal of Biological Chemistry* 268.15, pp. 11356–11363. ISSN: 0021-9258.

Bobrova, G. I. and M. A. Bukhtilova (Feb. 1, 1972). "Determination of mass-transfer coefficients". In: *Journal of engineering physics* 22.2, pp. 238–240. ISSN: 1573-871X. DOI: 10.1007/BF00825910. URL: https://doi.org/10.1007/BF00825910 (visited on 05/11/2022).

Bobrova, G. I. and G. D. Rabinovich (Jan. 1, 1967). *Determination of the soret coefficients and the concentration diffusion coefficients by an unsteady-state method.* NTRS Author Affiliations: Israel Oceanographic and Limnological Research Ltd. NTRS Document ID: 19670012719 NTRS Research Center: Legacy CDMS (CDMS). URL: https://ntrs.nasa.gov/citations/19670012719 (visited on 05/11/2022).

Boehning, D. and S. K. Joseph (Oct. 16, 2000). "Direct association of ligand-binding and pore domains in homo- and heterotetrameric inositol 1,4,5-trisphosphate receptors". In: *The EMBO journal* 19.20, pp. 5450–5459. ISSN: 0261-4189. DOI: 10.1093/emboj/19.20.5450.

Bononi, Angela et al. (June 22, 2017). "BAP1 regulates IP3R3-mediated Ca2+ flux to mitochondria suppressing cell transformation". In: *Nature* 546.7659, pp. 549–553. ISSN: 1476-4687. DOI: 10.1038/nature22798.

Bootman, Martin D. et al. (Aug. 2002). "2-aminoethoxydiphenyl borate (2-APB) is a reliable blocker of store-operated Ca2+ entry but an inconsistent inhibitor of InsP3-induced Ca2+ release". In: *FASEB journal: official publication of the Federation of American Societies for Experimental Biology* 16.10, pp. 1145–1150. ISSN: 1530-6860. DOI: 10.1096/fj.02-0037rev.

Bosanac, Ivan, Jean-René Alattia, et al. (Dec. 2002). "Structure of the inositol 1,4,5-trisphosphate receptor binding core in complex with its ligand". In: *Nature* 420.6916, pp. 696–700. ISSN: 1476-4687. DOI: 10.1038/nature01268. URL: http://www.nature.com/articles/nature01268 (visited on 01/15/2019).

Bosanac, Ivan, Takayuki Michikawa, et al. (Dec. 6, 2004). "Structural insights into the regulatory mechanism of IP3 receptor". In: *Biochimica et Biophysica Acta (BBA) - Molecular Cell Research*. 8th European Symposium on Calcium 1742.1, pp. 89–102. ISSN: 0167-4889. DOI: 10.1016/j.bbamcr.2004.09.016. URL: https://www.sciencedirect.com/science/article/pii/S0167488904002332 (visited on 05/13/2022).

Bosanac, Ivan, Haruka Yamazaki, et al. (Jan. 21, 2005). "Crystal Structure of the Ligand Binding Suppressor Domain of Type 1 Inositol 1,4,5-Trisphosphate Receptor". In: *Molecular Cell* 17.2, pp. 193–203. ISSN: 1097-2765. DOI: 10.1016/j.molcel.2004.11.047. URL: http://www.sciencedirect.com/science/article/pii/S1097276504007695 (visited on 01/14/2019).

Böttcher, B., S. A. Wynne, and R. A. Crowther (Mar. 6, 1997). "Determination of the fold of the core protein of hepatitis B virus by electron cryomicroscopy". In: *Nature* 386.6620, pp. 88–91. ISSN: 0028-0836. DOI: 10.1038/386088a0.

Brand, M D (Jan. 15, 1985a). "Electroneutral efflux of Ca2+ from liver mitochondria." In: *Biochemical Journal* 225.2, pp. 413–419. ISSN: 0264-6021. URL: https://www.ncbi.nlm.nih.gov/pmc/articles/PMC1144605/ (visited on 06/08/2022).

— (July 1, 1985b). "The stoichiometry of the exchange catalysed by the mitochondrial calcium/-sodium antiporter." In: *Biochemical Journal* 229.1, pp. 161–166. ISSN: 0264-6021. URL: https://www.ncbi.nlm.nih.gov/pmc/articles/PMC1145162/ (visited on 06/08/2022).

Braun, Dieter and Albert Libchaber (Oct. 28, 2002). "Trapping of DNA by thermophoretic depletion and convection". In: *Physical Review Letters* 89.18, p. 188103. ISSN: 0031-9007. DOI: 10.1103/PhysRevLett.89.188103.

Brautigam, Chad A. (Apr. 2015). "Fitting two- and three-site binding models to isothermal titration calorimetric data". In: *Methods (San Diego, Calif.)* 76, pp. 124–136. ISSN: 1046-2023. DOI: 10.1016/j.ymeth.2014.11.018. URL: https://www.ncbi.nlm.nih.gov/pmc/articles/PMC4591754/ (visited on 05/10/2022).

Brisac, Cynthia et al. (Dec. 2010). "Calcium Flux between the Endoplasmic Reticulum and Mitochondrion Contributes to Poliovirus-Induced Apoptosis". In: *Journal of Virology* 84.23, pp. 12226–12235. ISSN: 0022-538X. DOI: 10.1128/JVI.00994-10. URL: https://www.ncbi.nlm.nih.gov/pmc/articles/PMC2976416/ (visited on 06/09/2022).

Brown, Alan (Aug. 4, 2009). "Analysis of Cooperativity by Isothermal Titration Calorimetry". In: *International Journal of Molecular Sciences* 10.8, pp. 3457–3477. ISSN: 1422-0067. DOI: 10.3390/ijms10083457. URL: https://www.ncbi.nlm.nih.gov/pmc/articles/PMC2812830/ (visited on 05/10/2022).

Buckland, S. T. (1984). "Monte Carlo Confidence Intervals". In: *Biometrics* 40.3. Publisher: [Wiley, International Biometric Society], pp. 811–817. ISSN: 0006-341X. DOI: 10.2307/2530926. URL: https://www.jstor.org/stable/2530926 (visited on 05/12/2022).

Buczek, Pawel and Martin P. Horvath (June 23, 2006). "Thermodynamic Characterization of Binding Oxytricha nova Single Strand Telomere DNA with the Alpha Protein N-terminal Domain". In: *Journal of Molecular Biology* 359.5, pp. 1217–1234. ISSN: 0022-2836. DOI: 10.1016/j.jmb.2006.02.082. URL: https://www.sciencedirect.com/science/article/pii/S0022283606004761 (visited on 05/10/2022).

Butler, B. D. and J. C. R. Turner (Jan. 1, 1966). "Flow-cell studies of thermal diffusion in liquids. Part 2.—Phenomenological equations and their solution". In: *Transactions of the Faraday Society* 62.0. Publisher: The Royal Society of Chemistry, pp. 3121–3130. ISSN: 0014-7672. DOI: 10.1039/TF9666203121. URL: https://pubs.rsc.org/en/content/articlelanding/1966/tf/tf9666203121 (visited on 05/11/2022).

Bygrave, Fyfe L. and Angelo Benedetti (June 1, 1996). "What is the concentration of calcium ions in the endoplasmic reticulum?" In: *Cell Calcium* 19.6, pp. 547–551. ISSN: 0143-4160. DOI: 10.1016/S0143-4160(96)90064-0. URL: https://www.sciencedirect.com/science/article/pii/S0143416096900640 (visited on 06/05/2022).

Carafoli, Ernesto (Apr. 2003). "Historical review: mitochondria and calcium: ups and downs of an unusual relationship". In: *Trends in Biochemical Sciences* 28.4, pp. 175–181. ISSN: 0968-0004. DOI: 10.1016/S0968-0004(03)00053-7.

Carafoli, Ernesto and Izabela Roman (Jan. 1, 1980). "Mitochondria and disease". In: *Molecular Aspects of Medicine* 3.5, pp. 295–429. ISSN: 0098-2997. DOI: 10.1016/0098-2997(80)90005-9.

URL: https://www.sciencedirect.com/science/article/pii/0098299780900059 (visited on 06/08/2022).

Cárdenas, César et al. (July 23, 2010). "Essential regulation of cell bioenergetics by constitutive InsP3 receptor Ca2+ transfer to mitochondria". In: *Cell* 142.2, pp. 270–283. ISSN: 1097-4172. DOI: 10.1016/j.cell.2010.06.007.

Cardy, T J and C W Taylor (Sept. 1, 1998). "A novel role for calmodulin: Ca2+-independent inhibition of type-1 inositol trisphosphate receptors." In: *Biochemical Journal* 334 (Pt 2), pp. 447–455. ISSN: 0264-6021. URL: https://www.ncbi.nlm.nih.gov/pmc/articles/PMC1219708/ (visited on 05/17/2022).

Case, R. M. and T. Clausen (Nov. 1973). "The relationship between calcium exchange and enzyme secretion in the isolated rat pancreas". In: *The Journal of Physiology* 235.1, pp. 75–102. ISSN: 0022-3751. URL: https://www.ncbi.nlm.nih.gov/pmc/articles/PMC1350734/ (visited on 05/13/2022).

Castonguay, A and R Robitaille (July 1, 2002). "Xestospongin C is a potent inhibitor of SERCA at a vertebrate synapse". In: *Cell Calcium* 32.1, pp. 39–47. ISSN: 0143-4160. DOI: 10.1016/S0143-4160(02)00093-3. URL: https://www.sciencedirect.com/science/article/pii/S0143416002000933 (visited on 03/23/2022).

Catterall, William A. (Aug. 2011). "Voltage-Gated Calcium Channels". In: *Cold Spring Harbor Perspectives in Biology* 3.8, a003947. ISSN: 1943-0264. DOI: 10.1101/cshperspect.a003947. URL: https://www.ncbi.nlm.nih.gov/pmc/articles/PMC3140680/ (visited on 08/18/2022).

Chadwick, C C, A Saito, and S Fleischer (Mar. 1990). "Isolation and characterization of the inositol trisphosphate receptor from smooth muscle." In: *Proceedings of the National Academy of Sciences of the United States of America* 87.6, pp. 2132–2136. ISSN: 0027-8424. URL: https://www.ncbi.nlm.nih.gov/pmc/articles/PMC53640/ (visited on 05/17/2022).

Chan, Jenny et al. (Nov. 12, 2010). "Structural studies of inositol 1,4,5-trisphosphate receptor: coupling ligand binding to channel gating". In: *The Journal of Biological Chemistry* 285.46, pp. 36092–36099. ISSN: 1083-351X. DOI: 10.1074/jbc.M110.140160.

Chandran, Aneesh et al. (Feb. 21, 2019). "Exploration of inositol 1,4,5-trisphosphate (IP3) regulated dynamics of N-terminal domain of IP3 receptor reveals early phase molecular events during

receptor activation". In: *Scientific Reports* 9.1, p. 2454. ISSN: 2045-2322. DOI: 10.1038/s41598-019-39301-3.

Chang, Chi-Lun et al. (Nov. 14, 2013). "Feedback Regulation of Receptor-Induced Ca2+ Signaling Mediated by E-Syt1 and Nir2 at Endoplasmic Reticulum-Plasma Membrane Junctions". In: *Cell Reports* 5.3, pp. 813–825. ISSN: 2211-1247. DOI: 10.1016/j.celrep.2013.09.038. URL: https://www.sciencedirect.com/science/article/pii/S2211124713005615 (visited on 06/06/2022).

Chen, Dong-Hua et al. (Jan. 25, 2011). "Structural basis for scaffolding-mediated assembly and maturation of a dsDNA virus". In: *Proceedings of the National Academy of Sciences of the United States of America* 108.4, pp. 1355–1360. ISSN: 0027-8424. DOI: 10.1073/pnas.1015739108. URL: https://www.ncbi.nlm.nih.gov/pmc/articles/PMC3029737/ (visited on 06/11/2022).

Chirasani, Venkat R. et al. (Aug. 1, 2019). "A central core disease mutation in the Ca2+-binding site of skeletal muscle ryanodine receptor impairs single-channel regulation". In: *American Journal of Physiology - Cell Physiology* 317.2, pp. C358–C365. ISSN: 0363-6143. DOI: 10.1152/ajpcell.00052.2019. URL: https://www.ncbi.nlm.nih.gov/pmc/articles/PMC6732417/ (visited on 04/04/2022).

Clusius, Klaus and Gerhad Dickel (Aug. 1, 1938). "Neues Verfahren zur Gasentmischung und Isotopentrennung". In: *Naturwissenschaften* 26.33, pp. 546–546. ISSN: 1432-1904. DOI: 10.1007/BF01675498. URL: https://doi.org/10.1007/BF01675498 (visited on 05/11/2022).

Cohen, P. et al. (1980). "Calcium control of muscle phosphorylase kinase through the combined action of calmodulin and troponin". In: *Annals of the New York Academy of Sciences* 356, pp. 151–161. ISSN: 0077-8923. DOI: 10.1111/j.1749-6632.1980.tb29608.x.

Colombini, M. (June 1979). "A candidate for the permeability pathway of the outer mitochondrial membrane". In: *Nature* 279.5714. Number: 5714 Publisher: Nature Publishing Group, pp. 643–645. ISSN: 1476-4687. DOI: 10.1038/279643a0. URL: http://www.nature.com/articles/279643a0 (visited on 06/08/2022).

— (Aug. 2009). "The published 3D structure of the VDAC channel: native or not?" In: *Trends in Biochemical Sciences* 34.8, pp. 382–389. ISSN: 0968-0004. DOI: 10.1016/j.tibs.2009.05.001.

Conway, J. F. et al. (Mar. 6, 1997). "Visualization of a 4-helix bundle in the hepatitis B virus capsid by cryo-electron microscopy". In: *Nature* 386.6620, pp. 91–94. ISSN: 0028-0836. DOI: 10.1038/386091a0.

Correa, Vanessa et al. (May 1, 2001). "Structural Determinants of Adenophostin A Activity at Inositol Trisphosphate Receptors". In: *Molecular Pharmacology* 59.5. Publisher: American Society for Pharmacology and Experimental Therapeutics Section: Article, pp. 1206–1215. ISSN: 0026-895X, 1521-0111. DOI: 10.1124/mol.59.5.1206. URL: https://molpharm.aspetjournals.org/content/59/5/1206 (visited on 03/17/2022).

Criollo, A. et al. (May 2007). "Regulation of autophagy by the inositol trisphosphate receptor". In: *Cell Death and Differentiation* 14.5, pp. 1029–1039. ISSN: 1350-9047. DOI: 10.1038/sj.cdd.4402099.

Crowther, Richard Anthony, Hugh Esmor Huxley, and Aaron Klug (May 27, 1971). "Procedures for three-dimensional reconstruction of spherical viruses by Fourier synthesis from electron micrographs". In: *Philosophical Transactions of the Royal Society of London. B, Biological Sciences* 261.837. Publisher: Royal Society, pp. 221–230. DOI: 10.1098/rstb.1971.0054. URL: https://royalsocietypublishing.org/doi/10.1098/rstb.1971.0054 (visited on 09/14/2021).

Csordás, G, A P Thomas, and G Hajnóczky (Jan. 4, 1999). "Quasi-synaptic calcium signal transmission between endoplasmic reticulum and mitochondria." In: *The EMBO Journal* 18.1, pp. 96–108. ISSN: 0261-4189. DOI: 10.1093/emboj/18.1.96. URL: https://www.ncbi.nlm.nih.gov/pmc/articles/PMC1171106/ (visited on 06/08/2022).

Dam, T. K. et al. (May 12, 2000). "Binding of multivalent carbohydrates to concanavalin A and Dioclea grandiflora lectin. Thermodynamic analysis of the "multivalency effect"". In: *The Journal of Biological Chemistry* 275.19, pp. 14223–14230. ISSN: 0021-9258. DOI: 10.1074/jbc.275.19.14223.

Dash, Ranjan K and Daniel A Beard (July 1, 2008). "Analysis of cardiac mitochondrial Na+–Ca2+ exchanger kinetics with a biophysical model of mitochondrial Ca2+ handing suggests a 3: 1 stoichiometry". In: *The Journal of Physiology* 586 (Pt 13), pp. 3267–3285. ISSN: 0022-3751. DOI: 10.1113/jphysiol.2008.151977. URL: https://www.ncbi.nlm.nih.gov/pmc/articles/PMC2538784/ (visited on 06/08/2022).

Dasso, L L and C W Taylor (Dec. 15, 1991). "Heparin and other polyanions uncouple alpha 1-adrenoceptors from G-proteins." In: *Biochemical Journal* 280 (Pt 3), pp. 791–795. ISSN: 0264-6021. URL: https://www.ncbi.nlm.nih.gov/pmc/articles/PMC1130523/ (visited on 03/21/2022).

De Rosier, D. J. and A. Klug (Jan. 1968). "Reconstruction of Three Dimensional Structures from Electron Micrographs". In: *Nature* 217.5124. Number: 5124 Publisher: Nature Publishing Group, pp. 130–134. ISSN: 1476-4687. DOI: 10.1038/217130a0. URL: http://www.nature.com/articles/217130a0 (visited on 06/10/2022).

De Smedt, H et al. (Mar. 1, 1997). "Isoform diversity of the inositol trisphosphate receptor in cell types of mouse origin." In: *Biochemical Journal* 322 (Pt 2), pp. 575–583. ISSN: 0264-6021. URL: https://www.ncbi.nlm.nih.gov/pmc/articles/PMC1218228/ (visited on 06/03/2022).

De Smedt, H. et al. (Aug. 1994). "Determination of relative amounts of inositol trisphosphate receptor mRNA isoforms by ratio polymerase chain reaction." In: *Journal of Biological Chemistry* 269.34, pp. 21691–21698. ISSN: 00219258. DOI: 10.1016/S0021-9258(17)31861-6. URL: https://linkinghub.elsevier.com/retrieve/pii/S0021925817318616 (visited on 06/03/2022).

Decuypere, Jean-Paul et al. (May 1, 2011). "The IP3 receptor–mitochondria connection in apoptosis and autophagy". In: *Biochimica et Biophysica Acta (BBA) - Molecular Cell Research*. Including the Special Section: 11th European Symposium on Calcium 1813.5, pp. 1003–1013. ISSN: 0167-4889. DOI: 10.1016/j.bbamcr.2010.11.023. URL: http://www.sciencedirect.com/science/article/pii/S0167488910003095 (visited on 06/28/2019).

Deka, Ranjit K. et al. (Feb. 23, 2007). "Crystal structure of the Tp34 (TP0971) lipoprotein of treponema pallidum: implications of its metal-bound state and affinity for human lactoferrin". In: *The Journal of Biological Chemistry* 282.8, pp. 5944–5958. ISSN: 0021-9258. DOI: 10.1074/jbc.M610215200.

DeLuca, H. F. and G. W. Engstrom (Nov. 1961). "CALCIUM UPTAKE BY RAT KIDNEY MITOCHONDRIA*". In: *Proceedings of the National Academy of Sciences of the United States of America* 47.11, pp. 1744–1750. ISSN: 0027-8424. URL: https://www.ncbi.nlm.nih.gov/pmc/articles/PMC223205/ (visited on 06/08/2022).

Deng, Xiaoxiang et al. (Aug. 21, 2009). "STIM and Orai: Dynamic Intermembrane Coupling to Control Cellular Calcium Signals". In: *The Journal of Biological Chemistry* 284.34, pp. 22501–

22505. ISSN: 0021-9258. DOI: 10.1074/jbc.R109.018655. URL: https://www.ncbi.nlm.nih.gov/pmc/articles/PMC2755655/ (visited on 06/06/2022).

Dickinson, George D. et al. (Nov. 8, 2016). "Hindered cytoplasmic diffusion of inositol trisphosphate restricts its cellular range of action". In: *Science Signaling* 9.453. ISSN: 1945-0877, 1937-9145. DOI: 10.1126/scisignal.aag1625. URL: https://www.science.org/doi/10.1126/scisignal.aag1625 (visited on 06/06/2022).

Diercks, B.-P. et al. (Dec. 18, 2018). "ORAI1, stromal interaction molecules 1/2, and ryanodine receptor type 1 shape sub-second Ca2+ microdomains upon T cell activation". In: *Science signaling* 11.561, eaat0358. ISSN: 1945-0877. DOI: 10.1126/scisignal.aat0358. URL: https://www.ncbi.nlm.nih.gov/pmc/articles/PMC6728084/ (visited on 06/06/2022).

Dobson, Christopher M. (Sept. 1, 1999). "Protein misfolding, evolution and disease". In: *Trends in Biochemical Sciences* 24.9, pp. 329–332. ISSN: 0968-0004. DOI: 10.1016/S0968-0004(99)01445-0. URL: https://www.sciencedirect.com/science/article/pii/S0968000499014450 (visited on 05/17/2022).

Dohle, Wolfgang et al. (May 22, 2019). "A synthetic cyclitol-nucleoside conjugate polyphosphate is a highly potent second messenger mimic". In: *Chemical Science* 10.20. Publisher: The Royal Society of Chemistry, pp. 5382–5390. ISSN: 2041-6539. DOI: 10.1039/C9SC00445A. URL: https://pubs.rsc.org/en/content/articlelanding/2019/sc/c9sc00445a (visited on 03/20/2022).

Dolmetsch, R. E., K. Xu, and R. S. Lewis (Apr. 30, 1998). "Calcium oscillations increase the efficiency and specificity of gene expression". In: *Nature* 392.6679, pp. 933–936. ISSN: 0028-0836. DOI: 10.1038/31960.

Dolphin, Annette C (Oct. 23, 2020). "Functions of Presynaptic Voltage-gated Calcium Channels". In: *Function* 2.1, zqaa027. ISSN: 2633-8823. DOI: 10.1093/function/zqaa027. URL: https://www.ncbi.nlm.nih.gov/pmc/articles/PMC7709543/ (visited on 08/18/2022).

Doyle, D. A. et al. (Apr. 3, 1998). "The structure of the potassium channel: molecular basis of K+ conduction and selectivity". In: *Science (New York, N.Y.)* 280.5360, pp. 69–77. ISSN: 0036-8075. DOI: 10.1126/science.280.5360.69.

Dubochet, J. et al. (1982). "Electron microscopy of frozen water and aqueous solutions". In: *Journal of Microscopy* 128.3. _eprint: https://onlinelibrary.wiley.com/doi/pdf/10.1111/j.1365-2818.1982.tb04625.x, pp. 219–237. ISSN: 1365-2818. DOI: 10.1111/j.1365-2818.1982.

tb04625.x. URL: http://onlinelibrary.wiley.com/doi/abs/10.1111/j.1365-2818.1982.tb04625.x (visited on 06/10/2022).

Dufour, J., I. Arias, and T. Turner (Jan. 31, 1997). "Inositol 1,4,5-Trisphosphate and Calcium Regulate the Calcium Channel Function of the Hepatic Inositol 1,4,5-Trisphosphate Receptor*". In: *Journal of Biological Chemistry* 272.5, pp. 2675–2681. ISSN: 0021-9258. DOI: 10.1074/jbc.272.5.2675. URL: https://www.sciencedirect.com/science/article/pii/S002192581967359X (visited on 01/26/2022).

Duhr, Stefan and Dieter Braun (Apr. 27, 2006a). "Thermophoretic Depletion Follows Boltzmann Distribution". In: *Physical Review Letters* 96.16. ISSN: 0031-9007, 1079-7114. DOI: 10.1103/PhysRevLett.96.168301. URL: https://link.aps.org/doi/10.1103/PhysRevLett.96.168301 (visited on 03/17/2019).

— (Dec. 26, 2006b). "Why molecules move along a temperature gradient". In: *Proceedings of the National Academy of Sciences* 103.52, pp. 19678–19682. ISSN: 0027-8424, 1091-6490. DOI: 10.1073/pnas.0603873103. URL: https://www.pnas.org/content/103/52/19678 (visited on 03/17/2019).

Duncan, R. Scott, Sung-Yong Hwang, and Peter Koulen (Jan. 1, 2007). "Differential inositol 1,4,5-trisphosphate receptor signaling in a neuronal cell line". In: *The International Journal of Biochemistry & Cell Biology* 39.10, pp. 1852–1862. ISSN: 1357-2725. DOI: 10.1016/j.biocel.2007.05.003. URL: https://www.sciencedirect.com/science/article/pii/S135727250700146X (visited on 03/23/2022).

Dupont, Geneviève, Gérald Houart, and Paul De Koninck (Dec. 1, 2003). "Sensitivity of CaM kinase II to the frequency of Ca2+ oscillations: a simple model". In: *Cell Calcium* 34.6, pp. 485–497. ISSN: 0143-4160. DOI: 10.1016/S0143-4160(03)00152-0. URL: https://www.sciencedirect.com/science/article/pii/S0143416003001520 (visited on 06/07/2022).

Elmore, Susan (2007). "Apoptosis: A Review of Programmed Cell Death". In: *Toxicologic pathology* 35.4, pp. 495–516. ISSN: 0192-6233. DOI: 10.1080/01926230701320337. URL: https://www.ncbi.nlm.nih.gov/pmc/articles/PMC2117903/ (visited on 06/08/2022).

Emery, A. H. and H. G. Drickamer (Dec. 1955). "Thermal Diffusion in Polymer Solutions". In: *The Journal of Chemical Physics* 23.12. Publisher: American Institute of Physics, pp. 2252–2257.

ISSN: 0021-9606. DOI: 10.1063/1.1740733. URL: https://aip.scitation.org/doi/abs/10.1063/1.1740733 (visited on 05/12/2022).

Emsley, P. et al. (Apr. 1, 2010). "Features and development of Coot". In: *Acta Crystallographica Section D: Biological Crystallography* 66 (Pt 4), pp. 486–501. ISSN: 0907-4449. DOI: 10.1107/S0907444910007493. URL: https://www.ncbi.nlm.nih.gov/pmc/articles/PMC2852313/ (visited on 04/04/2022).

Endo, Makoto, Minoru Tanaka, and Yasuo Ogawa (Oct. 1970). "Calcium Induced Release of Calcium from the Sarcoplasmic Reticulum of Skinned Skeletal Muscle Fibres". In: *Nature* 228.5266. Number: 5266 Publisher: Nature Publishing Group, pp. 34–36. ISSN: 1476-4687. DOI: 10.1038/228034a0. URL: https://www.nature.com/articles/228034a0 (visited on 05/13/2022).

Estrozi, Leandro F. and Jorge Navaza (Dec. 1, 2010). "Ab initio high-resolution single-particle 3D reconstructions: The symmetry adapted functions way". In: *Journal of Structural Biology* 172.3, pp. 253–260. ISSN: 1047-8477. DOI: 10.1016/j.jsb.2010.06.023. URL: https://www.sciencedirect.com/science/article/pii/S1047847710002017 (visited on 06/11/2022).

Fan, Guizhen, Mariah R. Baker, Lara E. Terry, et al. (May 28, 2022). *Structural dynamics underlying gating and regulation in IP3R channel*. Pages: 2022.05.27.493711 Section: New Results. DOI: 10.1101/2022.05.27.493711. URL: https://www.biorxiv.org/content/10.1101/2022.05.27.493711v1 (visited on 06/29/2022).

Fan, Guizhen, Mariah R. Baker, Zhao Wang, et al. (Dec. 2018). "Cryo-EM reveals ligand induced allostery underlying InsP3R channel gating". In: *Cell Research* 28.12, pp. 1158–1170. ISSN: 1001-0602. DOI: 10.1038/s41422-018-0108-5. URL: https://www.ncbi.nlm.nih.gov/pmc/articles/PMC6274648/ (visited on 06/24/2022).

Fan, Guizhen, Matthew L. Baker, et al. (Nov. 19, 2015). "Gating machinery of InsP3R channels revealed by electron cryomicroscopy". In: *Nature* 527.7578, pp. 336–341. ISSN: 0028-0836. DOI: 10.1038/nature15249. URL: https://www.ncbi.nlm.nih.gov/pmc/articles/PMC4804758/ (visited on 01/15/2019).

Farber, Milton and W. F. Libby (Dec. 1940). "Effect of Gravitational Field on the Thermal Diffusion Separation Method". In: *The Journal of Chemical Physics* 8.12. Publisher: American Institute of Physics, pp. 965–969. ISSN: 0021-9606. DOI: 10.1063/1.1750611. URL: https://aip.scitation.org/doi/10.1063/1.1750611 (visited on 05/11/2022).

Faruqi, A. R. (1998). "Design principles and applications of a cooled CCD camera for electron microscopy". In: *Advances in Experimental Medicine and Biology* 453, pp. 63–72. ISSN: 0065-2598. DOI: 10.1007/978-1-4684-6039-1_8.

Fedrizzi, Laura, Dmitry Lim, and Ernesto Carafoli (2008). "Calcium and signal transduction". In: *Biochemistry and Molecular Biology Education* 36.3. _eprint: https://onlinelibrary.wiley.com/doi/pdf/10.1002/b pp. 175–180. ISSN: 1539-3429. DOI: 10.1002/bmb.20187. URL: https://onlinelibrary.wiley.com/doi/abs/10.1002/bmb.20187 (visited on 08/28/2022).

Fernández, Israel S., Xiao-Chen Bai, Tanweer Hussain, et al. (Nov. 15, 2013). "Molecular architecture of a eukaryotic translational initiation complex". In: *Science (New York, N.Y.)* 342.6160, 10.1126/science.1240585. ISSN: 0036-8075. DOI: 10.1126/science.1240585. URL: https://www.ncbi.nlm.nih.gov/pmc/articles/PMC3836175/ (visited on 06/14/2022).

Fernández, Israel S., Xiao-Chen Bai, Garib Murshudov, et al. (May 8, 2014). "Initiation of Translation by Cricket Paralysis Virus IRES Requires Its Translocation in the Ribosome". In: *Cell* 157.4, pp. 823–831. ISSN: 0092-8674. DOI: 10.1016/j.cell.2014.04.015. URL: https://www.ncbi.nlm.nih.gov/pmc/articles/PMC4017093/ (visited on 06/14/2022).

Fernández-Busnadiego, Rubén, Yasunori Saheki, and Pietro De Camilli (Apr. 21, 2015). "Three-dimensional architecture of extended synaptotagmin-mediated endoplasmic reticulum–plasma membrane contact sites". In: *Proceedings of the National Academy of Sciences* 112.16. ISSN: 0027-8424, 1091-6490. DOI: 10.1073/pnas.1503191112. URL: https://pnas.org/doi/full/10.1073/pnas.1503191112 (visited on 06/06/2022).

Ferris, C D, R L Huganir, and S H Snyder (Mar. 1990). "Calcium flux mediated by purified inositol 1,4,5-trisphosphate receptor in reconstituted lipid vesicles is allosterically regulated by adenine nucleotides." In: *Proceedings of the National Academy of Sciences of the United States of America* 87.6, pp. 2147–2151. ISSN: 0027-8424. URL: https://www.ncbi.nlm.nih.gov/pmc/articles/PMC53643/ (visited on 06/04/2022).

Ferris, C. et al. (Nov. 1989). "Purified inositol 1,4,5-trisphosphate receptor mediates calcium flux in reconstituted lipid vesicles". In: *Nature* 342.6245. Number: 6245 Publisher: Nature Publishing Group, pp. 87–89. ISSN: 1476-4687. DOI: 10.1038/342087a0. URL: https://www.nature.com/articles/342087a0 (visited on 05/13/2022).

Feske, Stefan et al. (May 2006). "A mutation in Orai1 causes immune deficiency by abrogating CRAC channel function". In: *Nature* 441.7090. Number: 7090 Publisher: Nature Publishing Group, pp. 179–185. ISSN: 1476-4687. DOI: 10.1038/nature04702. URL: https://www.nature.com/articles/nature04702 (visited on 05/03/2022).

Finch, E. A., T. J. Turner, and S. M. Goldin (Apr. 19, 1991a). "Calcium as a coagonist of inositol 1,4,5-trisphosphate-induced calcium release". In: *Science (New York, N.Y.)* 252.5004, pp. 443–446. ISSN: 0036-8075. DOI: 10.1126/science.2017683.

— (1991b). "Subsecond kinetics of inositol 1,4,5-trisphosphate-induced calcium release reveal rapid potentiation and subsequent inactivation by calcium". In: *Annals of the New York Academy of Sciences* 635, pp. 400–403. ISSN: 0077-8923. DOI: 10.1111/j.1749-6632.1991.tb36509.x.

Fitzgerald, Daniel J. et al. (Dec. 2006). "Protein complex expression by using multigene baculoviral vectors". In: *Nature Methods* 3.12, pp. 1021–1032. ISSN: 1548-7105. DOI: 10.1038/nmeth983. URL: https://www.nature.com/articles/nmeth983 (visited on 03/06/2019).

Fonseca, P. et al. (Apr. 1, 2003). "Domain organization of the type 1 inositol 1,4,5-trisphosphate receptor as revealed by single-particle analysis". In: *Proceedings of the National Academy of Sciences of the United States of America* 100.7. Publisher: National Academy of Sciences, p. 3936. DOI: 10.1073/pnas.0536251100. URL: https://www.ncbi.nlm.nih.gov/pmc/articles/PMC153026/ (visited on 10/06/2021).

Foskett, J. K. et al. (Apr. 2007). "Inositol Trisphosphate Receptor Ca2+ Release Channels". In: *Physiological reviews* 87.2, pp. 593–658. ISSN: 0031-9333. DOI: 10.1152/physrev.00035.2006. URL: https://www.ncbi.nlm.nih.gov/pmc/articles/PMC2901638/ (visited on 05/17/2022).

Foskett, J. Kevin and Don-On Daniel Mak (2010). "Regulation of IP3R Channel Gating by Ca2+ and Ca2+ Binding Proteins". In: *Current topics in membranes* 66, pp. 235–272. ISSN: 1063-5823. DOI: 10.1016/S1063-5823(10)66011-5. URL: https://www.ncbi.nlm.nih.gov/pmc/articles/PMC6707373/ (visited on 06/03/2022).

Frank, J et al. (Nov. 1, 1991). "Three-dimensional reconstruction of the 70S Escherichia coli ribosome in ice: the distribution of ribosomal RNA." In: *Journal of Cell Biology* 115.3, pp. 597–605. ISSN: 0021-9525. DOI: 10.1083/jcb.115.3.597. URL: https://doi.org/10.1083/jcb.115.3.597 (visited on 06/10/2022).

Frank, Joachim et al. (Jan. 1, 1996). "SPIDER and WEB: Processing and Visualization of Images in 3D Electron Microscopy and Related Fields". In: *Journal of Structural Biology* 116.1, pp. 190–199. ISSN: 1047-8477. DOI: 10.1006/jsbi.1996.0030. URL: https://www.sciencedirect.com/science/article/pii/S1047847796900301 (visited on 06/14/2022).

Franzini-Armstrong, C. (Dec. 1, 1963). "PORES IN THE SARCOPLASMIC RETICULUM". In: *Journal of Cell Biology* 19.3, pp. 637–641. ISSN: 0021-9525. DOI: 10.1083/jcb.19.3.637. URL: https://doi.org/10.1083/jcb.19.3.637 (visited on 05/13/2022).

Franzini-Armstrong, C. and A. O. Jorgensen (1994). "Structure and development of E-C coupling units in skeletal muscle". In: *Annual Review of Physiology* 56, pp. 509–534. ISSN: 0066-4278. DOI: 10.1146/annurev.ph.56.030194.002453.

Freire, Ernesto, Arne Schön, and Adrian Velazquez-Campoy (2009). "Isothermal titration calorimetry: general formalism using binding polynomials". In: *Methods in Enzymology* 455, pp. 127–155. ISSN: 1557-7988. DOI: 10.1016/S0076-6879(08)04205-5.

Freyer, Matthew W. and Edwin A. Lewis (Jan. 1, 2008). "Isothermal Titration Calorimetry: Experimental Design, Data Analysis, and Probing Macromolecule/Ligand Binding and Kinetic Interactions". In: *Methods in Cell Biology*. Vol. 84. Biophysical Tools for Biologists, Volume One: In Vitro Techniques. Academic Press, pp. 79–113. DOI: 10.1016/S0091-679X(07)84004-0. URL: http://www.sciencedirect.com/science/article/pii/S0091679X07840040 (visited on 03/17/2019).

Fritzke, Bernd (1994). "A Growing Neural Gas Network Learns Topologies". In: *Advances in Neural Information Processing Systems*. Vol. 7. MIT Press. URL: https://proceedings.neurips.cc/paper/1994/hash/d56b9fc4b0f1be8871f5e1c40c0067e7-Abstract.html (visited on 06/14/2022).

Fujiyoshi, Y. et al. (Jan. 1, 1980). "A new method for optimal-resolution electron microscopy of radiation-sensitive specimens". In: *Ultramicroscopy* 5.1, pp. 459–468. ISSN: 0304-3991. DOI: 10.1016/0304-3991(80)90046-7. URL: https://www.sciencedirect.com/science/article/pii/0304399180900467 (visited on 06/11/2022).

Fulton, John L. et al. (June 1, 2003). "Understanding the Effects of Concentration on the Solvation Structure of Ca2+ in Aqueous Solution. I: The Perspective on Local Structure from EXAFS and XANES". In: *The Journal of Physical Chemistry A* 107.23. Publisher: American Chemical

Society, pp. 4688–4696. ISSN: 1089-5639. DOI: 10.1021/jp0272264. URL: https://doi.org/10.1021/jp0272264 (visited on 05/18/2022).

Furuichi, Teiichi et al. (Nov. 1989). "Primary structure and functional expression of the inositol 1,4,5-trisphosphate-binding protein P400". In: *Nature* 342.6245. Number: 6245 Publisher: Nature Publishing Group, pp. 32–38. ISSN: 1476-4687. DOI: 10.1038/342032a0. URL: https://www.nature.com/articles/342032a0 (visited on 05/13/2022).

Gafni, Juliette et al. (Sept. 1, 1997). "Xestospongins: Potent Membrane Permeable Blockers of the Inositol 1,4,5-Trisphosphate Receptor". In: *Neuron* 19.3, pp. 723–733. ISSN: 0896-6273. DOI: 10.1016/S0896-6273(00)80384-0. URL: https://www.sciencedirect.com/science/article/pii/S0896627300803840 (visited on 03/21/2022).

Gambardella, Jessica, Angela Lombardi, et al. (Apr. 12, 2020). "Inositol 1,4,5-Trisphosphate Receptors in Human Disease: A Comprehensive Update". In: *Journal of Clinical Medicine* 9.4, p. 1096. ISSN: 2077-0383. DOI: 10.3390/jcm9041096. URL: https://www.ncbi.nlm.nih.gov/pmc/articles/PMC7231134/ (visited on 06/24/2022).

Gambardella, Jessica, Marco B. Morelli, et al. (June 2021). "The discovery and development of IP3 receptor modulators: An update." In: *Expert opinion on drug discovery* 16.6, pp. 709–718. ISSN: 1746-0441. DOI: 10.1080/17460441.2021.1858792. URL: https://www.ncbi.nlm.nih.gov/pmc/articles/PMC8169518/ (visited on 06/21/2022).

Gamper, Nikita and Mark S. Shapiro (July 2003). "Calmodulin Mediates Ca2+-dependent Modulation of M-type K+ Channels". In: *The Journal of General Physiology* 122.1, pp. 17–31. ISSN: 0022-1295. DOI: 10.1085/jgp.200208783. URL: https://www.ncbi.nlm.nih.gov/pmc/articles/PMC2234471/ (visited on 06/07/2022).

Georges, Amédée des et al. (Sept. 22, 2016). "Structural Basis for Gating and Activation of RyR1". In: *Cell* 167.1, 145–157.e17. ISSN: 1097-4172. DOI: 10.1016/j.cell.2016.08.075.

Ghosh, T K et al. (Aug. 15, 1988). "Competitive, reversible, and potent antagonism of inositol 1,4,5-trisphosphate-activated calcium release by heparin." In: *Journal of Biological Chemistry* 263.23, pp. 11075–11079. ISSN: 0021-9258. DOI: 10.1016/S0021-9258(18)37923-7. URL: https://www.sciencedirect.com/science/article/pii/S0021925818379237 (visited on 06/28/2022).

Giglio, M. and A. Vendramini (Nov. 15, 1974). "Thermal lens effect in a binary liquid mixture: A new effect". In: *Applied Physics Letters* 25.10. Publisher: American Institute of Physics, pp. 555–557. ISSN: 0003-6951. DOI: 10.1063/1.1655308. URL: https://aip.scitation.org/doi/10.1063/1.1655308 (visited on 05/11/2022).

Gincel, D, H Zaid, and V Shoshan-Barmatz (Aug. 15, 2001). "Calcium binding and translocation by the voltage-dependent anion channel: a possible regulatory mechanism in mitochondrial function." In: *Biochemical Journal* 358 (Pt 1), pp. 147–155. ISSN: 0264-6021. URL: https://www.ncbi.nlm.nih.gov/pmc/articles/PMC1222042/ (visited on 06/08/2022).

Giordano, Francesca et al. (June 20, 2013). "PI(4,5)P2-Dependent and Ca2+-Regulated ER-PM Interactions Mediated by the Extended Synaptotagmins". In: *Cell* 153.7, pp. 1494–1509. ISSN: 0092-8674. DOI: 10.1016/j.cell.2013.05.026. URL: https://www.sciencedirect.com/science/article/pii/S009286741300593X (visited on 06/06/2022).

Giorgi, Carlotta, Keisuke Ito, et al. (Nov. 26, 2010). "PML Regulates Apoptosis at Endoplasmic Reticulum by Modulating Calcium Release". In: *Science (New York, N.Y.)* 330.6008, pp. 1247–1251. ISSN: 0036-8075. DOI: 10.1126/science.1189157. URL: https://www.ncbi.nlm.nih.gov/pmc/articles/PMC3017677/ (visited on 04/02/2020).

Giorgi, Carlotta, Anna Romagnoli, et al. (Mar. 2008). "Ca2+ signaling, mitochondria and cell death". In: *Current Molecular Medicine* 8.2, pp. 119–130. ISSN: 1566-5240. DOI: 10.2174/156652408783769571.

Glaeser, Robert M. et al. (Apr. 1, 2011). "Precise beam-tilt alignment and collimation are required to minimize the phase error associated with coma in high-resolution cryo-EM". In: *Journal of Structural Biology* 174.1, pp. 1–10. ISSN: 1047-8477. DOI: 10.1016/j.jsb.2010.12.005. URL: https://www.sciencedirect.com/science/article/pii/S1047847710003825 (visited on 06/11/2022).

Gomis-Rüth, F. X., L. F. Kress, and W. Bode (Nov. 1, 1993). "First structure of a snake venom metalloproteinase: a prototype for matrix metalloproteinases/collagenases." In: *The EMBO Journal* 12.11. Publisher: John Wiley & Sons, Ltd, pp. 4151–4157. ISSN: 1460-2075. DOI: 10.1002/j.1460-2075.1993.tb06099.x. URL: http://www.embopress.org/doi/10.1002/j.1460-2075.1993.tb06099.x (visited on 08/15/2022).

Gonen, Tamir et al. (Dec. 1, 2005). "Lipid-protein interactions in double-layered two-dimensional AQP0 crystals". In: *Nature* 438.7068, pp. 633–638. ISSN: 0028-0836. DOI: 10.1038/nature04321. URL: https://www.ncbi.nlm.nih.gov/pmc/articles/PMC1350984/ (visited on 06/10/2022).

Gonzaga-Jauregui, Claudia et al. (Aug. 18, 2015). "Exome sequence analysis suggests genetic burden contributes to phenotypic variability and complex neuropathy". In: *Cell reports* 12.7, pp. 1169–1183. ISSN: 2211-1247. DOI: 10.1016/j.celrep.2015.07.023. URL: https://www.ncbi.nlm.nih.gov/pmc/articles/PMC4545408/ (visited on 04/04/2022).

Gorshkova, I. et al. (Sept. 15, 1995). "Thermodynamics of cyclic nucleotide binding to the cAMP receptor protein and its T127L mutant". In: *The Journal of Biological Chemistry* 270.37, pp. 21679–21683. ISSN: 0021-9258. DOI: 10.1074/jbc.270.37.21679.

Goto, Jun-Ichi et al. (Jan. 2010). "Two novel 2-aminoethyl diphenylborinate (2-APB) analogues differentially activate and inhibit store-operated Ca2+ entry via STIM proteins". In: *Cell calcium* 47.1, pp. 1–10. ISSN: 0143-4160. DOI: 10.1016/j.ceca.2009.10.004. URL: https://www.ncbi.nlm.nih.gov/pmc/articles/PMC2905153/ (visited on 03/23/2022).

Grant, Timothy, Alexis Rohou, and Nikolaus Grigorieff (Mar. 7, 2018). "cisTEM, user-friendly software for single-particle image processing". In: *eLife* 7. Ed. by Edward H Egelman. Publisher: eLife Sciences Publications, Ltd, e35383. ISSN: 2050-084X. DOI: 10.7554/eLife.35383. URL: https://doi.org/10.7554/eLife.35383 (visited on 06/14/2022).

Gregory, R B, G Rychkov, and G J Barritt (Mar. 1, 2001). "Evidence that 2-aminoethyl diphenylborate is a novel inhibitor of store-operated Ca2+ channels in liver cells, and acts through a mechanism which does not involve inositol trisphosphate receptors." In: *Biochemical Journal* 354 (Pt 2), pp. 285–290. ISSN: 0264-6021. URL: https://www.ncbi.nlm.nih.gov/pmc/articles/PMC1221654/ (visited on 03/23/2022).

Grigorieff, Nikolaus (Jan. 2007). "FREALIGN: high-resolution refinement of single particle structures". In: *Journal of Structural Biology* 157.1, pp. 117–125. ISSN: 1047-8477. DOI: 10.1016/j.jsb.2006.05.004.

Groswald, Douglas E. and Paul T. Kelly (1984). "Evidence that a Cerebellum-Enriched, Synaptic Junction Glycoprotein Is Related to Fodrin and Resists Extraction with Triton in a Calcium-Dependent Manner". In: *Journal of Neurochemistry* 42.2. _eprint: https://onlinelibrary.wiley.com/doi/pdf/10.11 4159.1984.tb02711.x, pp. 534–536. ISSN: 1471-4159. DOI: 10.1111/j.1471-4159.1984.

tb02711.x. URL: https://onlinelibrary.wiley.com/doi/abs/10.1111/j.1471-4159.1984.tb02711.x (visited on 05/13/2022).

Grotemeier, Antje et al. (June 1, 2010). "AMPK-independent induction of autophagy by cytosolic Ca2+ increase". In: *Cellular Signalling* 22.6, pp. 914–925. ISSN: 0898-6568. DOI: 10.1016/j.cellsig.2010.01.015. URL: https://www.sciencedirect.com/science/article/pii/S089865681000032X (visited on 06/09/2022).

Gudlur, Aparna et al. (Oct. 31, 2018). "Calcium sensing by the STIM1 ER-luminal domain". In: *Nature Communications* 9.1. Number: 1 Publisher: Nature Publishing Group, p. 4536. ISSN: 2041-1723. DOI: 10.1038/s41467-018-06816-8. URL: http://www.nature.com/articles/s41467-018-06816-8 (visited on 06/06/2022).

Guerrero-Hernandez, Agustin, Adan Dagnino-Acosta, and Alexei Verkhratsky (Aug. 1, 2010). "An intelligent sarco-endoplasmic reticulum Ca2+ store: Release and leak channels have differential access to a concealed Ca2+ pool". In: *Cell Calcium* 48.2, pp. 143–149. ISSN: 0143-4160. DOI: 10.1016/j.ceca.2010.08.001. URL: https://www.sciencedirect.com/science/article/pii/S014341601000117X (visited on 06/06/2022).

Guillemette, G et al. (Jan. 1987). "Intracellular receptors for inositol 1,4,5-trisphosphate in angiotensin II target tissues." In: *Journal of Biological Chemistry* 262.3, pp. 1010–1015. ISSN: 00219258. DOI: 10.1016/S0021-9258(19)75741-X. URL: https://linkinghub.elsevier.com/retrieve/pii/S002192581975741X (visited on 05/04/2022).

Guillemette, G. et al. (Mar. 1, 1989). "Differential effects of heparin on inositol 1,4,5-trisphosphate binding, metabolism, and calcium release activity in the bovine adrenal cortex." In: *Molecular Pharmacology* 35.3. Publisher: American Society for Pharmacology and Experimental Therapeutics, pp. 339–344. ISSN: 0026-895X, 1521-0111. URL: https://molpharm.aspetjournals.org/content/35/3/339 (visited on 03/21/2022).

Guo, H. et al. (Sept. 1, 2020). "Electron-event representation data enable efficient cryoEM file storage with full preservation of spatial and temporal resolution". In: *IUCrJ* 7.5. Number: 5 Publisher: International Union of Crystallography, pp. 860–869. ISSN: 2052-2525. DOI: 10.1107/S205225252000929X. URL: https://journals.iucr.org/m/issues/2020/05/00/fq5014/ (visited on 06/14/2022).

Guo, Wenting et al. (Nov. 13, 2020). "The central domain of cardiac ryanodine receptor governs channel activation, regulation, and stability". In: *The Journal of Biological Chemistry* 295.46, pp. 15622–15635. ISSN: 0021-9258. DOI: 10.1074/jbc.RA120.013512. URL: https://www.ncbi.nlm.nih.gov/pmc/articles/PMC7667974/ (visited on 04/04/2022).

Guse, A., D. Gil Montoya, and B. P. Diercks (Jan. 16, 2021). "Mechanisms and functions of calcium microdomains produced by ORAI channels, d-myo-inositol 1,4,5-trisphosphate receptors, or ryanodine receptors". In: *Pharmacology & Therapeutics*, p. 107804. ISSN: 1879-016X. DOI: 10.1016/j.pharmthera.2021.107804.

Gustchina, Elena et al. (Nov. 7, 2013). "Complexes of Neutralizing and Non-Neutralizing Affinity Matured Fabs with a Mimetic of the Internal Trimeric Coiled-Coil of HIV-1 gp41". In: *PLOS ONE* 8.11. Publisher: Public Library of Science, e78187. ISSN: 1932-6203. DOI: 10.1371/journal.pone.0078187. URL: https://journals.plos.org/plosone/article?id=10.1371/journal.pone.0078187 (visited on 05/10/2022).

Hagar, Robert E. et al. (Nov. 5, 1998). "Type III InsP3 receptor channel stays open in the presence of increased calcium". In: *Nature* 396.6706, pp. 81–84. ISSN: 0028-0836. DOI: 10.1038/23954. URL: https://www.ncbi.nlm.nih.gov/pmc/articles/PMC2825878/ (visited on 06/03/2022).

Hagemans, Dominique et al. (2015). "A script to highlight hydrophobicity and charge on protein surfaces". In: *Frontiers in Molecular Biosciences* 2, p. 56. ISSN: 2296-889X. DOI: 10.3389/fmolb.2015.00056.

Hamada, Kozo and Katsuhiko Mikoshiba (Feb. 10, 2020). "IP3 Receptor Plasticity Underlying Diverse Functions". In: *Annual Review of Physiology* 82.1. Publisher: Annual Reviews, pp. 151–176. ISSN: 0066-4278. DOI: 10.1146/annurev-physiol-021119-034433. URL: https://www.annualreviews.org/doi/10.1146/annurev-physiol-021119-034433 (visited on 02/04/2021).

Hamada, Kozo, Tomoko Miyata, et al. (June 14, 2002). "Two-state conformational changes in inositol 1,4,5-trisphosphate receptor regulated by calcium". In: *The Journal of Biological Chemistry* 277.24, pp. 21115–21118. ISSN: 0021-9258. DOI: 10.1074/jbc.C200244200.

Hamada, Kozo, Hideyuki Miyatake, et al. (May 2, 2017). "IP3-mediated gating mechanism of the IP3 receptor revealed by mutagenesis and X-ray crystallography". In: *Proceedings of the National Academy of Sciences of the United States of America* 114.18, pp. 4661–4666. ISSN:

0027-8424. DOI: 10.1073/pnas.1701420114. URL: https://www.ncbi.nlm.nih.gov/pmc/articles/PMC5422816/ (visited on 04/04/2022).

Hamada, Kozo, Akiko Terauchi, and Katsuhiko Mikoshiba (Dec. 26, 2003). "Three-dimensional rearrangements within inositol 1,4,5-trisphosphate receptor by calcium". In: *The Journal of Biological Chemistry* 278.52, pp. 52881–52889. ISSN: 0021-9258. DOI: 10.1074/jbc.M309743200.

Hamilton, Susan L. (Sept. 1, 2005). "Ryanodine receptors". In: *Cell Calcium*. Frontiers in calcium signalling 38.3, pp. 253–260. ISSN: 0143-4160. DOI: 10.1016/j.ceca.2005.06.037. URL: https://www.sciencedirect.com/science/article/pii/S0143416005001168 (visited on 06/06/2022).

Harnick, David J. et al. (Feb. 10, 1995). "The Human Type 1 Inositol 1,4,5-Trisphosphate Receptor from T Lymphocytes STRUCTURE, LOCALIZATION, AND TYROSINE PHOSPHORYLATION". In: *Journal of Biological Chemistry* 270.6, pp. 2833–2840. ISSN: 0021-9258, 1083-351X. DOI: 10.1074/jbc.270.6.2833. URL: http://www.jbc.org/content/270/6/2833 (visited on 01/15/2019).

Hasan, G. and M. Rosbash (Dec. 1992). "Drosophila homologs of two mammalian intracellular Ca(2+)-release channels: identification and expression patterns of the inositol 1,4,5-triphosphate and the ryanodine receptor genes". In: *Development (Cambridge, England)* 116.4, pp. 967–975. ISSN: 0950-1991. DOI: 10.1242/dev.116.4.967.

Hauser, Carl J. et al. (2001). "PAF-mediated Ca2+ influx in human neutrophils occurs via store-operated mechanisms". In: *Journal of Leukocyte Biology* 69.1. _eprint: https://onlinelibrary.wiley.com/doi/pdf/1 pp. 63–68. ISSN: 1938-3673. DOI: 10.1189/jlb.69.1.63. URL: https://onlinelibrary.wiley.com/doi/abs/10.1189/jlb.69.1.63 (visited on 03/23/2022).

Hayashi, Teruo and Tsung-Ping Su (Nov. 2, 2007). "Sigma-1 receptor chaperones at the ER-mitochondrion interface regulate Ca(2+) signaling and cell survival". In: *Cell* 131.3, pp. 596–610. ISSN: 0092-8674. DOI: 10.1016/j.cell.2007.08.036.

He, Bin, Nan Lu, and Zheng Zhou (Dec. 2009). "Cellular and Nuclear Degradation during Apoptosis". In: *Current opinion in cell biology* 21.6, pp. 900–912. ISSN: 0955-0674. DOI: 10.1016/j.ceb.2009.08.008. URL: https://www.ncbi.nlm.nih.gov/pmc/articles/PMC2787732/ (visited on 06/08/2022).

Heel, M. van et al. (Feb. 1996). "A new generation of the IMAGIC image processing system". In: *Journal of Structural Biology* 116.1, pp. 17–24. ISSN: 1047-8477. DOI: 10.1006/jsbi.1996.0004.

Henderson, R., J. M. Baldwin, et al. (June 20, 1990). "Model for the structure of bacteriorhodopsin based on high-resolution electron cryo-microscopy". In: *Journal of Molecular Biology* 213.4, pp. 899–929. ISSN: 0022-2836. DOI: 10.1016/S0022-2836(05)80271-2.

Henderson, R., A. Sali, et al. (Feb. 8, 2012). "Outcome of the First Electron Microscopy Validation Task Force Meeting". In: *Structure(London, England:1993)* 20-330.2, pp. 205–214. ISSN: 0969-2126. DOI: 10.1016/j.str.2011.12.014. URL: https://www.ncbi.nlm.nih.gov/pmc/articles/PMC3328769/ (visited on 05/17/2022).

Herndon, Robert M. (July 1, 1963). "THE FINE STRUCTURE OF THE PURKINJE CELL". In: *The Journal of Cell Biology* 18.1, pp. 167–180. ISSN: 0021-9525. URL: https://www.ncbi.nlm.nih.gov/pmc/articles/PMC2106278/ (visited on 05/17/2022).

Hirota, Junji et al. (Aug. 11, 1995). "Kinetics of Calcium Release by Immunoaffinity-purified Inositol 1,4,5-Trisphosphate Receptor in Reconstituted Lipid Vesicles *". In: *Journal of Biological Chemistry* 270.32, pp. 19046–19051. ISSN: 0021-9258. DOI: 10.1074/jbc.270.32.19046. URL: https://www.sciencedirect.com/science/article/pii/S002192581851944X (visited on 06/03/2022).

Hisatsune, Chihiro and Katsuhiko Mikoshiba (2017). "IP3 receptor mutations and brain diseases in human and rodents". In: *Journal of Neurochemistry* 141.6. _eprint: https://onlinelibrary.wiley.com/doi/pdf/10.1 pp. 790–807. ISSN: 1471-4159. DOI: 10.1111/jnc.13991. URL: https://onlinelibrary.wiley.com/doi/abs/10.1111/jnc.13991 (visited on 04/04/2022).

Hisatsune, Chihiro, Keiko Yasumatsu, et al. (Dec. 21, 2007). "Abnormal taste perception in mice lacking the type 3 inositol 1,4,5-trisphosphate receptor". In: *The Journal of Biological Chemistry* 282.51, pp. 37225–37231. ISSN: 0021-9258. DOI: 10.1074/jbc.M705641200.

Hogan, Patrick G (Oct. 1, 2015). "The STIM1–ORAI1 microdomain". In: *Cell Calcium*. Cell Signalling at Membrane Contact Sites 58.4, pp. 357–367. ISSN: 0143-4160. DOI: 10.1016/j.ceca.2015.07.001. URL: https://www.sciencedirect.com/science/article/pii/S0143416015001177 (visited on 06/06/2022).

Horbowicz, M., P. Brenac, and R. L. Obendorf (May 1998). "Fagopyritol B1, O-alpha-D-galactopyranosyl-(1–¿2)-D-chiro-inositol, a galactosyl cyclitol in maturing buckwheat seeds associated with desiccation tolerance". In: *Planta* 205.1, pp. 1–11. ISSN: 0032-0935. DOI: 10.1007/s004250050290.

Hou, Xiaowei et al. (Dec. 7, 2012). "Crystal structure of the calcium release-activated calcium channel Orai". In: *Science (New York, N.Y.)* 338.6112, pp. 1308–1313. ISSN: 0036-8075. DOI: 10.1126/science.1228757. URL: https://www.ncbi.nlm.nih.gov/pmc/articles/PMC3695727/ (visited on 06/06/2022).

Hoye, Thomas R., Jeffrey T. North, and Letitia J. Yao (Mar. 1, 1994). "A Total Synthesis of (+)-Xestospongin A/(+)-Araguspongine D". In: *Journal of the American Chemical Society* 116.6. Publisher: American Chemical Society, pp. 2617–2618. ISSN: 0002-7863. DOI: 10.1021/ja00085a051. URL: https://doi.org/10.1021/ja00085a051 (visited on 03/21/2022).

Høyer-Hansen, Maria et al. (Jan. 26, 2007). "Control of macroautophagy by calcium, calmodulin-dependent kinase kinase-beta, and Bcl-2". In: *Molecular Cell* 25.2, pp. 193–205. ISSN: 1097-2765. DOI: 10.1016/j.molcel.2006.12.009.

Iino, M (June 1, 1990). "Biphasic Ca2+ dependence of inositol 1,4,5-trisphosphate-induced Ca release in smooth muscle cells of the guinea pig taenia caeci." In: *Journal of General Physiology* 95.6, pp. 1103–1122. ISSN: 0022-1295. DOI: 10.1085/jgp.95.6.1103. URL: https://doi.org/10.1085/jgp.95.6.1103 (visited on 06/04/2022).

Irvine, R. F. (Apr. 9, 1990). "'Quanta' Ca2+ release and the control of Ca2+ entry by inositol phosphates - a possible mechanism". In: *FEBS Letters* 263.1, pp. 5–9. ISSN: 0014-5793. DOI: 10.1016/0014-5793(90)80692-C. URL: http://www.sciencedirect.com/science/article/pii/001457939080692C (visited on 04/01/2020).

Ivanova, Hristina et al. (Oct. 1, 2014). "Inositol 1,4,5-trisphosphate receptor-isoform diversity in cell death and survival". In: *Biochimica et Biophysica Acta (BBA) - Molecular Cell Research*. Calcium Signaling in Health and Disease 1843.10, pp. 2164–2183. ISSN: 0167-4889. DOI: 10.1016/j.bbamcr.2014.03.007. URL: http://www.sciencedirect.com/science/article/pii/S0167488914000913 (visited on 01/15/2019).

Iwai, Miwako, Takayuki Michikawa, et al. (Apr. 27, 2007). "Molecular Basis of the Isoform-specific Ligand-binding Affinity of Inositol 1,4,5-Trisphosphate Receptors". In: *Journal of Biological*

Chemistry 282.17, pp. 12755–12764. ISSN: 0021-9258, 1083-351X. DOI: 10.1074/jbc.M609833200. URL: http://www.jbc.org/content/282/17/12755 (visited on 02/12/2019).

Iwai, Miwako, Yoko Tateishi, et al. (Mar. 18, 2005). "Molecular cloning of mouse type 2 and type 3 inositol 1,4,5-trisphosphate receptors and identification of a novel type 2 receptor splice variant". In: *The Journal of Biological Chemistry* 280.11, pp. 10305–10317. ISSN: 0021-9258. DOI: 10.1074/jbc.M413824200.

Iwasaki, H. et al. (2001). "2-Aminoethoxydiphenyl borate (2-APB) inhibits capacitative calcium entry independently of the function of inositol 1,4,5-trisphosphate receptors". In: *Receptors & Channels* 7.6, pp. 429–439. ISSN: 1060-6823.

Jayaraman, T. et al. (June 7, 1996). "Regulation of the inositol 1,4,5-trisphosphate receptor by tyrosine phosphorylation". In: *Science (New York, N.Y.)* 272.5267, pp. 1492–1494. ISSN: 0036-8075. DOI: 10.1126/science.272.5267.1492.

Jenkins, D. J. and B. V. Potter (June 21, 1996). "A Ca(2+)-mobilising carbohydrate-based polyphosphate: synthesis of 2-hydroxyethyl alpha-D-glucopyranoside 2',3,4-trisphosphate". In: *Carbohydrate Research* 287.2, pp. 169–182. ISSN: 0008-6215. DOI: 10.1016/0008-6215(96)00078-x.

Jerabek-Willemsen, Moran, Timon André, et al. (Dec. 2014). "MicroScale Thermophoresis: Interaction analysis and beyond". In: *Journal of Molecular Structure* 1077, pp. 101–113. ISSN: 00222860. DOI: 10.1016/j.molstruc.2014.03.009. URL: https://linkinghub.elsevier.com/retrieve/pii/S0022286014002750 (visited on 03/03/2019).

Jerabek-Willemsen, Moran, Chistoph J. Wienken, et al. (Aug. 2011). "Molecular Interaction Studies Using Microscale Thermophoresis". In: *Assay and Drug Development Technologies* 9.4, pp. 342–353. ISSN: 1540-658X. DOI: 10.1089/adt.2011.0380. URL: https://www.ncbi.nlm.nih.gov/pmc/articles/PMC3148787/ (visited on 05/12/2022).

Jiang, Qiu-Xing et al. (July 15, 2002). "Three-dimensional structure of the type 1 inositol 1,4,5-trisphosphate receptor at 24 Å resolution". In: *The EMBO Journal* 21.14, pp. 3575–3581. ISSN: 0261-4189. DOI: 10.1093/emboj/cdf380. URL: https://www.ncbi.nlm.nih.gov/pmc/articles/PMC126125/ (visited on 10/06/2021).

Jiang, Youxing et al. (May 30, 2002a). "Crystal structure and mechanism of a calcium-gated potassium channel". In: *Nature* 417.6888, pp. 515–522. ISSN: 0028-0836. DOI: 10.1038/417515a.

Jiang, Youxing et al. (May 30, 2002b). "The open pore conformation of potassium channels". In: *Nature* 417.6888, pp. 523–526. ISSN: 0028-0836. DOI: 10.1038/417523a.

Johnson, Michael L. (2008). "Nonlinear least-squares fitting methods". In: *Methods in Cell Biology* 84, pp. 781–805. ISSN: 0091-679X. DOI: 10.1016/S0091-679X(07)84024-6.

Joseph, S K, S Pierson, and S Samanta (May 1, 1995). "Trypsin digestion of the inositol trisphosphate receptor: implications for the conformation and domain organization of the protein." In: *Biochemical Journal* 307 (Pt 3), pp. 859–865. ISSN: 0264-6021. URL: https://www.ncbi.nlm.nih.gov/pmc/articles/PMC1136727/ (visited on 05/18/2022).

Jung, D. W., K. Baysal, and G. P. Brierley (Jan. 13, 1995). "The sodium-calcium antiport of heart mitochondria is not electroneutral". In: *The Journal of Biological Chemistry* 270.2, pp. 672–678. ISSN: 0021-9258. DOI: 10.1074/jbc.270.2.672.

Kalinina, Juliya et al. (Jan. 11, 2012). "The alternatively spliced acid box region plays a key role in FGF receptor autoinhibition". In: *Structure (London, England: 1993)* 20.1, pp. 77–88. ISSN: 1878-4186. DOI: 10.1016/j.str.2011.10.022.

Kang, Sang Soo et al. (Feb. 1, 2010). "Caffeine-mediated inhibition of calcium release channel inositol 1,4,5-trisphosphate receptor subtype 3 blocks glioblastoma invasion and extends survival". In: *Cancer Research* 70.3, pp. 1173–1183. ISSN: 1538-7445. DOI: 10.1158/0008-5472.CAN-09-2886.

Katayama, E et al. (Sept. 16, 1996). "Native structure and arrangement of inositol-1,4,5-trisphosphate receptor molecules in bovine cerebellar Purkinje cells as studied by quick-freeze deep-etch electron microscopy." In: *The EMBO Journal* 15.18, pp. 4844–4851. ISSN: 0261-4189. URL: https://www.ncbi.nlm.nih.gov/pmc/articles/PMC452222/ (visited on 05/17/2022).

Kaul, Sunil C., Custer C. Deocaris, and Renu Wadhwa (Apr. 2007). "Three faces of mortalin: a housekeeper, guardian and killer". In: *Experimental Gerontology* 42.4, pp. 263–274. ISSN: 0531-5565. DOI: 10.1016/j.exger.2006.10.020.

Kawate, Toshimitsu and Eric Gouaux (Apr. 1, 2006). "Fluorescence-Detection Size-Exclusion Chromatography for Precrystallization Screening of Integral Membrane Proteins". In: *Structure* 14.4, pp. 673–681. ISSN: 0969-2126. DOI: 10.1016/j.str.2006.01.013. URL: https://www.sciencedirect.com/science/article/pii/S0969212606001092 (visited on 08/19/2022).

Kempers, L. J. T. M. (Oct. 8, 2001). "A comprehensive thermodynamic theory of the Soret effect in a multicomponent gas, liquid, or solid". In: *The Journal of Chemical Physics* 115.14, pp. 6330–6341. ISSN: 0021-9606, 1089-7690. DOI: 10.1063/1.1398315. URL: http://aip.scitation.org/doi/10.1063/1.1398315 (visited on 06/14/2022).

Kerkhofs, Martijn et al. (Nov. 1, 2018). "Pathophysiological consequences of isoform-specific IP3 receptor mutations". In: *Biochimica et Biophysica Acta (BBA) - Molecular Cell Research*. Calcium signaling in health, disease and therapy 1865.11, pp. 1707–1717. ISSN: 0167-4889. DOI: 10.1016/j.bbamcr.2018.06.004. URL: https://www.sciencedirect.com/science/article/pii/S0167488918301320 (visited on 04/04/2022).

Khan, M. Tariq and Suresh K. Joseph (May 28, 2010). "Role of Inositol Trisphosphate Receptors in Autophagy in DT40 Cells". In: *The Journal of Biological Chemistry* 285.22, pp. 16912–16920. ISSN: 0021-9258. DOI: 10.1074/jbc.M110.114207. URL: https://www.ncbi.nlm.nih.gov/pmc/articles/PMC2878024/ (visited on 06/09/2022).

Kim, Bongju and Satoshi Matsuoka (Mar. 15, 2008). "Cytoplasmic Na+-dependent modulation of mitochondrial Ca2+ via electrogenic mitochondrial Na+–Ca2+ exchange". In: *The Journal of Physiology* 586 (Pt 6), pp. 1683–1697. ISSN: 0022-3751. DOI: 10.1113/jphysiol.2007.148726. URL: https://www.ncbi.nlm.nih.gov/pmc/articles/PMC2375703/ (visited on 06/08/2022).

Kimanius, Dari, Liyi Dong, et al. (Dec. 16, 2021). "New tools for automated cryo-EM single-particle analysis in RELION-4.0". In: *Biochemical Journal* 478.24, pp. 4169–4185. ISSN: 0264-6021. DOI: 10.1042/BCJ20210708. URL: https://doi.org/10.1042/BCJ20210708 (visited on 06/14/2022).

Kimanius, Dari, Björn O Forsberg, et al. (Nov. 15, 2016). "Accelerated cryo-EM structure determination with parallelisation using GPUs in RELION-2". In: *eLife* 5. Ed. by Sriram Subramaniam. Publisher: eLife Sciences Publications, Ltd, e18722. ISSN: 2050-084X. DOI: 10.7554/eLife.18722. URL: https://doi.org/10.7554/eLife.18722 (visited on 06/14/2022).

Kirberger, Michael and Jenny J. Yang (2013). "Calcium-Binding Protein Site Types". In: *Encyclopedia of Metalloproteins*. Ed. by Robert H. Kretsinger, Vladimir N. Uversky, and Eugene A. Permyakov. New York, NY: Springer, pp. 511–521. ISBN: 978-1-4614-1533-6. DOI: 10.1007/978-1-4614-1533-6_35. URL: https://doi.org/10.1007/978-1-4614-1533-6_35 (visited on 08/15/2022).

Klionsky, Daniel J. (Nov. 2007). "Autophagy: from phenomenology to molecular understanding in less than a decade". In: *Nature Reviews Molecular Cell Biology* 8.11. Number: 11 Publisher: Nature Publishing Group, pp. 931–937. ISSN: 1471-0080. DOI: 10.1038/nrm2245. URL: http://www.nature.com/articles/nrm2245 (visited on 06/09/2022).

Kobayashi, Motomasa, Kazuyoshi Kawazoe, and Isao Kitagawa (1989). "Araguspongines B, C, D, E, F, G, H, and J, New Vasodilative Bis-1-Oxaquinolizidine Alkaloids from an Okinawan Marine Sponge, Xestospongia Sp." In: *Chemical & Pharmaceutical Bulletin* 37.6, pp. 1676–1678. DOI: 10.1248/cpb.37.1676.

Köhler, Werner and Konstantin I. Morozov (July 1, 2016). "The Soret Effect in Liquid Mixtures – A Review". In: *Journal of Non-Equilibrium Thermodynamics* 41.3. Publisher: De Gruyter, pp. 151–197. ISSN: 1437-4358. DOI: 10.1515/jnet-2016-0024. URL: https://www.degruyter.com/document/doi/10.1515/jnet-2016-0024/html?lang=en (visited on 05/11/2022).

Kohout, Susy C. et al. (Sept. 24, 2002). "C2 Domains of Protein Kinase C Isoforms , , and : Activation Parameters and Calcium Stoichiometries of the Membrane-Bound State". In: *Biochemistry* 41.38, pp. 11411–11424. ISSN: 0006-2960. URL: https://www.ncbi.nlm.nih.gov/pmc/articles/PMC3640336/ (visited on 08/15/2022).

Korte, F. Steven et al. (Oct. 1, 2012). "Enhanced Ca2+ binding of cardiac troponin reduces sarcomere length dependence of contractile activation independently of strong crossbridges". In: *American Journal of Physiology - Heart and Circulatory Physiology* 303.7, H863–H870. ISSN: 0363-6135. DOI: 10.1152/ajpheart.00395.2012. URL: https://www.ncbi.nlm.nih.gov/pmc/articles/PMC3469702/ (visited on 06/06/2022).

Kretsinger, R. H. and C. E. Nockolds (May 10, 1973). "Carp muscle calcium-binding protein. II. Structure determination and general description". In: *The Journal of Biological Chemistry* 248.9, pp. 3313–3326. ISSN: 0021-9258.

Krinke, O. et al. (Dec. 6, 2006). "Inositol trisphosphate receptor in higher plants: is it real?" In: *Journal of Experimental Botany* 58.3, pp. 361–376. ISSN: 0022-0957, 1460-2431. DOI: 10.1093/jxb/erl220. URL: https://academic.oup.com/jxb/article-lookup/doi/10.1093/jxb/erl220 (visited on 01/10/2022).

Kroemer, Guido, Lorenzo Galluzzi, and Catherine Brenner (Jan. 2007). "Mitochondrial membrane permeabilization in cell death". In: *Physiological Reviews* 87.1, pp. 99–163. ISSN: 0031-9333. DOI: 10.1152/physrev.00013.2006.

Kroemer, Guido and Beth Levine (Dec. 2008). "Autophagic cell death: the story of a misnomer". In: *Nature Reviews Molecular Cell Biology* 9.12. Number: 12 Publisher: Nature Publishing Group, pp. 1004–1010. ISSN: 1471-0080. DOI: 10.1038/nrm2529. URL: http://www.nature.com/articles/nrm2529 (visited on 06/09/2022).

Kuchay, Shafi et al. (June 2017). "PTEN counteracts FBXL2 to promote IP3R3- and Ca2+-mediated apoptosis limiting tumour growth". In: *Nature* 546.7659. Number: 7659 Publisher: Nature Publishing Group, pp. 554–558. ISSN: 1476-4687. DOI: 10.1038/nature22965. URL: http://www.nature.com/articles/nature22965 (visited on 06/16/2022).

Kucukelbir, Alp, Fred J. Sigworth, and Hemant D. Tagare (Jan. 2014). "Quantifying the local resolution of cryo-EM density maps". In: *Nature Methods* 11.1, pp. 63–65. ISSN: 1548-7105. DOI: 10.1038/nmeth.2727. URL: http://www.nature.com/articles/nmeth.2727 (visited on 01/15/2019).

Kukkonen, J. P., P. -E. Lund, and K. E. O. Åkerman (Aug. 1, 2001). "2-aminoethoxydiphenyl borate reveals heterogeneity in receptor-activated Ca2+discharge and store-operated Ca2+influx". In: *Cell Calcium* 30.2, pp. 117–129. ISSN: 0143-4160. DOI: 10.1054/ceca.2001.0219. URL: https://www.sciencedirect.com/science/article/pii/S0143416001902192 (visited on 03/23/2022).

Kuo, Anling et al. (June 20, 2003). "Crystal structure of the potassium channel KirBac1.1 in the closed state". In: *Science (New York, N.Y.)* 300.5627, pp. 1922–1926. ISSN: 1095-9203. DOI: 10.1126/science.1085028.

Lam, Andy K. M. and Antony Galione (Nov. 1, 2013). "The endoplasmic reticulum and junctional membrane communication during calcium signaling". In: *Biochimica et Biophysica Acta (BBA) - Molecular Cell Research*. Functional and structural diversity of the endoplasmic reticulum 1833.11, pp. 2542–2559. ISSN: 0167-4889. DOI: 10.1016/j.bbamcr.2013.06.004. URL: https://www.sciencedirect.com/science/article/pii/S0167488913002279 (visited on 06/06/2022).

Le, Vu H. et al. (Mar. 15, 2013). "Modeling complex equilibria in isothermal titration calorimetry experiments: Thermodynamic parameters estimation for a three-binding-site model". In: *Analytical Biochemistry* 434.2, pp. 233–241. ISSN: 0003-2697. DOI: 10.1016/j.ab.2012.11.030. URL: https://www.sciencedirect.com/science/article/pii/S0003269712006239 (visited on 05/10/2022).

Li, W. et al. (Apr. 30, 1998). "Cell-permeant caged InsP3 ester shows that Ca2+ spike frequency can optimize gene expression". In: *Nature* 392.6679, pp. 936–941. ISSN: 0028-0836. DOI: 10.1038/31965.

Li, Zhongyan et al. (May 21, 2019). "Self-binding peptides: Binding-upon-folding versus folding-upon-binding". In: *Journal of Theoretical Biology* 469, pp. 25–34. ISSN: 0022-5193. DOI: 10.1016/j.jtbi.2019.02.014. URL: http://www.sciencedirect.com/science/article/pii/S0022519319300839 (visited on 04/23/2019).

Lin, Chun-Chi, Kyuwon Baek, and Zhe Lu (Sept. 4, 2011). "Apo and InsP3-bound crystal structures of the ligand-binding domain of an InsP3 receptor". In: *Nature structural & molecular biology* 18.10, pp. 1172–1174. ISSN: 1545-9993. DOI: 10.1038/nsmb.2112. URL: https://www.ncbi.nlm.nih.gov/pmc/articles/PMC3242432/ (visited on 06/24/2022).

Lin, L. N. et al. (Sept. 14, 1993). "Calorimetric studies of the binding of ferric ions to human serum transferrin". In: *Biochemistry* 32.36, pp. 9398–9406. ISSN: 0006-2960. DOI: 10.1021/bi00087a019.

Liou, Jen et al. (July 12, 2005). "STIM Is a Ca2+ Sensor Essential for Ca2+-Store-Depletion-Triggered Ca2+ Influx". In: *Current biology : CB* 15.13, pp. 1235–1241. ISSN: 0960-9822. DOI: 10.1016/j.cub.2005.05.055. URL: https://www.ncbi.nlm.nih.gov/pmc/articles/PMC3186072/ (visited on 05/03/2022).

Liu, Hongrong et al. (Aug. 27, 2010). "Atomic structure of human adenovirus by cryoEM reveals interactions among protein networks". In: *Science (New York, N.Y.)* 329.5995, pp. 1038–1043. ISSN: 0036-8075. DOI: 10.1126/science.1187433. URL: https://www.ncbi.nlm.nih.gov/pmc/articles/PMC3412078/ (visited on 06/11/2022).

Lodish, H.F., N Kong, and L Wikström (June 1992). "Calcium is required for folding of newly made subunits of the asialoglycoprotein receptor within the endoplasmic reticulum." In: *Journal of Biological Chemistry* 267.18, pp. 12753–12760. ISSN: 00219258. DOI: 10.1016/S0021-9258(18)

42340-X. URL: https://linkinghub.elsevier.com/retrieve/pii/S002192581842340X (visited on 06/06/2022).

Long, Stephen B., Ernest B. Campbell, and Roderick Mackinnon (Aug. 5, 2005). "Crystal structure of a mammalian voltage-dependent Shaker family K+ channel". In: *Science (New York, N.Y.)* 309.5736, pp. 897–903. ISSN: 1095-9203. DOI: 10.1126/science.1116269.

Longsworth, L. G. (Nov. 1, 1957). "The Temperature Dependence of the Soret Coefficient of Aqueous Potassium Chloride". In: *The Journal of Physical Chemistry* 61.11. Publisher: American Chemical Society, pp. 1557–1562. ISSN: 0022-3654. DOI: 10.1021/j150557a023. URL: https://doi.org/10.1021/j150557a023 (visited on 05/11/2022).

Ludtke, S. et al. (Aug. 10, 2011). "Flexible Architecture of IP3R1 by Cryo-EM". In: *Structure (London, England : 1993)* 19.8, pp. 1192–1199. ISSN: 0969-2126. DOI: 10.1016/j.str.2011.05.003. URL: https://www.ncbi.nlm.nih.gov/pmc/articles/PMC3154621/ (visited on 04/29/2021).

Ludtke, S. J., P. R. Baldwin, and W. Chiu (Dec. 1, 1999). "EMAN: semiautomated software for high-resolution single-particle reconstructions". In: *Journal of Structural Biology* 128.1, pp. 82–97. ISSN: 1047-8477. DOI: 10.1006/jsbi.1999.4174.

Ludtke, Steven J. et al. (Aug. 2005). "The pore structure of the closed RyR1 channel". In: *Structure (London, England: 1993)* 13.8, pp. 1203–1211. ISSN: 0969-2126. DOI: 10.1016/j.str.2005.06.005.

Ludwig, C. (1856). *Diffusion zwischen ungleich erwärmten Orten gleich zusammengesetzter Lösungen.* Publisher: Aus der K.K. Hof- und Staatsdruckerei.

Ma, Ruifang et al. (Nov. 2020). "Structural basis for diamide modulation of ryanodine receptor". In: *Nature Chemical Biology* 16.11. Number: 11 Publisher: Nature Publishing Group, pp. 1246–1254. ISSN: 1552-4469. DOI: 10.1038/s41589-020-0627-5. URL: https://www.nature.com/articles/s41589-020-0627-5 (visited on 04/04/2022).

Maeda, N, T Kawasaki, et al. (Jan. 1991). "Structural and functional characterization of inositol 1,4,5-trisphosphate receptor channel from mouse cerebellum." In: *Journal of Biological Chemistry* 266.2, pp. 1109–1116. ISSN: 00219258. DOI: 10.1016/S0021-9258(17)35289-4. URL: https://linkinghub.elsevier.com/retrieve/pii/S0021925817352894 (visited on 05/13/2022).

Maeda, N, M Niinobe, and K Mikoshiba (Jan. 1990). "A cerebellar Purkinje cell marker P400 protein is an inositol 1,4,5-trisphosphate (InsP3) receptor protein. Purification and characterization of InsP3 receptor complex." In: *The EMBO Journal* 9.1, pp. 61–67. ISSN: 0261-4189. URL: https://www.ncbi.nlm.nih.gov/pmc/articles/PMC551630/ (visited on 05/17/2022).

Maeda, N. et al. (Dec. 1988). "Purification and characterization of P400 protein, a glycoprotein characteristic of Purkinje cell, from mouse cerebellum". In: *Journal of Neurochemistry* 51.6, pp. 1724–1730. ISSN: 0022-3042. DOI: 10.1111/j.1471-4159.1988.tb01151.x.

Maeda, Nobuaki et al. (May 1, 1989). "Developmental expression and intracellular location of P400 protein characteristic of Purkinje cells in the mouse cerebellum". In: *Developmental Biology* 133.1, pp. 67–76. ISSN: 0012-1606. DOI: 10.1016/0012-1606(89)90297-2. URL: https://www.sciencedirect.com/science/article/pii/0012160689902972 (visited on 05/13/2022).

Maekawa, Sadamichi et al. (June 22, 2004). *Physics of Transition Metal Oxides*. Google-Books-ID: iyNzfufnkBgC. Springer Science & Business Media. 356 pp. ISBN: 978-3-540-21293-5.

Maes, K. et al. (May 1, 2000). "Differential modulation of inositol 1,4,5-trisphosphate receptor type 1 and type 3 by ATP". In: *Cell Calcium* 27.5, pp. 257–267. ISSN: 0143-4160. DOI: 10.1054/ceca.2000.0121. URL: https://www.sciencedirect.com/science/article/pii/S0143416000901210 (visited on 01/26/2022).

Maes, Karlien et al. (Feb. 2, 2001). "Mapping of the ATP-binding Sites on Inositol 1,4,5-Trisphosphate Receptor Type 1 and Type 3 Homotetramers by Controlled Proteolysis and Photoaffinity Labeling*". In: *Journal of Biological Chemistry* 276.5, pp. 3492–3497. ISSN: 0021-9258. DOI: 10.1074/jbc.M006082200. URL: https://www.sciencedirect.com/science/article/pii/S0021925818465313 (visited on 01/26/2022).

Mak, Don-On Daniel, Sean McBride, and J. Kevin Foskett (Dec. 22, 1998). "Inositol 1,4,5-trisphosphate activation of inositol tris-phosphate receptor Ca2+ channel by ligand tuning of Ca2+ inhibition". In: *Proceedings of the National Academy of Sciences* 95.26, pp. 15821–15825. ISSN: 0027-8424, 1091-6490. DOI: 10.1073/pnas.95.26.15821. URL: https://www.pnas.org/content/95/26/15821 (visited on 01/15/2019).

Mak, Don-On Daniel, Sean McBride, Viswanathan Raghuram, et al. (Feb. 14, 2000). "Single-Channel Properties in Endoplasmic Reticulum Membrane of Recombinant Type 3 Inositol Trisphosphate Receptor". In: *Journal of General Physiology* 115.3, pp. 241–256. ISSN: 0022-

1295. DOI: 10.1085/jgp.115.3.241. URL: https://doi.org/10.1085/jgp.115.3.241 (visited on 06/06/2022).

Mak, Don-On Daniel, Sean M.J. McBride, et al. (Nov. 2003). "Novel Regulation of Calcium Inhibition of the Inositol 1,4,5-trisphosphate Receptor Calcium-release Channel". In: *The Journal of General Physiology* 122.5, pp. 569–581. ISSN: 0022-1295. DOI: 10.1085/jgp.200308808. URL: https://www.ncbi.nlm.nih.gov/pmc/articles/PMC2229581/ (visited on 06/03/2022).

Mallet, Jacques et al. (Feb. 20, 1976). "Anatomical, physiological and biochemical studies on the cerebellum from mutant mice. III. Protein differences associated with the weaver, staggerer and nervous mutations". In: *Brain Research* 103.2, pp. 291–312. ISSN: 0006-8993. DOI: 10.1016/0006-8993(76)90800-3. URL: https://www.sciencedirect.com/science/article/pii/0006899376908003 (visited on 05/13/2022).

Maranto, A. R. (Jan. 14, 1994). "Primary structure, ligand binding, and localization of the human type 3 inositol 1,4,5-trisphosphate receptor expressed in intestinal epithelium". In: *The Journal of Biological Chemistry* 269.2, pp. 1222–1230. ISSN: 0021-9258.

Marchant, J. S. and C. W. Taylor (July 1, 1997). "Cooperative activation of IP3 receptors by sequential binding of IP3 and Ca2+ safeguards against spontaneous activity". In: *Current biology: CB* 7.7, pp. 510–518. ISSN: 0960-9822. DOI: 10.1016/s0960-9822(06)00222-3.

Marchenko, Sergey M et al. (June 15, 2005). "Spontaneously active and InsP3-activated ion channels in cell nuclei from rat cerebellar Purkinje and granule neurones". In: *The Journal of Physiology* 565 (Pt 3), pp. 897–910. ISSN: 0022-3751. DOI: 10.1113/jphysiol.2004.081299. URL: https://www.ncbi.nlm.nih.gov/pmc/articles/PMC1464565/ (visited on 06/03/2022).

Marcus, Yizhak (Dec. 1, 1988). "Ionic radii in aqueous solutions". In: *Chemical Reviews* 88.8. Publisher: American Chemical Society, pp. 1475–1498. ISSN: 0009-2665. DOI: 10.1021/cr00090a003. URL: https://doi.org/10.1021/cr00090a003 (visited on 06/16/2022).

Martorana, Francesca et al. (Feb. 15, 2012). "The BH4 domain of Bcl-XL rescues astrocyte degeneration in amyotrophic lateral sclerosis by modulating intracellular calcium signals". In: *Human Molecular Genetics* 21.4, pp. 826–840. ISSN: 0964-6906, 1460-2083. DOI: 10.1093/hmg/ddr513. URL: https://academic.oup.com/hmg/article-lookup/doi/10.1093/hmg/ddr513 (visited on 06/09/2022).

Maruyama, T. et al. (Sept. 1997). "2APB, 2-aminoethoxydiphenyl borate, a membrane-penetrable modulator of Ins(1,4,5)P3-induced Ca2+ release". In: *Journal of Biochemistry* 122.3, pp. 498–505. ISSN: 0021-924X. DOI: 10.1093/oxfordjournals.jbchem.a021780.

Mastronarde, David N. (Aug. 2003). "SerialEM: A Program for Automated Tilt Series Acquisition on Tecnai Microscopes Using Prediction of Specimen Position". In: *Microscopy and Microanalysis* 9 (S02). Publisher: Cambridge University Press, pp. 1182–1183. ISSN: 1431-9276, 1435-8115. DOI: 10.1017/S1431927603445911. URL: https://www.cambridge.org/core/journals/microscopy-and-microanalysis/article/serialem-a-program-for-automated-tilt-series-acquisition-on-tecnai-microscopes-using-prediction-of-specimen-position/DB5EA0250C3803C2D7C145CD13B4ADE6 (visited on 06/14/2022).

— (Oct. 1, 2005). "Automated electron microscope tomography using robust prediction of specimen movements". In: *Journal of Structural Biology* 152.1, pp. 36–51. ISSN: 1047-8477. DOI: 10.1016/j.jsb.2005.07.007. URL: https://www.sciencedirect.com/science/article/pii/S1047847705001528 (visited on 04/04/2022).

McCormack, J. G., A. P. Halestrap, and R. M. Denton (Apr. 1990). "Role of calcium ions in regulation of mammalian intramitochondrial metabolism". In: *Physiological Reviews* 70.2, pp. 391–425. ISSN: 0031-9333. DOI: 10.1152/physrev.1990.70.2.391.

McGoldrick, Luke L. et al. (Jan. 2018). "Opening of the human epithelial calcium channel TRPV6". In: *Nature* 553.7687. Number: 7687 Publisher: Nature Publishing Group, pp. 233–237. ISSN: 1476-4687. DOI: 10.1038/nature25182. URL: http://www.nature.com/articles/nature25182 (visited on 06/16/2022).

McMullan, G., S. Chen, et al. (Aug. 1, 2009). "Detective quantum efficiency of electron area detectors in electron microscopy". In: *Ultramicroscopy* 109.9, pp. 1126–1143. ISSN: 0304-3991. DOI: 10.1016/j.ultramic.2009.04.002. URL: https://www.sciencedirect.com/science/article/pii/S0304399109001120 (visited on 06/11/2022).

McMullan, G., A.T. Clark, et al. (Nov. 2009). "Enhanced imaging in low dose electron microscopy using electron counting". In: *Ultramicroscopy* 109.12, pp. 1411–1416. ISSN: 0304-3991. DOI: 10.1016/j.ultramic.2009.07.004. URL: https://www.ncbi.nlm.nih.gov/pmc/articles/PMC2868354/ (visited on 06/11/2022).

McPhalen, Catherine A., Natalie C. J. Strynadka, and Michael N. G. James (Jan. 1, 1991). "Calcium-Binding Sites in Proteins: A Structural Perspective". In: *Advances in Protein Chemistry*. Ed. by C. B. Anfinsen et al. Vol. 42. Metalloproteins: Structural Aspects. Academic Press, pp. 77–144. DOI: 10.1016/S0065-3233(08)60535-5. URL: https://www.sciencedirect.com/science/article/pii/S0065323308605355 (visited on 08/15/2022).

McQuibban, Angus G. et al. (Mar. 15, 2010). "A Drosophila mutant of LETM1, a candidate gene for seizures in Wolf-Hirschhorn syndrome". In: *Human Molecular Genetics* 19.6, pp. 987–1000. ISSN: 1460-2083. DOI: 10.1093/hmg/ddp563.

Melville, Zephan et al. (Jan. 6, 2022). "High-resolution structure of the membrane-embedded skeletal muscle ryanodine receptor". In: *Structure* 30.1, 172–180.e3. ISSN: 0969-2126. DOI: 10.1016/j.str.2021.08.001. URL: https://www.sciencedirect.com/science/article/pii/S0969212621002963 (visited on 04/04/2022).

Mendes, Carolina C. P. et al. (Dec. 9, 2005). "The type III inositol 1,4,5-trisphosphate receptor preferentially transmits apoptotic Ca2+ signals into mitochondria". In: *The Journal of Biological Chemistry* 280.49, pp. 40892–40900. ISSN: 0021-9258. DOI: 10.1074/jbc.M506623200.

Mesirca, Pietro, Angelo G. Torrente, and Matteo E. Mangoni (Feb. 2, 2015). "Functional role of voltage gated Ca2+ channels in heart automaticity". In: *Frontiers in Physiology* 6, p. 19. ISSN: 1664-042X. DOI: 10.3389/fphys.2015.00019. URL: https://www.ncbi.nlm.nih.gov/pmc/articles/PMC4313592/ (visited on 08/18/2022).

Meyer, T., D. Holowka, and L. Stryer (Apr. 29, 1988). "Highly cooperative opening of calcium channels by inositol 1,4,5-trisphosphate". In: *Science (New York, N.Y.)* 240.4852, pp. 653–656. ISSN: 0036-8075. DOI: 10.1126/science.2452482.

Michell, Robert H. (Mar. 25, 1975). "Inositol phospholipids and cell surface receptor function". In: *Biochimica et Biophysica Acta (BBA) - Reviews on Biomembranes* 415.1, pp. 81–147. ISSN: 0304-4157. DOI: 10.1016/0304-4157(75)90017-9. URL: https://www.sciencedirect.com/science/article/pii/0304415775900179 (visited on 05/13/2022).

Michikawa, Takayuki et al. (Aug. 1999). "Calmodulin Mediates Calcium-Dependent Inactivation of the Cerebellar Type 1 Inositol 1,4,5-Trisphosphate Receptor". In: *Neuron* 23.4, pp. 799–808. ISSN: 08966273. DOI: 10.1016/S0896-6273(01)80037-4. URL: https://linkinghub.elsevier.com/retrieve/pii/S0896627301800374 (visited on 06/03/2022).

Mignery, G et al. (July 1990). "Structure and expression of the rat inositol 1,4,5-trisphosphate receptor." In: *Journal of Biological Chemistry* 265.21, pp. 12679–12685. ISSN: 00219258. DOI: 10.1016/S0021-9258(19)38397-8. URL: https://linkinghub.elsevier.com/retrieve/pii/S0021925819383978 (visited on 05/16/2022).

Mignery, G. and T. Südhof (Dec. 1, 1990). "The ligand binding site and transduction mechanism in the inositol-1,4,5-triphosphate receptor." In: *The EMBO Journal* 9.12. Publisher: John Wiley & Sons, Ltd, pp. 3893–3898. ISSN: 1460-2075. DOI: 10.1002/j.1460-2075.1990.tb07609.x. URL: http://www.embopress.org/doi/10.1002/j.1460-2075.1990.tb07609.x (visited on 08/12/2022).

Mignery, Gregory A. et al. (Nov. 1989). "Putative receptor for inositol 1,4,5-trisphosphate similar to ryanodine receptor". In: *Nature* 342.6246. Number: 6246 Publisher: Nature Publishing Group, pp. 192–195. ISSN: 1476-4687. DOI: 10.1038/342192a0. URL: https://www.nature.com/articles/342192a0 (visited on 05/13/2022).

Mikoshiba, K., M. Huchet, and J. P. Changeux (1979). "Biochemical and immunological studies on the P400 protein, a protein characteristic of the Purkinje cell from mouse and rat cerebellum". In: *Developmental Neuroscience* 2.6, pp. 254–275. ISSN: 0378-5866. DOI: 10.1159/000112489.

Mikoshiba, Katsuhiko (June 1, 1997). "The InsP3 receptor and intracellular Ca2+ signaling". In: *Current Opinion in Neurobiology* 7.3, pp. 339–345. ISSN: 0959-4388. DOI: 10.1016/S0959-4388(97)80061-X. URL: https://www.sciencedirect.com/science/article/pii/S095943889780061X (visited on 04/04/2022).

— (Jan. 1, 2015). "Role of IP3 receptor signaling in cell functions and diseases". In: *Advances in Biological Regulation*. 55th Symposium Issue 57, pp. 217–227. ISSN: 2212-4926. DOI: 10.1016/j.jbior.2014.10.001. URL: https://www.sciencedirect.com/science/article/pii/S2212492614000566 (visited on 05/13/2022).

Mikoshiba, Katsuhiko, Hideyuki Okano, and Yasuzo Tsukada (1985). "P400 Protein Characteristic to Purkinje Cells and Related Proteins in Cerebella from Neuropathological Mutant Mice: Autoradiographic Study by 14C-Leucine and Phosphorylation". In: *Developmental Neuroscience* 7.3. Publisher: Karger Publishers, pp. 179–187. ISSN: 0378-5866, 1421-9859. DOI: 10.1159/000112286. URL: https://www.karger.com/Article/FullText/112286 (visited on 05/13/2022).

Mills, Stephen J. et al. (Mar. 26, 2020). "d-chiro-Inositol Ribophostin: A Highly Potent Agonist of d-myo-Inositol 1,4,5-Trisphosphate Receptors: Synthesis and Biological Activities". In: *Journal of Medicinal Chemistry* 63.6. Publisher: American Chemical Society, pp. 3238–3251. ISSN: 0022-2623. DOI: 10.1021/acs.jmedchem.9b01986. URL: https://doi.org/10.1021/acs.jmedchem.9b01986 (visited on 03/20/2022).

Missiaen, L. et al. (Feb. 1, 2001). "2-Aminoethoxydiphenyl borate affects the inositol 1,4,5-trisphosphate receptor, the intracellular Ca2+pump and the non-specific Ca2+leak from the non-mitochondrial Ca2+stores in permeabilized A7r5 cells". In: *Cell Calcium* 29.2, pp. 111–116. ISSN: 0143-4160. DOI: 10.1054/ceca.2000.0163. URL: https://www.sciencedirect.com/science/article/pii/S0143416000901635 (visited on 03/23/2022).

Mitchell, Peter and Jennifer Moyle (Jan. 1967). "Chemiosmotic Hypothesis of Oxidative Phosphorylation". In: *Nature* 213.5072, pp. 137–139. ISSN: 0028-0836, 1476-4687. DOI: 10.1038/213137a0. URL: https://www.nature.com/articles/213137a0 (visited on 06/08/2022).

Miura, Hirohito et al. (Sept. 2007). "Expression of gustducin overlaps with that of type III IP3 receptor in taste buds of the rat soft palate". In: *Chemical Senses* 32.7, pp. 689–696. ISSN: 0379-864X. DOI: 10.1093/chemse/bjm036.

Miyakawa, T et al. (Mar. 1, 1999). "Encoding of Ca2+ signals by differential expression of IP3 receptor subtypes." In: *The EMBO Journal* 18.5, pp. 1303–1308. ISSN: 0261-4189. DOI: 10.1093/emboj/18.5.1303. URL: https://www.ncbi.nlm.nih.gov/pmc/articles/PMC1171220/ (visited on 03/20/2020).

Miyakawa, Tomoya et al. (Apr. 2, 2001). "Ca2+-sensor region of IP3 receptor controls intracellular Ca2+ signaling". In: *The EMBO Journal* 20.7, pp. 1674–1680. ISSN: 0261-4189. DOI: 10.1093/emboj/20.7.1674. URL: https://www.ncbi.nlm.nih.gov/pmc/articles/PMC145472/ (visited on 03/23/2020).

Miyawaki, A et al. (June 1, 1991). "Structure-function relationships of the mouse inositol 1,4,5-trisphosphate receptor." In: *Proceedings of the National Academy of Sciences of the United States of America* 88.11, pp. 4911–4915. ISSN: 0027-8424. URL: https://www.ncbi.nlm.nih.gov/pmc/articles/PMC51777/ (visited on 05/16/2022).

Miyawaki, Atsushi et al. (July 1, 1990). "Expressed cerebellar-type inositol 1,4,5-trisphosphate receptor, P400, has calcium release activity in a fibroblast L cell line". In: *Neuron* 5.1, pp. 11–18.

ISSN: 0896-6273. DOI: 10.1016/0896-6273(90)90029-F. URL: https://www.sciencedirect.com/science/article/pii/089662739090029F (visited on 05/13/2022).

Mochizuki, Tetsuya et al. (Feb. 10, 2010). "Design and synthesis of indole derivatives of adenophostin A. A entry into subtype-selective IP3 receptor ligands". In: *Tetrahedron Letters* 51.6, pp. 977–979. ISSN: 0040-4039. DOI: 10.1016/j.tetlet.2009.12.045. URL: https://www.sciencedirect.com/science/article/pii/S0040403909023314 (visited on 03/20/2022).

Montero, M et al. (Nov. 15, 1995). "Monitoring dynamic changes in free Ca2+ concentration in the endoplasmic reticulum of intact cells." In: *The EMBO Journal* 14.22, pp. 5467–5475. ISSN: 0261-4189. URL: https://www.ncbi.nlm.nih.gov/pmc/articles/PMC394660/ (visited on 06/05/2022).

Moore, Anthony L. and Walter D. Bonner (1982). "Measurements of Membrane Potentials in Plant Mitochondria with the Safranine Method". In: *Plant Physiology* 70.5. Publisher: American Society of Plant Biologists (ASPB), pp. 1271–1276. ISSN: 0032-0889. URL: http://www.jstor.org/stable/4267680 (visited on 06/08/2022).

Morgan, Anthony J. et al. (Nov. 1, 2011). "Molecular mechanisms of endolysosomal Ca2+ signalling in health and disease". In: *The Biochemical Journal* 439.3, pp. 349–374. ISSN: 1470-8728. DOI: 10.1042/BJ20110949.

Morin, Andrew et al. (Sept. 10, 2013). "Collaboration gets the most out of software". In: *eLife* 2. Publisher: eLife Sciences Publications, Ltd, e01456. ISSN: 2050-084X. DOI: 10.7554/eLife.01456. URL: https://doi.org/10.7554/eLife.01456 (visited on 06/16/2022).

Morris, Robert J. (June 1972). "Lavoisier and the Caloric Theory". In: *The British Journal for the History of Science* 6.1. Publisher: Cambridge University Press, pp. 1–38. ISSN: 1474-001X, 0007-0874. DOI: 10.1017/S000708740001195X. URL: https://www.cambridge.org/core/journals/british-journal-for-the-history-of-science/article/abs/lavoisier-and-the-caloric-theory/F37091B910E43FF7D61373A2EE2EAFE3 (visited on 06/15/2022).

Mound, Abdallah et al. (Aug. 18, 2017). "Downregulation of type 3 inositol (1,4,5)-trisphosphate receptor decreases breast cancer cell migration through an oscillatory Ca2+ signal". In: *Oncotarget* 8.42, pp. 72324–72341. ISSN: 1949-2553. DOI: 10.18632/oncotarget.20327. URL: https://www.ncbi.nlm.nih.gov/pmc/articles/PMC5641133/ (visited on 06/16/2022).

Nakade, S. et al. (Mar. 4, 1994). "Cyclic AMP-dependent phosphorylation of an immunoaffinity-purified homotetrameric inositol 1,4,5-trisphosphate receptor (type I) increases Ca2+ flux in reconstituted lipid vesicles". In: *The Journal of Biological Chemistry* 269.9, pp. 6735–6742. ISSN: 0021-9258.

Nakagawa, Masashi et al. (Jan. 1, 1984). "Structures of xestospongin A,B,C and D, novel vasodilativecompounds from marine sponge, xestospongia exigua". In: *Tetrahedron Letters* 25.30, pp. 3227–3230. ISSN: 0040-4039. DOI: 10.1016/S0040-4039(01)91016-0. URL: https://www.sciencedirect.com/science/article/pii/S0040403901910160 (visited on 03/21/2022).

Nakagawa, T et al. (July 15, 1991). "The subtypes of the mouse inositol 1,4,5-trisphosphate receptor are expressed in a tissue-specific and developmentally specific manner." In: *Proceedings of the National Academy of Sciences of the United States of America* 88.14, pp. 6244–6248. ISSN: 0027-8424. URL: https://www.ncbi.nlm.nih.gov/pmc/articles/PMC52059/ (visited on 04/04/2020).

Naraghi, Mohammad (Oct. 1, 1997). "T-jump study of calcium binding kinetics of calcium chelators". In: *Cell Calcium* 22.4, pp. 255–268. ISSN: 0143-4160. DOI: 10.1016/S0143-4160(97)90064-6. URL: https://www.sciencedirect.com/science/article/pii/S0143416097900646 (visited on 04/04/2022).

Nerou, E P et al. (Apr. 1, 2001). "Selective recognition of inositol phosphates by subtypes of the inositol trisphosphate receptor." In: *Biochemical Journal* 355 (Pt 1), pp. 59–69. ISSN: 0264-6021. URL: https://www.ncbi.nlm.nih.gov/pmc/articles/PMC1221712/ (visited on 06/15/2022).

Nicholls, David G. and Martin Crompton (1980). "Mitochondrial calcium transport". In: *FEBS Letters* 111.2. _eprint: https://febs.onlinelibrary.wiley.com/doi/pdf/10.1016/0014-5793%2880%2980806-4, pp. 261–268. ISSN: 1873-3468. DOI: 10.1016/0014-5793(80)80806-4. URL: http://onlinelibrary.wiley.com/doi/abs/10.1016/0014-5793%2880%2980806-4 (visited on 06/08/2022).

Nielsen, S. Pors and O. H. Petersen (June 1972). "Transport of calcium in the perfused submandibular gland of the cat". In: *The Journal of Physiology* 223.3, pp. 685–697. ISSN: 0022-3751. URL: https://www.ncbi.nlm.nih.gov/pmc/articles/PMC1331476/ (visited on 05/13/2022).

Nogales, E., S. G. Wolf, and K. H. Downing (Jan. 8, 1998). "Structure of the alpha beta tubulin dimer by electron crystallography". In: *Nature* 391.6663, pp. 199–203. ISSN: 0028-0836. DOI: 10.1038/34465.

Nogales, Eva (Jan. 2016). "The development of cryo-EM into a mainstream structural biology technique". In: *Nature methods* 13.1, pp. 24–27. ISSN: 1548-7091. URL: https://www.ncbi.nlm.nih.gov/pmc/articles/PMC4913480/ (visited on 06/10/2022).

Nordquist, DT, CA Kozak, and HT Orr (Dec. 1, 1988). "cDNA cloning and characterization of three genes uniquely expressed in cerebellum by Purkinje neurons". In: *The Journal of Neuroscience* 8.12, pp. 4780–4789. ISSN: 0270-6474. DOI: 10.1523/JNEUROSCI.08-12-04780.1988. URL: https://www.ncbi.nlm.nih.gov/pmc/articles/PMC6569577/ (visited on 05/13/2022).

Nucifora, F. C. et al. (Sept. 1995). "Molecular cloning of a cDNA for the human inositol 1,4,5-trisphosphate receptor type 1, and the identification of a third alternatively spliced variant". In: *Brain Research. Molecular Brain Research* 32.2, pp. 291–296. ISSN: 0169-328X. DOI: 10.1016/0169-328x(95)00089-b.

Ohtsuki, M. and E. Zeitler (Jan. 1, 1975). "Minimal beam exposure with a field emission source". In: *Ultramicroscopy* 1.2, pp. 163–165. ISSN: 0304-3991. DOI: 10.1016/S0304-3991(75)80021-0. URL: https://www.sciencedirect.com/science/article/pii/S0304399175800210 (visited on 06/11/2022).

Oka, Tatsuya et al. (Apr. 2002). "Xestospongin C, a novel blocker of IP3 receptor, attenuates the increase in cytosolic calcium level and degranulation that is induced by antigen in RBL-2H3 mast cells". In: *British Journal of Pharmacology* 135.8, pp. 1959–1966. ISSN: 0007-1188. DOI: 10.1038/sj.bjp.0704662. URL: https://www.ncbi.nlm.nih.gov/pmc/articles/PMC1573325/ (visited on 03/23/2022).

Ong, H. et al. (Jan. 13, 2015). "STIM2 enhances receptor-stimulated Ca2+ signaling by promoting recruitment of STIM1 to the endoplasmic reticulum–plasma membrane junctions". In: *Science Signaling* 8.359. Publisher: American Association for the Advancement of Science Section: Research Article, ra3–ra3. ISSN: 1945-0877, 1937-9145. DOI: 10.1126/scisignal.2005748. URL: https://stke.sciencemag.org/content/8/359/ra3 (visited on 04/01/2020).

Osawa, Masanori et al. (May 6, 2005). "Mg2+ and Ca2+ differentially regulate DNA binding and dimerization of DREAM". In: *The Journal of Biological Chemistry* 280.18, pp. 18008–18014. ISSN: 0021-9258. DOI: 10.1074/jbc.M500338200.

Ozaki, Hiroshi et al. (Dec. 2002). "Inhibitory mechanism of xestospongin-C on contraction and ion channels in the intestinal smooth muscle". In: *British Journal of Pharmacology* 137.8, pp. 1207–1212. ISSN: 0007-1188. DOI: 10.1038/sj.bjp.0704988. URL: https://www.ncbi.nlm.nih.gov/pmc/articles/PMC1573613/ (visited on 03/23/2022).

Ozaki, Shoichiro (Feb. 27, 2014). "2-Aminoethyl diphenylborinate (2-APB) analogues: part 2. regulators of Ca2+ release and consequent cellular processes". In: *Archives of Physiology* 1.1. ISBN: 9782055089810 Number: 1 Publisher: Herbert Publications Section: Original Research, p. 1. ISSN: 2055-0898. URL: http://www.hoajonline.com/physiology/2055-0898/1/1 (visited on 05/03/2022).

Ozaki, Shoichiro, Etsuko Ebisui, et al. (Feb. 1, 2010). "Potent transglutaminase inhibitors, aryl -aminoethyl ketones". In: *Bioorganic & Medicinal Chemistry Letters* 20.3, pp. 1141–1144. ISSN: 0960-894X. DOI: 10.1016/j.bmcl.2009.12.011. URL: https://www.sciencedirect.com/science/article/pii/S0960894X09017168 (visited on 05/03/2022).

Ozaki, Shoichiro, Akinobu Z. Suzuki, et al. (Nov. 15, 2013). "2-Aminoethyl diphenylborinate (2-APB) analogues: Regulation of Ca2+ signaling". In: *Biochemical and Biophysical Research Communications* 441.2, pp. 286–290. ISSN: 0006-291X. DOI: 10.1016/j.bbrc.2013.08.102. URL: https://www.sciencedirect.com/science/article/pii/S0006291X13014605 (visited on 05/03/2022).

Paknejad, Navid and Richard K. Hite (Aug. 2018). "Structural basis for the regulation of inositol trisphosphate receptors by Ca 2+ and IP 3". In: *Nature Structural & Molecular Biology* 25.8, p. 660. ISSN: 1545-9985. DOI: 10.1038/s41594-018-0089-6. URL: https://www.nature.com/articles/s41594-018-0089-6 (visited on 01/14/2019).

Palmer, Amy E. et al. (Dec. 14, 2004). "Bcl-2-mediated alterations in endoplasmic reticulum Ca2+ analyzed with an improved genetically encoded fluorescent sensor". In: *Proceedings of the National Academy of Sciences of the United States of America* 101.50, pp. 17404–17409. ISSN: 0027-8424. DOI: 10.1073/pnas.0408030101. URL: https://www.ncbi.nlm.nih.gov/pmc/articles/PMC535104/ (visited on 06/05/2022).

Palty, Raz et al. (Jan. 5, 2010). "NCLX is an essential component of mitochondrial Na+/Ca2+ exchange". In: *Proceedings of the National Academy of Sciences of the United States of America* 107.1, pp. 436–441. ISSN: 0027-8424. DOI: 10.1073/pnas.0908099107. URL: https://www.ncbi.nlm.nih.gov/pmc/articles/PMC2806722/ (visited on 06/08/2022).

Parsons, MR R. et al. (Nov. 1995). "Crystal structure of a quinoenzyme: copper amine oxidase of Escherichia coli at 2 å resolution". In: *Structure with Folding & design* 3.11, pp. 1171–1184. ISSN: 0969-2126. DOI: 10.1016/S0969-2126(01)00253-2. URL: http://www.scopus.com/inward/record.url?scp=0029645871&partnerID=8YFLogxK (visited on 08/15/2022).

Partington, J. R. (1960). "Joseph Black's "Lectures on the Elements of Chemistry"". In: *Chymia* 6. Publisher: University of California Press, pp. 27–67. ISSN: 0095-9367. DOI: 10.2307/27757192. URL: https://www.jstor.org/stable/27757192 (visited on 05/04/2022).

Parys, J. and H. De Smedt (2012). "Inositol 1,4,5-Trisphosphate and Its Receptors". In: *Calcium Signaling*. Ed. by Md. Shahidul Islam. Advances in Experimental Medicine and Biology. Dordrecht: Springer Netherlands, pp. 255–279. ISBN: 978-94-007-2888-2. DOI: 10.1007/978-94-007-2888-2_11. URL: https://doi.org/10.1007/978-94-007-2888-2_11 (visited on 06/05/2022).

Patel, Sandip et al. (Oct. 14, 1997). "Ca2+-independent inhibition of inositol trisphosphate receptors by calmodulin: Redistribution of calmodulin as a possible means of regulating Ca2+mobilization". In: *Proceedings of the National Academy of Sciences* 94.21. Publisher: Proceedings of the National Academy of Sciences, pp. 11627–11632. DOI: 10.1073/pnas.94.21.11627. URL: https://www.pnas.org/doi/10.1073/pnas.94.21.11627 (visited on 05/17/2022).

Payton, A. D. and J. C. R. Turner (Jan. 1, 1962). "Soret coefficients and heats of transport of some salts of alkaline earth metals in water at 25°C". In: *Transactions of the Faraday Society* 58.0. Publisher: The Royal Society of Chemistry, pp. 55–59. ISSN: 0014-7672. DOI: 10.1039/TF9625800055. URL: https://pubs.rsc.org/en/content/articlelanding/1962/tf/tf9625800055 (visited on 05/11/2022).

Penczek, Pawel A., Robert A. Grassucci, and Joachim Frank (Mar. 1, 1994). "The ribosome at improved resolution: New techniques for merging and orientation refinement in 3D cryo-electron microscopy of biological particles". In: *Ultramicroscopy* 53.3, pp. 251–270. ISSN: 0304-3991. DOI:

10.1016/0304-3991(94)90038-8. URL: https://www.sciencedirect.com/science/article/pii/0304399194900388 (visited on 06/13/2022).

Peng, Wei et al. (Oct. 21, 2016). "Structural basis for the gating mechanism of the type 2 ryanodine receptor RyR2". In: *Science* 354.6310. Publisher: American Association for the Advancement of Science, aah5324. DOI: 10.1126/science.aah5324. URL: https://www-science-org.proxy.library.vanderbilt.edu/doi/10.1126/science.aah5324 (visited on 04/04/2022).

Pettersen, Eric F., Thomas D. Goddard, Conrad C. Huang, Gregory S. Couch, et al. (Oct. 2004). "UCSF Chimera–a visualization system for exploratory research and analysis". In: *Journal of Computational Chemistry* 25.13, pp. 1605–1612. ISSN: 0192-8651. DOI: 10.1002/jcc.20084.

Pettersen, Eric F., Thomas D. Goddard, Conrad C. Huang, Elaine C. Meng, et al. (Jan. 2021). "UCSF ChimeraX: Structure visualization for researchers, educators, and developers". In: *Protein Science : A Publication of the Protein Society* 30.1, pp. 70–82. ISSN: 0961-8368. DOI: 10.1002/pro.3943. URL: https://www.ncbi.nlm.nih.gov/pmc/articles/PMC7737788/ (visited on 04/04/2022).

Pidcock, Eina and Geoffrey R. Moore (June 2001). "Structural characteristics of protein binding sites for calcium and lanthanide ions". In: *JBIC Journal of Biological Inorganic Chemistry* 6.5, pp. 479–489. ISSN: 0949-8257, 1432-1327. DOI: 10.1007/s007750100214. URL: http://link.springer.com/10.1007/s007750100214 (visited on 08/15/2022).

Pinton, P, T Pozzan, and R Rizzuto (Sept. 15, 1998). "The Golgi apparatus is an inositol 1,4,5-trisphosphate-sensitive Ca2+ store, with functional properties distinct from those of the endoplasmic reticulum." In: *The EMBO Journal* 17.18, pp. 5298–5308. ISSN: 0261-4189. DOI: 10.1093/emboj/17.18.5298. URL: https://www.ncbi.nlm.nih.gov/pmc/articles/PMC1170857/ (visited on 06/05/2022).

Platten, J. K. and P. Costesèque (Nov. 1, 2004). "Charles Soret. A short biographya". In: *The European Physical Journal E* 15.3, pp. 235–239. ISSN: 1292-895X. DOI: 10.1140/epje/i2004-10062-8. URL: https://doi.org/10.1140/epje/i2004-10062-8 (visited on 05/11/2022).

Pozzan, T. and G. F. Azzone (Nov. 15, 1976). "The coupling of electrical ion fluxes in rat liver mitochondria". In: *FEBS letters* 72.1, pp. 62–66. ISSN: 0014-5793. DOI: 10.1016/0014-5793(76)80899-x.

Prakriya, M. and R. Lewis (Oct. 2015). "Store-Operated Calcium Channels". In: *Physiological Reviews* 95.4, pp. 1383–1436. ISSN: 1522-1210. DOI: 10.1152/physrev.00020.2014.

Prakriya, Murali et al. (Sept. 2006). "Orai1 is an essential pore subunit of the CRAC channel". In: *Nature* 443.7108. Number: 7108 Publisher: Nature Publishing Group, pp. 230–233. ISSN: 1476-4687. DOI: 10.1038/nature05122. URL: http://www.nature.com/articles/nature05122 (visited on 06/06/2022).

Prole, David L. and Colin W. Taylor (2016). "Inositol 1,4,5-trisphosphate receptors and their protein partners as signalling hubs". In: *The Journal of Physiology* 594.11, pp. 2849–2866. ISSN: 1469-7793. DOI: 10.1113/JP271139.

Punjani, Ali et al. (Mar. 2017). "cryoSPARC: algorithms for rapid unsupervised cryo-EM structure determination". In: *Nature Methods* 14.3. Number: 3 Publisher: Nature Publishing Group, pp. 290–296. ISSN: 1548-7105. DOI: 10.1038/nmeth.4169. URL: http://www.nature.com/articles/nmeth.4169 (visited on 04/04/2022).

Radermacher, M. et al. (May 1987). "Three-dimensional reconstruction from a single-exposure, random conical tilt series applied to the 50S ribosomal subunit of Escherichia coli". In: *Journal of Microscopy* 146 (Pt 2), pp. 113–136. ISSN: 0022-2720. DOI: 10.1111/j.1365-2818.1987.tb01333.x.

Rainard, Julie M., George C. Pandarakalam, and Stuart P. McElroy (Mar. 2018). "Using Microscale Thermophoresis to Characterize Hits from High-Throughput Screening: A European Lead Factory Perspective". In: *Slas Discovery* 23.3, pp. 225–241. ISSN: 2472-5552. DOI: 10.1177/2472555217744728. URL: https://www.ncbi.nlm.nih.gov/pmc/articles/PMC5824829/ (visited on 05/12/2022).

Ramos-Franco, J, D Bare, et al. (Sept. 2000). "Single-channel function of recombinant type 2 inositol 1,4, 5-trisphosphate receptor." In: *Biophysical Journal* 79.3, pp. 1388–1399. ISSN: 0006-3495. URL: https://www.ncbi.nlm.nih.gov/pmc/articles/PMC1301033/ (visited on 06/03/2022).

Ramos-Franco, J, S Caenepeel, et al. (Dec. 1998). "Single channel function of recombinant type-1 inositol 1,4,5-trisphosphate receptor ligand binding domain splice variants." In: *Biophysical Journal* 75.6, pp. 2783–2793. ISSN: 0006-3495. URL: https://www.ncbi.nlm.nih.gov/pmc/articles/PMC1299951/ (visited on 06/03/2022).

Ramos-Franco, J, M Fill, and G A Mignery (Aug. 1998). "Isoform-specific function of single inositol 1,4,5-trisphosphate receptor channels." In: *Biophysical Journal* 75.2, pp. 834–839. ISSN: 0006-3495. URL: https://www.ncbi.nlm.nih.gov/pmc/articles/PMC1299757/ (visited on 06/03/2022).

Rasola, Andrea and Paolo Bernardi (May 2007). "The mitochondrial permeability transition pore and its involvement in cell death and in disease pathogenesis". In: *Apoptosis: An International Journal on Programmed Cell Death* 12.5, pp. 815–833. ISSN: 1360-8185. DOI: 10.1007/s10495-007-0723-y.

Rasola, Andrea, Marco Sciacovelli, et al. (May 17, 2010). "Signal Transduction to the Permeability Transition Pore". In: *FEBS letters* 584.10, pp. 1989–1996. ISSN: 0014-5793. DOI: 10.1016/j.febslet.2010.02.022. URL: https://www.ncbi.nlm.nih.gov/pmc/articles/PMC2866765/ (visited on 06/08/2022).

Rassoul, G. a. R. and T. R. Bott (June 15, 1970). "Soret Coefficients of Some Binary Mixtures". In: *The Journal of Chemical Physics* 52.12. Publisher: American Institute of Physics, pp. 6445–6446. ISSN: 0021-9606. DOI: 10.1063/1.1672977. URL: https://aip.scitation.org/doi/10.1063/1.1672977 (visited on 05/11/2022).

Rees, Douglas C., Eric Johnson, and Oded Lewinson (Mar. 2009). "ABC transporters: The power to change". In: *Nature reviews. Molecular cell biology* 10.3, pp. 218–227. ISSN: 1471-0072. DOI: 10.1038/nrm2646. URL: https://www.ncbi.nlm.nih.gov/pmc/articles/PMC2830722/ (visited on 08/13/2022).

Rickert, Mathias et al. (June 18, 2004). "Compensatory energetic mechanisms mediating the assembly of signaling complexes between interleukin-2 and its alpha, beta, and gamma(c) receptors". In: *Journal of Molecular Biology* 339.5, pp. 1115–1128. ISSN: 0022-2836. DOI: 10.1016/j.jmb.2004.04.038.

Riley, Andrew M. et al. (June 1, 2001). "Bicyclic Analogues of d-myo-Inositol 1,4,5-Trisphosphate Related to Adenophostin A: Synthesis and Biological Activity". In: *Journal of Medicinal Chemistry* 44.13. Publisher: American Chemical Society, pp. 2108–2117. ISSN: 0022-2623. DOI: 10.1021/jm0005499. URL: https://doi.org/10.1021/jm0005499 (visited on 03/17/2022).

Rizzuto, Rosario, Marisa Brini, et al. (Oct. 29, 1993). "Microdomains with High Ca2+ Close to IP3-Sensitive Channels that Are Sensed by Neighboring Mitochondria". In: *Science* 262.5134.

Publisher: American Association for the Advancement of Science, pp. 744–747. DOI: 10.1126/science.8235595. URL: http://www.science.org/doi/10.1126/science.8235595 (visited on 06/08/2022).

Rizzuto, Rosario, Michael R. Duchen, and Tullio Pozzan (Jan. 13, 2004). "Flirting in Little Space: The ER/Mitochondria Ca2+ Liaison". In: *Science's STKE* 2004.215. Publisher: American Association for the Advancement of Science, re1–re1. DOI: 10.1126/stke.2152004re1. URL: http://www.science.org/doi/10.1126/stke.2152004re1 (visited on 06/08/2022).

Rohou, Alexis and Nikolaus Grigorieff (Nov. 1, 2015). "CTFFIND4: Fast and accurate defocus estimation from electron micrographs". In: *Journal of Structural Biology*. Recent Advances in Detector Technologies and Applications for Molecular TEM 192.2, pp. 216–221. ISSN: 1047-8477. DOI: 10.1016/j.jsb.2015.08.008. URL: http://www.sciencedirect.com/science/article/pii/S1047847715300460 (visited on 01/15/2019).

Rondestvedt, Christian, Richard Scribner, and Carl Wulfman (1954). *Alcoholysis of Triarylboranes*. datapdf.com. URL: https://datapdf.com/alcoholysis-of-triarylboranes-american-chemical-society.html (visited on 03/23/2022).

Rosenthal, Peter B. and Richard Henderson (Oct. 31, 2003). "Optimal Determination of Particle Orientation, Absolute Hand, and Contrast Loss in Single-particle Electron Cryomicroscopy". In: *Journal of Molecular Biology* 333.4, pp. 721–745. ISSN: 0022-2836. DOI: 10.1016/j.jmb.2003.07.013. URL: https://www.sciencedirect.com/science/article/pii/S0022283603010222 (visited on 08/12/2021).

Rossi, Ana M. et al. (Sept. 2009). "Synthetic partial agonists reveal key steps in IP3 receptor activation". In: *Nature Chemical Biology* 5.9, pp. 631–639. ISSN: 1552-4469. DOI: 10.1038/nchembio.195.

Rossi, C. S., F. D. Vasington, and E. Carafoli (Feb. 5, 1973). "The effect of ruthenium red on the uptake and release of Ca 2+ by mitochondria". In: *Biochemical and Biophysical Research Communications* 50.3, pp. 846–852. ISSN: 0006-291X. DOI: 10.1016/0006-291x(73)91322-3.

Royer, Catherine A. (May 1, 2006). "Probing Protein Folding and Conformational Transitions with Fluorescence". In: *Chemical Reviews* 106.5. Publisher: American Chemical Society, pp. 1769–1784. ISSN: 0009-2665. DOI: 10.1021/cr0404390. URL: https://doi.org/10.1021/cr0404390 (visited on 05/12/2022).

Ruska, Ernst (Aug. 1, 1987). "The development of the electron microscope and of electron microscopy". In: *Bioscience Reports* 7.8, pp. 607–629. ISSN: 1573-4935. DOI: 10.1007/BF01127674. URL: https://doi.org/10.1007/BF01127674 (visited on 06/10/2022).

Ruskin, Rachel S., Zhiheng Yu, and Nikolaus Grigorieff (Dec. 2013). "Quantitative characterization of electron detectors for transmission electron microscopy". In: *Journal of structural biology* 184.3, 10.1016/j.jsb.2013.10.016. ISSN: 1047-8477. DOI: 10.1016/j.jsb.2013.10.016. URL: https://www.ncbi.nlm.nih.gov/pmc/articles/PMC3876735/ (visited on 06/11/2022).

Saibil, Helen R. (Aug. 31, 2017). "Blob-ology and biology of cryo-EM: an interview with Helen Saibil". In: *BMC Biology* 15.1, p. 77. ISSN: 1741-7007. DOI: 10.1186/s12915-017-0417-z. URL: https://doi.org/10.1186/s12915-017-0417-z (visited on 06/11/2022).

Sakakura, Chouhei et al. (Oct. 2003). "Possible involvement of inositol 1,4,5-trisphosphate receptor type 3 (IP3R3) in the peritoneal dissemination of gastric cancers". In: *Anticancer Research* 23.5, pp. 3691–3697. ISSN: 0250-7005.

Saleem, Huma et al. (July 2014). "Interactions of antagonists with subtypes of inositol 1,4,5-trisphosphate (IP3) receptor". In: *British Journal of Pharmacology* 171.13, pp. 3298–3312. ISSN: 0007-1188. DOI: 10.1111/bph.12685. URL: https://www.ncbi.nlm.nih.gov/pmc/articles/PMC4080982/ (visited on 06/25/2022).

Samanta, Krishna and Anant B. Parekh (May 15, 2017). "Spatial Ca2+ profiling: decrypting the universal cytosolic Ca2+ oscillation". In: *The Journal of Physiology* 595.10, pp. 3053–3062. ISSN: 0022-3751. DOI: 10.1113/JP272860. URL: https://www.ncbi.nlm.nih.gov/pmc/articles/PMC5430209/ (visited on 06/05/2022).

Sander, B., M. M. Golas, and H. Stark (July 1, 2005). "Advantages of CCD detectors for de novo three-dimensional structure determination in single-particle electron microscopy". In: *Journal of Structural Biology* 151.1, pp. 92–105. ISSN: 1047-8477. DOI: 10.1016/j.jsb.2005.04.004. URL: https://www.sciencedirect.com/science/article/pii/S1047847705001061 (visited on 06/11/2022).

Santo-Domingo, Jaime and Nicolas Demaurex (July 2010). "Calcium uptake mechanisms of mitochondria". In: *Biochimica Et Biophysica Acta* 1797.6, pp. 907–912. ISSN: 0006-3002. DOI: 10.1016/j.bbabio.2010.01.005.

Santulli, Gaetano et al. (May 15, 2017). "Intracellular calcium release channels: an update". In: *The Journal of Physiology* 595.10, pp. 3041–3051. ISSN: 0022-3751. DOI: 10.1113/JP272781. URL: https://www.ncbi.nlm.nih.gov/pmc/articles/PMC5430224/ (visited on 06/24/2022).

Sarkar, Sovan et al. (Sept. 26, 2005). "Lithium induces autophagy by inhibiting inositol monophosphatase". In: *The Journal of Cell Biology* 170.7, pp. 1101–1111. ISSN: 0021-9525. DOI: 10.1083/jcb.200504035. URL: https://www.ncbi.nlm.nih.gov/pmc/articles/PMC2171537/ (visited on 06/09/2022).

Sato, C., K. Hamada, et al. (Feb. 6, 2004). "Inositol 1,4,5-trisphosphate receptor contains multiple cavities and L-shaped ligand-binding domains". In: *Journal of Molecular Biology* 336.1, pp. 155–164. ISSN: 0022-2836. DOI: 10.1016/j.jmb.2003.11.024.

Sato, C., M. Sato, et al. (1998). "The sodium channel has four domains surrounding a central pore". In: *Journal of Structural Biology* 121.3, pp. 314–325. ISSN: 1047-8477. DOI: 10.1006/jsbi.1998.3990.

Sato-Miyaoka, Mai et al. (Sept. 2012). "Regulation of hair shedding by the type 3 IP3 receptor". In: *The Journal of Investigative Dermatology* 132.9, pp. 2137–2147. ISSN: 1523-1747. DOI: 10.1038/jid.2012.141.

Saxton, R. L., E. L. Dougherty, and H. G. Drickamer (July 1954). "Thermal Diffusion in Binary Liquid Mixtures of Molecules of Simple Symmetry". In: *The Journal of Chemical Physics* 22.7. Publisher: American Institute of Physics, pp. 1166–1168. ISSN: 0021-9606. DOI: 10.1063/1.1740324. URL: https://aip.scitation.org/doi/10.1063/1.1740324 (visited on 05/11/2022).

Scheres, S. H. W. (Jan. 1, 2016). "Chapter Six - Processing of Structurally Heterogeneous Cryo-EM Data in RELION". In: *Methods in Enzymology*. Ed. by R. A. Crowther. Vol. 579. The Resolution Revolution: Recent Advances In cryoEM. Academic Press, pp. 125–157. DOI: 10.1016/bs.mie.2016.04.012. URL: https://www.sciencedirect.com/science/article/pii/S0076687916300301 (visited on 04/04/2022).

Scheres, Sjors H. W. (Dec. 1, 2012). "RELION: Implementation of a Bayesian approach to cryo-EM structure determination". In: *Journal of Structural Biology* 180.3, pp. 519–530. ISSN: 1047-8477. DOI: 10.1016/j.jsb.2012.09.006. URL: https://www.sciencedirect.com/science/article/pii/S1047847712002481 (visited on 06/14/2022).

Scheres, Sjors H.W. (2010). "Maximum-likelihood methods in cryo-EM. Part II: application to experimental data". In: *Methods in enzymology* 482, pp. 295–320. ISSN: 0076-6879. DOI: 10.1016/S0076-6879(10)82012-9. URL: https://www.ncbi.nlm.nih.gov/pmc/articles/PMC3080752/ (visited on 06/14/2022).

Scheuermann, Thomas H. et al. (Mar. 1, 2016). "On the acquisition and analysis of microscale thermophoresis data". In: *Analytical biochemistry* 496, pp. 79–93. ISSN: 0003-2697. DOI: 10.1016/j.ab.2015.12.013. URL: https://www.ncbi.nlm.nih.gov/pmc/articles/PMC4873313/ (visited on 05/12/2022).

Schmidt, Carla and Henning Urlaub (Oct. 2017). "Combining cryo-electron microscopy (cryo-EM) and cross-linking mass spectrometry (CX-MS) for structural elucidation of large protein assemblies". In: *Current Opinion in Structural Biology* 46, pp. 157–168. ISSN: 1879-033X. DOI: 10.1016/j.sbi.2017.10.005.

Schmitz, Emily A., Hirohide Takahashi, and Erkan Karakas (Mar. 17, 2022). "Structural basis for activation and gating of IP3 receptors". In: *Nature Communications* 13.1. Number: 1 Publisher: Nature Publishing Group, p. 1408. ISSN: 2041-1723. DOI: 10.1038/s41467-022-29073-2. URL: https://www.nature.com/articles/s41467-022-29073-2 (visited on 03/22/2022).

Schug, Zachary T. and Suresh K. Joseph (Aug. 25, 2006). "The role of the S4-S5 linker and C-terminal tail in inositol 1,4,5-trisphosphate receptor function". In: *The Journal of Biological Chemistry* 281.34, pp. 24431–24440. ISSN: 0021-9258. DOI: 10.1074/jbc.M604190200.

Schwaller, B. (Jan. 1, 2009). "The continuing disappearance of "pure" Ca2+ buffers". In: *Cellular and Molecular Life Sciences* 66.2, pp. 275–300. ISSN: 1420-9071. DOI: 10.1007/s00018-008-8564-6. URL: https://doi.org/10.1007/s00018-008-8564-6 (visited on 01/15/2019).

Seidel, Susanne A. I. et al. (Mar. 1, 2013). "Microscale thermophoresis quantifies biomolecular interactions under previously challenging conditions". In: *Methods*. Biophysical Methods for the Study of Protein Interactions 59.3, pp. 301–315. ISSN: 1046-2023. DOI: 10.1016/j.ymeth.2012.12.005. URL: https://www.sciencedirect.com/science/article/pii/S1046202312003064 (visited on 05/11/2022).

Seo, Min-Duk et al. (Jan. 29, 2012). "Structural and functional conservation of key domains in InsP3 and ryanodine receptors". In: *Nature* 483.7387, pp. 108–112. ISSN: 0028-0836. DOI: 10.

1038/nature10751. URL: https://www.ncbi.nlm.nih.gov/pmc/articles/PMC3378505/ (visited on 01/15/2019).

Serysheva, Irina I., Mariah R. Baker, and Guizhen Fan (2017). "Structural Insights into IP3R Function". In: *Membrane Dynamics and Calcium Signaling*. Ed. by Joachim Krebs. Advances in Experimental Medicine and Biology. Cham: Springer International Publishing, pp. 121–147. ISBN: 978-3-319-55858-5. DOI: 10.1007/978-3-319-55858-5_6. URL: https://doi.org/10.1007/978-3-319-55858-5_6 (visited on 06/24/2022).

Serysheva, Irina I., Dan J. Bare, et al. (June 13, 2003). "Structure of the Type 1 Inositol 1,4,5-Trisphosphate Receptor Revealed by Electron Cryomicroscopy". In: *Journal of Biological Chemistry* 278.24, pp. 21319–21322. ISSN: 0021-9258, 1083-351X. DOI: 10.1074/jbc.C300148200. URL: http://www.jbc.org/content/278/24/21319 (visited on 07/12/2019).

Serysheva, Irina I., Susan L. Hamilton, et al. (Jan. 21, 2005). "Structure of Ca2+ Release Channel at 14 Å Resolution". In: *Journal of molecular biology* 345.3, pp. 427–431. ISSN: 0022-2836. DOI: 10.1016/j.jmb.2004.10.073. URL: https://www.ncbi.nlm.nih.gov/pmc/articles/PMC2978512/ (visited on 10/06/2021).

Serysheva, Irina I. and Steven J. Ludtke (Jan. 1, 2010). "Chapter 8 - 3D Structure of IP3 Receptor". In: *Current Topics in Membranes*. Ed. by Irina I. Serysheva. Vol. 66. Structure and Function of Calcium Release Channels. Academic Press, pp. 171–189. DOI: 10.1016/S1063-5823(10)66008-5. URL: https://www.sciencedirect.com/science/article/pii/S1063582310660085 (visited on 05/14/2022).

Settembre, Ethan C et al. (Jan. 19, 2011). "Atomic model of an infectious rotavirus particle". In: *The EMBO Journal* 30.2, pp. 408–416. ISSN: 0261-4189. DOI: 10.1038/emboj.2010.322. URL: https://www.ncbi.nlm.nih.gov/pmc/articles/PMC3025467/ (visited on 06/11/2022).

Shibao, Kazunori et al. (Dec. 2010). "The type III inositol 1,4,5-trisphosphate receptor is associated with aggressiveness of colorectal carcinoma". In: *Cell Calcium* 48.6, pp. 315–323. ISSN: 1532-1991. DOI: 10.1016/j.ceca.2010.09.005.

Shimomura, Osamu, Frank H. Johnson, and Yo Saiga (1962). "Extraction, Purification and Properties of Aequorin, a Bioluminescent Protein from the Luminous Hydromedusan, Aequorea". In: *Journal of Cellular and Comparative Physiology* 59.3. _eprint: https://onlinelibrary.wiley.com/doi/pdf/10.1002/

pp. 223–239. ISSN: 1553-0809. DOI: 10.1002/jcp.1030590302. URL: http://onlinelibrary.wiley.com/doi/abs/10.1002/jcp.1030590302 (visited on 06/06/2022).

Shipton, Megan L. et al. (May 28, 2020). "Both d- and l-Glucose Polyphosphates Mimic d-myo-Inositol 1,4,5-Trisphosphate: New Synthetic Agonists and Partial Agonists at the Ins(1,4,5)P3 Receptor". In: *Journal of Medicinal Chemistry* 63.10. Publisher: American Chemical Society, pp. 5442–5457. ISSN: 0022-2623. DOI: 10.1021/acs.jmedchem.0c00215. URL: https://doi.org/10.1021/acs.jmedchem.0c00215 (visited on 03/20/2022).

Shoshan-Barmatz, Varda et al. (June 1, 2010). "VDAC, a multi-functional mitochondrial protein regulating cell life and death". In: *Molecular Aspects of Medicine*. VDAC, a multi-functional mitochondrial protein regulating both cell life and death 31.3, pp. 227–285. ISSN: 0098-2997. DOI: 10.1016/j.mam.2010.03.002. URL: http://www.sciencedirect.com/science/article/pii/S009829971000021X (visited on 04/02/2020).

Sienaert, I. et al. (Oct. 25, 1996). "Characterization of a cytosolic and a luminal Ca2+ binding site in the type I inositol 1,4,5-trisphosphate receptor". In: *The Journal of Biological Chemistry* 271.43, pp. 27005–27012. ISSN: 0021-9258. DOI: 10.1074/jbc.271.43.27005.

Sienaert, Ilse et al. (Oct. 10, 1997). "Molecular and Functional Evidence for Multiple Ca2+-binding Domains in the Type 1 Inositol 1,4,5-Trisphosphate Receptor *". In: *Journal of Biological Chemistry* 272.41. Publisher: Elsevier, pp. 25899–25906. ISSN: 0021-9258, 1083-351X. DOI: 10.1074/jbc.272.41.25899. URL: https://www.jbc.org/article/S0021-9258(18)60191-7/abstract (visited on 08/15/2022).

Sigworth, F. J. (1998). "A maximum-likelihood approach to single-particle image refinement". In: *Journal of Structural Biology* 122.3, pp. 328–339. ISSN: 1047-8477. DOI: 10.1006/jsbi.1998.4014.

Sipma, Henk et al. (Apr. 23, 1999). "Modulation of Inositol 1,4,5-Trisphosphate Binding to the Recombinant Ligand-binding Site of the Type-1 Inositol 1,4,5-Trisphosphate Receptor by Ca2+ and Calmodulin*". In: *Journal of Biological Chemistry* 274.17, pp. 12157–12162. ISSN: 0021-9258. DOI: 10.1074/jbc.274.17.12157. URL: https://www.sciencedirect.com/science/article/pii/S0021925819735443 (visited on 05/17/2022).

Smart, Oliver S. et al. (Dec. 1, 1996). "HOLE: A program for the analysis of the pore dimensions of ion channel structural models". In: *Journal of Molecular Graphics* 14.6, pp. 354–360. ISSN:

0263-7855. DOI: 10.1016/S0263-7855(97)00009-X. URL: https://www.sciencedirect.com/science/article/pii/S026378559700009X (visited on 04/04/2022).

Smet, P. De et al. (July 1, 1999). "Xestospongin C is an equally potent inhibitor of the inositol 1,4,5-trisphosphate receptor and the endoplasmic-reticulum Ca2+pumps". In: *Cell Calcium* 26.1, pp. 9–13. ISSN: 0143-4160. DOI: 10.1054/ceca.1999.0047. URL: https://www.sciencedirect.com/science/article/pii/S0143416099900477 (visited on 03/23/2022).

Smith, Emma F., Pamela J. Shaw, and Kurt J. De Vos (Sept. 25, 2019). "The role of mitochondria in amyotrophic lateral sclerosis". In: *Neuroscience Letters*. Mitochondria in degenerative and inflammatory neurological disorders 710, p. 132933. ISSN: 0304-3940. DOI: 10.1016/j.neulet.2017.06.052. URL: https://www.sciencedirect.com/science/article/pii/S030439401730544X (visited on 09/11/2022).

Smith, Ian F. et al. (Aug. 19, 2014). "Single-Molecule Tracking of Inositol Trisphosphate Receptors Reveals Different Motilities and Distributions". In: *Biophysical Journal* 107.4, pp. 834–845. ISSN: 0006-3495. DOI: 10.1016/j.bpj.2014.05.051. URL: https://www.ncbi.nlm.nih.gov/pmc/articles/PMC4142249/ (visited on 06/06/2022).

Smith, M K, R J Colbran, and T R Soderling (Feb. 5, 1990). "Specificities of autoinhibitory domain peptides for four protein kinases. Implications for intact cell studies of protein kinase function." In: *Journal of Biological Chemistry* 265.4, pp. 1837–1840. ISSN: 0021-9258. DOI: 10.1016/S0021-9258(19)39904-1. URL: https://www.sciencedirect.com/science/article/pii/S0021925819399041 (visited on 09/12/2022).

Sokolova, O., L. Kolmakova-Partensky, and N. Grigorieff (Mar. 7, 2001). "Three-dimensional structure of a voltage-gated potassium channel at 2.5 nm resolution". In: *Structure (London, England: 1993)* 9.3, pp. 215–220. ISSN: 0969-2126. DOI: 10.1016/s0969-2126(01)00578-0.

Solovyova, N et al. (July 1, 2002). "Xestospongin C empties the ER calcium store but does not inhibit InsP3-induced Ca2+ release in cultured dorsal root ganglia neurones". In: *Cell Calcium* 32.1, pp. 49–52. ISSN: 0143-4160. DOI: 10.1016/S0143-4160(02)00094-5. URL: https://www.sciencedirect.com/science/article/pii/S0143416002000945 (visited on 03/23/2022).

Soulsby, M. D and R. J. H Wojcikiewicz (Oct. 1, 2002). "2-Aminoethoxydiphenyl borate inhibits inositol 1,4,5-trisphosphate receptor function, ubiquitination and downregulation, but acts with variable characteristics in different cell types". In: *Cell Calcium* 32.4, pp. 175–181. ISSN: 0143-

4160. DOI: 10.1016/S0143416002001525. URL: https://www.sciencedirect.com/science/article/pii/S0143416002001525 (visited on 03/23/2022).

South, Sarah T., Steven B. Bleyl, and John C. Carey (Sept. 15, 2007). "Two unique patients with novel microdeletions in 4p16.3 that exclude the WHS critical regions: implications for critical region designation". In: *American Journal of Medical Genetics. Part A* 143A.18, pp. 2137–2142. ISSN: 1552-4825. DOI: 10.1002/ajmg.a.31900.

Spahn, Christian M. T. et al. (Aug. 20, 2004). "Cryo-EM Visualization of a Viral Internal Ribosome Entry Site Bound to Human Ribosomes: The IRES Functions as an RNA-Based Translation Factor". In: *Cell* 118.4, pp. 465–475. ISSN: 0092-8674. DOI: 10.1016/j.cell.2004.08.001. URL: https://www.sciencedirect.com/science/article/pii/S0092867404007469 (visited on 06/14/2022).

Spät, A, A Fabiato, and R P Rubin (Feb. 1, 1986). "Binding of inositol trisphosphate by a liver microsomal fraction." In: *Biochemical Journal* 233.3, pp. 929–932. ISSN: 0264-6021. URL: https://www.ncbi.nlm.nih.gov/pmc/articles/PMC1153121/ (visited on 05/04/2022).

Srivastava, Vijay Kumar and Rupali Yadav (Jan. 1, 2019). "Chapter 9 - Isothermal titration calorimetry". In: *Data Processing Handbook for Complex Biological Data Sources*. Ed. by Gauri Misra. Academic Press, pp. 125–137. ISBN: 978-0-12-816548-5. DOI: 10.1016/B978-0-12-816548-5.00009-5. URL: https://www.sciencedirect.com/science/article/pii/B9780128165485000095 (visited on 05/10/2022).

Stewart, A. and N. Grigorieff (Dec. 1, 2004). "Noise bias in the refinement of structures derived from single particles". In: *Ultramicroscopy* 102.1, pp. 67–84. ISSN: 0304-3991. DOI: 10.1016/j.ultramic.2004.08.008. URL: https://www.sciencedirect.com/science/article/pii/S0304399104001706 (visited on 05/17/2022).

Strausberg, Robert L. et al. (Dec. 24, 2002). "Generation and initial analysis of more than 15,000 full-length human and mouse cDNA sequences". In: *Proceedings of the National Academy of Sciences of the United States of America* 99.26, pp. 16899–16903. ISSN: 0027-8424. DOI: 10.1073/pnas.242603899.

Streb, H. et al. (Nov. 1983). "Release of Ca 2+ from a nonmitochondrial intracellular store in pancreatic acinar cells by inositol-1,4,5-trisphosphate". In: *Nature* 306.5938, p. 67. ISSN: 1476-

4687. DOI: 10.1038/306067a0. URL: https://www.nature.com/articles/306067a0 (visited on 06/27/2019).

Striggow, F. and B. E. Ehrlich (Aug. 1996). "The inositol 1,4,5-trisphosphate receptor of cerebellum. Mn2+ permeability and regulation by cytosolic Mn2+". In: *The Journal of General Physiology* 108.2, pp. 115–124. ISSN: 0022-1295. DOI: 10.1085/jgp.108.2.115.

Südhof, T C et al. (Nov. 1991). "Structure of a novel InsP3 receptor." In: *The EMBO Journal* 10.11, pp. 3199–3206. ISSN: 0261-4189. URL: https://www.ncbi.nlm.nih.gov/pmc/articles/PMC453043/ (visited on 04/04/2020).

Supattapone, S et al. (Jan. 25, 1988). "Solubilization, purification, and characterization of an inositol trisphosphate receptor." In: *Journal of Biological Chemistry* 263.3, pp. 1530–1534. ISSN: 0021-9258. DOI: 10.1016/S0021-9258(19)57336-7. URL: https://www.sciencedirect.com/science/article/pii/S0021925819573367 (visited on 03/21/2022).

Sureshan, Kana M. et al. (Mar. 14, 2009). "Activation of IP3 receptors by synthetic bisphosphate ligands †Dedicated to Dr Melanie N. Trusselle (1973–2008)." In: *Chemical Communications (Cambridge, England)* 10, pp. 1204–1206. ISSN: 1359-7345. DOI: 10.1039/b819328b. URL: https://www.ncbi.nlm.nih.gov/pmc/articles/PMC2898634/ (visited on 07/11/2019).

Suzuki, Akinobu Z. et al. (Feb. 15, 2010). "Synthesis of bisboron compounds and their strong inhibitory activity on store-operated calcium entry". In: *Bioorganic & Medicinal Chemistry Letters* 20.4, pp. 1395–1398. ISSN: 0960-894X. DOI: 10.1016/j.bmcl.2009.12.108. URL: https://www.sciencedirect.com/science/article/pii/S0960894X09018319 (visited on 05/03/2022).

Szabadkai, György et al. (Dec. 18, 2006). "Chaperone-mediated coupling of endoplasmic reticulum and mitochondrial Ca2+ channels". In: *The Journal of Cell Biology* 175.6, pp. 901–911. ISSN: 0021-9525. DOI: 10.1083/jcb.200608073. URL: https://www.ncbi.nlm.nih.gov/pmc/articles/PMC2064700/ (visited on 06/08/2022).

Szado, Tania et al. (Feb. 19, 2008). "Phosphorylation of inositol 1,4,5-trisphosphate receptors by protein kinase B/Akt inhibits Ca2+ release and apoptosis". In: *Proceedings of the National Academy of Sciences of the United States of America* 105.7, pp. 2427–2432. ISSN: 1091-6490. DOI: 10.1073/pnas.0711324105.

Szalai, G, R Krishnamurthy, and G Hajnóczky (Nov. 15, 1999). "Apoptosis driven by IP(3)-linked mitochondrial calcium signals." In: *The EMBO Journal* 18.22, pp. 6349–6361. ISSN: 0261-4189. DOI: 10.1093/emboj/18.22.6349. URL: https://www.ncbi.nlm.nih.gov/pmc/articles/PMC1171698/ (visited on 06/08/2022).

Szlufcik, Karolina et al. (Apr. 1, 2006). "The suppressor domain of inositol 1,4,5-trisphosphate receptor plays an essential role in the protection against apoptosis". In: *Cell Calcium* 39.4, pp. 325–336. ISSN: 0143-4160. DOI: 10.1016/j.ceca.2005.11.007. URL: https://www.sciencedirect.com/science/article/pii/S0143416005002307 (visited on 01/26/2022).

Ta, Tram Anh et al. (Feb. 1, 2006). "Hydroxylated Xestospongins Block Inositol-1,4,5-trisphosphate-Induced Ca2+ Release and Sensitize Ca2+-Induced Ca2+ Release Mediated by Ryanodine Receptors". In: *Molecular Pharmacology* 69.2. Publisher: American Society for Pharmacology and Experimental Therapeutics Section: Article, pp. 532–538. ISSN: 0026-895X, 1521-0111. DOI: 10.1124/mol.105.019125. URL: https://molpharm.aspetjournals.org/content/69/2/532 (visited on 03/21/2022).

Tait, Stephen W. G. and Douglas R. Green (Sept. 2010). "Mitochondria and cell death: outer membrane permeabilization and beyond". In: *Nature Reviews Molecular Cell Biology* 11.9. Number: 9 Publisher: Nature Publishing Group, pp. 621–632. ISSN: 1471-0080. DOI: 10.1038/nrm2952. URL: http://www.nature.com/articles/nrm2952 (visited on 06/08/2022).

Takahashi, Masaaki et al. (Nov. 25, 1993). "ADENOPHOSTINS A AND B: POTENT AGONISTS OF INOSITOL-1, 4, 5-TRISPHOSPHATE RECEPTOR PRODUCED BY Penicillium brevicompactum TAXONOMY, FERMENTATION, ISOLATION, PHYSICO-CHEMICAL AND BIOLOGICAL PROPERTIES". In: *The Journal of Antibiotics* 46.11. Publisher: JAPAN ANTIBIOTICS RESEARCH ASSOCIATION, pp. 1643–1647. ISSN: 0021-8820, 1881-1469. DOI: 10.7164/antibiotics.46.1643. URL: https://www.jstage.jst.go.jp/article/antibiotics1968/46/11/46_11_1643/_article (visited on 03/17/2022).

Takei, K. et al. (Feb. 1, 1994). "Inositol 1,4,5-Trisphosphate receptor causes formation of ER cisternal stacks in transfected fibroblasts and in cerebellar purkinje cells". In: *Neuron* 12.2, pp. 327–342. ISSN: 0896-6273. DOI: 10.1016/0896-6273(94)90275-5. URL: http://www.sciencedirect.com/science/article/pii/0896627394902755 (visited on 06/28/2019).

Tang, Guang et al. (Jan. 2007). "EMAN2: an extensible image processing suite for electron microscopy". In: *Journal of Structural Biology* 157.1, pp. 38–46. ISSN: 1047-8477. DOI: 10.1016/j.jsb.2006.05.009.

Tang, Tie-Shan et al. (Jan. 15, 2003). "Modulation of Type 1 Inositol (1,4,5)-Trisphosphate Receptor Function by Protein Kinase A and Protein Phosphatase 1". In: *The Journal of Neuroscience* 23.2, pp. 403–415. ISSN: 0270-6474. DOI: 10.1523/JNEUROSCI.23-02-00403.2003. URL: https://www.ncbi.nlm.nih.gov/pmc/articles/PMC6741879/ (visited on 06/03/2022).

Tansey, M. G. et al. (Apr. 1, 1994). "Ca(2+)-dependent phosphorylation of myosin light chain kinase decreases the Ca2+ sensitivity of light chain phosphorylation within smooth muscle cells". In: *Journal of Biological Chemistry* 269.13, pp. 9912–9920. ISSN: 0021-9258. DOI: 10.1016/S0021-9258(17)36969-7. URL: https://www.sciencedirect.com/science/article/pii/S0021925817369697 (visited on 06/07/2022).

Tao, Xiao et al. (Dec. 18, 2009). "Crystal structure of the eukaryotic strong inward-rectifier K+ channel Kir2.2 at 3.1 A resolution". In: *Science (New York, N.Y.)* 326.5960, pp. 1668–1674. ISSN: 1095-9203. DOI: 10.1126/science.1180310.

Taufiq-Ur-Rahman et al. (Apr. 2, 2009). "Clustering of IP3 receptors by IP3 retunes their regulation by IP3 and Ca2+". In: *Nature* 458.7238, pp. 655–659. ISSN: 0028-0836. DOI: 10.1038/nature07763. URL: https://www.ncbi.nlm.nih.gov/pmc/articles/PMC2702691/ (visited on 03/30/2020).

Taylor, C., P. da Fonseca, and E. Morris (Apr. 2004). "IP3 receptors: the search for structure". In: *Trends in Biochemical Sciences* 29.4, pp. 210–219. ISSN: 09680004. DOI: 10.1016/j.tibs.2004.02.010. URL: https://linkinghub.elsevier.com/retrieve/pii/S0968000404000544 (visited on 06/04/2022).

Taylor, C. and S. Tovey (Dec. 2010). "IP3 Receptors: Toward Understanding Their Activation". In: *Cold Spring Harbor Perspectives in Biology* 2.12, a004010. ISSN: 1943-0264. DOI: 10.1101/cshperspect.a004010. URL: https://www.ncbi.nlm.nih.gov/pmc/articles/PMC2982166/ (visited on 04/25/2022).

Taylor, C.W., A.A. Genazzani, and S.A. Morris (Dec. 1999). "Expression of inositol trisphosphate receptors". In: *Cell Calcium* 26.6, pp. 237–251. ISSN: 01434160. DOI: 10.1054/ceca.1999.0090.

URL: https://linkinghub.elsevier.com/retrieve/pii/S0143416099900908 (visited on 06/03/2022).

Taylor, K. A. and R. M. Glaeser (Dec. 13, 1974). "Electron diffraction of frozen, hydrated protein crystals". In: *Science (New York, N.Y.)* 186.4168, pp. 1036–1037. ISSN: 0036-8075. DOI: 10.1126/science.186.4168.1036.

Terry, Lara E. et al. (Oct. 22, 2020). "Disease-associated mutations in inositol 1,4,5-trisphosphate receptor subunits impair channel function". In: *Journal of Biological Chemistry*. Publisher: American Society for Biochemistry and Molecular Biology, jbc.RA120.015683. ISSN: 0021-9258, 1083-351X. DOI: 10.1074/jbc.RA120.015683. URL: http://www.jbc.org/content/early/2020/10/22/jbc.RA120.015683 (visited on 11/09/2020).

Thomas, Mark P., Stephen J. Mills, and Barry V. L. Potter (Jan. 26, 2016). "The "Other" Inositols and Their Phosphates: Synthesis, Biology, and Medicine (with Recent Advances in myo-Inositol Chemistry)". In: *Angewandte Chemie (International Ed. in English)* 55.5, pp. 1614–1650. ISSN: 1521-3773. DOI: 10.1002/anie.201502227.

Thompson, Rebecca F. et al. (May 1, 2016). "An introduction to sample preparation and imaging by cryo-electron microscopy for structural biology". In: *Methods (San Diego, Calif.)* 100, pp. 3–15. ISSN: 1046-2023. DOI: 10.1016/j.ymeth.2016.02.017. URL: https://www.ncbi.nlm.nih.gov/pmc/articles/PMC4854231/ (visited on 06/11/2022).

Thyagarajan, K. and P. Lallemand (July 1, 1978). "Determination of the thermal diffusion ratio in a binary mixture by forced Rayleigh scattering". In: *Optics Communications* 26.1, pp. 54–57. ISSN: 0030-4018. DOI: 10.1016/0030-4018(78)90340-1. URL: https://www.sciencedirect.com/science/article/pii/0030401878903401 (visited on 05/11/2022).

Trajkovic, Sanja et al. (Sept. 6, 2011). "Atomic Force Microscopy Study of Conformational Change of Immobilized Calmodulin". In: *Langmuir : the ACS journal of surfaces and colloids* 27.17, pp. 10793–10799. ISSN: 0743-7463. DOI: 10.1021/la2016885. URL: https://www.ncbi.nlm.nih.gov/pmc/articles/PMC3164926/ (visited on 08/15/2022).

Tsai, Ming-Feng et al. (Jan. 2014). "Functional reconstitution of the mitochondrial Ca2+/H+ antiporter Letm1". In: *The Journal of General Physiology* 143.1, pp. 67–73. ISSN: 0022-1295. DOI: 10.1085/jgp.201311096. URL: https://www.ncbi.nlm.nih.gov/pmc/articles/PMC3874562/ (visited on 06/08/2022).

Tso, Shih-Chia and Chad A. Brautigam (2021). "Measuring the KD of Protein–Ligand Interactions Using Microscale ThermophoresisMicroscale thermophoresis (MST)". In: *Protein-Ligand Interactions: Methods and Applications*. Ed. by Tina Daviter et al. Methods in Molecular Biology. New York, NY: Springer US, pp. 161–181. ISBN: 978-1-07-161197-5. DOI: 10.1007/978-1-0716-1197-5_6. URL: https://doi.org/10.1007/978-1-0716-1197-5_6 (visited on 05/12/2022).

Tu, Huiping, Tomoya Miyakawa, et al. (Apr. 2002). "Functional characterization of the type 1 inositol 1,4,5-trisphosphate receptor coupling domain SII(+/-) splice variants and the Opisthotonos mutant form." In: *Biophysical Journal* 82.4, pp. 1995–2004. ISSN: 0006-3495. URL: https://www.ncbi.nlm.nih.gov/pmc/articles/PMC1301995/ (visited on 01/26/2022).

Tu, Huiping, Elena Nosyreva, et al. (July 2003). "Functional and Biochemical Analysis of the Type 1 Inositol (1,4,5)-Trisphosphate Receptor Calcium Sensor". In: *Biophysical Journal* 85.1, pp. 290–299. ISSN: 0006-3495. URL: https://www.ncbi.nlm.nih.gov/pmc/articles/PMC1303085/ (visited on 06/03/2022).

Tu, Huiping, Zhengnan Wang, and Ilya Bezprozvanny (Feb. 2005). "Modulation of Mammalian Inositol 1,4,5-Trisphosphate Receptor Isoforms by Calcium: A Role of Calcium Sensor Region". In: *Biophysical Journal* 88.2, pp. 1056–1069. ISSN: 0006-3495. DOI: 10.1529/biophysj.104.049601. URL: https://www.ncbi.nlm.nih.gov/pmc/articles/PMC1305112/ (visited on 06/03/2022).

Tu, Huiping, Zhengnan Wang, Elena Nosyreva, et al. (Feb. 2005). "Functional Characterization of Mammalian Inositol 1,4,5-Trisphosphate Receptor Isoforms". In: *Biophysical Journal* 88.2, pp. 1046–1055. ISSN: 0006-3495. DOI: 10.1529/biophysj.104.049593. URL: https://www.ncbi.nlm.nih.gov/pmc/articles/PMC1305111/ (visited on 04/04/2022).

Uchida, K. et al. (Oct. 2008). "Observation of the spin Seebeck effect". In: *Nature* 455.7214. Number: 7214 Publisher: Nature Publishing Group, pp. 778–781. ISSN: 1476-4687. DOI: 10.1038/nature07321. URL: https://www.nature.com/articles/nature07321 (visited on 05/04/2022).

Uchida, Keiko et al. (May 9, 2003). "Critical Regions for Activation Gating of the Inositol 1,4,5-Trisphosphate Receptor *". In: *Journal of Biological Chemistry* 278.19. Publisher: Elsevier, pp. 16551–16560. ISSN: 0021-9258, 1083-351X. DOI: 10.1074/jbc.M300646200. URL: https://www.jbc.org/article/S0021-9258(19)58365-X/abstract (visited on 04/04/2022).

Unwin, P. N. and R. Henderson (May 25, 1975). "Molecular structure determination by electron microscopy of unstained crystalline specimens". In: *Journal of Molecular Biology* 94.3, pp. 425–440. ISSN: 0022-2836. DOI: 10.1016/0022-2836(75)90212-0.

Van Heel, Marin (Jan. 1, 1987). "Angular reconstitution: A posteriori assignment of projection directions for 3D reconstruction". In: *Ultramicroscopy* 21.2, pp. 111–123. ISSN: 0304-3991. DOI: 10.1016/0304-3991(87)90078-7. URL: https://www.sciencedirect.com/science/article/pii/0304399187900787 (visited on 09/14/2021).

VANDERHEYDEN, Veerle et al. (June 2009). "Regulation of inositol 1,4,5-trisphosphate-induced Ca2+ release by reversible phosphorylation and dephosphorylation". In: *Biochimica et biophysica acta* 1793.6, pp. 959–970. ISSN: 0006-3002. DOI: 10.1016/j.bbamcr.2008.12.003. URL: https://www.ncbi.nlm.nih.gov/pmc/articles/PMC2693466/ (visited on 09/12/2022).

Vasington, Frank D. and Jerome V. Murphy (Aug. 1962). "Ca++ Uptake by Rat Kidney Mitochondria and Its Dependence on Respiration and Phosphorylation". In: *Journal of Biological Chemistry* 237.8, pp. 2670–2677. ISSN: 00219258. DOI: 10.1016/S0021-9258(19)73805-8. URL: https://linkinghub.elsevier.com/retrieve/pii/S0021925819738058 (visited on 06/08/2022).

Venkatachalam, Kartik and Craig Montell (2007). "TRP Channels". In: *Annual review of biochemistry* 76, p. 387. DOI: 10.1146/annurev.biochem.75.103004.142819. URL: http://www.ncbi.nlm.nih.gov/pmc/articles/PMC4196875/ (visited on 06/06/2022).

Verkhratsky, Alexei (Jan. 2005). "Physiology and Pathophysiology of the Calcium Store in the Endoplasmic Reticulum of Neurons". In: *Physiological Reviews* 85.1. Publisher: American Physiological Society, pp. 201–279. ISSN: 0031-9333. DOI: 10.1152/physrev.00004.2004. URL: https://journals.physiology.org/doi/full/10.1152/physrev.00004.2004 (visited on 05/13/2022).

Vervloessem, Tamara et al. (Sept. 2015). "The type 2 inositol 1,4,5-trisphosphate receptor, emerging functions for an intriguing Ca^{2}-release channel". In: *Biochimica Et Biophysica Acta* 1853.9, pp. 1992–2005. ISSN: 0006-3002. DOI: 10.1016/j.bbamcr.2014.12.006.

Vibhute, Amol M., Vera Konieczny, et al. (June 28, 2015). "Triazolophostins: a library of novel and potent agonists of IP3 receptors †Electronic supplementary information (ESI) available: Synthetic procedures and spectral data for all new compounds, crystal data for disaccharide 4

and details of the docking study. CCDC 1022279. For ESI and crystallographic data in CIF or other electronic format see DOI: 10.1039/c5ob00440c Click here for additional data file. Click here for additional data file." In: *Organic & Biomolecular Chemistry* 13.24, pp. 6698–6710. ISSN: 1477-0520. DOI: 10.1039/c5ob00440c. URL: https://www.ncbi.nlm.nih.gov/pmc/articles/PMC4533600/ (visited on 03/20/2022).

Vibhute, Amol M., Poornenth Pushpanandan, et al. (Sept. 8, 2016). "Synthesis of dimeric analogs of adenophostin A that potently evoke Ca2+ release through IP3 receptors". In: *RSC Advances* 6.89. Publisher: The Royal Society of Chemistry, pp. 86346–86351. ISSN: 2046-2069. DOI: 10.1039/C6RA19413C. URL: https://pubs.rsc.org/en/content/articlelanding/2016/ra/c6ra19413c (visited on 03/20/2022).

Vicencio, J. M. et al. (July 2009). "The inositol 1,4,5-trisphosphate receptor regulates autophagy through its interaction with Beclin 1". In: *Cell Death and Differentiation* 16.7, pp. 1006–1017. ISSN: 1476-5403. DOI: 10.1038/cdd.2009.34.

Voit, A. et al. (June 3, 2005). "Thermal patterning of a critical polymer blend". In: *Physical Review Letters* 94.21, p. 214501. ISSN: 0031-9007. DOI: 10.1103/PhysRevLett.94.214501.

W, Kühlbrandt and Wang Dn (Mar. 14, 1991). "Three-dimensional structure of plant light-harvesting complex determined by electron crystallography". In: *Nature* 350.6314. Publisher: Nature. ISSN: 0028-0836. DOI: 10.1038/350130a0. URL: http://pubmed.ncbi.nlm.nih.gov/2005962/ (visited on 06/10/2022).

Wadhwa, Renu, Kazunari Taira, and Sunil C. Kaul (July 2002). "An Hsp70 family chaperone, mortalin/mthsp70/PBP74/Grp75: what, when, and where?" In: *Cell Stress & Chaperones* 7.3, pp. 309–316. ISSN: 1355-8145. DOI: 10.1379/1466-1268(2002)007<0309:ahfcmm>2.0.co;2.

Wagner, Larry E., Matthew J. Betzenhauser, and David I. Yule (June 23, 2006). "ATP Binding to a Unique Site in the Type-1 S2- Inositol 1,4,5-Trisphosphate Receptor Defines Susceptibility to Phosphorylation by Protein Kinase A*". In: *Journal of Biological Chemistry* 281.25, pp. 17410–17419. ISSN: 0021-9258. DOI: 10.1074/jbc.M601340200. URL: https://www.sciencedirect.com/science/article/pii/S0021925820557700 (visited on 01/26/2022).

Walaas, SI, AC Nairn, and P Greengard (Apr. 1, 1986). "PCPP-260, a Purkinje cell-specific cyclic AMP-regulated membrane phosphoprotein of Mr 260,000". In: *The Journal of Neuroscience*

6.4, pp. 954–961. ISSN: 0270-6474. DOI: 10.1523/JNEUROSCI.06-04-00954.1986. URL: https://www.ncbi.nlm.nih.gov/pmc/articles/PMC6568447/ (visited on 05/13/2022).

Wei, Risheng et al. (Sept. 2016). "Structural insights into Ca2+-activated long-range allosteric channel gating of RyR1". In: *Cell Research* 26.9, pp. 977–994. ISSN: 1001-0602. DOI: 10.1038/cr.2016.99. URL: https://www.ncbi.nlm.nih.gov/pmc/articles/PMC5034117/ (visited on 04/04/2022).

Wienken, Christoph J. et al. (Oct. 19, 2010). "Protein-binding assays in biological liquids using microscale thermophoresis". In: *Nature Communications* 1.1. Number: 1 Publisher: Nature Publishing Group, p. 100. ISSN: 2041-1723. DOI: 10.1038/ncomms1093. URL: http://www.nature.com/articles/ncomms1093 (visited on 08/15/2022).

Wierenga, Rik K. and Wim G. J. Hol (Apr. 1983). "Predicted nucleotide-binding properties of p21 protein and its cancer-associated variant". In: *Nature* 302.5911. Bandiera_abtest: a Cg_type: Nature Research Journals Number: 5911 Primary_atype: Research Publisher: Nature Publishing Group, pp. 842–844. ISSN: 1476-4687. DOI: 10.1038/302842a0. URL: https://www.nature.com/articles/302842a0 (visited on 01/26/2022).

Wilcox, R. A. et al. (June 1, 1995). "2-Hydroxyethyl-alpha-D-glucopyranoside-2,3',4'-trisphosphate, a novel, metabolically resistant, adenophostin A and myo-inositol-1,4,5-trisphosphate analogue, potently interacts with the myo-inositol-1,4,5-trisphosphate receptor." In: *Molecular Pharmacology* 47.6. Publisher: American Society for Pharmacology and Experimental Therapeutics, pp. 1204–1211. ISSN: 0026-895X, 1521-0111. URL: http://molpharm.aspetjournals.org/content/47/6/1204 (visited on 06/15/2022).

Wilcox, Robert A et al. (Nov. 1998). "New developments in the molecular pharmacology of the myo-inositol 1,4,5-trisphosphate receptor". In: *Trends in Pharmacological Sciences* 19.11, pp. 467–475. ISSN: 01656147. DOI: 10.1016/S0165-6147(98)01260-7. URL: https://linkinghub.elsevier.com/retrieve/pii/S0165614798012607 (visited on 03/17/2022).

Williams, A. J., D. J. West, and R. Sitsapesan (Feb. 2001). "Light at the end of the Ca(2+)-release channel tunnel: structures and mechanisms involved in ion translocation in ryanodine receptor channels". In: *Quarterly Reviews of Biophysics* 34.1, pp. 61–104. ISSN: 0033-5835. DOI: 10.1017/s0033583501003675.

Williams, Andrea et al. (May 2008). "Novel targets for Huntington's disease in an mTOR-independent autophagy pathway". In: *Nature Chemical Biology* 4.5. Number: 5 Publisher: Nature Publishing Group, pp. 295–305. ISSN: 1552-4469. DOI: 10.1038/nchembio.79. URL: http://www.nature.com/articles/nchembio.79 (visited on 06/09/2022).

Williams, Christopher J. et al. (Jan. 2018). "MolProbity: More and better reference data for improved all-atom structure validation". In: *Protein Science : A Publication of the Protein Society* 27.1, pp. 293–315. ISSN: 0961-8368. DOI: 10.1002/pro.3330. URL: https://www.ncbi.nlm.nih.gov/pmc/articles/PMC5734394/ (visited on 04/04/2022).

Williams, R. C. and H. W. Fisher (Aug. 28, 1970). "Electron microscopy of tobacco mosaic virus under conditions of minimal beam exposure". In: *Journal of Molecular Biology* 52.1, pp. 121–123. ISSN: 0022-2836. DOI: 10.1016/0022-2836(70)90181-6.

Willuweit, B and K Aktories (Feb. 1, 1988). "Heparin uncouples alpha 2-adrenoceptors from the Gi-protein in membranes of human platelets." In: *Biochemical Journal* 249.3, pp. 857–863. ISSN: 0264-6021. URL: https://www.ncbi.nlm.nih.gov/pmc/articles/PMC1148785/ (visited on 03/21/2022).

Wiseman, Thomas et al. (May 15, 1989). "Rapid measurement of binding constants and heats of binding using a new titration calorimeter". In: *Analytical Biochemistry* 179.1, pp. 131–137. ISSN: 0003-2697. DOI: 10.1016/0003-2697(89)90213-3. URL: https://www.sciencedirect.com/science/article/pii/0003269789902133 (visited on 05/06/2022).

Wojcikiewicz, R. J. and S. G. Luo (Mar. 6, 1998). "Phosphorylation of inositol 1,4,5-trisphosphate receptors by cAMP-dependent protein kinase. Type I, II, and III receptors are differentially susceptible to phosphorylation and are phosphorylated in intact cells". In: *The Journal of Biological Chemistry* 273.10, pp. 5670–5677. ISSN: 0021-9258. DOI: 10.1074/jbc.273.10.5670.

Wojcikiewicz, Richard J. H. (May 12, 1995). "Type I, II, and III Inositol 1,4,5-Trisphosphate Receptors Are Unequally Susceptible to Down-regulation and Are Expressed in Markedly Different Proportions in Different Cell Types*". In: *Journal of Biological Chemistry* 270.19, pp. 11678–11683. ISSN: 0021-9258. DOI: 10.1074/jbc.270.19.11678. URL: https://www.sciencedirect.com/science/article/pii/S0021925817502495 (visited on 06/03/2022).

Wojcikiewicz, Richard J. H. and Su Ge Luo (Apr. 1, 1998). "Differences Among Type I, II, and III Inositol-1,4,5-Trisphosphate Receptors in Ligand-Binding Affinity Influence the Sensitivity

of Calcium Stores to Inositol-1,4,5-Trisphosphate". In: *Molecular Pharmacology* 53.4, pp. 656–662. ISSN: 0026-895X, 1521-0111. DOI: 10.1124/mol.53.4.656. URL: http://molpharm.aspetjournals.org/lookup/doi/10.1124/mol.53.4.656 (visited on 02/12/2019).

Wolf, Matthias et al. (Apr. 6, 2010). "Subunit interactions in bovine papillomavirus". In: *Proceedings of the National Academy of Sciences of the United States of America* 107.14, pp. 6298–6303. ISSN: 0027-8424. DOI: 10.1073/pnas.0914604107. URL: https://www.ncbi.nlm.nih.gov/pmc/articles/PMC2852008/ (visited on 06/11/2022).

Woll, Kellie A. and Filip Van Petegem (Jan. 1, 2022). "Calcium-release channels: structure and function of IP3 receptors and ryanodine receptors". In: *Physiological Reviews* 102.1, pp. 209–268. ISSN: 1522-1210. DOI: 10.1152/physrev.00033.2020.

Worley, P. F. et al. (Sept. 5, 1987). "Characterization of inositol trisphosphate receptor binding in brain. Regulation by pH and calcium." In: *Journal of Biological Chemistry* 262.25. Publisher: Elsevier, pp. 12132–12136. ISSN: 0021-9258, 1083-351X. DOI: 10.1016/S0021-9258(18)45326-4. URL: https://www.jbc.org/article/S0021-9258(18)45326-4/abstract (visited on 05/04/2022).

Worley, Paul F. et al. (Jan. 1987). "Inositol trisphosphate receptor localization in brain: variable stoichiometry with protein kinase C". In: *Nature* 325.6100. Number: 6100 Publisher: Nature Publishing Group, pp. 159–161. ISSN: 1476-4687. DOI: 10.1038/325159a0. URL: https://www.nature.com/articles/325159a0 (visited on 05/04/2022).

Worley, PF, JM Baraban, and SH Snyder (Jan. 1, 1989). "Inositol 1,4,5-trisphosphate receptor binding: autoradiographic localization in rat brain". In: *The Journal of Neuroscience* 9.1, pp. 339–346. ISSN: 0270-6474. DOI: 10.1523/JNEUROSCI.09-01-00339.1989. URL: https://www.ncbi.nlm.nih.gov/pmc/articles/PMC6569993/ (visited on 05/13/2022).

Wright, F. A. and R. J. H. Wojcikiewicz (Jan. 1, 2016). "Chapter 4 - Inositol 1,4,5-Trisphosphate Receptor Ubiquitination". In: *Progress in Molecular Biology and Translational Science*. Ed. by Sudha K. Shenoy. Vol. 141. Ubiquitination and Transmembrane Signaling. Academic Press, pp. 141–159. DOI: 10.1016/bs.pmbts.2016.02.004. URL: https://www.sciencedirect.com/science/article/pii/S1877117316000442 (visited on 09/12/2022).

Xu, Haoxing and Dejian Ren (2015). "Lysosomal Physiology". In: *Annual review of physiology* 77, pp. 57–80. ISSN: 0066-4278. DOI: 10.1146/annurev-physiol-021014-071649. URL: https://www.ncbi.nlm.nih.gov/pmc/articles/PMC4524569/ (visited on 06/05/2022).

Xu, Le et al. (Dec. 14, 2018). "Ca2+-mediated activation of the skeletal-muscle ryanodine receptor ion channel". In: *The Journal of Biological Chemistry* 293.50, pp. 19501–19509. ISSN: 0021-9258. DOI: 10.1074/jbc.RA118.004453. URL: https://www.ncbi.nlm.nih.gov/pmc/articles/PMC6302159/ (visited on 04/04/2022).

Xue, Renhao et al. (2021). "The Role of Calmodulin vs. Synaptotagmin in Exocytosis". In: *Frontiers in Molecular Neuroscience* 14. ISSN: 1662-5099. URL: https://www.frontiersin.org/article/10.3389/fnmol.2021.691363 (visited on 06/06/2022).

Yamada, N et al. (Sept. 15, 1994). "Human inositol 1,4,5-trisphosphate type-1 receptor, InsP3R1: structure, function, regulation of expression and chromosomal localization." In: *Biochemical Journal* 302 (Pt 3), pp. 781–790. ISSN: 0264-6021. URL: https://www.ncbi.nlm.nih.gov/pmc/articles/PMC1137299/ (visited on 04/04/2020).

Yamamoto-Hino, M. et al. (1994). "Cloning and characterization of human type 2 and type 3 inositol 1,4,5-trisphosphate receptors". In: *Receptors & Channels* 2.1, pp. 9–22. ISSN: 1060-6823.

Yamazaki, Haruka et al. (Nov. 12, 2010). "Tyr-167/Trp-168 in Type 1/3 Inositol 1,4,5-Trisphosphate Receptor Mediates Functional Coupling between Ligand Binding and Channel Opening". In: *The Journal of Biological Chemistry* 285.46, pp. 36081–36091. ISSN: 0021-9258. DOI: 10.1074/jbc.M110.140129. URL: https://www.ncbi.nlm.nih.gov/pmc/articles/PMC2975230/ (visited on 04/04/2022).

Yang, Chao et al. (Feb. 23, 2015). "Self-Binding Peptides: Folding or Binding?" In: *Journal of Chemical Information and Modeling* 55.2. Publisher: American Chemical Society, pp. 329–342. ISSN: 1549-9596. DOI: 10.1021/ci500522v. URL: https://doi.org/10.1021/ci500522v (visited on 06/28/2022).

Yen, M., L. Lokteva, and R. Lewis (Nov. 1, 2016). "Functional Analysis of Orai1 Concatemers Supports a Hexameric Stoichiometry for the CRAC Channel". In: *Biophysical Journal* 111.9, pp. 1897–1907. ISSN: 0006-3495. DOI: 10.1016/j.bpj.2016.09.020. URL: https://www.sciencedirect.com/science/article/pii/S0006349516308207 (visited on 06/06/2022).

Yim, Willa Wen-You and Noboru Mizushima (Feb. 11, 2020). "Lysosome biology in autophagy". In: *Cell Discovery* 6, p. 6. ISSN: 2056-5968. DOI: 10.1038/s41421-020-0141-7. URL: https://www.ncbi.nlm.nih.gov/pmc/articles/PMC7010707/ (visited on 06/09/2022).

Yoshikawa, F., H. Iwasaki, et al. (Jan. 1, 1999). "Cooperative formation of the ligand-binding site of the inositol 1,4, 5-trisphosphate receptor by two separable domains". In: *The Journal of Biological Chemistry* 274.1, pp. 328–334. ISSN: 0021-9258. DOI: 10.1074/jbc.274.1.328.

Yoshikawa, F., M. Morita, et al. (July 26, 1996). "Mutational Analysis of the Ligand Binding Site of the Inositol 1,4,5-Trisphosphate Receptor *". In: *Journal of Biological Chemistry* 271.30. Publisher: Elsevier, pp. 18277–18284. ISSN: 0021-9258, 1083-351X. DOI: 10.1074/jbc.271.30.18277. URL: https://www.jbc.org/article/S0021-9258(19)87052-7/abstract (visited on 05/04/2022).

Yoshikawa, S et al. (Aug. 1992). "Molecular cloning and characterization of the inositol 1,4,5-trisphosphate receptor in Drosophila melanogaster." In: *Journal of Biological Chemistry* 267.23, pp. 16613–16619. ISSN: 00219258. DOI: 10.1016/S0021-9258(18)42047-9. URL: https://linkinghub.elsevier.com/retrieve/pii/S0021925818420479 (visited on 05/16/2022).

Yu, Xuekui et al. (May 11, 2011). "Atomic Model of CPV Reveals the Mechanism Used by This Single-Shelled Virus to Economically Carry Out Functions Conserved in Multishelled Reoviruses". In: *Structure* 19.5, pp. 652–661. ISSN: 0969-2126. DOI: 10.1016/j.str.2011.03.003. URL: https://www.sciencedirect.com/science/article/pii/S0969212611001006 (visited on 06/11/2022).

Zhang, Dan et al. (May 29, 2007). "The inositol 1,4,5-trisphosphate receptor (Itpr) gene family in Xenopus: identification of type 2 and type 3 inositol 1,4,5-trisphosphate receptor subtypes". In: *Biochemical Journal* 404.3, pp. 383–391. ISSN: 0264-6021. DOI: 10.1042/BJ20070101. URL: https://doi.org/10.1042/BJ20070101 (visited on 08/18/2022).

Zhang, K. J. et al. (May 1996). "Optical measurement of the Soret coefficient and the diffusion coefficient of liquid mixtures". In: *The Journal of Chemical Physics* 104.17. Publisher: American Institute of Physics, pp. 6881–6892. ISSN: 0021-9606. DOI: 10.1063/1.471355. URL: https://aip.scitation.org/doi/10.1063/1.471355 (visited on 05/11/2022).

Zhang, Kai (Jan. 2016). "Gctf: Real-time CTF determination and correction". In: *Journal of Structural Biology* 193.1, pp. 1–12. ISSN: 1047-8477. DOI: 10.1016/j.jsb.2015.11.003. URL: https://www.ncbi.nlm.nih.gov/pmc/articles/PMC4711343/ (visited on 04/04/2022).

Zhang, Xing et al. (Feb. 12, 2008). "Near-atomic resolution using electron cryomicroscopy and single-particle reconstruction". In: *Proceedings of the National Academy of Sciences of the United States of America* 105.6, pp. 1867–1872. ISSN: 0027-8424. DOI: 10.1073/pnas.0711623105. URL: https://www.ncbi.nlm.nih.gov/pmc/articles/PMC2542862/ (visited on 06/11/2022).

Zhang, Xinzheng et al. (Nov. 6, 2012). "Structure of Sputnik, a virophage, at 3.5-Å resolution". In: *Proceedings of the National Academy of Sciences of the United States of America* 109.45, pp. 18431–18436. ISSN: 0027-8424. DOI: 10.1073/pnas.1211702109. URL: https://www.ncbi.nlm.nih.gov/pmc/articles/PMC3494952/ (visited on 06/11/2022).

Zheng, Shawn Q. et al. (Apr. 2017). "MotionCor2: anisotropic correction of beam-induced motion for improved cryo-electron microscopy". In: *Nature Methods* 14.4. Number: 4 Publisher: Nature Publishing Group, pp. 331–332. ISSN: 1548-7105. DOI: 10.1038/nmeth.4193. URL: http://www.nature.com/articles/nmeth.4193 (visited on 06/15/2022).

Zhou, Hong et al. (Jan. 12, 2007). "2-Aminoethyl diphenylborinate analogues: Selective inhibition for store-operated Ca2+ entry". In: *Biochemical and Biophysical Research Communications* 352.2, pp. 277–282. ISSN: 0006-291X. DOI: 10.1016/j.bbrc.2006.10.174. URL: https://www.sciencedirect.com/science/article/pii/S0006291X06023928 (visited on 05/03/2022).

Zhou, Qingtong et al. (Dec. 19, 2019). "Common activation mechanism of class A GPCRs". In: *eLife* 8. Ed. by Yibing Shan and Olga Boudker. Publisher: eLife Sciences Publications, Ltd, e50279. ISSN: 2050-084X. DOI: 10.7554/eLife.50279. URL: https://doi.org/10.7554/eLife.50279 (visited on 06/06/2022).

Zhou, Yubin et al. (Jan. 2010). "STIM1 gates the store-operated calcium channel ORAI1 in vitro". In: *Nature Structural & Molecular Biology* 17.1. Number: 1 Publisher: Nature Publishing Group, pp. 112–116. ISSN: 1545-9985. DOI: 10.1038/nsmb.1724. URL: http://www.nature.com/articles/nsmb.1724 (visited on 06/06/2022).

Zhou, Zheng Hong and Wah Chiu (Feb. 1, 1993). "Prospects for using an IVEM with a FEG for imaging macromolecules towards atomic resolution". In: *Ultramicroscopy* 49.1, pp. 407–416.

ISSN: 0304-3991. DOI: 10.1016/0304-3991(93)90246-T. URL: https://www.sciencedirect.com/science/article/pii/030439919390246T (visited on 06/11/2022).

Zivanov, Jasenko, Takanori Nakane, Björn O Forsberg, et al. (Nov. 9, 2018). "New tools for automated high-resolution cryo-EM structure determination in RELION-3". In: *eLife* 7. Ed. by Edward H Egelman and John Kuriyan. Publisher: eLife Sciences Publications, Ltd, e42166. ISSN: 2050-084X. DOI: 10.7554/eLife.42166. URL: https://doi.org/10.7554/eLife.42166 (visited on 04/04/2022).

Zivanov, Jasenko, Takanori Nakane, and Sjors H. W. Scheres (Jan. 1, 2019). "A Bayesian approach to beam-induced motion correction in cryo-EM single-particle analysis". In: *IUCrJ* 6 (Pt 1), pp. 5–17. ISSN: 2052-2525. DOI: 10.1107/S205225251801463X. URL: https://www.ncbi.nlm.nih.gov/pmc/articles/PMC6327179/ (visited on 04/04/2022).

Zollino, Marcella et al. (Mar. 2003). "Mapping the Wolf-Hirschhorn Syndrome Phenotype Outside the Currently Accepted WHS Critical Region and Defining a New Critical Region, WHSCR-2". In: *American Journal of Human Genetics* 72.3, pp. 590–597. ISSN: 0002-9297. URL: https://www.ncbi.nlm.nih.gov/pmc/articles/PMC1180235/ (visited on 06/08/2022).